HIGHWAY SIGN SUPPORT STRUCTURES

Volume 1

BREAK-AWAY ROADSIDE SIGN SUPPORT STRUCTURES

PROJECT HPR-2(104), CONTRACT NO. CPR-11-3550

TEXAS TRANSPORTATION INSTITUTE

Texas A&M University
College Station, Texas

HIGHWAY SIGN SUPPORT RESEARCH PROJECT HPR-2(104)

Project Policy Committee

OFFICERS

T. S. Huff, Chairman

J. E. Wilson, Vice Chairman

M. D. Shelby, Secretary (ex officio)

MEMBERS

V. Adam, Research and Development Engineer, Louisiana Department of Highways.

R. L. Anderson, Squad Chief, Bridge Section, State Highway Commission of Kansas.

J. E. Burke, Engineer of Research and Development, Illinois Division of Highways.

A. H. Dederman, Bridge Engineer, Nebraska Department of Roads.

F. W. Ellerman, Research Civil Engineer, District of Columbia Department of Highways and Traffic.

B. C. Hartronft, Research and Development Engineer, Oklahoma Department of Highways.

L. E. Hinds, Sr. Bridge Design Engineer, Tennessee Department of Highways.

P. A. Hoffman, Assistant Engineer, Bridge Section, South Dakota Department of Highways.

T. S. Huff, Chief Engineer of Highway Design, Texas Highway Department.

F. C. Marshall, Traffic Engineer, Minnesota Department of Highways.

A. Taragin, Assistant Deputy Director, Office of R&D, Bureau of Public Roads, Department of Transportation.

J. F. Tribble, Chief, Bureau of Research and Development, Alabama Highway Department.

A. M. White, Traffic Control & Safety Engineer and Equipment Manager, Mississippi Highway Department.

J. E. Wilson, Traffic Engineer, California Division of Highways, Department of Public Works.

L. L. Zink, Planning and Research Engineer, North Dakota Highway Department.

ALTERNATES

J. L. Beaton, Materials and Research Engineer, California Division of Highways.

H. M. Brooks, Senior Bridge Design Engineer, Tennessee Department of Highways.

G. C. Carlson, Traffic Research Engineer, Minnesota Department of Highways.

F. L. Holman, Jr., Assistant Research and Development Engineer, Alabama Highway Department.

S. Q. Kidd, Assistant Traffic Control and Safety Engineer, Mississippi State Highway Department.

R. L. Lewis, Research Engineer, Texas Highway Department.

J. D. McNeal, Engineer of Planning & Research, State Highway Commission of Kansas.

R. L. Meyer, Traffic Engineer, Nebraska Department of Roads.

R. S. O'Neill, Assistant Bridge Engineer, South Dakota Department of Highways.

C. F. Scheffey, Chief, Structures and Applied Mechanics Division, Office of R&D, Bureau of Public Roads, Department of Transportation.

V. E. Staff, Chief Highway Engineer, Chief Administrative Officer, Illinois Division of Highways.

G. J. Stelzmiller, Highway Design Engineer, North Dakota Highway Department.

W. T. Taylor, Jr., Assistant Traffic and Planning Engineer, Louisiana Department of Highways.

A STATEMENT FROM THE POLICY COMMITTEE

Someone has said "the penalty for leaving the traveled way should not be capital punishment." Unfortunately, there are still too many people killed in collisions with fixed objects such as sign posts, trees, and bridge piers along the edges of our highways. The results of this research now provide the highway engineer with a solution, at least for the roadside sign post portion of this problem. The attached report provides criteria for the design of break-away sign supports that will fail under collision with little or no injury to the vehicle occupants.

The work herein was performed by the Texas Transportation Institute as a part of the Highway Planning and Research Program sponsored by 13 states and the District of Columbia in cooperation with the United States Bureau of Public Roads. Representatives of these sponsoring agencies served on a Policy Committee to guide the program and judge the results of the study. It is the judgment of the Policy Committee that the results are very practical and can be put into practice immediately in every state in the Union.

This research study extended beyond the formulation of just a break-away design. The report outlines design criteria that will enable each designer to consider various assumptions, configurations and materials. Actually three additional designs other than the break-away cantilever support were considered and all were found to be satisfactory to varying degrees. They were as follows:

(1) A deforming "A" frame type constructed of light rail steel members which shear upon impact.

(2) An "A" frame support made of aluminum which fails by fracture of the cast joints upon impact.

(3) A wooden post with a shear plane introduced near its base. This support was not crash tested under this project; however, it is felt that limited testing of this design to establish its value is a matter of record.

By use of the design criteria outlined in the report, supports of existing signs can be modified at a nominal expense to conform to the break-away concept. In addition, the findings can be applied to all new construction.

At the time of publication of this report at least seven of the cooperating states, Kansas, Louisiana, Minnesota, Nebraska, Oklahoma, Tennessee, and Texas, have already erected several hundred break-away installations. The other participating states are in the process of implementing such programs. Accidents with the sign posts in the above states erected in compliance with the findings of this report have behaved as predicted and have already resulted in the saving of many lives as well as reducing the severity of injuries.

This research and experience point to the advantages of the break-away sign support. We recommend to highway engineers, administrators, and in particular AASHO to give serious consideration to the findings of this research project.

Through the cooperative efforts of this study a long step has been taken to minimize the hazard of ground mounted sign support structures to the highway user. The Policy Committee believes that the multi-state cooperative research concept is sound and that "feed back" and early implementation of results in itself are worthy of its keep. Research endeavors of this type and general interest should be continued especially to further explore the "off pavement" elements of our highways as they may be related to safety. Areas of research might include the study of highway illumination, overhead sign supports, impact attenuation devices and roadside appurtenances including the placement of signs and signals.

HIGHWAY SIGN SUPPORT STRUCTURES

VOLUME 1

BREAK-AWAY ROADSIDE SIGN SUPPORT STRUCTURES

Final Report

of

PROJECT HPR-2(104), CONTRACT NO. CPR-11-3550
HIGHWAY SIGN SUPPORT RESEARCH

AREA I SIGN SUPPORT STRUCTURES

TEXAS TRANSPORTATION INSTITUTE
TEXAS A&M UNIVERSITY
COLLEGE STATION, TEXAS

JULY 1967

FOREWORD

The information contained herein was developed on Research Project HPR-2(104), entitled "Highway Sign Support Research," which was a pooled fund research project sponsored jointly by the U. S. Department of Transportation, Federal Highway Administration, Bureau of Public Roads, and the following highway departments: Alabama, California, Illinois, Kansas, Louisiana, Minnesota, Mississippi, Nebraska, North Dakota, Oklahoma, South Dakota, Tennessee, Texas, and the District of Columbia.

The result of this Research Project have been reported in three separate volumes, each concerning itself with the specific area of investigation as follows:

VOLUME 1	BREAK-AWAY ROADSIDE SIGN SUPPORT STRUCTURES
VOLUME 2	WIND LOADS ON ROADSIDE SIGNS
VOLUME 3	FEASIBILITY STUDY OF IMPACT ATTENUATION OR PROTECTIVE DEVICES FOR FIXED HIGHWAY OBSTACLES

Each volume is complete within itself, presenting the objectives, work done, conclusions, and recommendations.

The Contract Manager of this project was R. F. Baker of the Office of Research and Development, Bureau of Public Roads. A Policy Committee composed of engineers from the various participating highway departments and the Bureau of Public Roads was established to represent the participating agencies to (1) insure that the contractor would be responsive to the desires of the cooperating highway agencies, (2) provide a means for keeping all parties informed of progress and action on the subject, and

(3) provide adequate liaison between the technical personnel on the project and those of the technical staff of the Bureau of Public Roads and the participating agencies to insure the success of the work and its early acceptance.

This Policy Committee was composed of the following members and alternates

Chairman: T. S. Huff

Vice Chairman: J. E. Wilson

Secretary: M. D. Shelby (ex officio)

STATE	MEMBER	ALTERNATE
Alabama	J. F. Tribble	F. L. Holman
California	J. E. Wilson	J. L. Beaton
Illinois	J. E. Burke	V. E. Staff
Kansas	R. L. Anderson	J. D. McNeal
Louisiana	V. Adam	W. T. Taylor, Jr.
Minnesota	F. C. Marshall	G. Carlson
Mississippi	A. M. White	S. Q. Kidd
Nebraska	A. H. Dederman	R. L. Meyer
North Dakota	V. Zink	G. J. Stelzmiller
Oklahoma	B. C. Hartronft	
South Dakota	P. A. Hoffman	R. S. O'Neill
Tennessee	L. E. Hinds	H. M. Brooks
Texas	T. S. Huff	R. L. Lewis
District of Columbia	F. W. Ellerman	
Bureau of Public Roads	A. Taragin	C. F. Scheffey

In addition, a Technical Subcommittee was established to provide continuous and critical review of the progress of the work. This committee was selected by the Policy Committee and was composed of engineers with special technical competence and ability to contribute to the success of the project and implementation of its findings. The members of the Technical Subcommittee were as follows:

Chairman: T. S. Huff

Secretary: M. D. Shelby (ex officio)

STATE	MEMBER
California	J. L. Beaton
Kansas	R. L. Anderson
Louisiana	W. T. Taylor, Jr.
Tennessee	L. E. Hinds
Texas	T. S. Huff

The opinions, findings and conclusions expressed in this report are those of the authors and not necessarily those of the Bureau of Public Roads.

ACKNOWLEDGEMENTS

This project was conducted by the Texas Transportation Institute, C. J. Keese, Director, through the Texas A&M Research Foundation, Fred J. Benson, Vice President. The work was accomplished through combined efforts of the Structural Research Department, T. J. Hirsch, Head, and the Highway Design and Traffic Department, Charles Pinnell, Head.

The organization of the research team in responsible charge for accomplishing the objectives of the research was under the Co-Directorship of R. M. Olson (Structures) and Neilon J. Rowan (Highway Design and Traffic). The three specific research efforts were under the supervision of three research area supervisors as follows:

Area I	Sign Support Structures Thomas C. Edwards, Supervisor
Area II	Protective Devices Peter D. Weiner, Supervisor
Area III	Reduction of Wind Loads Hayes E. Ross, Jr., Supervisor

In addition to the research area supervisors, a support group under the supervision of Thomas Williams and James Mahle provided purchasing, procurement, fabrication, and test installation services.

James Bradley supervised the photographic coverage of all crash tests and assisted Rowan and Olson in the preparation of the 16 mm sound movie summarizing the results of the Break-Away Roadside Sign Research.

Mrs. Diantha Langley was in charge of data reduction and processing from the high speed movie film records and oscillogram records from all

crash tests. Mrs. Langley also made significant contributions in preparing this final report by documenting crash tests with selected photographs and tabulated data.

Electronic instrumentation, including transducers, recordings, and other devices was accomplished by A. M. Gaddis, Gerald Clark, James Byram, and Monroe White.

The typing and preparation of the manuscript for this report was accomplished by Mrs. Ruth DeShaw and Mrs. Sylvia Velasco.

M. D. Shelby, Research Engineer of TTI, was Secretary (ex officio) of both the Project Policy Committee and Technical Subcommittee and worked tirelessly in coordinating the efforts of the researchers in response to the requirements of the sponsoring agencies.

Charles F. Scheffey, Chief of Structures and Applied Mechanics Division, Office of Research and Development, BPR, is due particular acknowledgement for the many hours spent in counseling the researchers concerning the technical aspects of this research. His advice and counsel based on many years of experience were invaluable to the researchers.

The suggestions and encouragement of A. C. Taylor, Regional Engineer, Bureau of Public Roads, were a continuing source of inspiration which are sincerely and gratefully acknowledged.

Last, but not least, the significant contributions of Leon Hawkins, Texas Highway Department Engineer, are acknowledged. Mr. Hawkins deserves credit for developing the original concept and design of the break-away base for use on cantilever type roadside signs. From the beginning and throughout this project, Mr. Hawkins has worked closely with the

researchers of TTI offering his technical and practical advice concerning the development and implementation of the break-away design concept. He supervised the preparation and revision of standards for design and installation of the many break-away signs now installed along Texas highways. He has worked tirelessly in collecting information concerning the behavior and performance of sign installations in Texas.

A distinguishing characteristic of this research study has been the activities of the Project Policy Committee, whose interest in the primary objective of eliminating roadside hazards, and whose examination of the detailed information developed in this investigation, has proven invaluable to the research staff. It is believed that the liaison between the practicing engineers and the researchers during this investigation has resulted in a clearer understanding of the nature of the hazard and its elimination through a cooperative research effort. It is apparent that the elapsed time between research investigation and field application has been substantially reduced by the continuing deliberations of the Project Policy Committee.

TABLE OF CONTENTS

OF

VOLUME 1

BREAK-AWAY ROADSIDE SIGN SUPPORT STRUCTURES

PART I	SUMMARY OF RESEARCH
PART II	MATHEMATICAL SIMULATION, CORRELATION AND PARAMETER STUDY
PART III	LABORATORY INVESTIGATIONS, DATA ACQUISITION, DATA ANALYSIS, CRASH TESTS, CASE STUDIES OF ACTUAL ROADSIDE INSTALLATIONS

PART I

SUMMARY OF RESEARCH

TABLE OF CONTENTS

Chapter		Page
1		
	1.1 Introduction	1:1
	1.2 Other Concepts	1:2
	1.3 Break-Away Cantilever Support References	1:3

LIST OF FIGURES

Figure		Page
1.3.1	Loading Conditions for Break-Away Support	1:5
1.3.2	Break-Away Sign Support Behavior	1:6

LIST OF TABLES

Table		Page
1.3.1	Recommendations for Design of "Break-Away" Supports	1:7

CHAPTER 1

1.1 Introduction

The need for safer roadside support structures for highway signs and utilities is apparent from accident statistics. Statistics for single-vehicle accidents on completed sections of the Interstate System for the period of July to December, 1966, show that of 993 fatal accidents, 566, or 57% involved the vehicle running off the road. Of these 566 fatal accidents, 443, or 78% were caused by collisions with obstacles. The remaining 123, or 22% of the fatalities were caused by the vehicle overturning without contacting an obstacle. Of the 443 accidents involving roadside obstacles, 148, or 33% were with guardrails; 95, or 21% with bridge elements; 44, or 10% with sign supports; and 16, or 4% with luminaire supports. Out of the total 443 single-vehicle off-the-road accidents involving obstacles, there were 511 fatalities, or 1.18 deaths per accident. Fifty-two (52) of these deaths can be attributed to collisions with sign supports.[1]

It is interesting to note that in Texas alone, since December of 1965, there have been 82 accidents involving break-away supports. In 43 of these the vehicle did not remain at the scene. In the remaining 36 accidents, there were 8 cases of minor injury (bruises or complaint of pain). Only 1 case of serious injury occurred in an accident in which the colliding vehicle struck a culvert headwall after the vehicle had passed through the sign support.

At the inception of this investigation, the objectives of the research effort were stated, in part, as follows: "To develop new designs and installations criteria for support structures for highway signs and utilities to

reduce the injury and damage effects of motor vehicle accidents resulting from collisions with these structures." In order to be responsive to the stated objective and the cooperative nature of the research, the Project Policy Committee requested information concerning roadside sign installations from each of the 50 state highway departments. The request was sent out in August, 1966, and 38 replies were received by October 15, 1966. All of the replies indicated that cantilever type supports were employed. Thirteen (13) of the respondents had adopted, or were considering adopting, break-away details for these types of supports. On August 1, 1966, the Federal Highway Administration issued Instructional Memorandum 21-6-66 which said in part:

> "When it is necessary to locate sign supports and lighting standards adjacent to the shoulder, a break-away or yielding support should be used. Pending the development of generally accepted criteria on break-away sign supports, a preliminary design for sign supports developed jointly by the Texas Highway Department and Texas A&M University will be accepted if the states so request."

Since criteria for the design, detailing, construction, and maintenance was becoming more essential with the passage of time, emphasis has been placed on the development of information concerning the break-away concept for cantilever supports.

1.2 Other Concepts

In earlier studies by the Texas Transportation Institute, other types of sign support structures were subjected to full-scale tests. An A-frame constructed of tubular steel sections, with preformed failure planes, was tested and proved to perform satisfactorily.[2] Timber supports for small signs containing stress raisers in the form of notches or slots produced only minor damage to the colliding vehicle.[3]

Other types of roadside sign supports have also been considered as part of this research. Several A-frame concepts were studied, including (1) an A-frame fabricated from rail grade rolled steel "U-sections," and (2) a tubular aluminum A-frame employing cast aluminum joint connections. These signs performed satisfactorily and are more fully described in Sections 8.6 and 8.8 of Part III.

For the reasons previously mentioned, the concept and design recommendations for the break-away cantilever support are presented.

1.3 Break-Away Cantilever Support

The basic concept of the break-away sign support is to provide a structure that will resist wind loads yet fail, at preselected locations, when struck by a vehicle. The loading conditions for which the support must be designed are shown in Figure 1.3.1. Three critical connection locations and their required characteristics under each loading condition are indicated. When these connections are properly designed, the support will be stable and will possess the break-away characteristics, when struck by a vehicle, shown in Figure 1.3.2.

The major objective of the research effort in Area I has been to provide information for the design of safe break-away cantilever supports. Emphasis has been placed on developing design recommendations for the three critical connections. This information has been developed through laboratory tests (see Part III) and the use of a mathematical model (see Part II). Table 1.3.1 is a summary of the design recommendations presented in Section 5.1 of Part II. With a thorough understanding of the conceptual principles of the break-away support and the prudent application

of the design recommendations, a safe support can be constructed. Full-scale crash tests and accident records indicate that the break-away concept will function for the types of collisions which are most probable.

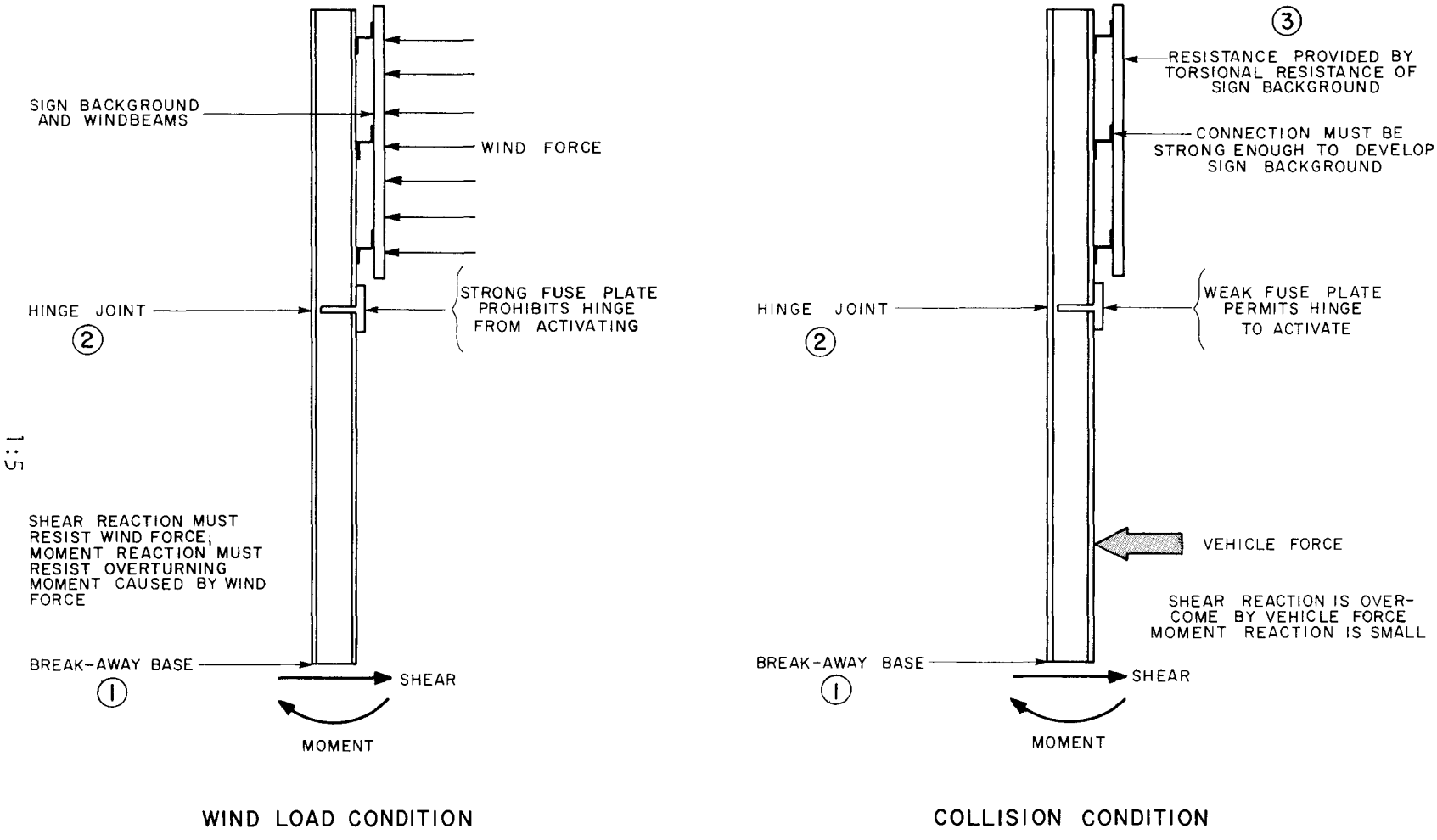

FIGURE 1.3.1 BREAKAWAY SIGN LOADING CONDITIONS

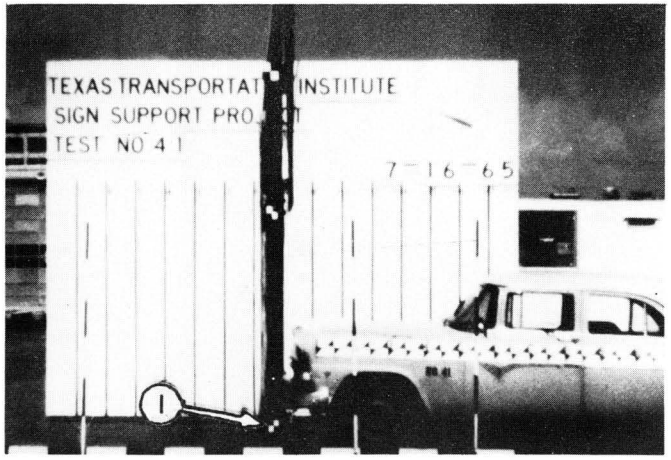

a) BREAK-AWAY BASE (1) DISENGAGES

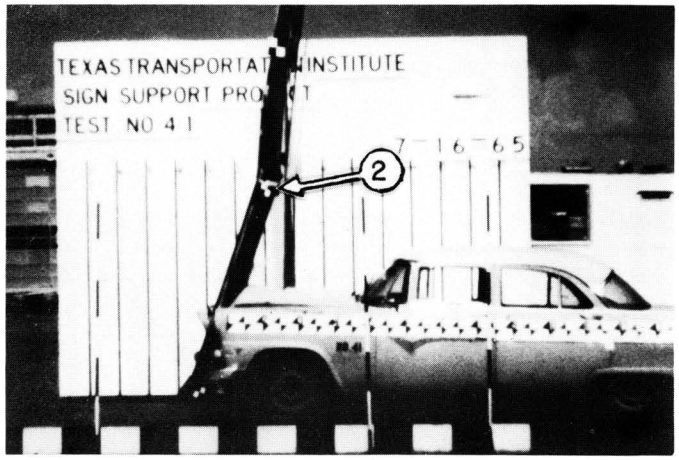

b) HINGE JOINT (2) ACTIVATES

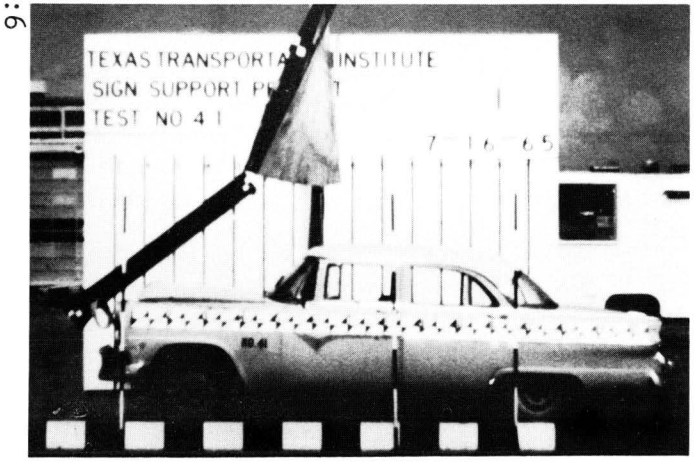

c) POST LOSES CONTACT WITH VEHICLE

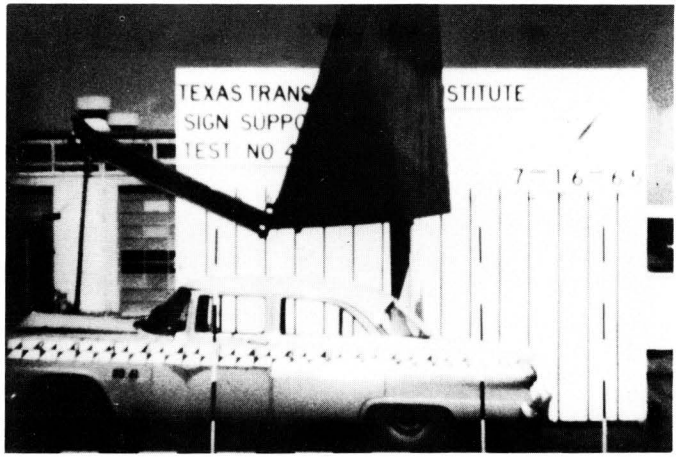

d) SIGN SUPPORT POST CLEARS VEHICLE

FIGURE 1.3.2 BREAK-AWAY SIGN SUPPORT BEHAVIOR

TABLE 1.3.1 RECOMMENDATIONS FOR DESIGN OF "BREAK-AWAY" SUPPORTS

1. Post Sizes — Ref.

A standard structural section weighing less than 45 lb/ft. selected to resist the maximum wind load moment. — Section 5.1 Part II Vol. I

2. Base Plate and Base Connection

The base plate should be designed for the maximum wind loads and not weigh more than the maximum values shown in the table below. The base bolts should be designed to resist the maximum wind load assuming no pretension. The initial bolt forces in the table below are recommended: — Section 5.1 Part II Vol. I

Post Size (lb/ft.)	Bolt Diam. (in.)	Bolt Force (lb.)	Torque (A325, galv.) (lb.-in.)	(lb.-ft)	Base Plate Wt. (lb.)
0-8	1/2	920-1380	200-300	16.7-25.0	8.0
9-20	5/8	1740-2660	460-680	37.5-56.5	12.0
21-30	3/4	2400-3600	750-1060	67.5-88.3	21.0
30+	7/8	2400-3600	850-1280	70.8-106.8	21.0
30+	1	2400-3600	450-1470	77.1-118.2	21.0

Table 5.1.1 Part II Vol. I

3. Fuse Connection

The moment capacity for the fuse connection is determined by the maximum wind load moment at the fuse. If slotted plates are used the initial bolt force can be determined by — Section 5.1 Part II Vol. I

$$N' = \frac{M}{mnf(s)r}, \text{ where } f(s)_{max} = 0.26,\ f(s)_{avg} = 0.21,\ f(s)_{min} = 0.17$$

ASTM turn-of-nut tightening methods are satisfactory if background-to-post connections are adequately designed. For torque wrench tightening, the bolt force may be calculated using

$$N' = K_T \tau \text{ , where } \tau = \text{bolt torque in in.-lb.}$$

TABLE 1.3.1 (Continued)

Bolt Diameter (ASTM A325 galvanized) (in.)	K_T	Ref.
1/2 - 13UNC	4.940	Table 3.3.1 Part III Vol. I
5/8 - 11UNC	3.870	
3/4 - 10UNC	3.185	

4. Background-to-Post Connection

The maximum connection force anticipated is 10,000 lb. — Section 5.1 Part II Vol. I

5. Rotational Stiffness of Sign Background

A minimum stiffness of 100 ft.-lb./degree (5,730 ft.-lb./radian). — Section 5.1 Part II Vol. I

REFERENCES

1. "Fatal accidents on completed sections of the Interstate System, July - December, 1966," Circular Memorandum to Regional Federal Highway Administration and Division Engineers, from J. D. Lacy, Director, Office of Traffic Operations, Washington, D. C., U. S. Department of Transportation, Federal Highway Administration, Bureau of Public Roads, June 13, 1967, Page 12.

2. Samson, C. H., Rowan, N. J., Olson, R. M. and Tidwell, D. R., "Impact Behavior of Sign Supports," A Research Report 68-1, Texas Transportation Institute, College Station, Texas, March 1965, Page 4-17.

3. Rowan, N. J., Olson, R. M., Edwards, T. C., Gaddis, A. M. and Williams, T. G., "Impact Behavior of Sign Supports-II," Staff Progress Report 68-2, Texas Transportation Institute, College Station, Texas, September 1965, Page 39.

PART II

MATHEMATICAL SIMULATION, CORRELATION AND PARAMETER STUDY

TABLE OF CONTENTS

CHAPTER		PAGE
1	INTRODUCTION	1:1
	1.1 Need for the Model	1:1
2	DEVELOPMENT OF THE MATHEMATICAL MODEL	2:2
	2.1 Basic Concepts of the "Break-Away" System and Their Model Simulation	2:2
	The "break-away" sign model	2:2
	2.2 The Finite Difference Equations of Motion	2:4
	Matrix formulation of the equations of motion	2:6
	2.3 Determination of Bending Moments	2:9
	2.4 Boundary Conditions on the Post	2:13
	2.5 Translational Response of the Sign Background	2:17
	2.6 Derivation of Numerical Integration Techniques for Torsional Response	2:20
	Boundary conditions on the sign background	2:22
	2.7 Formulation of Technique to Include Sign Background Restraint	2:24
	2.8 Vehicle Model	2:26
	Simulation of vehicle crash characteristics	2:27
	Passenger simulation	2:31
	2.9 The "Plastic Hinge"	2:33
	2.10 The Slip Base	2:38
3	CORRELATION WITH TEST RESULTS	3:42
	3.1 Introduction	3:42
	3.2 Philosophy of the Correlation	3:42
	3.3 Simulation Input Values	3:44
	The slip base	3:44
	"Plastic hinge" fuse plate	3:46
	The support post	3:48
	Sign background	3:48
	Sign background-to-post connection	3:51
	The vehicle and passenger	3:54
	3.4 Correlation	3:54
	Base displacement	3:54

TABLE OF CONTENTS (Continued)

CHAPTER		PAGE
	Vehicle velocity	3:59
	Vehicle displacement	3:62
	Mechanical fuse plate force	3:62
	Bending 2' - 0" above base	3:66
	Force in the base bolts	3:68
	Vehicle deceleration	3:70
	Passenger response	3:70
	Event times	3:73
	3.5 Conclusions	3.75
4	PARAMETER STUDY	4:76
	4.1 Introduction	4:76
	4.2 Philosophy of the Study	4:76
	4.3 Range of Study Parameters	4:78
	Sign support size	4:78
	Vehicles	4:80
	Simulated passenger	4:80
	Description of problem runs	4:87
	4.4 Results	4:87
	Summary of all problems	4:87
	Effects of vehicle velocity and vehicle weight	4:87
	Effects of initial base bolt tension	4:105
	Base plate weight	4:105
	Effect of sign background torsional stiffness	4:113
	Effect of vehicle stiffness	4:113
	Effect of initial fuse plate bolt tension	4:113
	Effect of background-to-post connection stiffness	4:117
	Effects of support post weight	4:117
	4.5 Conclusions	4:121
	The sign background	4:121
	Background-to-post connection	4:121
	Initial fuse plate bolt tension	4:121
	Initial base plate bolt tension	4:122
	The vehicle	4:122
	The support post	4:122
5	RECOMMENDATIONS	5:124
	5.1 "Break-Away" Supports	5:124
	REFERENCES	129

LIST OF FIGURES

FIGURE		PAGE
2.1.1	Sign Support Idealization	2:3
2.2.1	Sign Convention and Free Bodies	2:5
2.3.1	Elastic-Plastic M - ϕ Diagram	2:9
2.3.2	Idealization of Support Base	2:12
2.4.1	Stages of Post Bending	2:14
2.4.2	Equation (2.2.8) for Restrained End Condition	2:16
2.4.3	Equation (2.2.8) for Free End	2:18
2.6.1	General Torsional Model	2:21
2.6.2	Equation (2.6.1) for Torsional Response of Sign Background	2:23
2.7.1	Post-Sign Background Connection	2:25
2.8.1	Vehicle Simulation	2:28
2.8.2	Idealized Vehicle	2:30
2.8.3	Passenger Simulation	2:32
2.9.1	The "Plastic Hinge"	2:34
2.9.2	"Plastic Hinge" Behavior	2:36
2.10.1	"Break-Away" Support Base Plate	2:39
3.1.1	Post Configuration for Tests 41 and 446-5	3:43
3.3.1	Slip vs. Base Coefficient of Friction Curve	3:45
3.3.2	Fuse Plate Friction Factor (8WF17)	3:47
3.3.3	Sign Support for Test No. 41	3:49
3.3.4	Sign Support for Test 446-5	3:50
3.3.5	Section Properties of Background	3:52
3.3.6	Background-to-Post Connection	3:53

LIST OF FIGURES (Continued)

FIGURE		PAGE
3.4.1	Test 41, Base Plate Displacement	3:57
3.4.2	Test 446-5, Base Plate Displacement	3:58
3.4.3	Test 41, Vehicle Velocity	3:60
3.4.4	Test 446-5, Vehicle Velocity	3:61
3.4.5	Vehicle Displacement	3:63
3.4.6	Test 41, Fuse Plate Force Correlation	3:64
3.4.7	Test 446-5, Fuse Force	3:65
3.4.8	Test 446-5, Bending Moment 2' - 0" from Base	3:67
3.4.9	Test 446-5, Base Bolt Force	3:69
3.4.10	Frame Acceleration	3:71
3.4.11	Passenger Response	3:72
4.3.1	Distribution of Sign Depth and Width	4:79
4.3.2	3I5.7 Post and Sign	4:81
4.3.3	6B8.5 Post and Sign	4:82
4.3.4	8WF20 Post and Sign	4:83
4.3.5	10WF25 Post and Sign	4:84
4.4.1	3I5.7 Support	4:96
4.4.2	6B8.5 Support	4:97
4.4.3	8WF20 Support	4:98
4.4.4	10WF25 Support	4:99
4.4.5	Time of Critical Events (3I5.7)	4:100
4.4.6	Time of Critical Events (6B8.5)	4:101
4.4.7	Time of Critical Events (8WF20)	4:102
4.4.8	Time of Critical Events (10WF25)	4:103
4.4.9	1800 Lb. Vehicle, V_o = 40 mph	4:106

LIST OF FIGURES (Continued)

FIGURE		PAGE
4.4.10	3600 lb. Vehicle, V_o = 40 mph	4:107
4.4.11	4800 lb. Vehicle, V_o = 40 mph	4:108
4.4.12	Effects of Support Weight (40 mph Collision Velocity)	4:119

LIST OF TABLES

TABLE		PAGE
3.3.1	Vehicle Simulation	3:55
3.4.1	Correlation Parameters	3:56
3.4.2	Comparison of Event Times	3:74
4.3.1	Fixed Parameters for Study Supports	4:85
4.3.2	Vehicle Parameters	4:86
4.3.3	List of Parameter Study Problems	4:88
4.4.1	Summary of Parameter Study Results	4:91
4.4.2	Critical Base Bolt Tension to Stop Vehicle for 40 MPH Collision	4:109
4.4.3	Effect of Base Bolt Tension on Simulated Passenger Acceleration	4:110
4.4.4	Effect of Base Plate Weight (1800 lb. Vehicle, 40 mph)	4:111
4.4.5	Effect of Base Plate Weight (3600 lb. Vehicle, 40 mph)	4:112
4.4.6	Effect of Sign Background Torsional Stiffness	4:114
4.4.7	Effect of Vehicle Stiffness	4:115
4.4.8	Effect of Initial Fuse Bolt Tension	4:116
4.4.9	Effect of Background-to-Post Connection Stiffness	4:118
5.1.1	Recommended Range of Base Plate Variables	5:125

CHAPTER 1

INTRODUCTION

1.1 Need for the Model

In order to develop the concept of the "break-away" sign support post into a design that can be utilized under field conditions, it is necessary to explore the effects of the various parameters of the concept on the response of the vehicle and the support. Studies of this type would develop the required criteria for the design of supports that could be relied upon to operate safely on the highway. A full-scale testing program obviously would be prohibitively expensive, if not impractical, considering the number of variables involved. It is therefore logical to develop an analytical model which can be used to evaluate the various parameters which affect the design of the sign support. The following sections are devoted to the development of a mathematical model, its verification by correlation with full-scale crash tests and the formulation of criteria based on a parameter study conducted with the model.

C H A P T E R 2

DEVELOPMENT OF THE MATHEMATICAL MODEL

2.1 Basic Concepts of the "Break-Away" System and Their Model Simulation

The concept of the "break-away" sign post was explained and illustrated in Section 1.3 of Part I. It may be recalled that the post is attached at its base by a slip plate or friction plate which offers some resistance to slipping. The post is weakened by the insertion of a "plastic hinge" in the upper portion of the post near the attachment point of the lower windbeam on the sign background. The background is normally a thin plate of plywood or built up of metal sections. It is strengthened by two or more horizontal beams to distribute the wind loads to the posts (in some instances these beams are an integral part of the sign face). The size of the sign background varies according to the amount of advisory information placed on it. The size of the posts, or support members, is directly related to the size of the background. As the background becomes large, the size of the posts must be increased proportionately to resist wind forces. Hence, it is possible to encounter very large and stiff post members in practice.

The "break-away" sign model. The post mass and sign background are idealized as discrete elements as shown in Figure 2.1.1. The background is broken into rigid plate elements connected by elastic torsional springs. The background is assumed to be rigidly connected to a support which represents the opposite leg of the two-post sign. This assumption presupposes that the opposite leg does not rotate. The background is

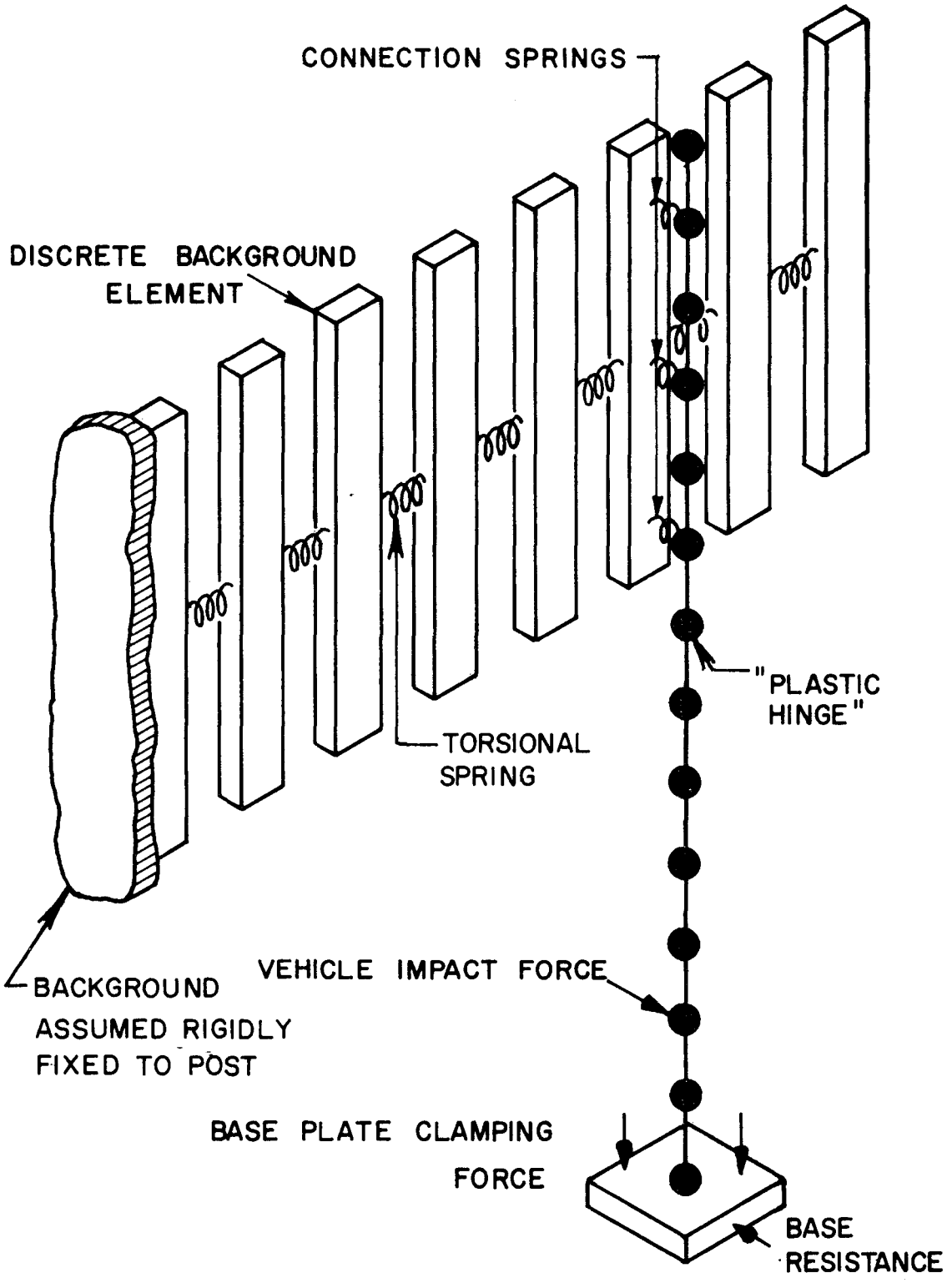

FIGURE 2.1.1 SIGN SUPPORT IDEALIZATION

connected to the post leg by elastic springs which represent the physical connections. The post is discretized as a lumped-mass system as shown. The slip-base is idealized as a friction device, the resistance of which is a function of the clamping force and the friction factor between the faying surfaces.

2.2 The Finite Difference Equations of Motion

Figure 2.2.1(a) is a section from the model showing the free bodies related to a typical mass point and adjacent beam segments. Figure 2.2.1(b) gives the sign conventions adopted in this development. The origin of the x (vertical) axis is taken at the bottom of the post.

Consider the system of Figure 2.2.1(c) as displaced in the positive y direction. The deformation of the beam is assumed to be influenced by flexural deflection only. Deformations due to shear are neglected as well as effects of strain rate, geometry changes and rotary inertia. The relation between moment and curvature is, in general, assumed to be bilinear although other relations may be used. The forces acting on the mass are the end shears, external actions and reactions, and the inertia force of the mass itself, derived from D'Alembert's principle.

Summation of the forces in the y direction yields

$$m_j \ddot{y}_j + V_{ji} - V_{jk} - F_j(t) = 0 \qquad (2.2.1)$$

Since forces are applied only at mass points, the relations between end shears and end moments are

$$V_{jk} = \frac{M_k - M_j}{h_{jk}} \qquad (2.2.2)$$

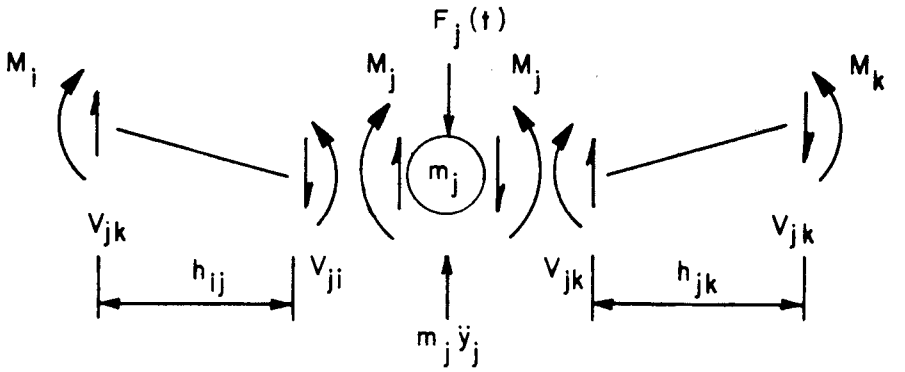

(a) BEAM SEGMENT ijk

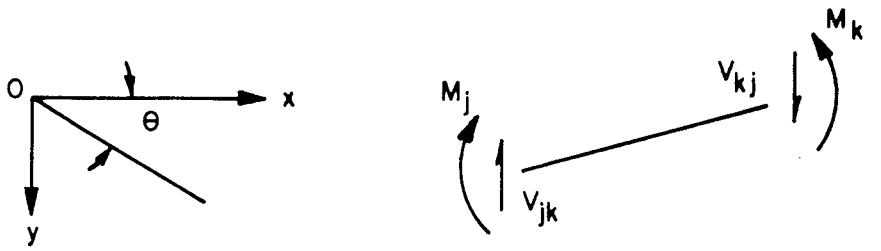

(b) SIGN CONVENTION (POSITIVE AS SHOWN)

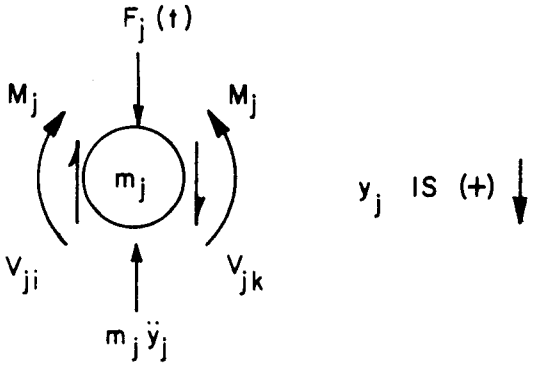

(c) DYNAMIC EQUILIBRIUM FREE BODY

FIGURE 2.2.1 SIGN CONVENTION AND FREE BODIES

$$V_{ji} = \frac{M_j - M_i}{h_{ij}} \qquad (2.2.3)$$

Substituting from Eq. (2.2.2) and Eq. (2.2.3) into Eq. (2.2.1) yields

$$m_j \ddot{y}_j + \frac{M_j - M_i}{h_{ij}} - \frac{M_k - M_j}{h_{jk}} = F_j(t) \qquad (2.2.4)$$

If a reference segment length (h_o) is chosen, all segments can be expressed by

$$a_{ij} = \frac{h_o}{h_{ij}} \quad , \quad a_{jk} = \frac{h_o}{h_{jk}} \quad , \text{ etc.}$$

and Eq. (2.2.4) becomes

$$m_j \ddot{y}_j - \frac{1}{h_o} [a_{ij} M_j - (a_{ij} + a_{jk}) M_j + a_{jk} M_k] = F_j(t) \qquad (2.2.5)$$

Eq. (2.2.5) is the difference equation for the motion of the single mass point m_j.

Matrix formulation of the equations of motion. Dividing the beam into n segments, having n + 1 lumped masses, requires n + 1 equations of the form of Eq. (2.2.5) to describe the system. The resulting set of simultaneous equations can be expressed in matrix form

$$[m] \{\ddot{y}\} - \frac{1}{h_o} [a] \{M\} = \{F\} \qquad (2.2.6)$$

where

[m] is a diagonal matrix of the lumped mass values:

$$[m] = \begin{bmatrix} \cdots & & & & \\ & \cdots & & & \\ & & m_i & & \\ & & & m_j & \\ & & & & m_k \\ & & & & \cdots \end{bmatrix}$$

$\{\ddot{y}\}$ is a column matrix of mass point accelerations:

$$\{\ddot{y}\} = \begin{Bmatrix} \cdots \\ \cdots \\ \ddot{y}_i \\ \ddot{y}_j \\ \ddot{y}_k \\ \cdots \end{Bmatrix}$$

[a] is a tri-diagonal matrix of the segment ratios:

$$[a] = \begin{bmatrix} \cdots & & & \\ \cdots & & & \\ a_{hi} - (a_{hi} + a_{ij})\, a_{ij} & & & \\ & a_{ij} - (a_{ij} + a_{jk})\, a_{jk} & & \\ & & \cdots & \\ & & \cdots & \end{bmatrix}$$

$\{M\}$ and $\{F\}$ are column matrices:

$$\{M\} = \begin{Bmatrix} \cdots \\ \cdots \\ M_i \\ M_j \\ M_k \\ \cdots \\ \cdots \end{Bmatrix} \qquad \{F\} = \begin{Bmatrix} \cdots \\ \cdots \\ F_i(t) \\ F_j(t) \\ F_k(t) \\ \cdots \\ \cdots \end{Bmatrix}$$

Eq. (2.2.5) can be integrated numerically by introducing the difference approximation for acceleration.[1]

$$\frac{d^2y}{dt^2} = \frac{y(t + \Delta t) - 2y(t) + y(t + \Delta t)}{\Delta t^2}$$

The use of this approximation is equivalent to a constant acceleration technique.[2] The acceleration vector $\{\ddot{y}\}$ in Eq. (2.2.5) can be written as

$$\{\ddot{y}(t)\} = \frac{1}{\Delta t^2} \{y(t - \Delta t)\} - \frac{2}{\Delta t^2} \{y(t)\} + \frac{1}{\Delta t^2} \{y(t + \Delta t)\} \quad (2.2.7)$$

Note that since finite differences are introduced, each displacement vector has a functional relation to the time-differencing interval Δt. Substitution from Eq. (2.2.7) into Eq. (2.2.5) yields

$$\{y(t + \Delta t)\} = \Delta t^2 [m]^{-1} \{F(t)\} + \frac{\Delta t^2}{h_o} [m]^{-1} [a] \{M(t)\} + 2\{y(t)\} - \{y(t - \Delta t)\} \quad (2.2.8)$$

These equations are used to numerically integrate the equations of motion. The process consists of the following steps:

(1) Set up the boundary and starting conditions.

(2) Calculate $\{F\}$.

(3) Calculate $\{y(t + \Delta t)\}$ from Eq. (2.2.8).

(4) Calculate $\{M(t)\}$ using the moment-curvature relation for the beam material.

(5) Repeat procedure, starting with step (2).

It should be noted that in order to complete step (3), for the first iteration (time = $0+\Delta t$), the bending moment at each mass point must be known. In most problems the beam is assumed to be initially in an unstressed condition, hence the bending moments are zero. If other initial conditions are imposed, the bending moments must be known in order to start the integration. Note from Eq. (2.2.8) that the determination of $y(0+\Delta t)$ requires specific knowledge of prior time dependent events, i.e., of $y(0-\Delta t)$. The starting conditions are determined,

therefore, so that the recursive equations, Eq.(2.2.8), are forced to fit the prescribed initial conditions. The initial conditions for the specific problem of this paper are

$$\{y(o)\} = 0., \quad \{\dot{y}(o)\} = 0.$$

$$\{M(o)\} = 0., \quad \{F(o)\} = 0.$$

For these conditions

$$\{y(o - \Delta t)\} = 0.$$

2.3 Determination of Bending Moments

In Eq. (2.2.8), it is necessary to know the bending moment on each mass point at time t. These moments are present in the form of the column matrix $\{M\}$. The value of the moment on any particular mass point can be determined from the moment-curvature characteristics of the beam material.

It is assumed that the beam is of a material which exhibits a typical elastic-plastic moment-curvature relationship as shown in Figure 2.3.1.

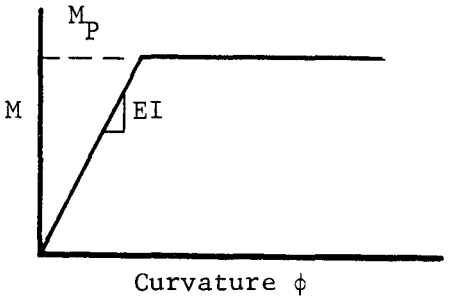

FIGURE 2.3.1 ELASTIC-PLASTIC M-ϕ DIAGRAM

This assumption is in accordance with the approach used in the treatment of elastic-plastic beam and frame structures. The modulus of elasticity of the material will be denoted by E at the mass point under consideration. If the cross section is not uniform the moment of inertia, I, would refer to the average value over the half-segment on each side of the mass point.

The curvature at a typical interior mass point can be determined by using divided differences. Since the differencing interval is not constant, one obtains

$$\left(\frac{d^2y}{dx^2}\right)_j = \phi_j = \frac{2}{h_{ij} + h_{jk}} \left[\frac{y_k - y_j}{h_{jk}} - \frac{y_j - y_i}{h_{ij}} \right] \quad (2.3.1)$$

In the elastic range the bending moment is

$$M = -EI\left(\frac{d^2y}{dx^2}\right) = -Q\left(\frac{d^2y}{dx^2}\right) \quad (2.3.2)$$

where Q denotes the stiffness EI.

Substituting from Eq. (2.3.1) into Eq. (2.3.2) yields

$$M_j = -\frac{2Q_j}{(h_{ij} + h_{jk})} \left[\frac{y_i}{h_{ij}} - \left(\frac{1}{h_{ij}} + \frac{1}{h_{jk}}\right) y_j + \frac{y_k}{h_{jk}} \right] \quad (2.3.3)$$

Note that since finite differences are used, the curvature has in effect been lumped at the mass points. This is in agreement with the assumption of lumped-mass and lumped-flexibility. As long as $Mj \leq Mp$, the yield moment, Eq. (2.3.3), is valid. When $Mj > M_p$, the value of Mp must be substituted for Mj so that plastic behavior will be taken into account.

At the base end of the post, special consideration must be given to the rotational restraint offered by the base bolts. The base is idealized as shown in Figure 2.3.2(a). The base is assumed to be composed of rigid plates connected by a frictionless roller. The rotational resistance of the base is offered by the couple of the forces produced in the connection bolts. As shown in Figure 2.3.2(b), the couple is composed of the tensile force in the bolt T_2 and the bearing T_1 on the washer.

The strain in the tension bolt is

$$\varepsilon_2 = \frac{T_2}{A_2 E}$$

The strain in the washer is

$$\varepsilon_1 = \frac{T_1}{A_1 E} \qquad \text{where } T_1 = T_2 = \frac{M_1}{2C}$$

The curvature at the base is

$$\alpha = \frac{\varepsilon_1 + \varepsilon_2}{C} = \frac{1}{CE}\left(\frac{T_1}{A_1} + \frac{T_2}{A_2}\right)$$

$$\alpha = \frac{M_1}{2C^2E}\left(\frac{1}{A_1} + \frac{1}{A_2}\right) = \frac{M_1}{2C^2E}\left(\frac{A_1 + A_2}{A_1 A_2}\right)$$

The total curvature at mass point 1 is

$$\phi\ (1) = \frac{2}{h^2}\left[y(2) - y(1)\right] - \frac{M_1}{2C^2E}\left(\frac{A_1 + A_2}{A_1 A_2}\right)$$

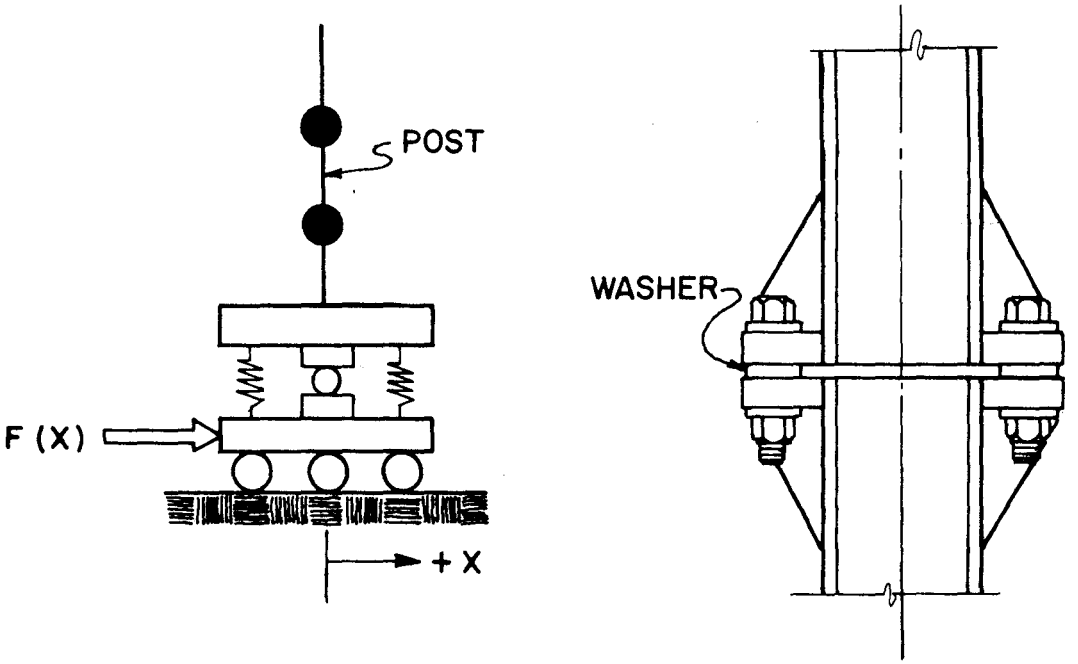

IDEALIZATION OF BASE

(a)

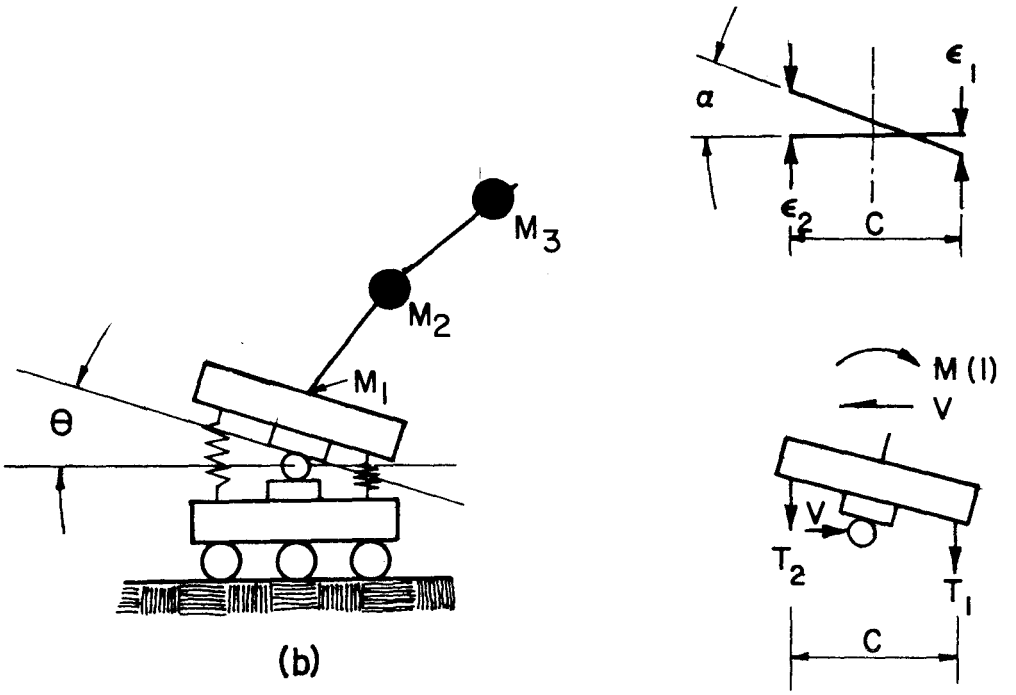

(b)

FIGURE 2.3.2 IDEALIZATION OF SUPPORT BASE

Since

$$M_1 = -\phi(1)\ EI,$$

$$M_1 = -EI_1 \left\{ \frac{2[y(2) - y(1)]}{h^2} - \frac{M_1}{2C^2E} \left(\frac{A_1 + A_2}{A_1 A_2} \right) \right\}$$

$$M_1 = -EI_1 \left\{ \frac{\frac{2}{h^2}[y(2) - y(1)]}{[1 + \frac{I_1}{2C^2} \left(\frac{A_1 + A_2}{A_1 A_2} \right)]} \right\} \qquad (2.3.4)$$

Eq. (2.3.4) reflects the effect of base flexibility on the moment at the base. If the moment at the base becomes plastic,

$$M_1 = M_p$$

2.4 Boundary Conditions on the Post

A study of the details of the behavior of a typical "break-away" post reveals that there are two distinct stages of bending during the response of the post to an impact force. These stages are introduced by the boundary conditions imposed on the post by the mechanical features of the "break-away" concept. Figure 2.4.1 illustrates these stages.

In stage I, the base rotation is restrained by the base bolts and its motion is resisted by friction between the slip planes. This stage lasts until the total deflection of the base exceeds the allowable slip. The allowable slip is taken to be the total depth of the slot in the base plate. At this time in the event, stage I ends and stage II begins.

Stage II is a free-end condition since no restraining devices or actions are present at the base. This stage lasts until the event is terminated when the post loses contact with the vehicle.

It should be noted that the "plastic hinge" can be activated in either stage depending upon the bending moment at the hinge line.

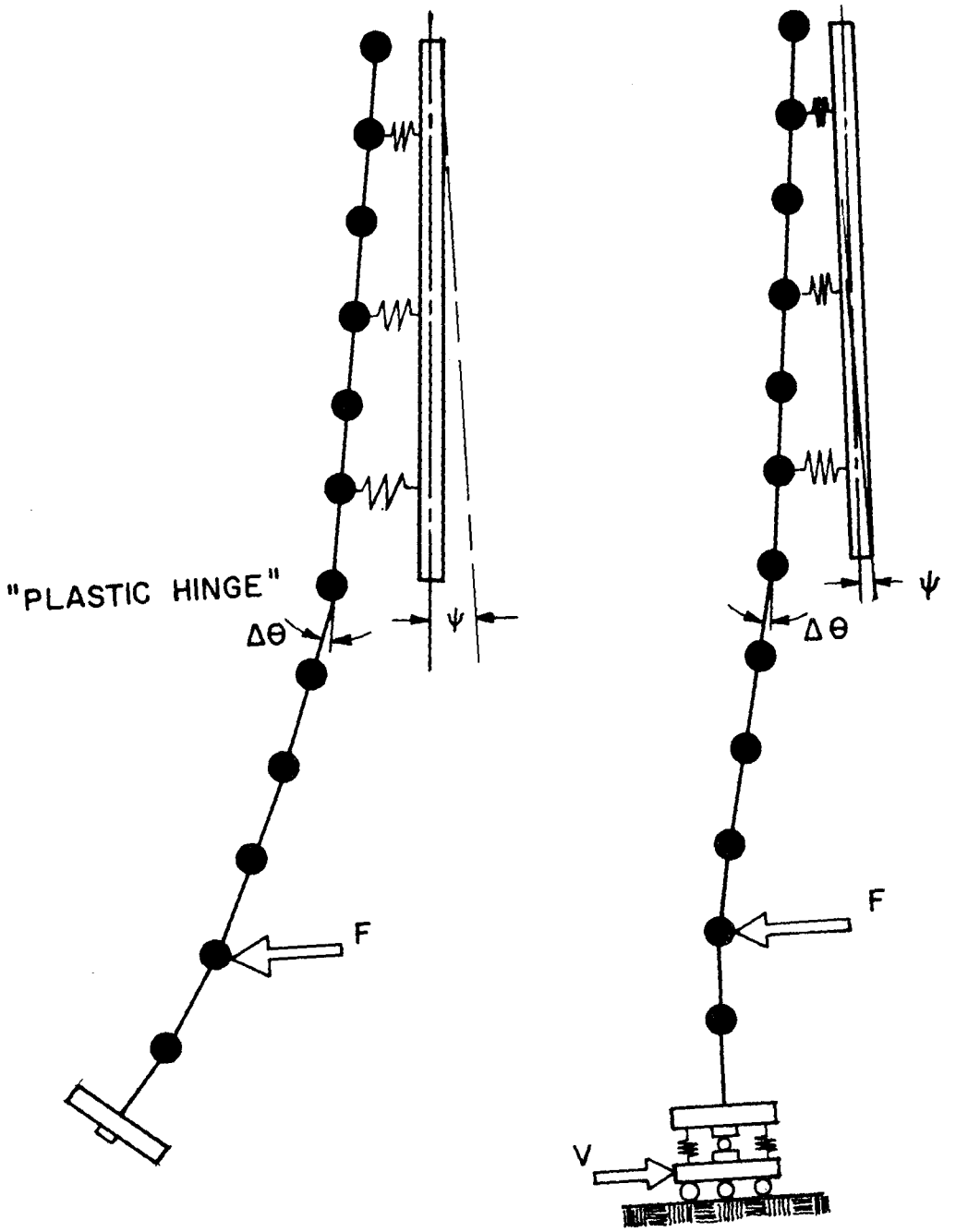

FIGURE 2.4.1 STAGES OF POST BENDING

The boundary conditions and matrix formulation for the restrained-end condition (stage I) are given in Figure 2.4.2. The displacement at M_1 is not zero for all time intervals, thus Eq. (2.2.8) can be satisfied by introducing a dummy mass point to the left of M_1. Consider the recursive relation for y_1 $(t+\Delta t)$ from Eq. (2.2.8).

$$y_1 (t + \Delta t) = \frac{\Delta t^2}{m_1} F_1 (t)$$

$$+ \frac{\Delta t^2}{h_o m_1} \left[a_{12'} M_{2'} - (a_{12'} + a_{12}) M_1 + a_{12} M_2 \right]$$

$$+ 2y_1 (t) - y_1 (t - \Delta t)$$

From boundary condition 1

$$V_{12'} = \frac{M_1 - M_{2'}}{h_{12'}} = 0$$

Therefore

$$M_1 = M_{2'}$$

By letting $h_{12'} = h_{12}$ and $a_{12'} = a_{12}$, one obtains

$$y_1 (t + \Delta t) = \frac{\Delta t^2}{m_1} F_1 (t) + \frac{\Delta t^2}{h_o m_1} (-a_{12} M_1 + a_{12} M_2)$$

$$+ 2y_1 (t) - y_1 (t - \Delta t)$$

From boundary condition 2

$$\theta_{12'} = \theta_{12}$$

Hence,

$$y_{2'} - y_1 = y_2 - y_1$$

or

$$y_{2'} = y_2$$

Boundary Conditions:

$$\left.\begin{array}{ll} (1) & V_{12'} = 0. \\ (2) & \theta_{12'} = \theta_{12} \end{array}\right\} \text{all } t$$

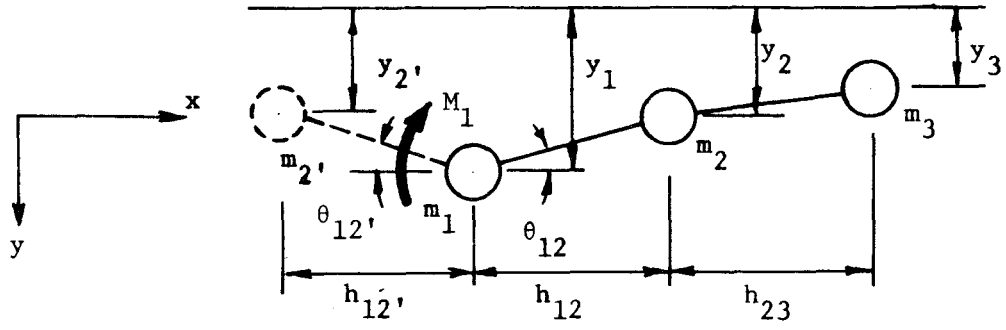

Since $y_{2'} = y_2$

$$M_1 = -\frac{2Q_1}{h_{12}^2}\left[\frac{y(2) - y(1)}{1 + \frac{I_1}{2c^2}\left(\frac{A_1 + A_2}{A_1 A_2}\right)}\right] \qquad \text{for } M_1 < M_p$$

$$\begin{bmatrix} y_1(t+\Delta t) \\ y_2(t+\Delta t) \\ y_3(t+\Delta t) \\ \vdots \end{bmatrix} = \Delta t^2 \begin{bmatrix} 1/m_1 & & & \\ & 1/m_2 & & \\ & & 1/m_3 & \\ & & & \ddots \end{bmatrix} \begin{bmatrix} F_1(t) \\ F_2(t) \\ F_3(t) \\ \vdots \end{bmatrix} + \frac{\Delta t^2}{h_o} \begin{bmatrix} 1/m_1 & & & \\ & 1/m_2 & & \\ & & 1/m_3 & \\ & & & \ddots \end{bmatrix} \begin{bmatrix} -a_{12} & a_{12} & 0 & & \\ a_{12} & -(a_{12}+a_{23}) & a_{23} & & \\ & a_{23} & -(a_{23}+a_{34}) & a_{34} & \\ & & \ddots & \ddots & \ddots \end{bmatrix} \begin{bmatrix} M_1 \\ M_2 \\ M_3 \\ \vdots \end{bmatrix}$$

$$+2 \begin{bmatrix} y_1(t) \\ y_2(t) \\ y_3(t) \\ \vdots \end{bmatrix} - \begin{bmatrix} y_1(t-\Delta t) \\ y_2(t-\Delta t) \\ y_3(t-\Delta t) \\ \vdots \end{bmatrix}$$

FIGURE 2.4.2 EQUATION (2.2.8) FOR RESTRAINED END CONDITION

The bending moment at M_1 is determined using this relation and Eq. (2.3.4).

The boundary conditions and matrix formulation for a free-end are given in Figure 2.4.3. Since the deflection at m_1 is not zero for all times, Eq. (2.2.8) can be satisfied only if a dummy mass point is introduced to the left of m_1. Consider the expansion of Eq. (2.2.8) for $y_1\ (t + \Delta t)$, one finds

$$y_1\ (t + \Delta t) = \frac{\Delta t^2}{m_1}\ F_1\ (t) - \frac{\Delta t^2}{m_1}\ a_{12'}M_{2'}$$

$$- (a_{12'} + a_{12})M_1 + a_{12}M_2$$

$$+ 2y_1\ (t) - y_1\ (t - \Delta t)$$

Since

$$V_{12'} = \frac{M_1 - M_{2'}}{h_{12'}} = 0, \text{ and } M_1 = 0, \text{ then } M_{2'} = 0$$

By letting $h_{12'} = h_{12}$, and $a_{12'} = a_{12}$, one finds

$$y_1\ (t + \Delta t) = \frac{\Delta t^2}{m_1} F_1(t) + \frac{\Delta t^2}{h_o m_1}\ a_{12}M_2 + 2y_1(t) - y_1(t - \Delta t)$$

The boundary condition at the top of the post is that of a free end.

2.5 Translational Response of the Sign Background

The background is lumped into n masses as shown in Figure 2.1.1. Eq. (2.2.8), the matrix formulation of the recursive equations for the translatory motion of the n mass points, is

$$y(t + \Delta t) = \Delta t^2[m]^{-1}\ \{F\}\ - \frac{\Delta t^2}{h_o}\ [m]^{-1}[a]\ \{M\}$$

$$+ 2\ \{y(t)\}\ - \{y(t - \Delta t)\}$$

Boundary Conditions:

(1) $M_1 = 0.$

(2) $V_{12'} = \dfrac{M_1 - M_2}{h_{12'}}$

and $M_1 = 0.$, then $M_{2'} = 0.$

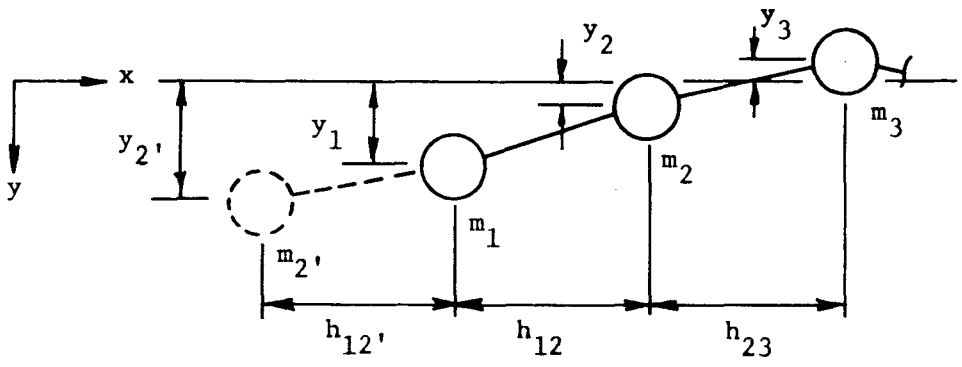

$$M_2 = -\frac{2Q_2}{(h_{12}+h_{23})}\left[\frac{y_1}{h_{12}} - \left(\frac{1}{h_{12}} + \frac{1}{h_{23}}\right) y_2 + \frac{y_3}{h_{23}}\right] \qquad \text{for } M_2 < M_p$$

$$\begin{bmatrix} y_1(t+\Delta t) \\ y_2(t+\Delta t) \\ y_3(t+\Delta t) \\ \vdots \end{bmatrix} = \Delta t^2 \begin{bmatrix} 1/m_1 & & & \\ & 1/m_2 & & \\ & & 1/m_3 & \\ & & & \ddots \end{bmatrix} \begin{bmatrix} F_1(t) \\ F_2(t) \\ F_3(t) \\ \vdots \end{bmatrix} - t^2 \begin{bmatrix} 1/m_1 & & & \\ & 1/m_2 & & \\ & & 1/m_3 & \\ & & & \ddots \end{bmatrix} \begin{bmatrix} R_1(y_1) \\ R_2(y_2) \\ R_3(y_3) \\ \vdots \end{bmatrix}$$

$$+ \frac{\Delta t^2}{h_o} \begin{bmatrix} 1/m_1 & & & \\ & 1/m_2 & & \\ & & 1/m_3 & \\ & & & \ddots \end{bmatrix} \begin{bmatrix} 0 & a_{12} & 0 & & \\ a_{12} & -(a_{12}+a_{23}) & a_{23} & & \\ & a_{23} & -(a_{23}+a_{34}) & a_{34} & \\ & & \ddots & \ddots & \ddots \end{bmatrix} \begin{bmatrix} 0 \\ M_2 \\ M_3 \\ \vdots \end{bmatrix} + 2 \begin{bmatrix} y_1(t) \\ y_2(t) \\ y_3(t) \\ \vdots \end{bmatrix} - \begin{bmatrix} y_1(t-\Delta t) \\ y_2(t-\Delta t) \\ y_3(t-\Delta t) \\ \vdots \end{bmatrix}$$

FIGURE 2.4.3 EQUATION (2.2.8) FOR FREE END

If the system is assumed to behave elastically, the bending moment at each mass point can be related to the curvature at the point by

$$M_j = -EI\left(\frac{d^2y}{dx^2}\right)_j \qquad (2.5.1)$$

Using Eq. (2.3.1) with $h_{ij} = h_{jk} = h$, one obtains the curvature in finite difference form

$$\left(\frac{d^2y}{dx^2}\right)_j = \frac{y_i - 2y_j + y_k}{h^2} \qquad (2.5.2)$$

Substituting from Eq. (2.5.2) into Eq. (2.5.1) yields

$$M_j = -\frac{EI}{h^2}(y_i - 2y_j + y_k)] \qquad (2.5.3)$$

Note that I, the moment of inertia of the background, is used as a constant in Eq. (2.5.3). This assumes that the rotation of the background is small and does not significantly influence the moment of inertia of the cross section.

Equation (2.2.8) and Eq. (2.5.3) can now be used as explained in Section 2.2 to solve for the translational response of the background.

The background is free at one end and assumed fixed to the opposite post (see Figure 2.1.1). The boundary conditions and Eq. (2.2.8) for the free end are shown in Figure 2.4.3. For the fixed end, Eq. (2.2.8) must be modified to reflect the following boundary conditions:

(1) $\theta_{n,\ n-1} = \theta_{n,\ n+1}$

(2) $Y_n = 0$

Condition (2) can be satisfied by setting the first row of all matrices in Eq. (2.2.8) equal to zero except {M}. Condition (1) is

satisfied by entering the value of M from Eq. (2.5.3) in the first row.

2.6 Derivation of Numerical Integration Technique for Torsional Response

The techniques used in the previous derivation for flexural response can be applied to the solution of the difference approximation of the differential equations of torsional motion. The rod is assumed to behave elastically and is acted upon by time-dependent torques T_1 (t), T_2 (t), ...T_n (t). The continuous rod can be discretized by breaking it into a series of lumped masses connected by elastic torsional springs as shown in Figure 2.6.1. The mass moment of inertia (J) of the cross section with respect to the axis of rotation is averaged over the interval h and is assumed concentrated at the mass point. The torsional spring represents the average torsional stiffness (λ) over the interval.

Following the same steps used in the previous developments, the recursive expression for the numerical integration for the torsional motion is

$$\{\psi\ (t + \Delta t)\} = \Delta t^2[J]^{-1}\ \{T\ (t)\} + \lambda \Delta t^2[J]^{-1}\{\beta\ (t)\} + 2\{\psi\ (t)\} - \{\psi\ (t + \Delta t)\} \qquad (2.6.1)$$

where $\psi \equiv$ rotational displacement of each mass point.

In Eq. 2.6.1

$$[J] = \begin{bmatrix} \cdot & & & & \\ & \cdot & & & \\ & & J_i & & \\ & & & J_j & \\ & & & & J_k \\ & & & & & \cdot \\ & & & & & & \cdot \end{bmatrix} \qquad \{\psi\} = \begin{Bmatrix} \cdot \\ \cdot \\ \psi_i \\ \psi_j \\ \psi_k \\ \cdot \\ \cdot \end{Bmatrix}$$

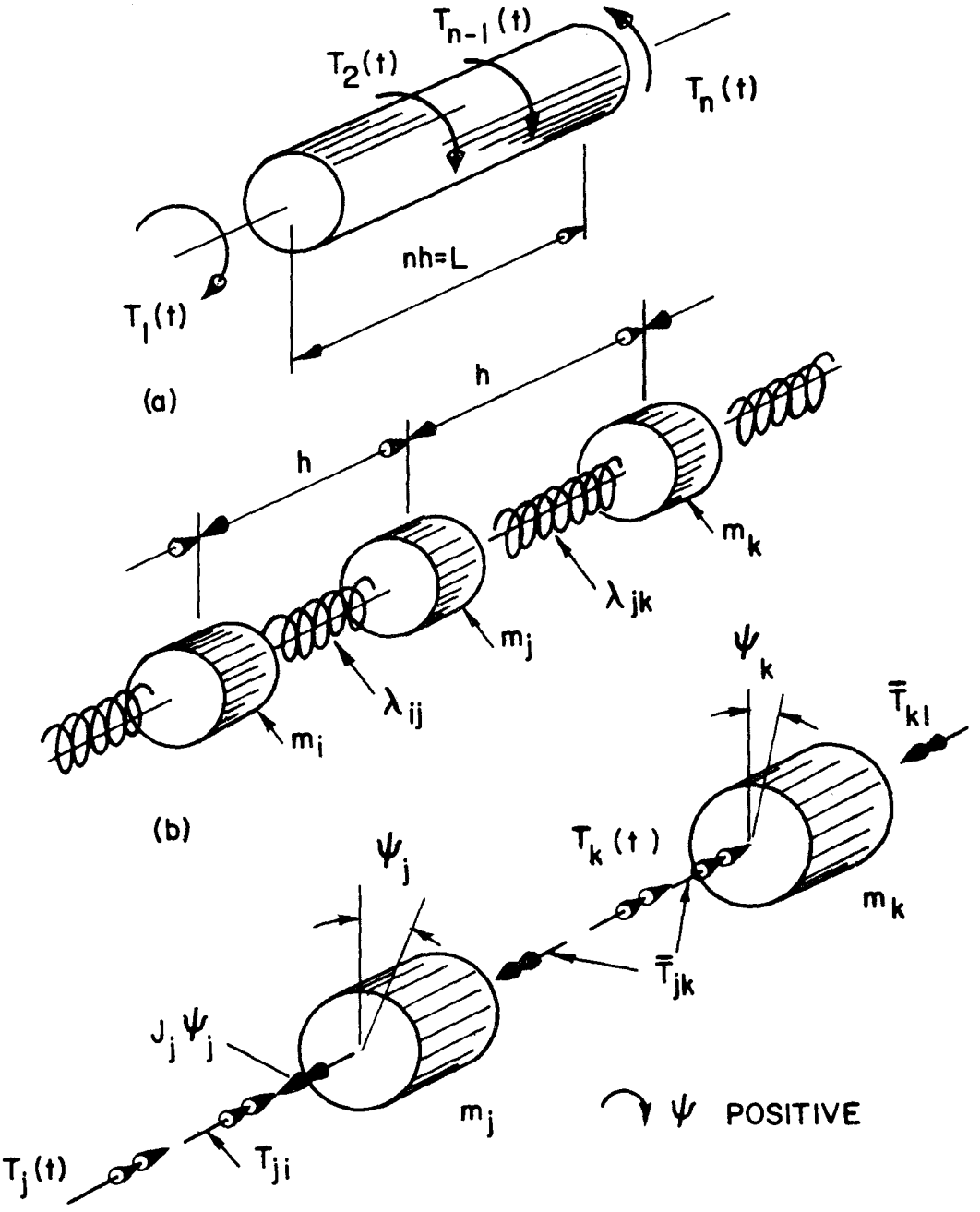

FIGURE 2.6.1 GENERAL TORSIONAL MODEL

$$\{\beta\} = \begin{Bmatrix} \cdots \\ \cdots \\ \psi_h - 2\psi_i + \psi_j \\ \psi_i - 2\psi_j + \psi_k \\ \cdots \\ \cdots \end{Bmatrix} \qquad \{T\ (t)\} = \begin{Bmatrix} T_i\ (t) \\ T_j\ (t) \\ T_k\ (t) \\ \cdot \\ \cdot \end{Bmatrix}$$

Boundary conditions on the sign background. Reference to Figure 2.2.1 will establish the boundary conditions on the sign background in the torsional mode. In torsion, the background is free at one end and assumed fixed at the other as shown in Figure 2.6.2. For the free-end, one boundary condition is

$$T_{12'} = 0$$

In order to satisfy Eq. (2.6.1) for m_1, a dummy mass ($m_{2'}$) must be placed to the left of m_1 as shown in Figure 2.6.2(a). From Eq. (2.6.1),

$$\bar{T}_{12'} = (\psi_{2'} - \psi_1)\lambda_{12'} = 0$$

Therefore, $\psi_{2'} = \psi_1$, and the matrix $\{\beta\}$ of Eq. (2.6.1) is modified as shown in Figure 2.6.2

For the fixed end, the boundary conditions are shown in Figure 2.6.2(b). In order to satisfy boundary condition 2, the dummy mass (m_n) may be visualized to the right of m_{n+1}. Using the relation

$$\bar{T}_{ji} = (\psi_i - \psi_j)\lambda_{ij}$$

and

$$\bar{T}_{jk} = (\psi_j - \psi_k)\lambda_{jk}$$

then

$$\psi_n - \psi_{n+1} = \psi_{n'} - \psi_{n+1}$$

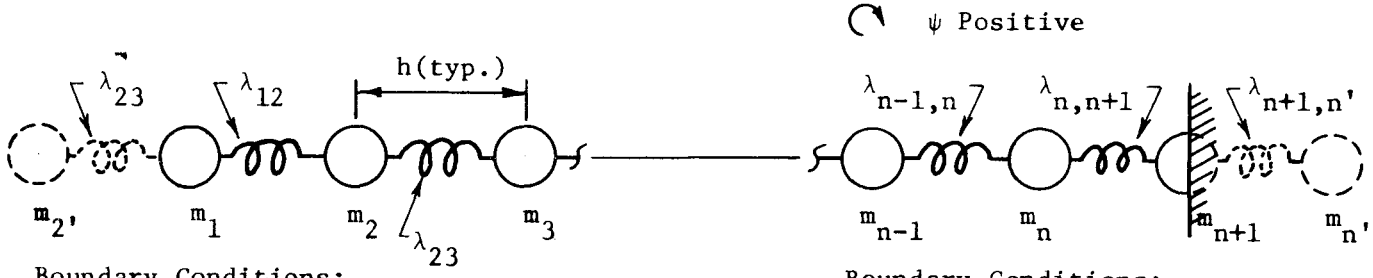

Boundary Conditions:

(1) $T_{12'} = 0.$

(a) Free End

Boundary Conditions:

(1) $\psi_{n+1} = 0.$

(2) $T_{n+1,n} = -T_{n+1,n'}$

(b) Fixed End

$$\begin{bmatrix} \psi_1(t+\Delta t) \\ \psi_2(t+\Delta t) \\ \psi_3(t+\Delta t) \\ \vdots \\ \psi_n(t+\Delta t) \\ 0. \end{bmatrix} = \Delta t^2 \begin{bmatrix} 1/J_1 & & & & & \\ & 1/J_2 & & & & \\ & & 1/J_3 & & & \\ & & & \ddots & & \\ & & & & 1/J_n & \\ & & & & & 1/J_{n+1} \end{bmatrix} \begin{bmatrix} T_1(t) \\ T_2(t) \\ T_3(t) \\ \vdots \\ T_n(t) \\ 0. \end{bmatrix} = \lambda \Delta t^2 \begin{bmatrix} 1/J_1 & & & & & \\ & 1/J_2 & & & & \\ & & 1/J_3 & & & \\ & & & \ddots & & \\ & & & & 1/J_n & \\ & & & & & 1/J_{n+1} \end{bmatrix} \begin{bmatrix} 0-\psi_1+\psi_2 \\ \psi_1-2\psi_2+\psi_3 \\ \psi_2-2\psi_3+\psi_4 \\ \vdots \\ \psi_{n-1}-2\psi_n \\ 2\psi_n \\ 0. \end{bmatrix} + 2 \begin{bmatrix} \psi_1(t) \\ \psi_2(t) \\ \psi_3(t) \\ \vdots \\ \psi_n(t) \\ 0. \end{bmatrix} + \begin{bmatrix} \psi_1(t-\Delta t) \\ \psi_2(t-\Delta t) \\ \psi_3(t-\Delta t) \\ \vdots \\ \psi_n(t-\Delta t) \\ 0. \end{bmatrix}$$

FIGURE 2.6.2 EQUATION (2.6.1) FOR TORSIONAL RESPONSE OF SIGN BACKGROUND

but from boundary condition 1

$$\psi_{n+1} = 0$$

therefore

$$\psi_n = \psi_{n'}$$

The complete matrix formulation for the torsional response of the background is shown in Figure 2.6.2.

2.7 Formulation of Technique to Include Sign Background Restraint

Figure 2.7.1 shows the idealization of the post-sign background connection. The structural connection is idealized as a linear spring having a stiffness that depends on the particular type of connection employed. The static position of the background and post are chosen as the reference datums for the displacements. Positive deflections of the post masses and background element are to the right.

At some time during the response to an impact, the post masses and background element will assume the positions shown in Figure 2.7.1(b). The various springs will be compressed or extended because of the relative positions of the masses and background elements. Consider a typical spring at n with stiffness K_n. The spring deformation is

$$\delta_h = y_h - Y_h$$

The spring will be in compression if δ_h is positive and in tension if δ_n is negative.

The force exerted by the spring on the mass is

$$F_h(t) = K_h (y_h - Y_h) \qquad (2.7.1)$$

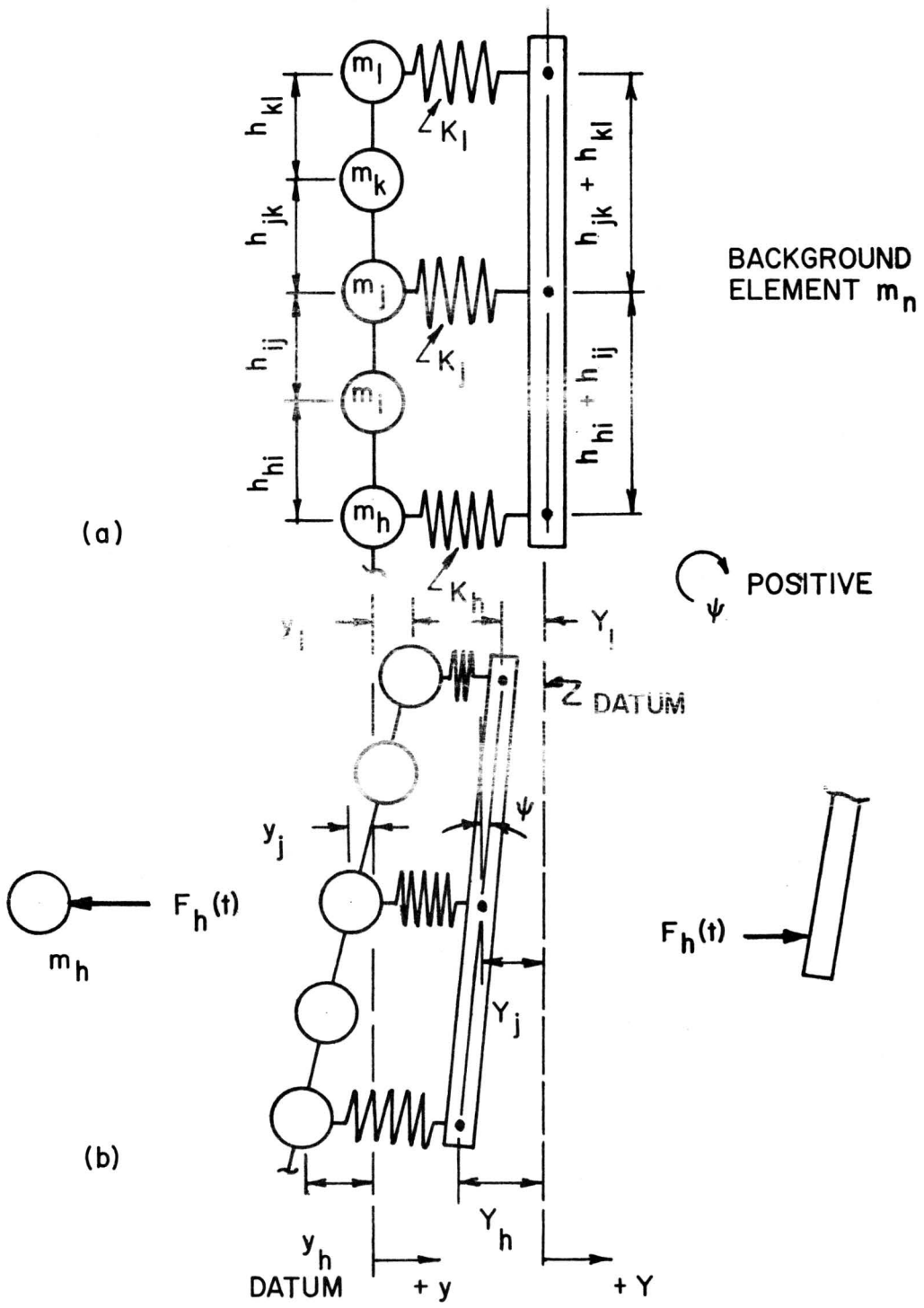

FIGURE 2.7.1 POST-SIGN BACKGROUND CONNECTION

assuming positive forces act to the right. If the connection springs have different stiffnesses in tension and compression, the value of K_h can be changed accordingly in Equation (2.7.1) depending on the algebraic sign of δ_h. The forces, F_h (t), F_j (t), and F_1 (t) are forcing functions, since they vary with time, and hence are elements of the column matrix of forcing functions {F (t)} in Equation (2.2.8).

An equal and opposite force acts on the background. The moment of these forces about point 0 produce a torque,

$$T_n\ (t) = F_h\ (t)(h_{hi} + h_{ij}) + F_1\ (t)(h_{jk} + h_{kl}) \qquad (2.7.2)$$

which is positive when clockwise. This torque is an element of {T (t)} in Eq. (2.6.1).

Equations (2.7.1) and (2.7.2) provide a means for coupling the response of the background and post.

2.8 Vehicle Model

To this stage in the development of the "break-away" sign model, attention has been focused entirely on the post and sign background. The concept of the vehicle model and the techniques that will be employed to include it in the overall problem will now be considered.

An automobile is a complex structural system composed of various plate, shell, column and beam structural elements. All these elements are combined to give a highly redundant multidegree-of-freedom vibrational system. Under impact forces, these elements are capable of absorbing various amounts of energy. The sum of all the incremental energies of the component parts equals the total energy absorbed by the vehicle during an impact. The model vehicle is assumed to be a single degree-

of-freedom system. It is represented by a rigid mass and massless springs as shown in Figure 2.8.1. The rigid mass and its velocity account for the momentum of the vehicle and the force-deformation characteristics of the springs provide for the energy absorbed by the vehicle during impact. As long as the springs are capable of absorbing an amount of energy equivalent to that of an actual vehicle, it is considered that satisfactory results can be obtained with this simple simulation. The data used for the force-deformation input was derived from full scale fixed barrier tests utilizing a barrier presenting the same frontal impact area as a sign support post.

Simulation of vehicle crash characteristics. The force-deformation characteristics of a vehicle are simulated using the model shown in Figure 2.8.1. For illustration, the vehicle is assumed to have three springs. Each spring comes into play when the vehicle has deformed a specified amount. When the total relative deformation between the post and vehicle is less than C_1 only spring K_1 is deformed and the resultant force acts on the post at mass m(i) as shown in Figure 2.8.1(c). When the relative deformation is between C_1 and C_2, both spring K_1 and K_2 are compressed, the resultant spring force F_1 (from K_1) acts on post mass m(i) and F_2 (from K_2) acts on post mass m(j) as shown in Figure 2.8.1(d). Finally, when the relative deformation is larger than $C_1 + C_2$ all three springs are compressed and the spring forces act on all three masses in contact. This action simulates the progressive crushing of the vehicle as the post penetrates into the vehicle. In this approach, an attempt is made to simulate the movement of the center of pressure up the post as the penetration progresses. It is recognized

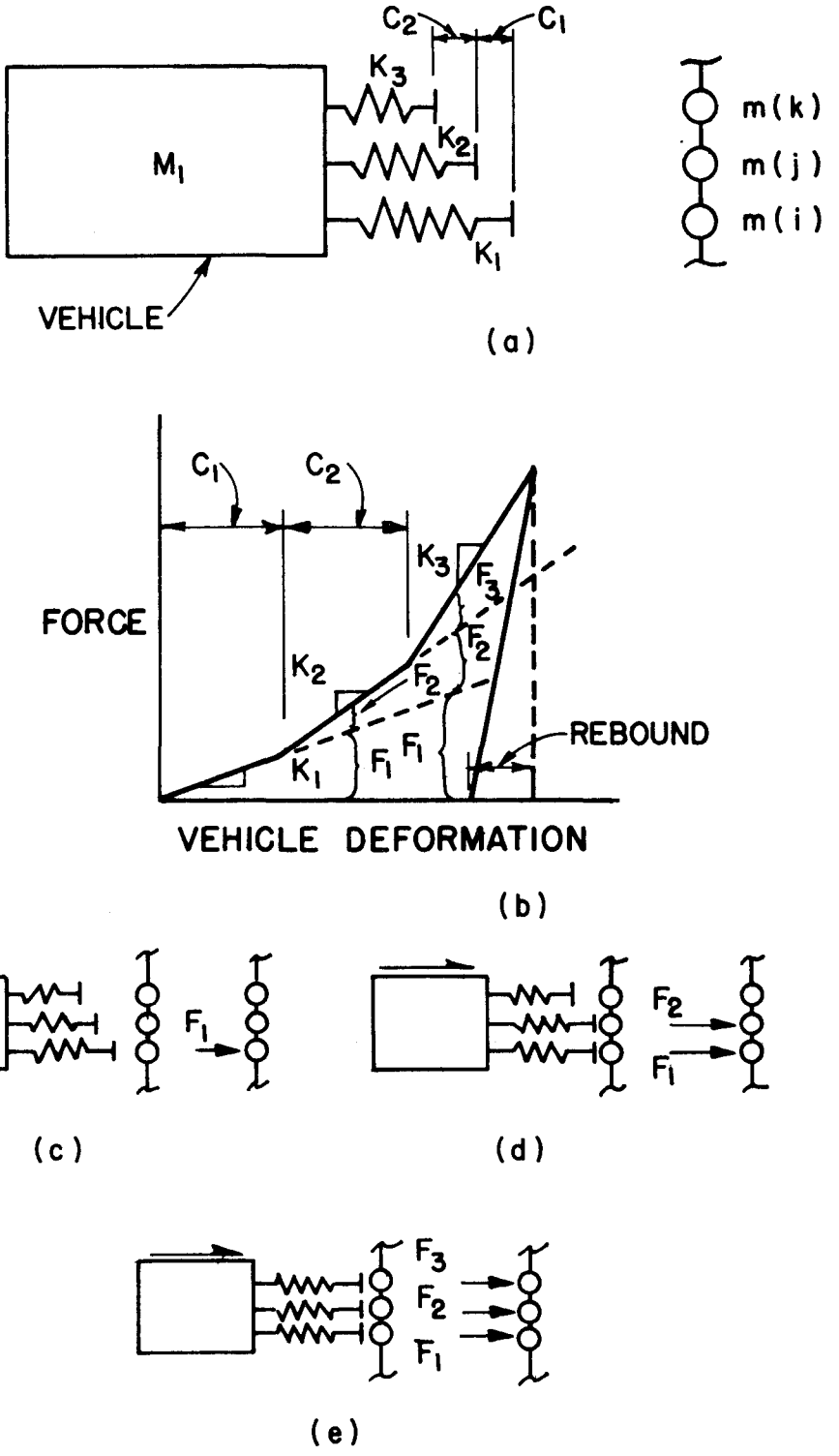

FIGURE 2.8.1 VEHICLE SIMULATION

that the distribution of the spring forces on the post are determined by the assumed action of the springs. In order to effect a gradual release of force as the springs release (when the relative deformation reverses), a restitution function has been built into the routine.

In order to present the equations necessary to describe the motion of the vehicle, consider the single mass and spring shown in Figure 2.8.2(a). Figure 2.8.2(b) shows the initial conditions at the instant of impact of the simulated vehicle and a representative mass of the post (m_j). At this instant, m_j is undeflected and at rest. The vehicle spring is uncompressed and the vehicle mass m_1 has an initial velocity $\dot{X}_o$.

At some time t after initial impact, the mass (m_j) will have a deformation x_j (t). The vehicle mass, by virtue of its motion, will have a displacement X_1 (t). Displacements are measured from some convenient datum as shown in Figure 2.8.2(c). The datum for the post mass m_j is chosen as the unstressed neutral line of the post. If $|X_1\ (t)|$ is assumed larger than $|x_j\ (t)|$, the compression in the spring is

$$\Delta X = |X_1\ (t)| - |x_j\ (t)|$$

If the displacements are positive to the right in Figure 2.8.2(c)

$$\Delta X\ (t) = -\ [X_1\ (t) - x_j\ (t)]$$

The force in the spring is

$$F(X_1,t) = -[K_j(X)]\ [\Delta X(t)] \qquad (2.8.1)$$

The forces acting on the vehicle mass (m_1) are the spring force $F(X_1,t)$ and the inertia of the mass itself. The free body of M_1 is shown in Figure 2.8.2(d). Summation of the forces yields

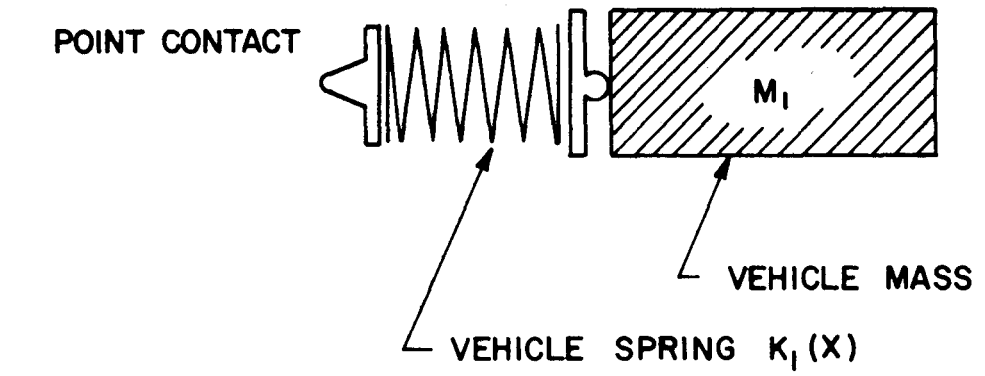

(a) SINGLE DEGREE-OF-FREEDOM VEHICLE MODEL

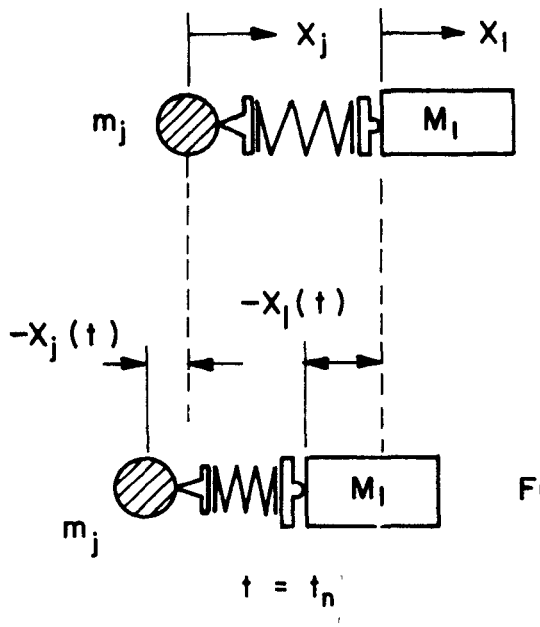

INITIAL CONDITIONS:

$X_1(0)=0.$, $\dot{X}_1(0)=\dot{X}_0$

$\dot{X}_j(0)=0.$, $\ddot{X}_j(0)=0.$

(b) INITIAL CONDITIONS

(c) DURING IMPACT

(d) VEHICLE FREE BODY

FIGURE 2.8.2 IDEALIZED VEHICLE

$$M_1 \ddot{X}_1 (t) = F(X_1, t)$$

This differential equation can be integrated using a forward step integration in time procedure.

The displacement of M_1 at any time is

$$X_1 (t + \Delta t) = X_1 (t) + \Delta t \dot{X}_1 (t) \qquad (2.8.2)$$

The acceleration using Eq. (2.8.1) is

$$\ddot{X}_1 (t + \Delta t) = - \frac{F (t + \Delta t)}{M_1}$$

$$= - \frac{K[X_1 (t + \Delta t) - x_j (t + \Delta t)]}{M_1} \qquad (2.8.3)$$

The velocity is

$$\dot{X}_1 (t + \Delta t) = \dot{X}_1 (t) + \Delta t \ddot{X}_1 (t + \Delta t) \qquad (2.8.4)$$

The forward step method proceeds in the order of these equations. The displacement $x_j (t + \Delta t)$ is found from Eq. (2.2.8) using the force F (t) from Eq. (2.8.1), as the forcing function for that time.

Passenger simulation. The response of a human passenger to a collision is difficult to simulate. In order to obtain an approximation, a rough simulation was attempted. The passenger is simulated by a one degree-of-freedom spring and mass system attached to the mass simulating the vehicle. Figure 2.8.3(a) shows the model configuration. The passenger mass is assumed to be restrained by a linear spring representing a seat belt.

The reference axis for displacements of the vehicle and passenger mass is the same as used in the development of the foregoing relations for the vehicle response. Consider Figure 2.8.3(b) and the free bodies

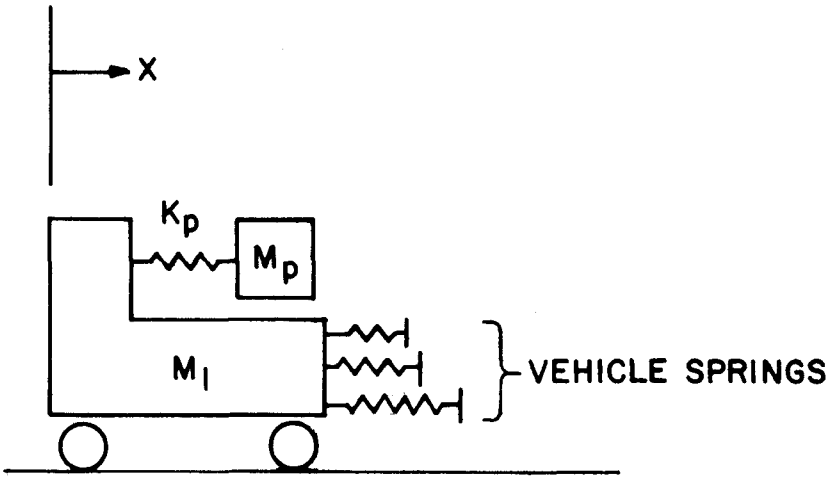

(a) VEHICLE - PASSENGER SIMULATION

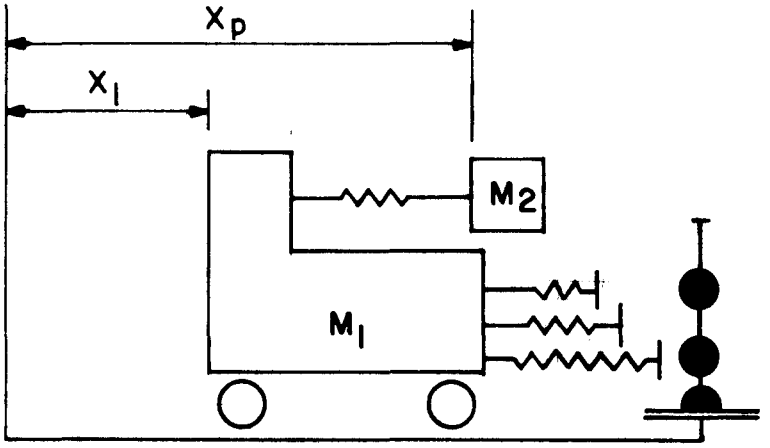

(b) VEHICLE AND PASSENGER DURING COLLISION EVENT

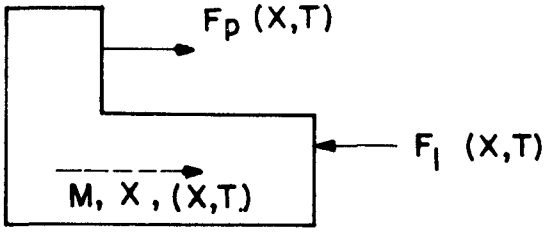

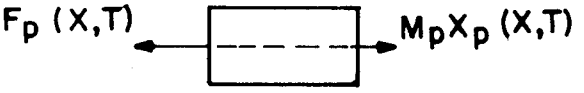

(c) VEHICLE FREE BODY (d) PASSENGER FREE BODY

FIGURE 2.8.3 PASSENGER SIMULATION

shown in parts (c) and (d). Once the vehicle makes contact with the support post the contact force is expressed by Eq. (2.8.1) and the displacement by Eq. (2.8.2). The force in the seat belt spring (K_p) is

$$F_p(x,t) = -K_p[X_p(t) - X_1(t)] \qquad (2.8.5)$$

where $X_p(t)$ and $X_1(t)$ are the respective displacements of the two masses. The displacement $X_p(t)$ is expressed as

$$X_p(t+\Delta t) = X_p(t) + \Delta t\, \dot{X}_p(t) \qquad (2.8.6)$$

where $\dot{X}_p(t)$ is the passenger velocity relative to the reference axis. The acceleration of the passenger mass can be determined by summing forces in Figure 2.8.3(d)

$$M_p \ddot{X}_p(t) = F_p(x,t)$$

$$\ddot{X}_p(t) = \frac{F_p(x,t)}{M_p}$$

Substituting from Eq. (2.8.5)

$$\ddot{X}_p(t) = -\frac{K_p[X_p(t) - X_1(t)]}{M_p} \qquad (2.8.7)$$

The velocity can be expressed as

$$\dot{X}_p(t+\Delta t) = \dot{X}_p(t) + \Delta t\, \ddot{X}_p(t+\Delta t) \qquad (2.8.8)$$

The numerical integration proceeds in the same order as previously described for the vehicle response.

2.9 The "Plastic Hinge"

Figure 2.9.1 shows the "plastic hinge" and its behavior under positive and negative bending moment. In this illustration positive moment tends to initiate slipping in the fuse plate. It should be noted

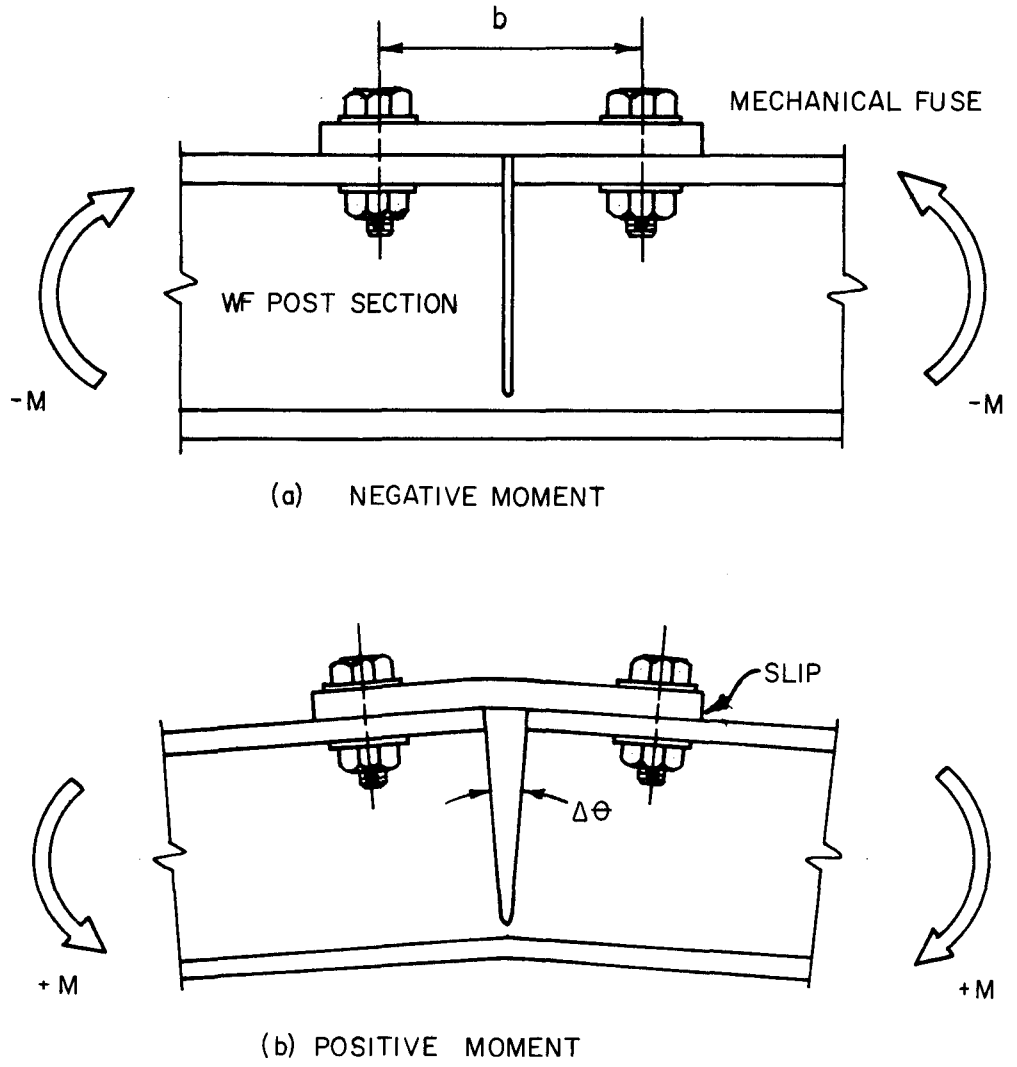

FIGURE 2.9.1 THE "PLASTIC HINGE"

that under the action of a negative moment the fuse plate is forced to transmit compression across the flanges of the post. In this mode the integrity of the post section is maintained and the moment can be obtained using Eq. (2.3.3). Since the flange of the post is physically separated, the value of the moment of inertia must be calculated using only the areas of the fuse plate and the bottom flange. Because the fuse plate is of ductile steel, the moment-curvature relationship can be idealized as elastic-plastic. The moment can be calculated by

$$M_j = - \frac{2Q_j}{(h_{ij} + h_{jk})} \left[\frac{y_i}{h_{ij}} - \left(\frac{1}{h_{ij}} + \frac{1}{h_{jk}} \right) y_j + \frac{y_k}{h_{jk}} \right] \qquad (2.9.1)$$

in the elastic range and

$$M_j = - M_p$$

in the plastic range.

Under the action of a positive moment, as shown in Figure 2.9.1(b), the beam tends to pivot about the compression flange as the fuse plate slips. This rotation is impeded by the action of the slip plate. The resisting force on the slip plane is a function of the normal force acting on the plane and the friction coefficient of the faying surfaces. Laboratory tests were conducted (see Chapter 4 of Part III) to determine the force slip characteristics of several typical "plastic hinge" fuse plates. These tests indicated that the resistance to movement was a function of the amount of slip, see Figure 2.9.2(a). If N' denotes the tension in the bolts, the resistance, F, can be expressed as

$$F = mnN'f(s) \qquad (2.9.2)$$

where f(s) is the coefficient of friction on the faying surfaces and n is the number of faying surfaces.

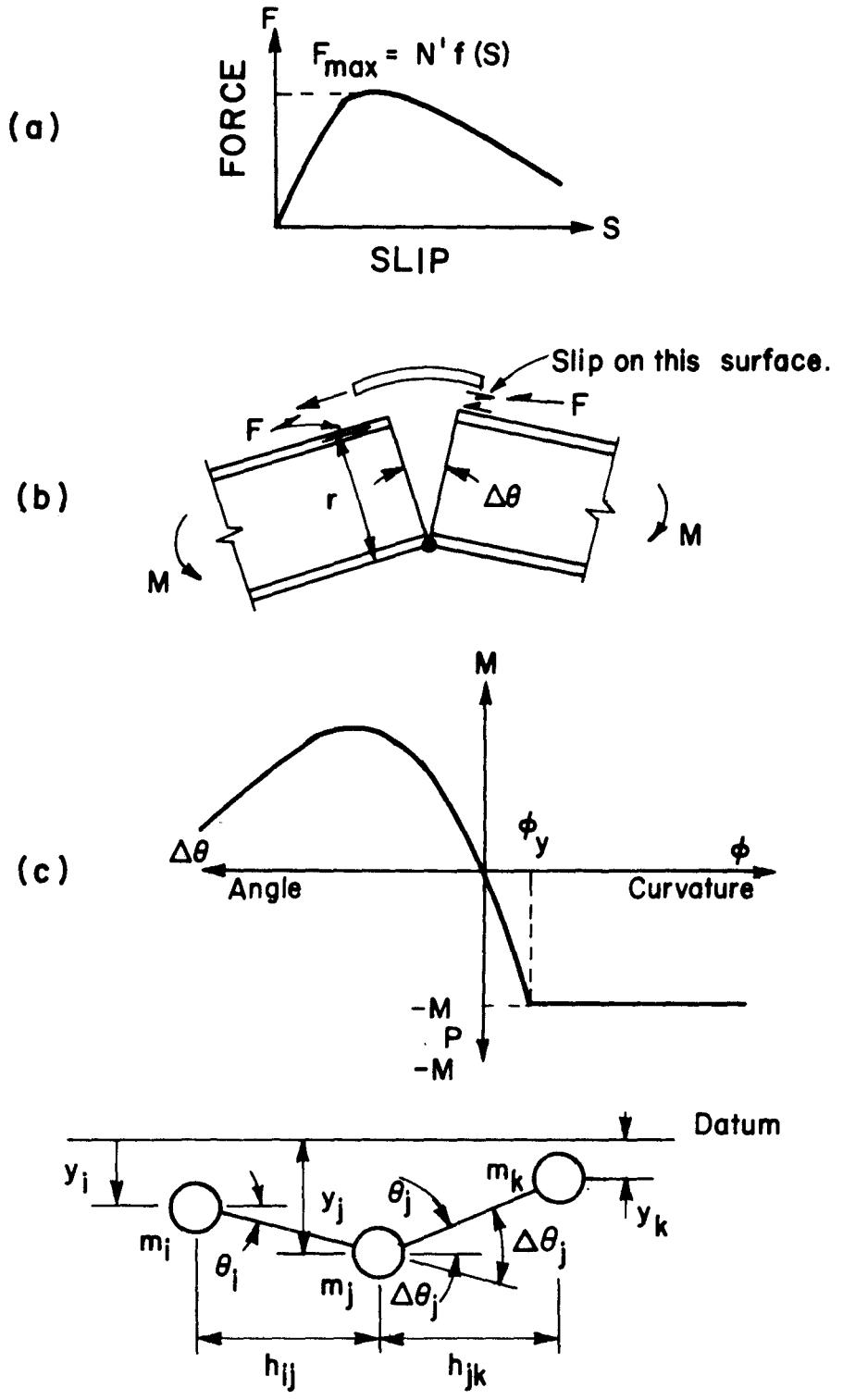

FIGURE 2.9.2 "PLASTIC HINGE" BEHAVIOR

Referring to Figure 2.9.2(b), the plastic hinge bending moment is

$$M = Fr$$

where r is the distance from the apparent center of rotation to the resultant of the slip force F. Since F is a function of N' and f(s) the moment can be expressed as

$$M = mnN'f(s)r \tag{2.9.3}$$

The friction coefficient, f(s), depends upon the value of slip. The slip at any time during the event is

$$s = r\Delta\theta \tag{2.9.4}$$

where $\Delta\theta$ is the relative rotation of the joint. Referring to Figure 2.9.2(c), the relative rotation for a typical mass point, m_j, is

$$\Delta\theta j = \theta i - \theta j \tag{2.9.5}$$

where

$$\theta i = \frac{Y_j - Y_i}{h_{ij}} \tag{2.9.6}$$

$$\theta_j = \frac{Y_k - Y_j}{h_{jk}} \tag{2.9.7}$$

Substitution from Equation (2.9.6) and Equation (2.9.7) into Equation (2.9.5) yields,

$$\Delta\theta_j = \frac{Y_j - Y_i}{h_{ij}} - \frac{Y_k - Y_j}{h_{jk}} \tag{2.9.8}$$

With the use of Equation (2.9.3), Equation (2.9.4), and Equation (2.9.8), an expression for the moment-relative rotation of the "plastic hinge" can be developed. This relation can be used in place of Equation (2.9.1) when the "plastic hinge" is subjected to a positive moment (moment tending to cause fuse plate to slip).

2.10 The Slip Base

The slip force, or friction force, between the two halves of the "break-away" base is dependent upon the normal force, or clamping force, of the base bolts on the faying surfaces, and the friction factor. The base is also subjected to bending moments introduced by wind loads and collision forces. The base must be designed so that it will be capable of resisting wind induced bending and shear and still not offer excessive resistance to slip under collision loads.

Figure 2.10.1 shows a "break-away" sign support post subject to a general set of forces which are typical of those present under a collision condition. Figure 2.10.1(a) is a free body of the base showing the forces present under the preload in the bolts only. Note that since there are four bolts in the base, the resultant compressive forces at front and rear are 2N'; N' is the tension in one bolt due to the initial torqueing. When loading is applied to the base, the bolts are required to carry additional load as shown in Figure 2.10.1(b). The bolt forces induced by the bending moment are

$$T = \frac{M}{2C}$$

Where T is the force in one bolt produced by the couple only. Since the bolts are preloaded, the load in the bolt on the tension side will not increase appreciably until the preload has been exceeded. The total normal force on the faying surfaces under this condition is shown in Figure 2.10.1(b).

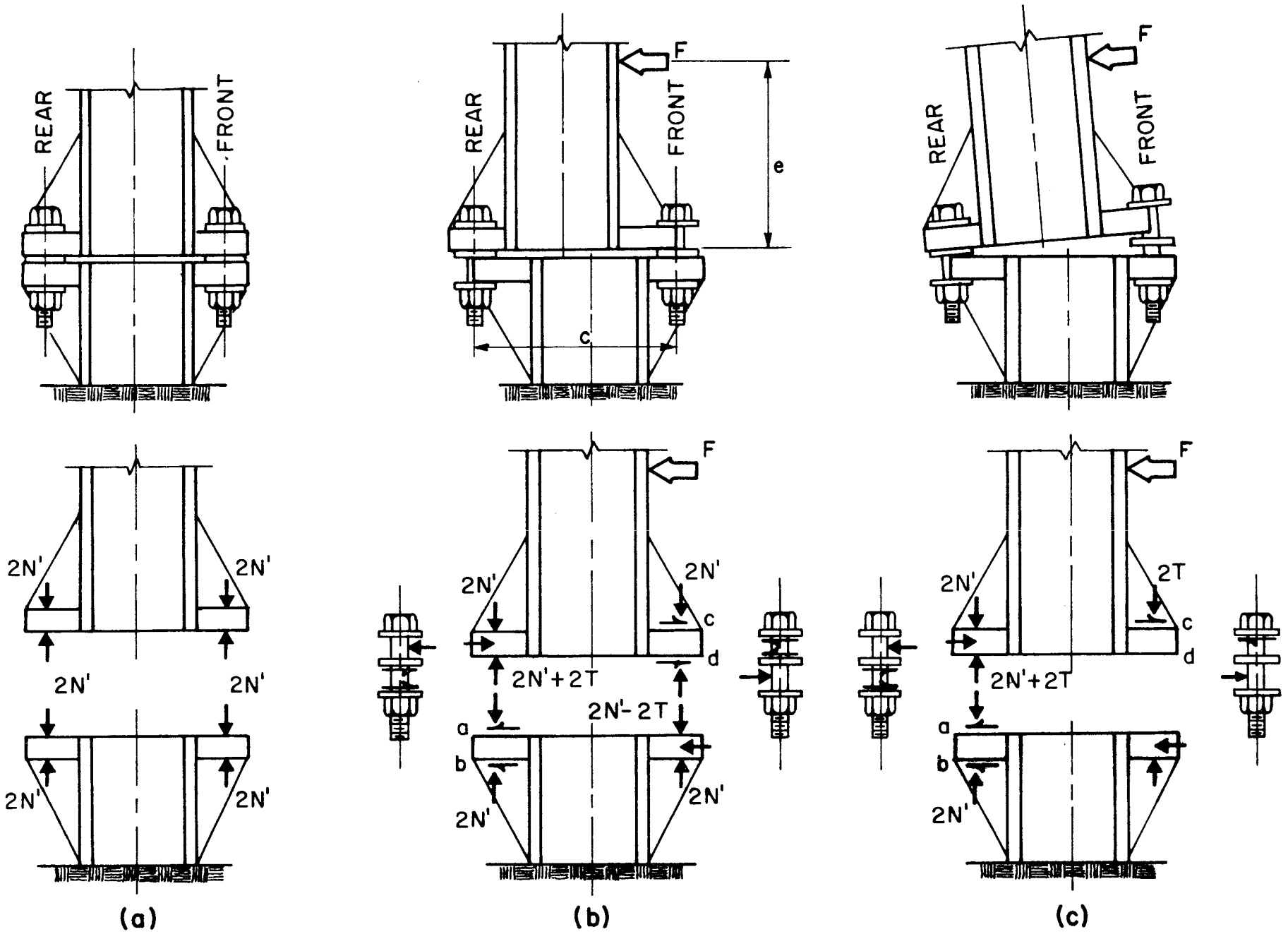

FIGURE 2.10.1 "BREAK-AWAY" SUPPORT BASE PLATE

Surfaces	Normal Force	No. of Faying Surfaces
a	2N' + 2T	2
b	2N'	2
c	2N'	2
d	2N' - 2T	2
Total	8N'	8

When the load in the tension bolt exceeds the preload, the joint will open, as shown in Figure 2.10.1(c), and the faying surface of the front bolt will be lost. Under this condition, the total normal force is

Surface	Normal Force	No. of Faying Surfaces
a	2N' + 2T	2
b	2N'	2
c	2T	2
d	0	-
Total	4N' + 4T	6

The resistance of the base to movement is a function of several variables, the type and number of faying surfaces, the normal forces on the surfaces, and the initial bolt tension. Laboratory tests were conducted to determine representative values for the coefficient of friction on the faying surfaces (see Part III, Chapter 2). It was found that the coefficient of friction varied with the slip. Two types of tests were conducted, one series for the case of a pure shear loading on the base (no external moment), and a series of shear with external moment.

By expressing the coefficient of friction as a function of slip, the following relation can be developed for the resistance of the base to applied forces:

$$F = mnN'f(s) \quad \text{for } \frac{M}{2C} \leq N' \qquad (2.10.1)$$

$$F = \frac{mn}{2}\left(N' + \frac{M}{2C}\right)f(s) \text{ for } \frac{M}{2C} \geq N' \qquad (2.10.2)$$

where m ≡ number of bolts crossing the slip plane

n ≡ number of faying surfaces per bolt

N' ≡ tension in bolt due to preload

f(s) ≡ coefficient of friction or a function of base slip

M ≡ external moment acting on the base

C ≡ distance between bolt lines in the plane of the load

CHAPTER 3

CORRELATION WITH TEST RESULTS

3.1 Introduction

Results from two full-scale tests were used to obtain quantitative correlations with the mathematical model. These tests, designated as Tests No. 41 and No. 446-5, involved controlled collisions with a sign support with the configuration shown in Figure 3.1.1 Both tests used a 1955 Ford sedan travelling at an initial velocity of approximately 40 mph. Slotted steel fuse plates were used in both tests. Instrumentation for the tests employed: (1) a displacement transducer on the slip-base, (2) strain gages on the post and fuse plate, (3) an accelerometer in the vehicle, and (4) high speed motion pictures of the event. The data from the above transducers, excepting the motion pictures, were recorded simultaneously on a continuous trace recording oscillograph.

The data from Test No. 41 have been analyzed and reported by Olson.[3] The results of Test No. 446-5 are presented in Chapters 7 and 8 of Part III.

3.2 Philosophy of the Correlation

In order to use the model, it is necessary to have a knowledge of the physical properties of the various parameters that are input information to the program, i.e., the characteristics of the slip-base, "plastic hinge", etc. Information on the parameters was obtained by laboratory tests of the respective component parts. The

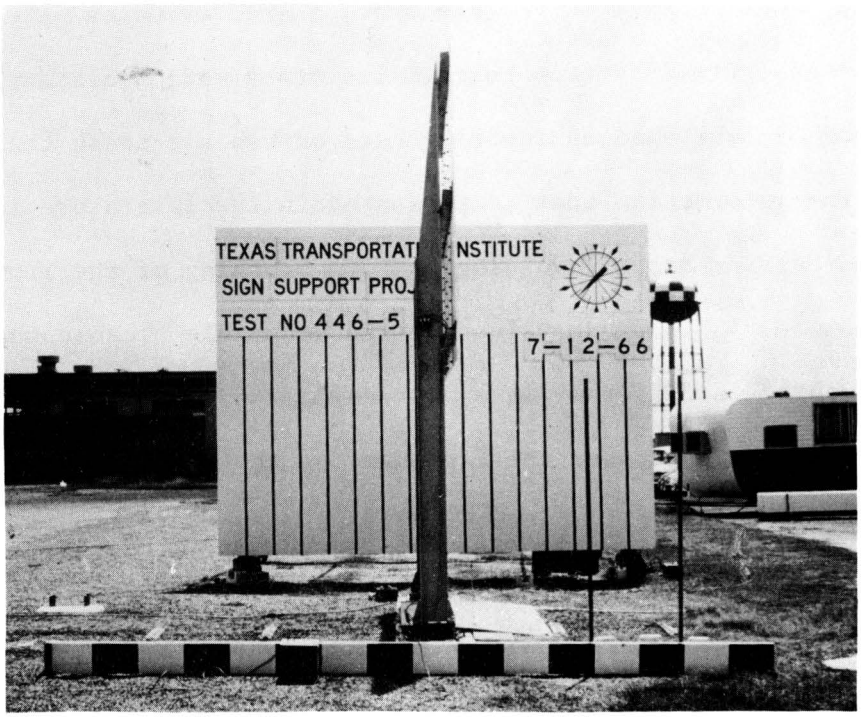

FIGURE 3.1.1-POST CONFIGURATION FOR TESTS 41 & 446-5

tests were conducted under static loading conditions and the results used in the model. Data on vehicle crash characteristics were obtained from full-scale fixed barrier tests. The tests were necessary because of the lack of published engineering data on vehicle crash characteristics. The information that is presented in the literature is derived from fixed barrier tests involving uniform crushing of the front end of the vehicle.[4,5,6] These values are unacceptable because the nature of the crushing is different in a post collision. In the post collision, the post penetrates the front end of the vehicle and the full energy absorption capacity of the front end is not utilized.

3.3 Simulation Input Values

The slip base. The slip base force is expressed by the following equations.

$$F = mnN'f(s) \text{ for } N' \geq \frac{M}{2C} \qquad (3.3.1)$$

$$F = \frac{mn}{2} \left(N' + \frac{M}{2C}\right) f(s) \text{ for } N \leq \frac{M}{2C} \qquad (3.3.2)$$

The coefficient of friction, f(s), is a function of the slip of the base plates and has been established by laboratory tests (see Section 2.5 of Part III). Figure 3.3.1 shows the mean multilinear function used in the correlations. Also plotted are the upper and lower limit curves of the experimentally determined values of f(s). The computer program has the capability of approximating a curve by passing straightline segments through any five points on a predetermined f(s) vs. slip curve. The mean multilinear curve is assumed to apply for all bolt torques and hence is independent of the bolt torque (clamping force); therefore it can

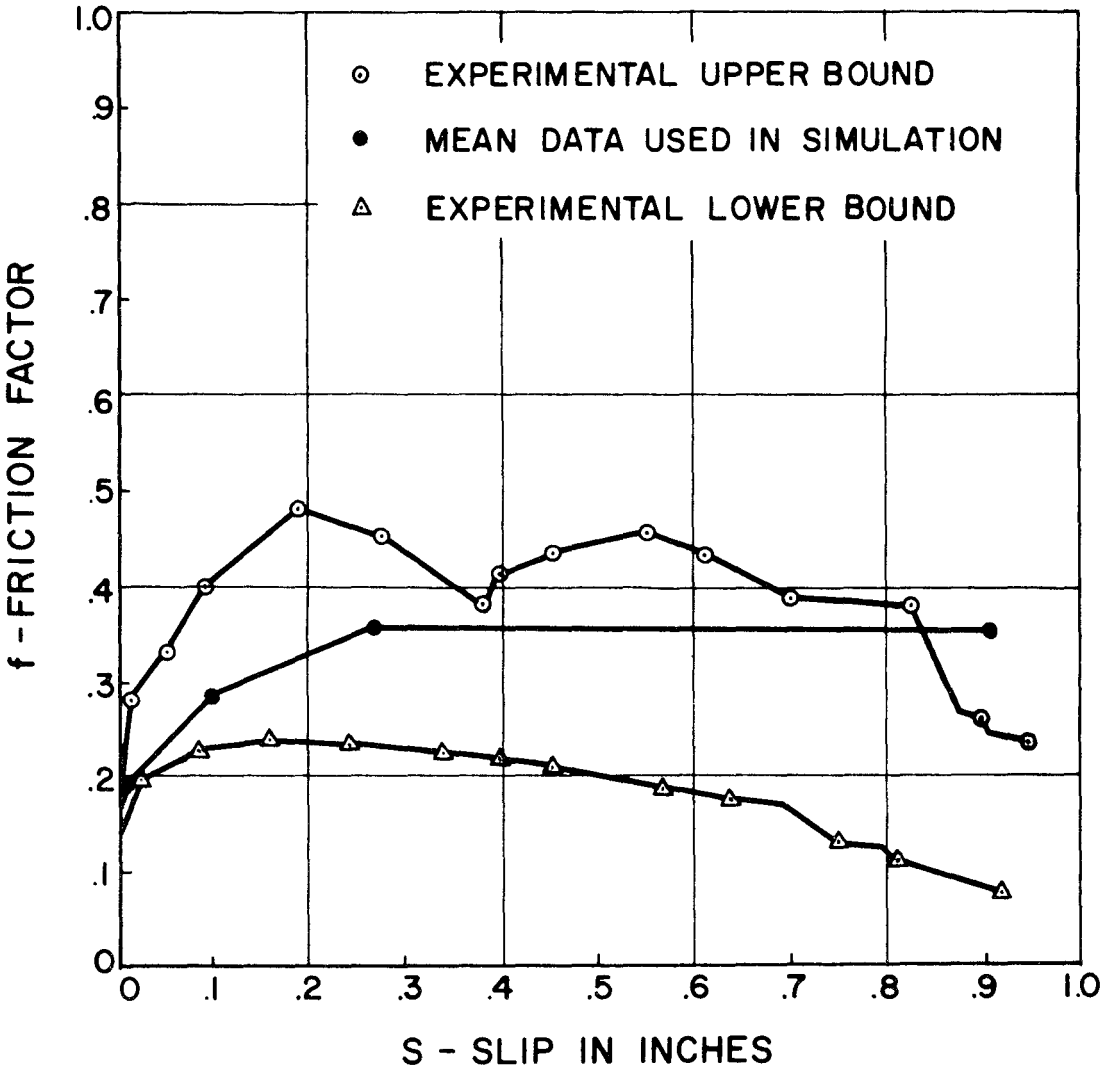

FIGURE 3.3.1 SLIP VS. BASE COEFFICIENT OF FRICTION CURVE

be applied to all bases.

The bases used in Test No. 41 and Test No. 446-5 had four bolts, each bolt had two friction faces, therefore, m = 4, n = 2 and Eq. (3.3.1) and Eq. (3.3.2) become

$$F = (4)\ (2)\ N'\ f(s) = 8N'\ f(s) \text{ for } N' \geq \frac{M}{2C}$$

$$F = \frac{(4)\ (2)}{2}\ (N' + \frac{M}{2C}) = 4\ (N' + \frac{M}{2C})\ f(s) \text{ for } N' \leq \frac{M}{2C}$$

"Plastic hinge" fuse plate. The resisting moment supplied by the "plastic hinge" is proportional to the coefficient of friction on the faying surface between the fuse plate and the support post flange. For Test 41 and Test 446-5, a slotted steel fuse plate was used. There were two bolts crossing the slip plane with two faying surfaces per bolt, therefore m = 2, n = 2 and Eq. (2.9.2) for the force in the plate, is

$$F = 4N'f(s)$$

The functional relation between the fuse plate slip and the coefficient of friction, for an 8WF17 post, is shown by the experimental data presented in Figure 3.3.2. These data were obtained from laboratory investigations carried out under Research Project No. 2-5-63-68, sponsored by the Texas Highway Department in cooperation with the Bureau of Public Roads. The results of the tests in this series are reported in Section 4.6 of Part III. For purpose of the correlation, the mean data curve was used. The data was simulated by the use of a

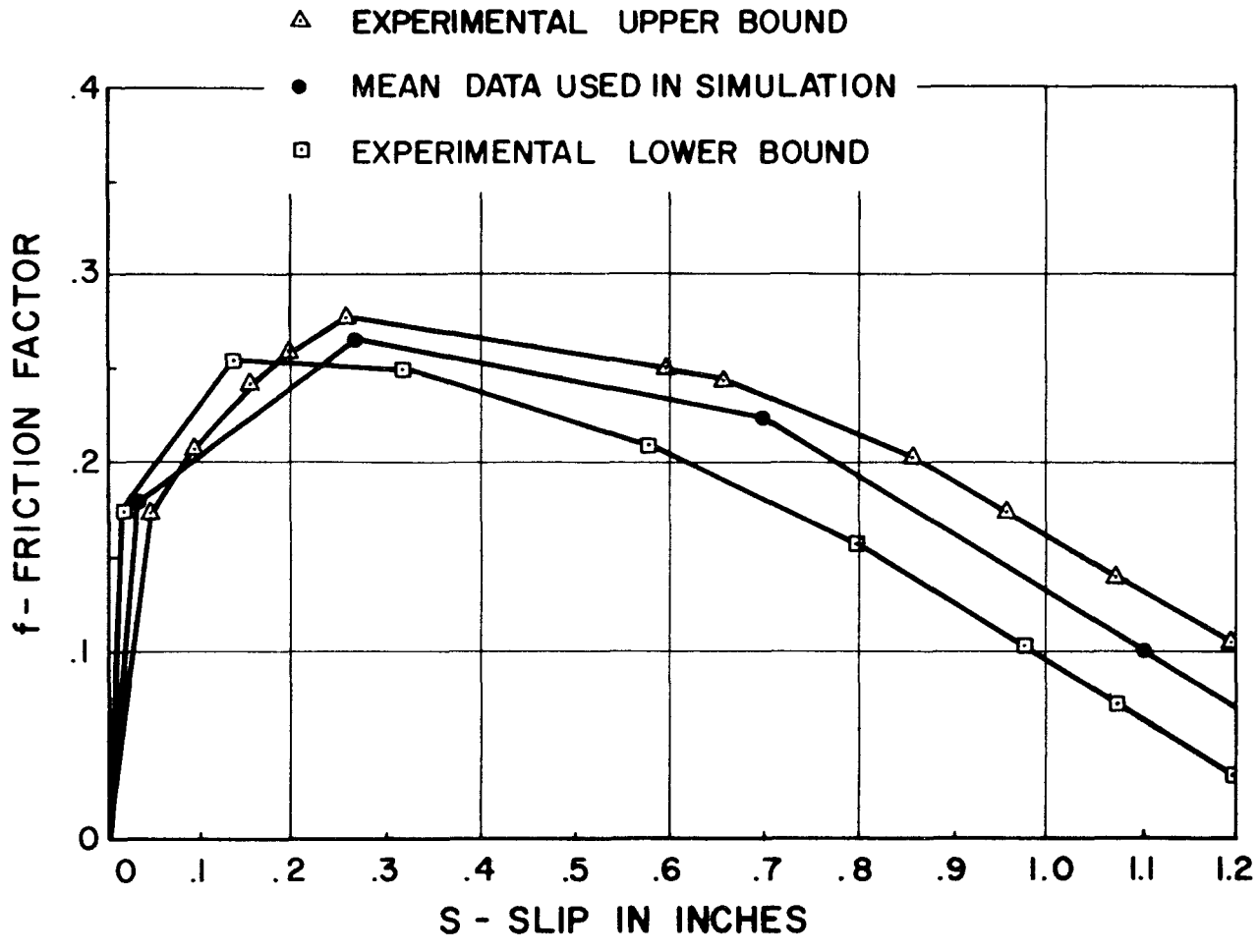

FIGURE 3.3.2 FUSE PLATE FRICTION FACTOR (8WF17)

multilinear curve passed through five points.

The support post. The support posts used in each test are shown in Figure 3.3.3 and Figure 3.3.4. For the simulation, the post is broken into 30 segments. The "plastic hinge" is assumed to be concentrated at m_{14} and the vehicle is assumed to apply concentrated forces at m_3 through m_7 (the location of forces at any time is dependent on the crushing of the vehicle, see Section 2.8). The sign background-to-post connections are located at m_{16}, m_{23} and m_{30}.

Sign background. The support posts have a lateral separation of 9' - 6". For the simulation, the background is divided into 12 equal segments. The post is assumed to be connected to the background three feet (on a lumped mass) from the end, giving a post separation in the model of 9' - 0". This difference introduced no significant error in the results.

Laboratory tests of several types of sign background material (see Section 5.6 of Part III) indicate that the torsional stiffness of the sign background can be approximated by

$$\frac{T}{\psi} = \frac{2}{3} G\, ab^3 \left[L - \frac{a}{12} \frac{1}{\sqrt{10E/G}}\right]$$

where

G = shear modulus of background material (psi)

E = modulus of elasticity of sign material (psi)

a = background width (in.)

b = background thickness (in.)

L = length of background (in.)

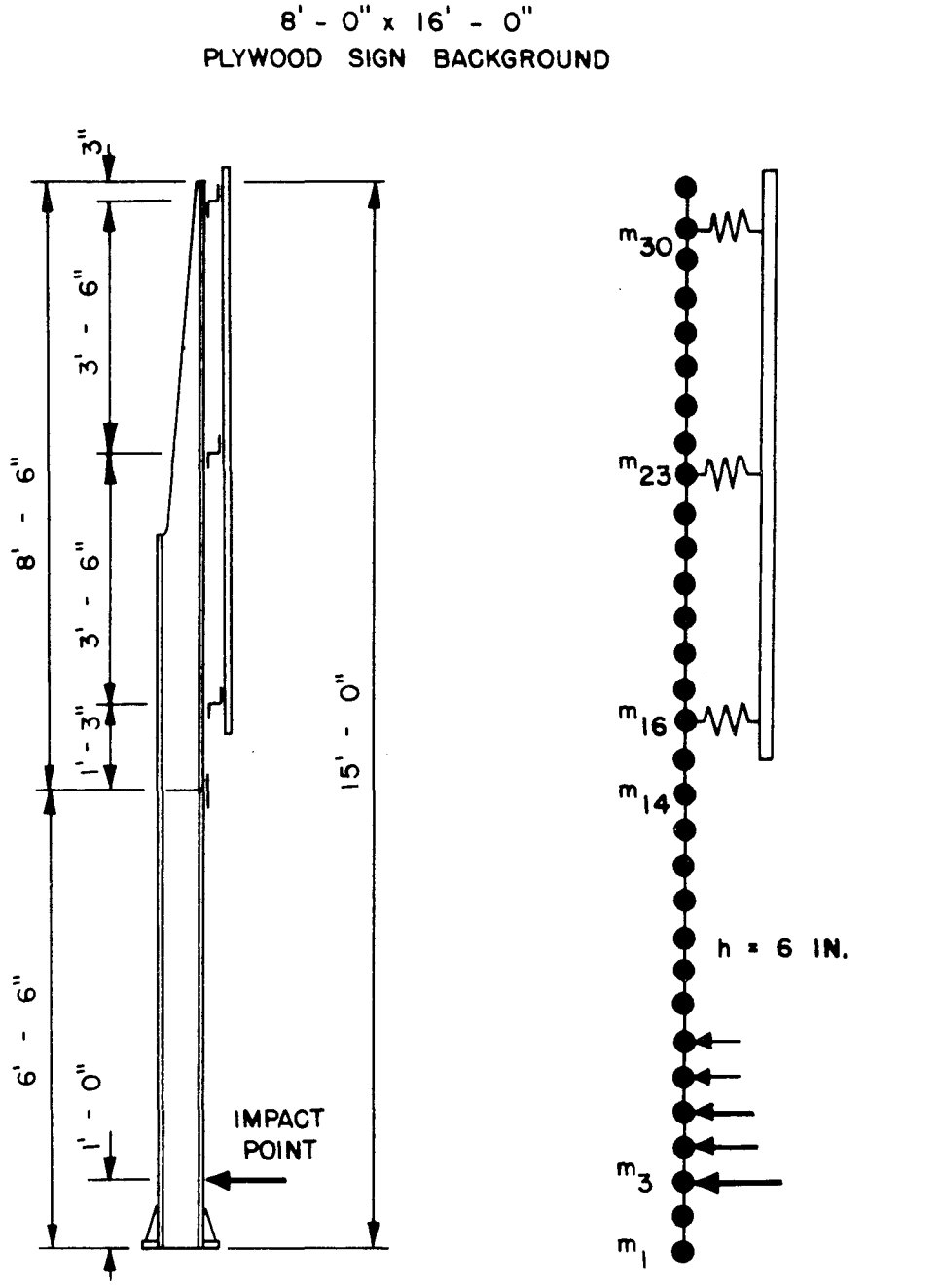

FIGURE 3.3.3 SIGN SUPPORT FOR TEST NO. 41

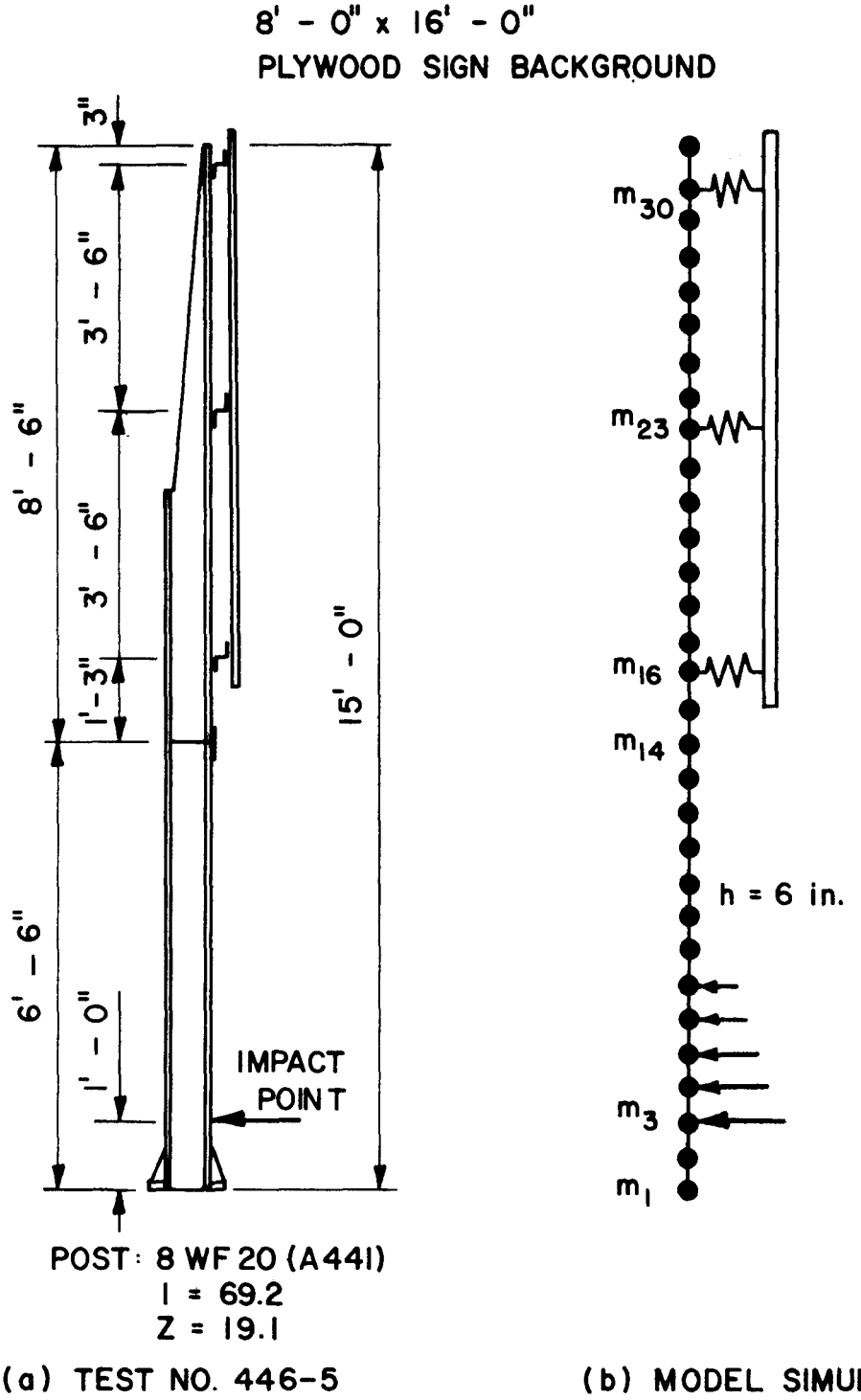

FIGURE 3.3.4 SIGN SUPPORT FOR TEST 446-5

T = torque (in.-lb.)

ψ = angle of rotation (radians)

The translational response of the background is handled as previously described. The aluminum windbeam is transformed to an equivalent area having the same mechanical properties as the plywood sign board. The modulus of elasticity values used are

$$E \text{ (plywood)} = 1.5 \times 10^6 \text{ psi}$$

$$E \text{ (aluminum)} = 10.0 \times 10^6 \text{ psi}$$

The moment of inertia calculation for the translational response is shown in Figure 3.3.5.

Sign background-to-post connection. A very simple calculation is made to determine the spring constant for the connection. Figure 3.3.6 shows a detail of the connection. It is assumed that the major part of the deformation of the connection takes place in the background sign face (5/8 in. - thick plywood). Then

$$K_i = \frac{AE}{L}$$

Using an assumed modulus of elasticity for the plywood (perpendicular to the grain) of 15,000 psi and an A/L ratio of 2,

$$K_i = 2(15{,}000) = 30{,}000 \text{ lb./in.}$$

It is noted that the spring constant will probably be different in compression than in tension. This fact is considered in the

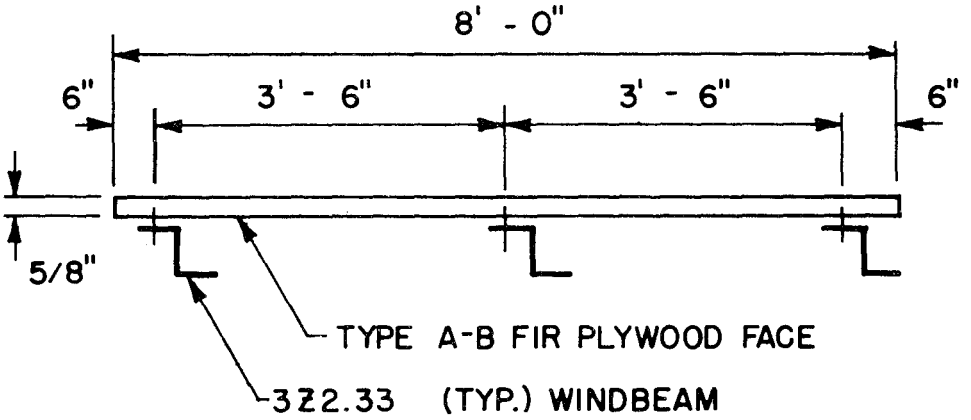

(a) CROSS SECTION OF SIGN BACKGROUND

FACE AREA:

$A_1 = (8.0)\,(12.0)\,(0.625) = 60.0\ \text{IN.}^2$

WIND BEAM AREA:

$A_2 = 3.0(1.98)(10.0\times10^6)/(1.5\times10^6) = 39.5\ \text{IN.}^2$

TOTAL= 99.5 IN.^{2}

(b) GROSS AREA OF BACKGROUND

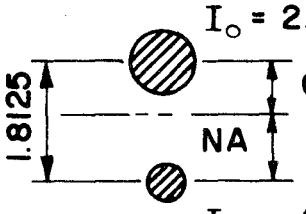

$I_o = 2.717\ \text{IN}^4$

$I_o = \dfrac{(10.0\times10^6)}{(1.5\times10^6)}\ (8.67)$

$I_o = 57.70\ \text{IN}$

$A_1D_1^2 = (60.0)\,(0.6605)^2 = 26.17$

$A_2D_2^2 = (39.4)\,(1.1520)^2 = 57.50$

$\Sigma AD^2 = 78.67$

$\Sigma I_o = 57.70$

$I_{NA} = 136.37\ \text{IN}^4$

(c) MOMENT OF INERTIA CALCULATION

FIGURE 3.3.5 SECTION PROPERTIES OF BACK-GROUND

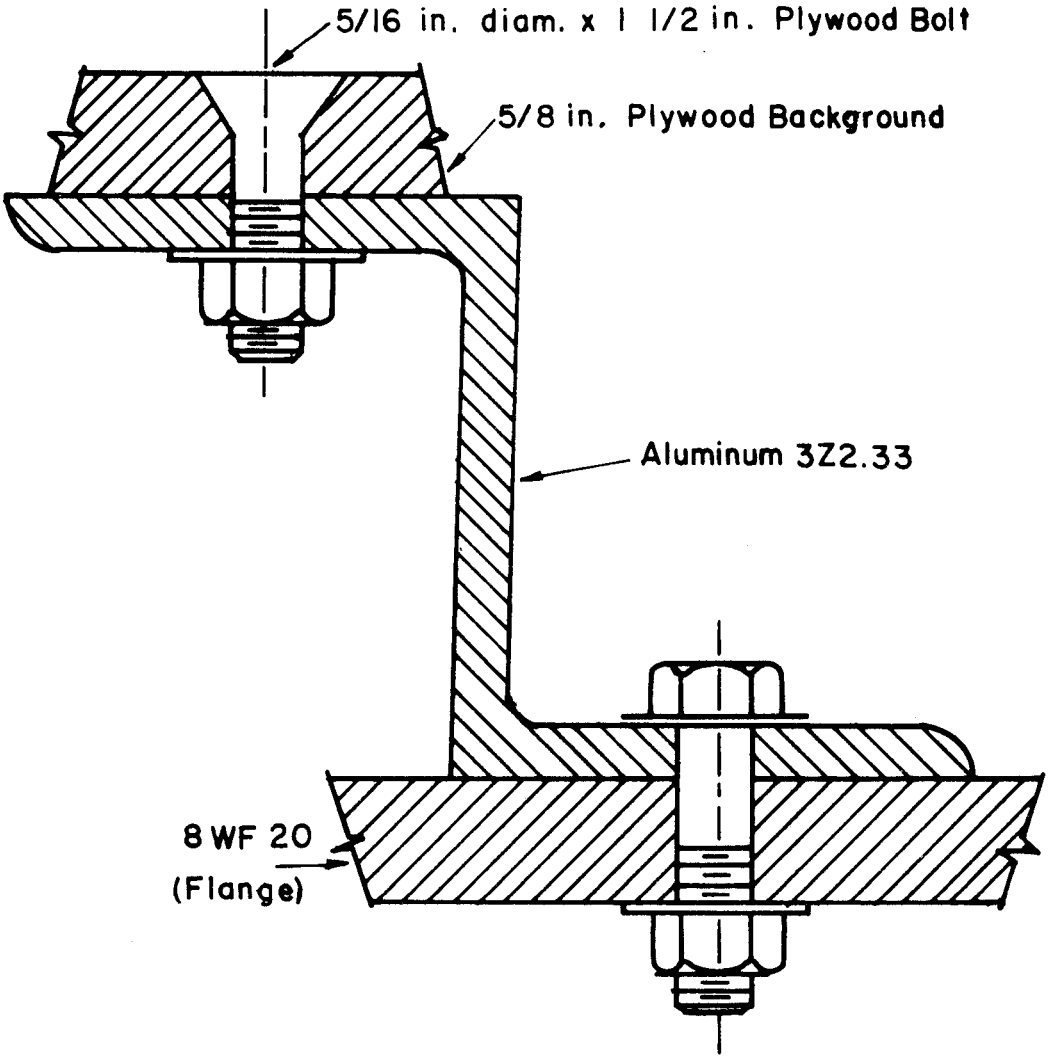

FIGURE 3.3.6 BACKGROUND-TO-POST CONNECTION

correlation runs by assuming that the compression stiffness is 3 K_i.

The vehicle and passenger. The passenger is simulated with a 150 lb. weight and a 2500 lb./ft. simulated restraint. The vehicle crush characteristics are simulated using the data developed in Section 8.3 of Part III. Note that five springs have been used. The range of values used are shown in Table 3.3.1 The vehicle weight in Test 41 was 3620 lbs. and in Test 446-5, 3500 lbs. Both vehicles were 1955 Fords.

3.4 Correlation

Table 3.4.1 shows the parameters that were correlated for each full-scale crash test of a "break-away" support post. The parameters were not identical for each test due to changes in instrumentation and availability of transducers.

Base displacement. In Figure 3.4.1 and Figure 3.4.2 the plot of base displacement from the simulation is compared with the measured data from the tests.

Figure 3.4.1, the correlation for Test 41, shows good agreement, with the displacement from the simulation lagging the measured displacement. Note that the test data, as recorded, are shown as well as the assumed path with the discontinuities eliminated. It is believed that these discontinuities were caused by the instrumentation and do not represent physical quantities. This is supported by the fact that the method of attachment of the slide arm on the transducer precluded a movement in the direction opposite to the motion of the base.

Figure 3.4.2 is the base displacement-time plot for Test 446-5. The test data presented were obtained from the high speed film record.

TABLE 3.3.1 VEHICLE SIMULATION (Ref. to Figure 2.8.1)

SPRING NO.	RANGE (in.)	STIFFNESS (lb./ft.)
1	0 - 6.72	17,000
2	6.72 - 15.48	11,350
3	6.72 - 15.48	11,350
4	15.48 -	2,533
5	15.48 -	2,533

TABLE 3.4.1 CORRELATION PARAMETERS

	TEST NUMBER	
Parameter	41	446-5
Base Displacement	✓	✓
Vehicle Velocity	✓	✓
Vehicle Displacement	✓	✓
Mechanical Fuse Plate Force	✓	✓
Bending Moment 2' - 0" Above Base		✓
Force in Base Bolts		✓
Vehicle Deceleration	✓	✓
Response of Simulated Passenger	✓	
Event Times	✓	✓

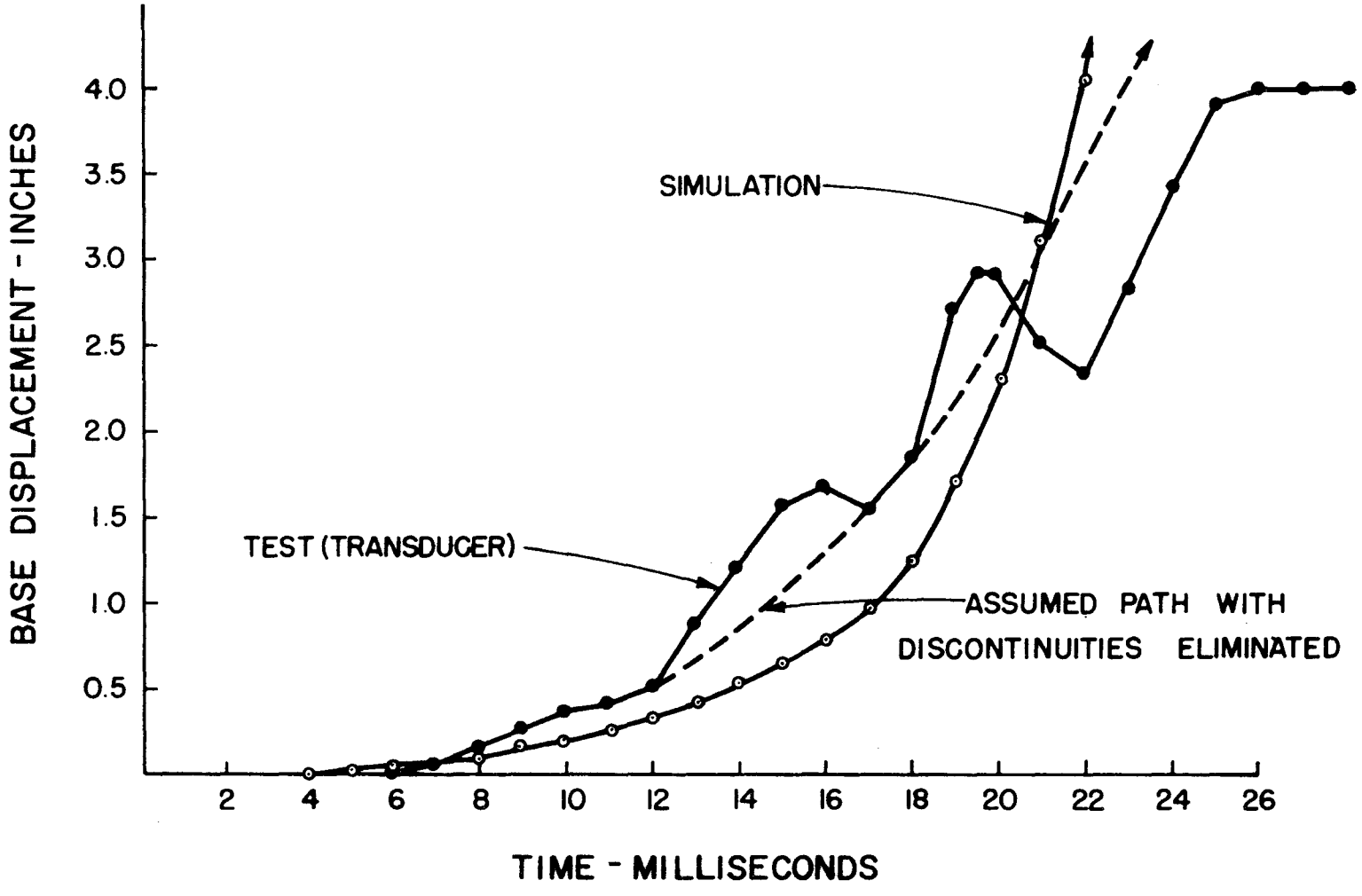

FIGURE 3.4.1 TEST 41, BASE PLATE DISPLACEMENT

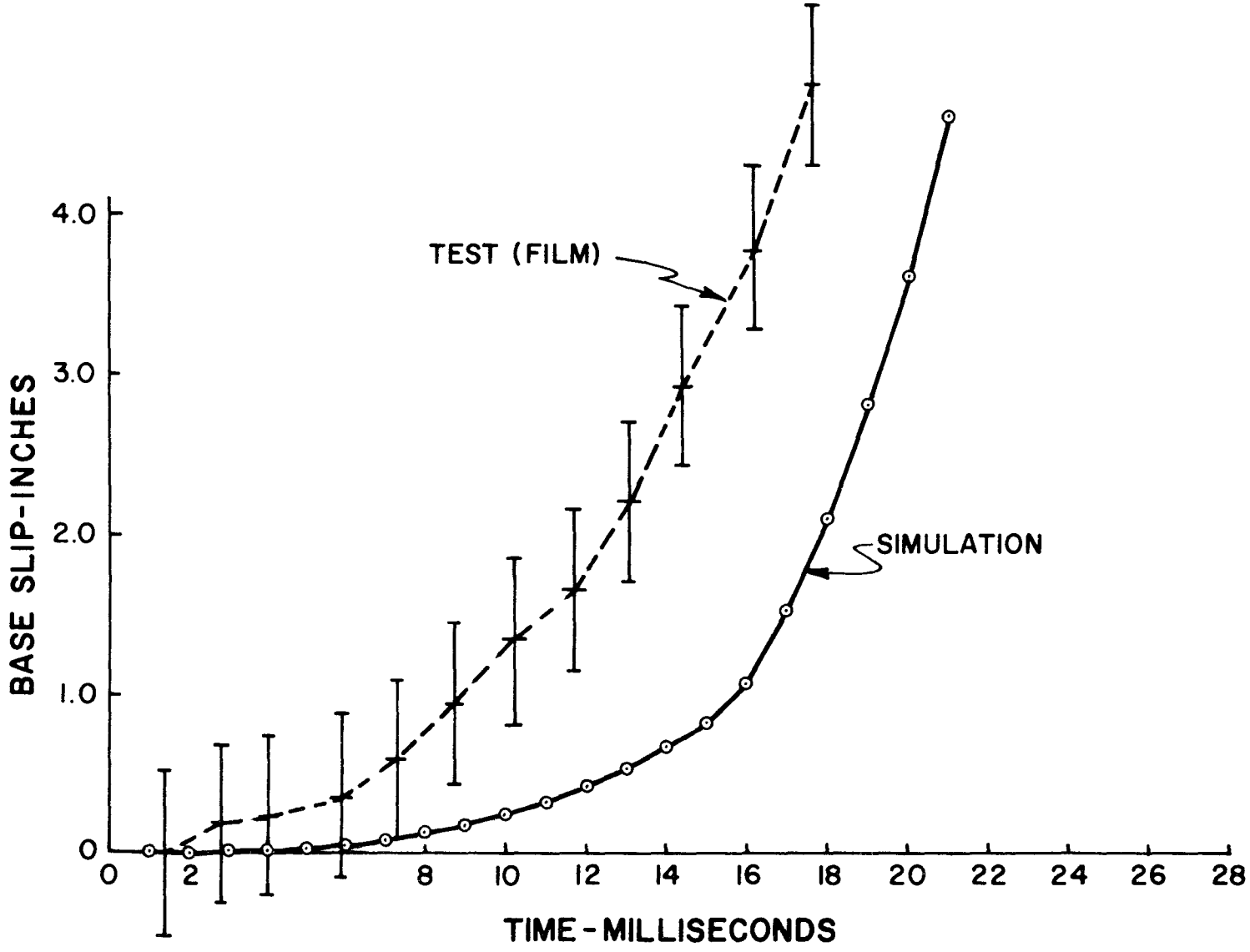

FIGURE 3.4.2 TEST 446-5, BASE PLATE DISPLACEMENT

As mentioned in Section 6.3 of Part III, the displacement transducer on the base of the post did not operate. The data have an inherent error of approximately ± 1/2 inch in displacement and ± 5% in time base. It is therefore reasonable to expect the data to fall anywhere within the limits shown. The mean data curve has been drawn. While the correlation for this test is not as close as in Test 41 (Figure 3.4.1) the comparisons for both tests indicate that the simulation is capable of predicting the base displacement in the early stages of the collision event.

Vehicle velocity. Figure 3.4.3 and Figure 3.4.4 show plots of vehicle velocity vs. time after initial contact. The test values were obtained by integration of the accelerometer data (see Section 7.1 of Part III). The initial velocities used in these calculations were obtained from the time-displacement data from the high speed film and from velocity measuring devices (see Section 7.3 of Part III).

Both figures indicate that the simulation is very accurate for times less than 10 to 12 milliseconds. Good agreement is obtained for the final velocity in the case of Test 446-5. It should be noted that the accelerometer was mounted on the frame of the vehicle and hence was measuring the dynamic forces introduced through the frame at that point. The velocities determined by integration therefore represent the motion of the transducer and not the vehicle as a whole, hence the discontinuities in the data. However, the general trend of the data must reflect the velocity of the whole vehicle, consequently, the comparison is valid.

From the comparison of data in Figure 3.4.3 and Figure 3.4.4,

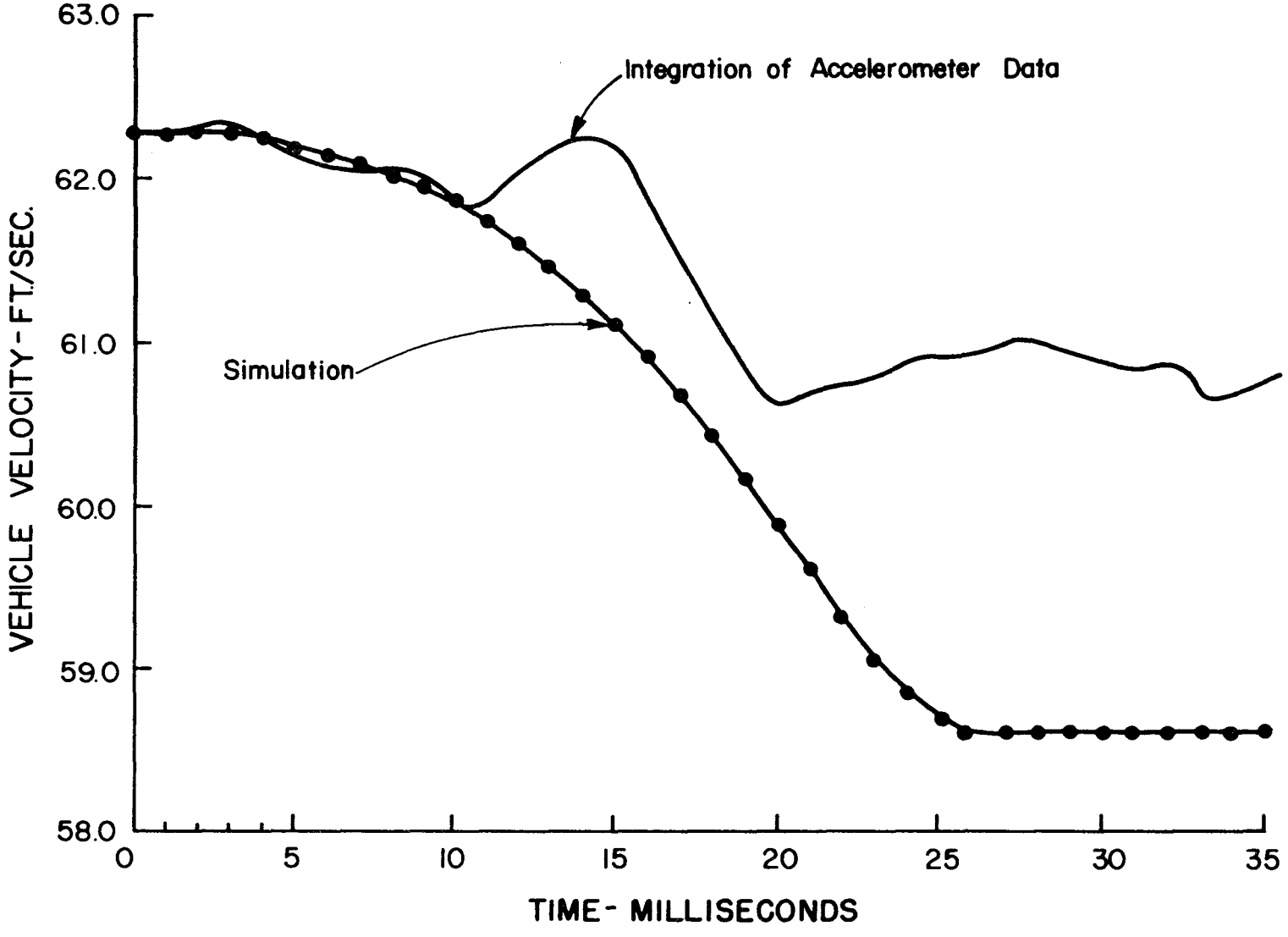

FIGURE 3.4.3 TEST 41, VEHICLE VELOCITY

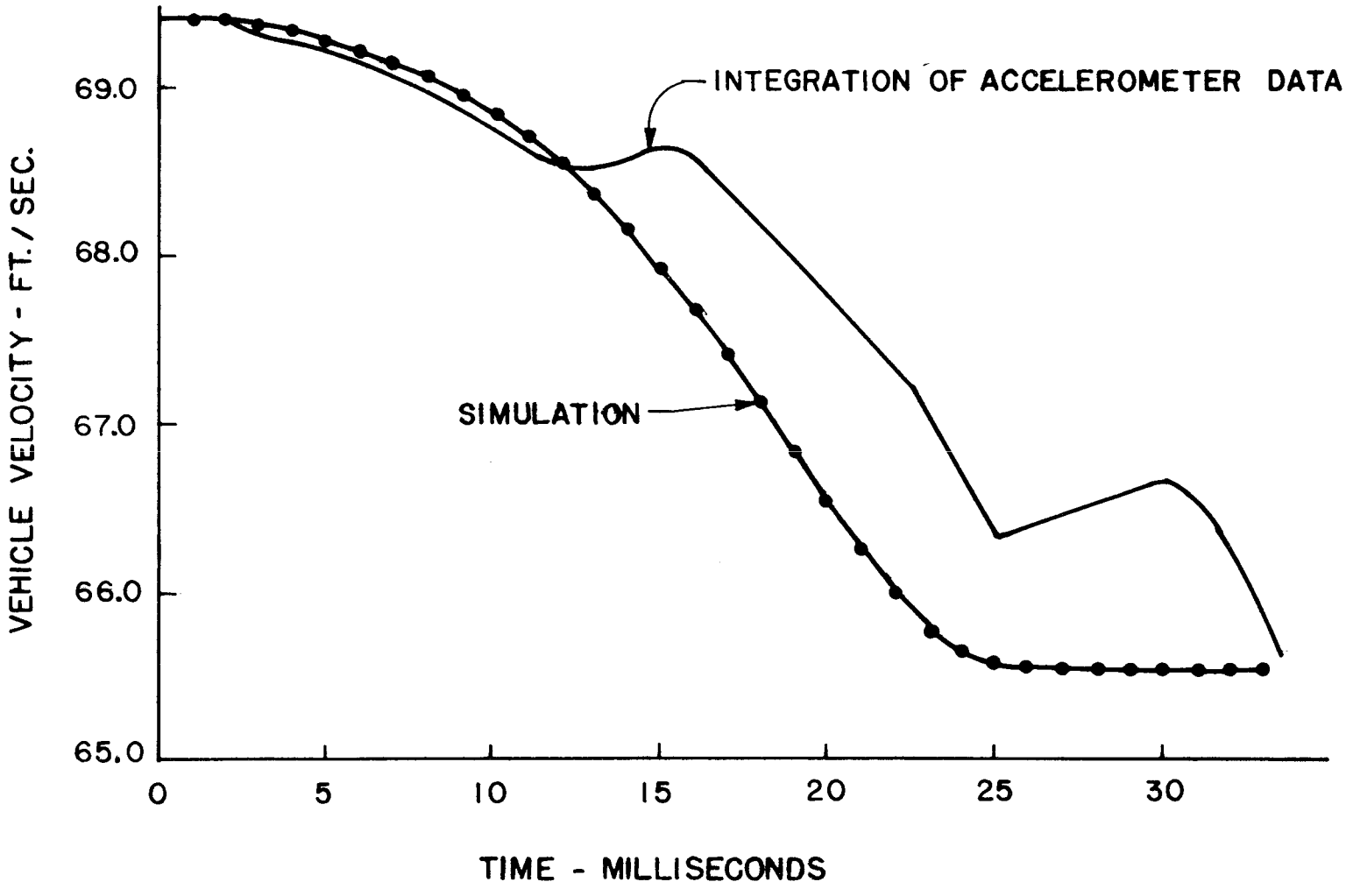

FIGURE 3.4.4 TEST 446-5 VEHICLE VELOCITY

it can be concluded that the simulation can be used to predict vehicle velocities within engineering accuracy.

Vehicle displacement. Figure 3.4.5 shows the comparison of vehicle displacement vs. time for each of three sources of data: (1) values from the simulation, (2) from double integration of the accelerometer data and (3) measurements from the high-speed film record. Note that in both tests excellent agreement between the test and simulation was achieved. It should be noted that vehicle displacement is very insensitive to changes in other parameters. It can be concluded that the simulation gives very accurate results on the displacement of the vehicle.

Mechanical fuse plate force. Figure 3.4.6 and Figure 3.4.7 show the plots of the fuse plate force vs. time. For Test 41, the initial fuse plate bolt force was chosen such that the maximum fuse plate force, observed in the test, could be attained. This was done because at the time Test 41 was conducted, no suitable means of measuring the bolt force was available. In Figure 3.4.6, note that the two curves have the same characteristic shape. The undulations are probably due to the influence of the flexural vibrations of the support post. The time (approximately 17 milliseconds) at which the fuse is activated (force goes to zero) is in good agreement. This time is influenced by the stiffness of the vehicle spring (the rate at which the vehicle force is applied) and the coefficient of friction-slip data entered as input information.

In Test 446-5, Figure 3.4.7, the fuse plate force from the simulation is considerably larger than that observed in the test. In

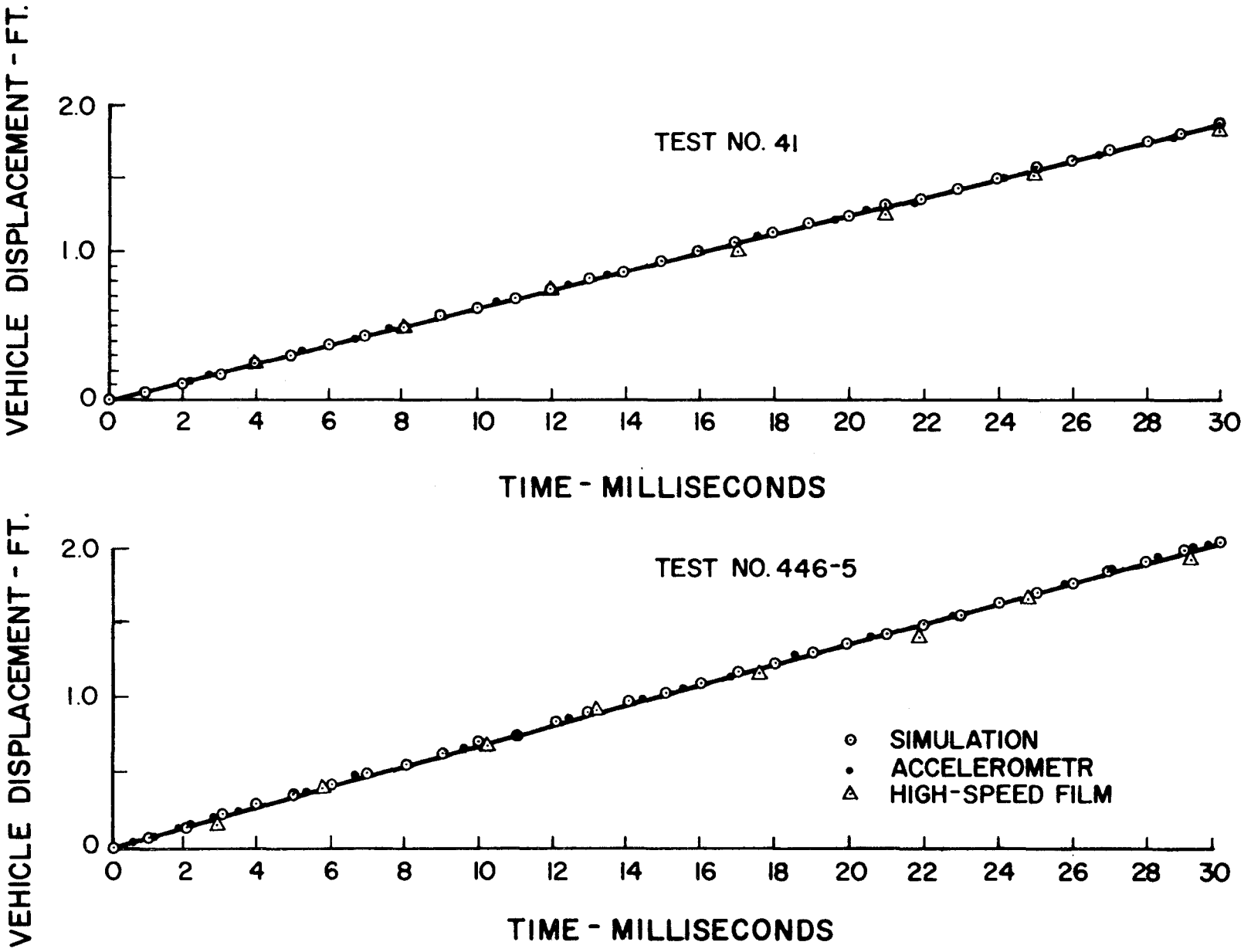

FIGURE 3.4.5 VEHICLE DISPLACEMENT

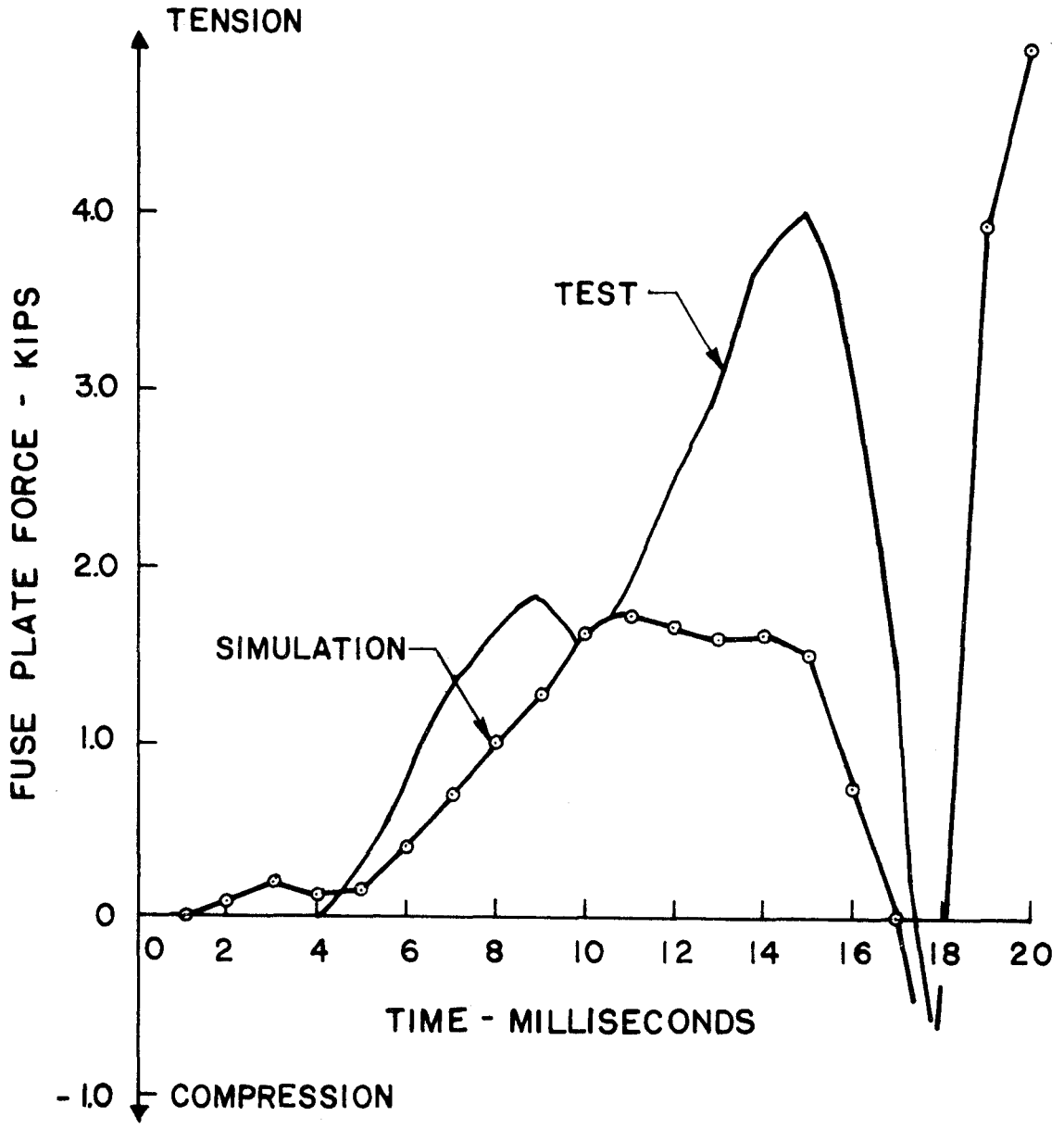

FIGURE 3.4.6 TEST 41, FUSE PLATE FORCE CORRELATION

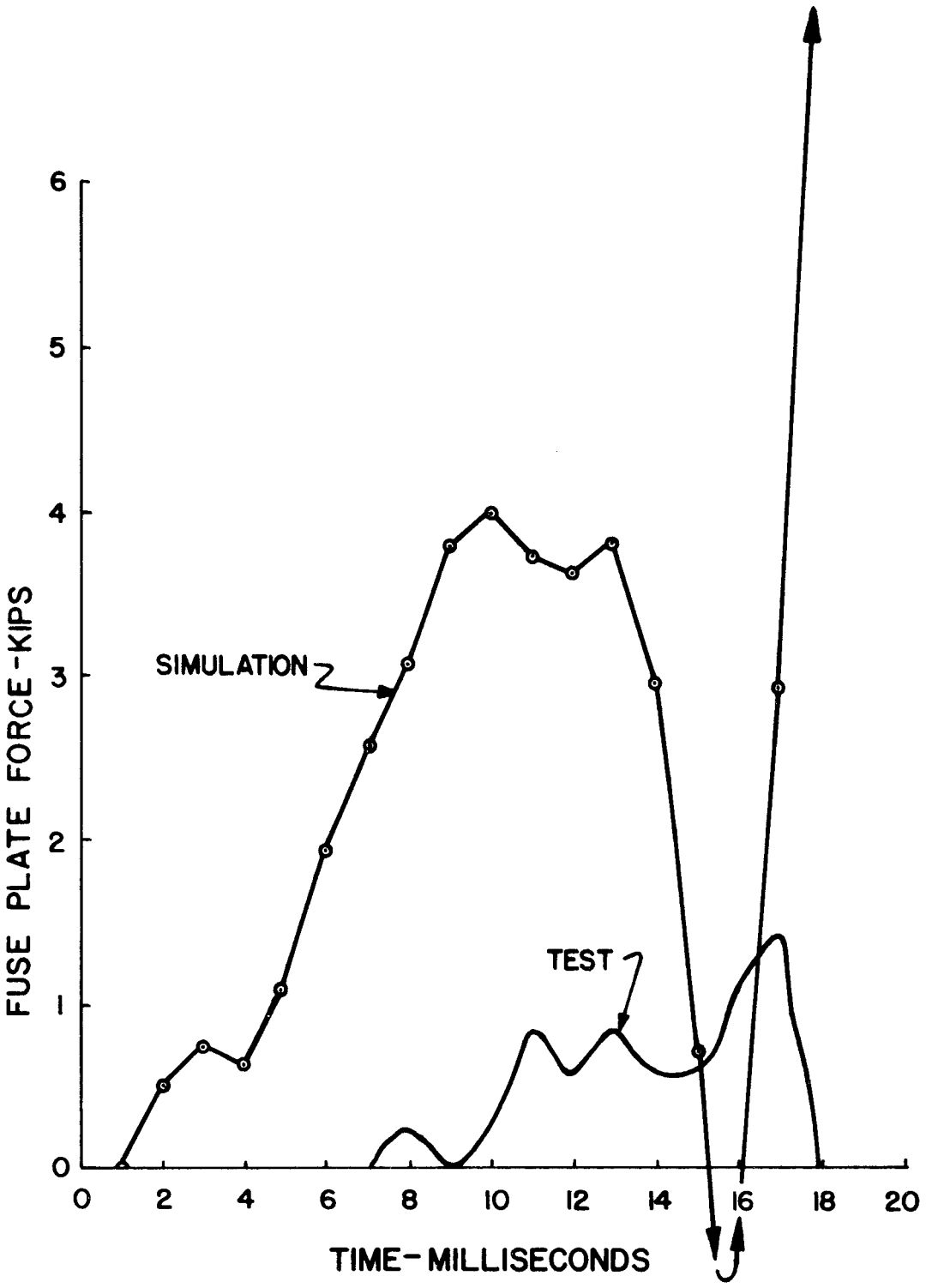

FIGURE 3.4.7 TEST 446-5, FUSE FORCE

Test 41, the bolts in the fuse plate were tightened to an apparent value of 3800 lbs. per bolt. In Test 446-5 they were tightened by the turn-of-the-nut method to their proof load of 36050 lbs. per bolt. Due to the relative initial bolt tensions employed, it appears that the fuse plate in Test 446-5 should develop higher force than in Test 41. The test data do not show this behavior. Note that the time correlation in Test 446-5 is satisfactory. It appears that the test data from Test 446-5 are in error. The source of this error has not been determined.

This correlation leaves some doubt as to the validity of the routines used to simulate the fuse plate behavior. However, the results of the comparison in Test 41 (Figure 3.4.6) indicate that the simulation is satisfactory. Several unsuccessful attempts were made to develop routines which would correlate more closely with Test 446-5.

Bending 2' - 0" above base. Figure 3.4.8 shows the correlation for the bending moment at a point 2' - 0" above the base plate. Note that the values from the simulation exhibit the same behavior with respect to time. Up to the time of release, at 17 milliseconds, the post experiences a negative bending moment (flange away from the input side in tension). The magnitudes of the values from the simulation are considerably larger than those measured. This is probably due to the assumed distribution of the impact force on the post. In the early stages of impact, from 0 to 7 milliseconds, the bumper alone is in contact with the post and the force on the post is approximately a point load as assumed in the simulation. Note the correlation in this range. As the grille and hood come into contact with the post, the impact force is spread over an increasingly larger segment of the post. This would tend to lower the peak moment value. An

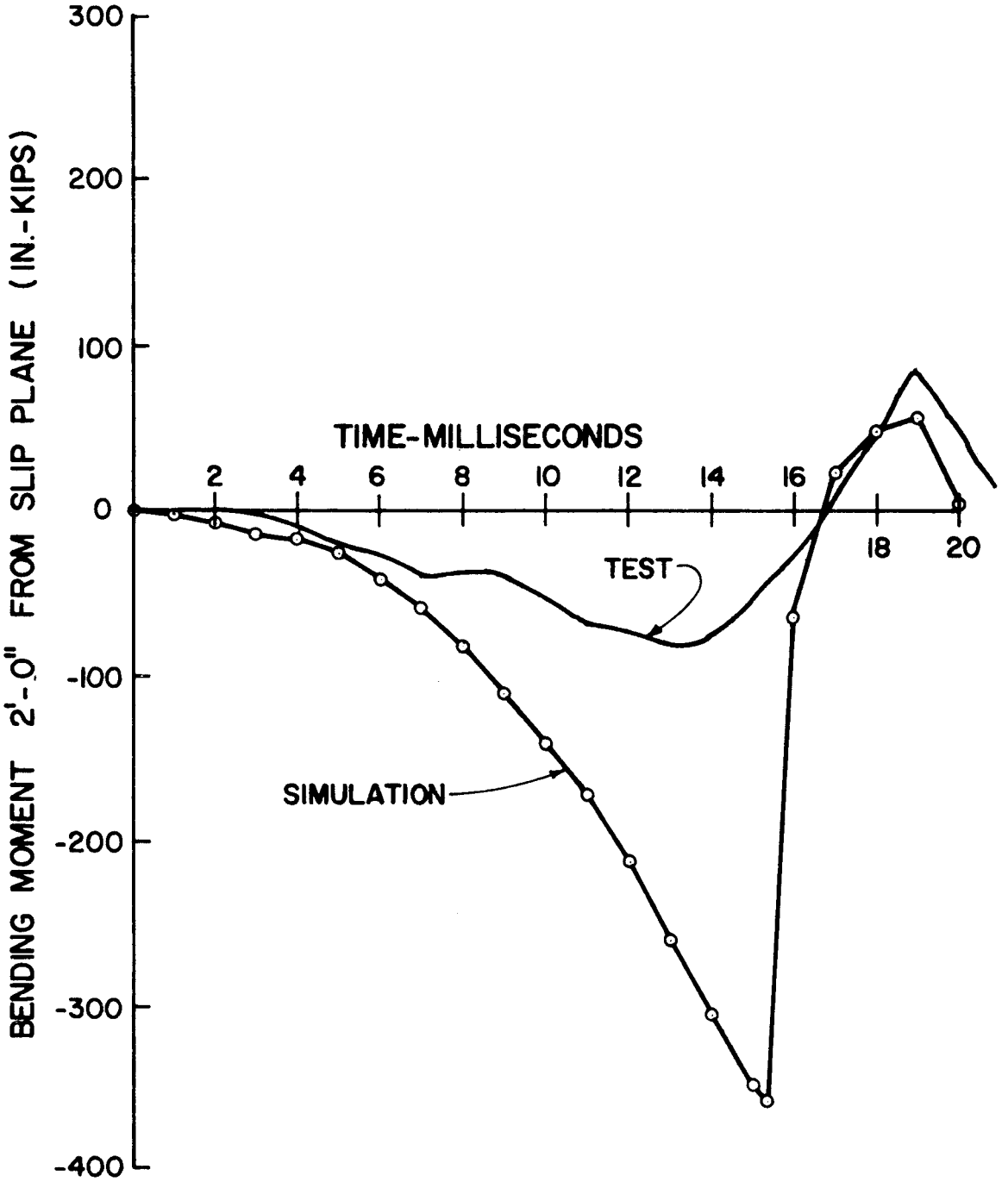

FIGURE 3.4.8 TEST 446-5, BENDING MOMENT 2'-0" FROM BASE

attempt was made to simulate the spreading of force but this did not reduce the moment values significantly.

Considering the foregoing discussion it can be concluded that the mathematical model, as presently formulated, gives good qualitative correlation for the bending moment 2' - 0" above the base, but some doubt is cast on its ability to simulate the magnitude of material stresses.

Force in the base bolts. Figure 3.4.9 shows the correlation of the base bolt force for Test 446-5. The base bolts were instrumented to measure axial tension. Bolts 2 and 3 were 3/4-10 UNC of 4140 steel and Bolts 1 and 4 were 3/4-10 UNC ASTM A325 of galvanized steel. During the test Bolt 2 failed to operate. All bolts were initially torqued to a tension of approximately 2000 lbs. During the test Bolt 3 was placed in tension due to the moment induced at the base by the impact force. Bolts 1 and 4 were on the compressive face of the base plate and show little change in tension throughout the event. At approximately eight milliseconds, the tension in Bolt 3 began to increase and dropped to zero when release occurred. Note that the tension in Bolt 3, from the simulation, shows the same behavior as exhibited by the test data for Bolt 3. The maximum tension reached, in the simulated bolt, is larger than actually measured. This is to be expected and causes no alarm since the correlation, in general, is good. No correlation is shown for the other bolts as the simulation technique (see Section 2.10 of Part II) assumes that the load in the bolts in the compression zone do not change. Note the excellent time agreement.

It appears from this correlation that the technique used to

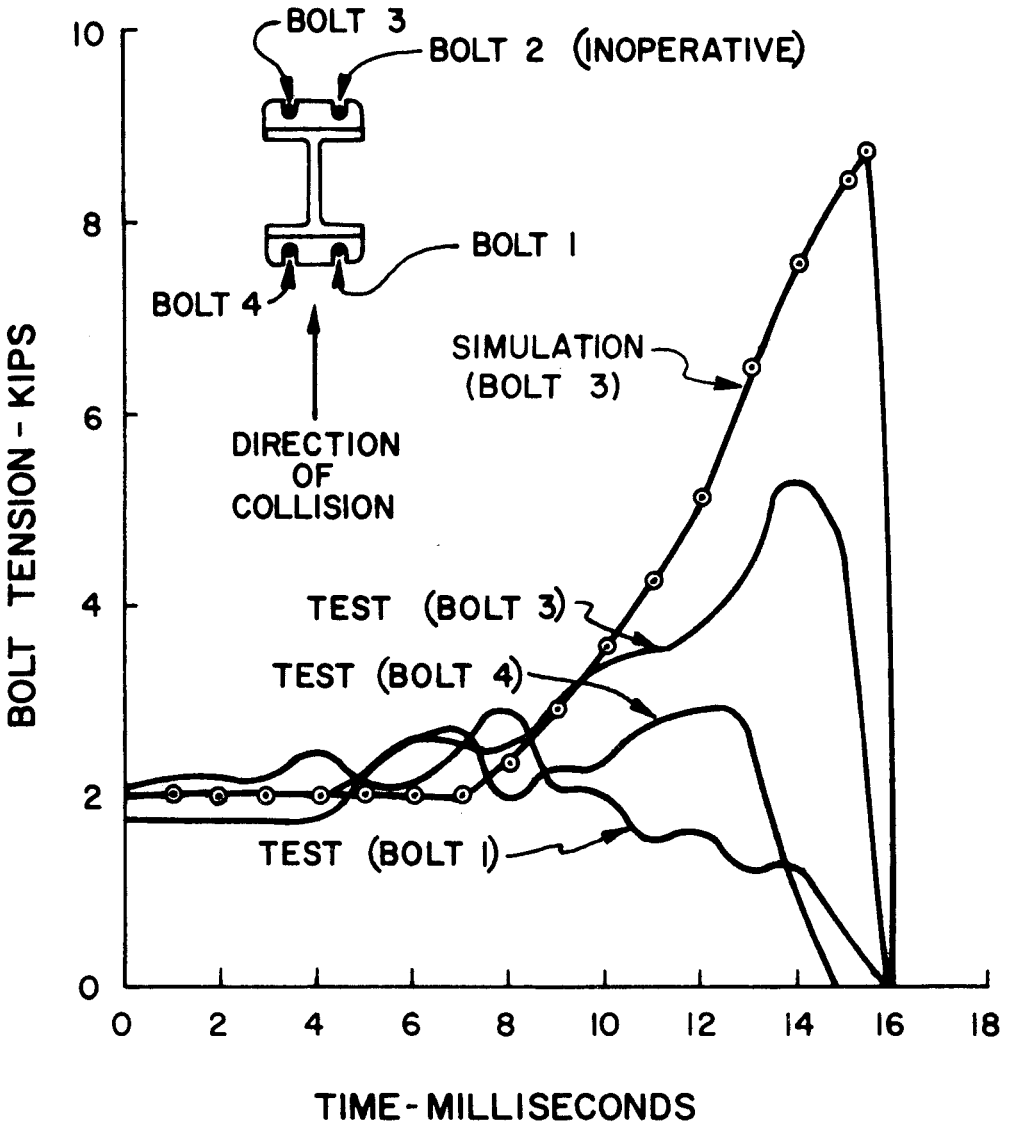

FIGURE 3.4.9 TEST 446-5, BASE BOLT FORCE

simulate the base plate behavior is adequate.

Vehicle deceleration. Figure 3.4.10 (a) is a correlation of the measured accelerations of a point on the vehicle frame and the deceleration of the rigid mass simulating the vehicle. Note that the deceleration from the simulation is approximately the mean of the values from the frame accelerometer. The peak decelerations occur at approximately the same time after impact. At 20 milliseconds, the vehicle spring ceases to compress, and the simulated vehicle acceleration begins to return to zero. The real post stays in contact longer and hence accelerations were recorded. Note that the mean value of these accelerations is relatively small.

Figure 3.4.10 (b) is the acceleration time plot for Test 446-5. The same observations made above apply to these data.

Passenger response. Figure 3.4.11 shows the comparison between the simulation for a 150 lb. passenger restrained with a 2500 lb./ft. seat belt spring stiffness. The test data were obtained from an instrumented 150 lb. block of concrete which was placed in the driver's seat in Test 41 and restrained with a seat belt. Also shown in the comparison are data derived by the use of Eq.(2.8.7)

$$\ddot{X}_p\ (t) = - \frac{K_p\ [X_p\ (t) - X_1\ (t)]}{M_p}$$

where the value of $X_1\ (t)$ is calculated using Eq. (2.8.4) and Eq. (2.8.2). In Eq. (2.8.4) the value of $\ddot{X}_1\ (t + \Delta t)$ is measured from the accelerometer trace of Figure 3.4.10 (a). In Figure 3.4.11, the passenger acceleration as calculated from the mathematical model (simulation)

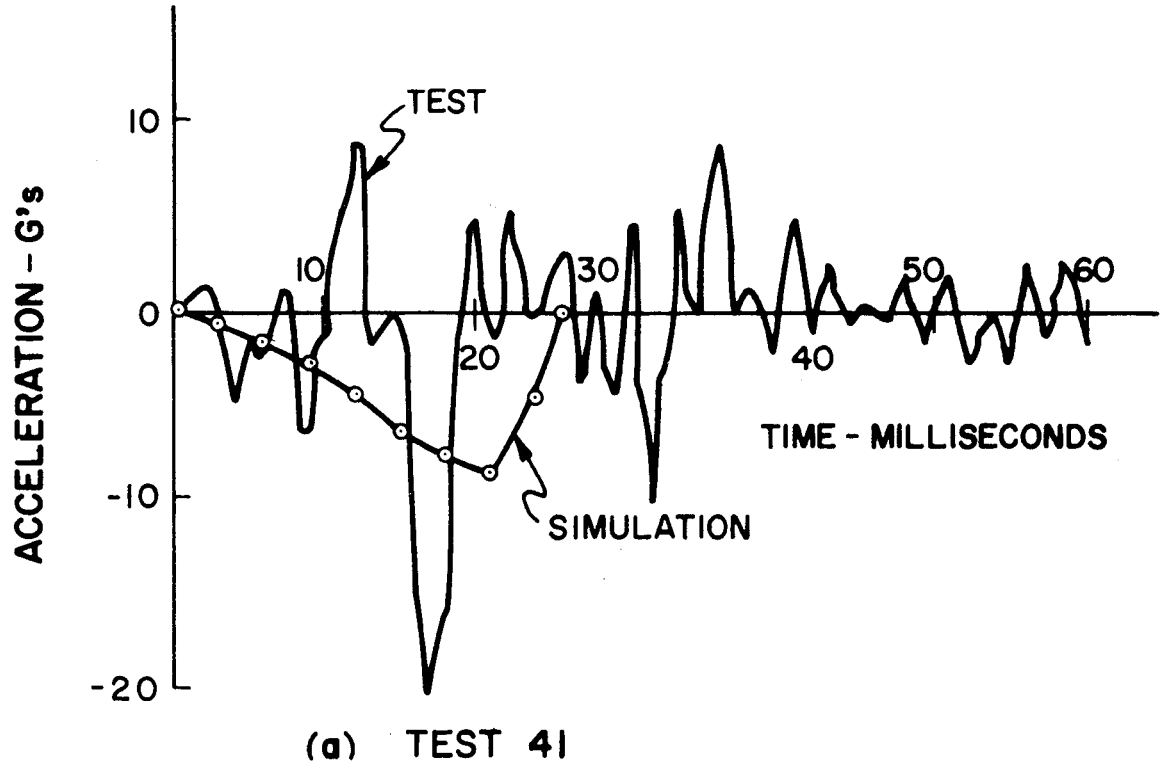

(a) TEST 41

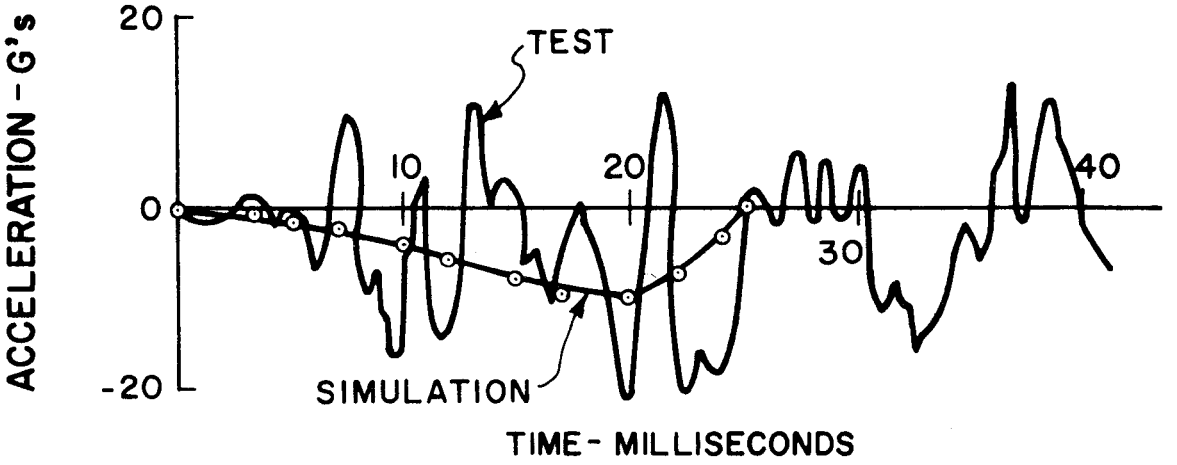

(b) TEST 446-5

FIGURE 3.4.10 FRAME ACCELERATION

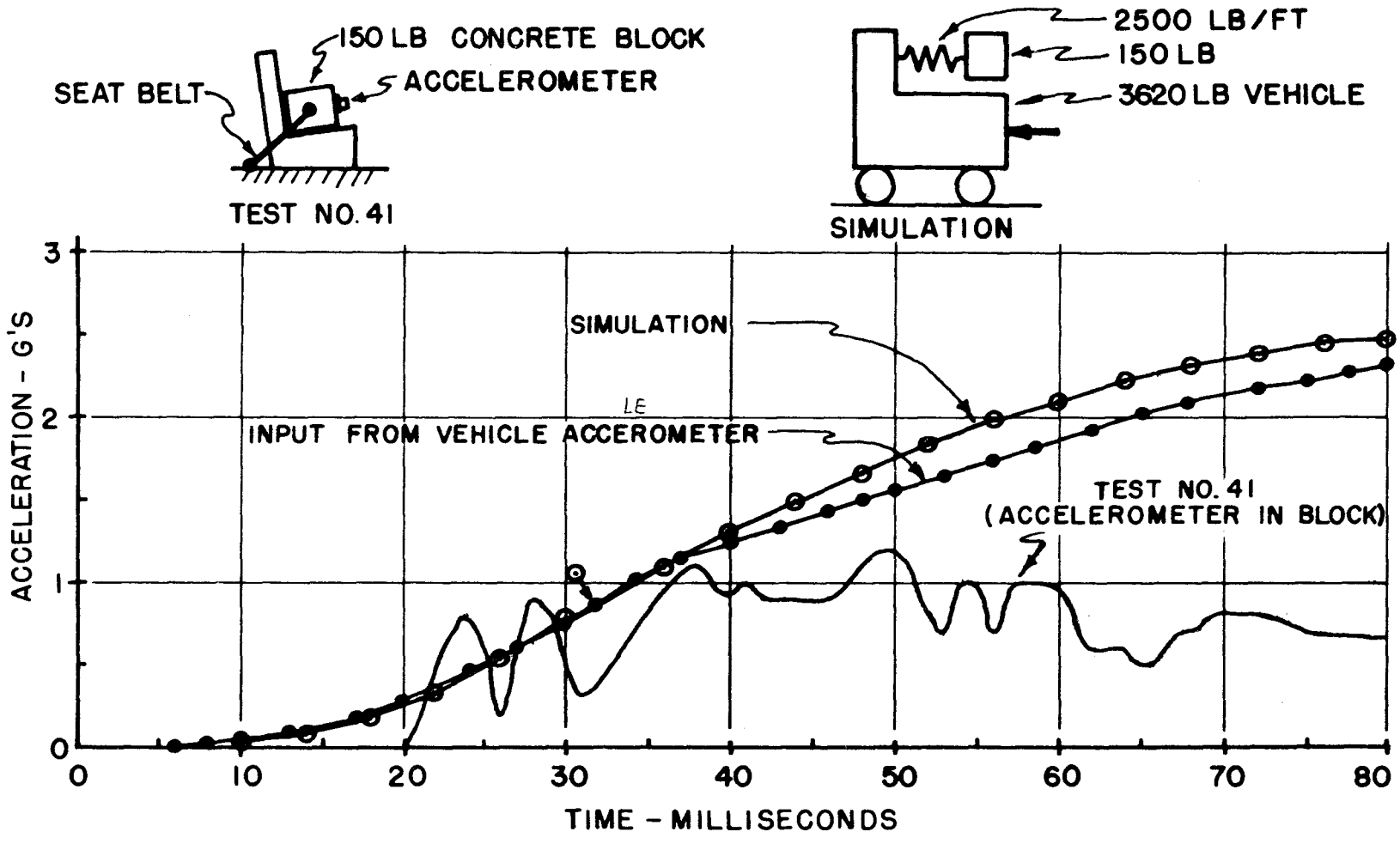

FIGURE 3.4.11 - PASSENGER RESPONSE

and from Eq. (2.8.7) agree very well, especially for times below 40 milliseconds. This indicates that the measured deceleration of the vehicle causes the simulated passenger to respond in the same manner as the rigid body deceleration of the simulated vehicle, i.e., the higher frequencies of vibration of the vehicle do not affect the response of the simulated passenger. Note that both curves fall above the measured acceleration of the 150 lb. concrete block for time greater than 40 milliseconds. This discrepancy could be due to several causes: (1) the seat belt spring stiffness (2500 lb./ft.) used for the calculations in Figure 3.4.11 could be smaller since it acts in combination with the seat, and (2) the accelerometer on the concrete block measured only the acceleration component tangential to the path of the center of gravity, which was not horizontal as assumed in the other calculations. No attempt was made to find the belt stiffness that would make the data agree since the agreement was close enough to allow the use of the simulation techniques for qualitative comparison of passenger response. Also, the comparison of the two calculated curves established the significance of the frame accelerometer readings as it related to passenger response.

Event times. Table 3.4.2 compares the times at which certain events, important to the behavior of the "break-away" concept occur. The test values shown are taken from the high-speed film records. Due to the difficulty in determining the times exactly, several determinations were made for each event by different observers. The

TABLE 3.4.2 COMPARISON OF EVENT TIMES

EVENT	TIME (MILLISECONDS)					
	TEST 41			TEST 446-5		
	SIMULATION	TEST*		SIMULATION	TEST	
		RANGE	AVERAGE		RANGE	AVERAGE
Base Disengaged	17	12-20	15	15	5-15	10
Fuse Activated	26	14-28	22	Not Activated	Not Activated	
Vehicle-Post Contact Terminated	26	37-88	69	26	56-136	98

*Test values from ref. 3 p. 58

maximum and minimum values of the observation are listed as the range of values and the mean of the observations is listed as the average value.

3.5 Conclusions

The correlations presented in the previous section indicate that in general the mathematical model, as formulated, can be used to predict the behavior of the "break-away" sign support. More significant perhaps is the ability of the simulation to reproduce the response of the vehicle, i.e., vehicle displacement, deceleration, and velocity change. The model is also capable of giving an insight into the response of a belted passenger. Caution should be exercised however in drawing conclusions as to human response from the results of a collision on the simulated passenger. This should be used only as an indicator of passenger safety.

It appears, from the correlation presented, that the motion and behavior of the support post as calculated with the model, is accurate enough to permit its use in the evaluation of most parameters of the system. There was some doubt cast as to the accuracy of results on flexural bending stresses in the post. However, the comparison made is not conclusive evidence that the model values are as much in error as it appears. In view of the results of the other comparisons, this one anomaly alone could not invalidate the use of the model for its intended purpose.

The following chapter will explore the effects of the significant parameters on the behavior of the "break-away" support. Studies will also be conducted to develop criteria that should be useful in design.

CHAPTER 4

PARAMETER STUDY

4.1 Introduction

To date limited information is available on the in-service behavior of the "break-away sign support. The operational concepts have been clearly defined but the effects of the system parameters on the support behavior have not. Test data from full-scale tests have served only to validate the concept and have been used primarily as a developmental tool. They have provided the necessary information for the development and validation of a mathematical model that will simulate the vehicle-support collision. The model was used to extend the knowledge of the effects of system parameters. The results of the parameter study provided the information necessary for the development of design recommendations. These recommendations are presented in Part II, Chapter 5.

4.2 Philosophy of the Study

The sign system consists of the sign and support, the "break-away" features, and the vehicle. The parameters that affect the operation of the system are as follows:

for the sign,

1. the background,
2. the background-to-support post connections,
3. the mechanical fuse,
4. the support post;

for the vehicle,

1. force-deformation (crush) characteristics,
2. weight,
3. velocity at impact, and
4. angle of incidence of impact.

All of the above parameters were included in the study except the angle of incidence. The present model is formulated for impacts normal to the sign face (0° angle of incidence). It is believed that results of the head-on collisions can be applied to angles of incidence up to 15 degrees without appreciable error. The conclusion is based on highway accident data in Texas and the results of one test conducted for the Texas Highway Department.[7,8]

It would be impractical to conduct a study of such scope to include all combinations of the variables listed previously. In place of such an exhaustive study, a cross section of the practical spectrum was taken. A study of this type limits the number of problems and at the same time indicates the trends that the various parameters have on the system.

In the study that follows, four different sign support structures were chosen. These supports represent the sizes that would normally be employed under present signing practices. The vehicles were selected to represent typical small, medium and large passenger vehicles. Trucks have been excluded from the study. Truck-sign collisions do not present a significant safety problem since most large vehicles have the mass and kinetic energy, at impact, to "ride-down" the signs that present the greatest hazard to passenger vehicles.

It must be emphasized that the study was conducted on operational sign supports in order to gain the necessary experience on the behavior of the supports chosen under operational conditions. This approach would better serve the objectives of the study than would a systematic evaluation of the effects of each parameter independently.

4.3 Range of Study Parameters

Sign support size. The sign support sizes used were based upon designs for four representative sign background sizes. The design wind was chosen as 80 mph. This represents an average design wind for most of the continental United States. The choice of background sizes was based upon a Texas Highway Department tabulation of sign sizes for 1027 guide signs on the Interstate System in Texas. Figure 4.3.1 shows the distribution of sign background width and depth as a function of the percent of signs which have widths or depths equal to or less than the values plotted as the ordinate. Approximately 70% of signs have backgrounds 8' x 16' or smaller. In order to cover the range of sign sizes anticipated in present day signing, the following sizes were shown for the parameter study:

(1) 4' depth x 6' width

(2) 6' depth x 10' width

(3) 8' depth x 16' width

(4) 14' depth x 19' width

The larger sizes were chosen to obtain the largest practical size of support post.

The designs for the supports were made following the provision

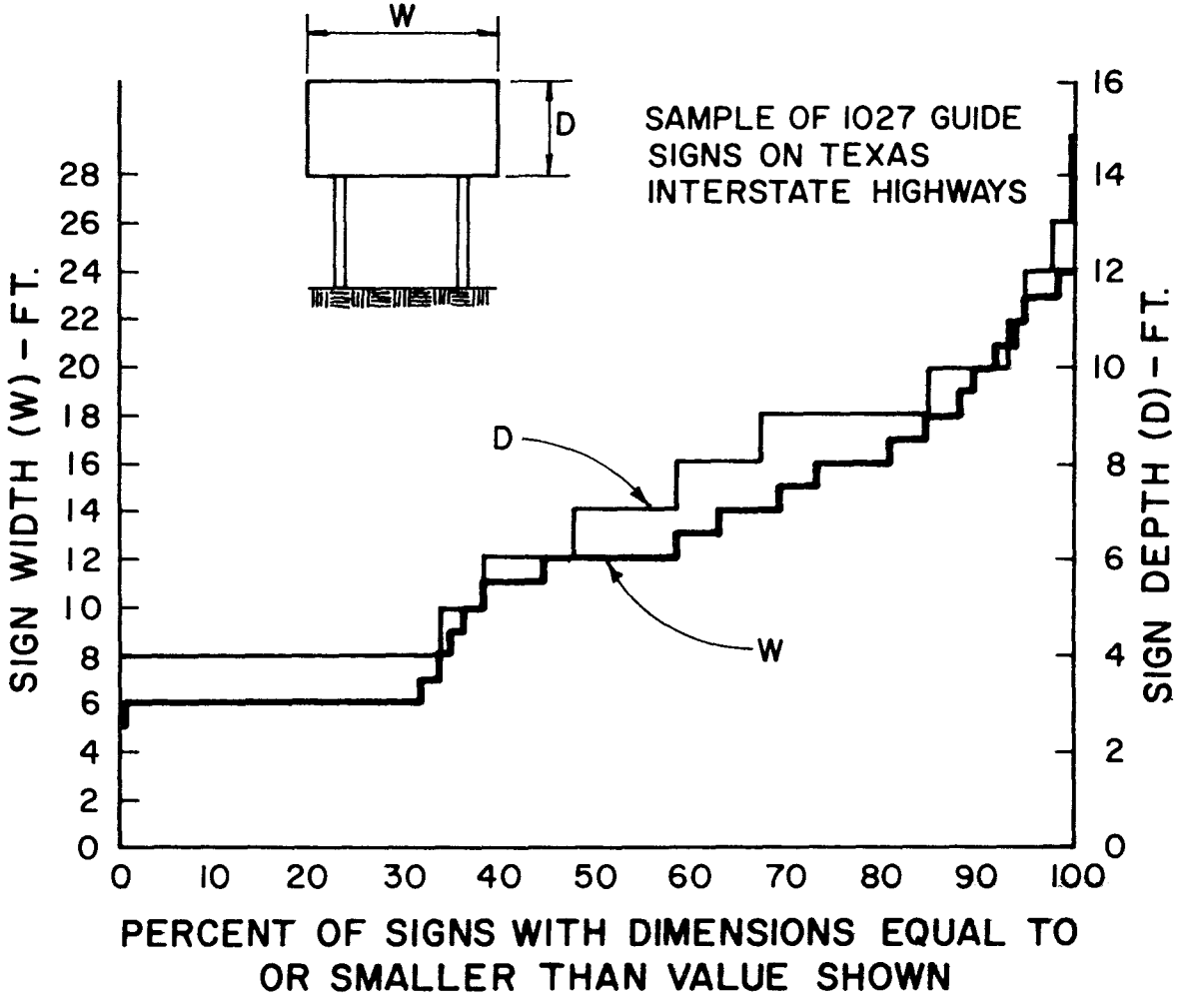

FIGURE 4.3.1 DISTRIBUTION OF SIGN DEPTH AND WIDTH

of the Specifications for the Design and Construction of Structural Supports for Highway Signs (1960) using ASTM A441 steel. The study is limited to two support posts per sign. Signs with more than two support posts will behave like two support signs as long as the span between posts is similar. The support posts were chosen from the available sections (those that would satisfy the design criteria) so that a good distribution of stiffness to weight was obtained. Figure 4.3.2 through Figure 4.3.5 show the supports chosen and the model simulation. All backgrounds were assumed to be 5/8" plywood with aluminum windbeams. Table 4.3.1 gives the fixed parameters for the supports. Fuse plate bolts were assumed to be tightened by the turn-of-nut method.[9]

Vehicles. Vehicles were chosen to represent the average, small, medium and large class of passenger vehicles. Vehicle velocities were chosen to represent low, medium and high speed collisions. The vehicle parameters are shown in Table 4.3.2.

Vehicle force-deformation characteristics (spring stiffness) similar to those developed in Section 8.3 of Part III, were used in the parameter study. The small vehicle characteristics were similar to Figure 8.3.3, the medium vehicle to Figure 8.3.2, and the large vehicle similar to Figure 8.3.5 in Part III.

Simulated passenger. The passenger is simulated as previously described using a 150 lb. weight and a restraint spring whose stiffness is 5000 lb./ft. (nominal value of seat belt stiffness). Note that this value is different from the 2500 lb./ft. value used in Section 3.4 of Part II.

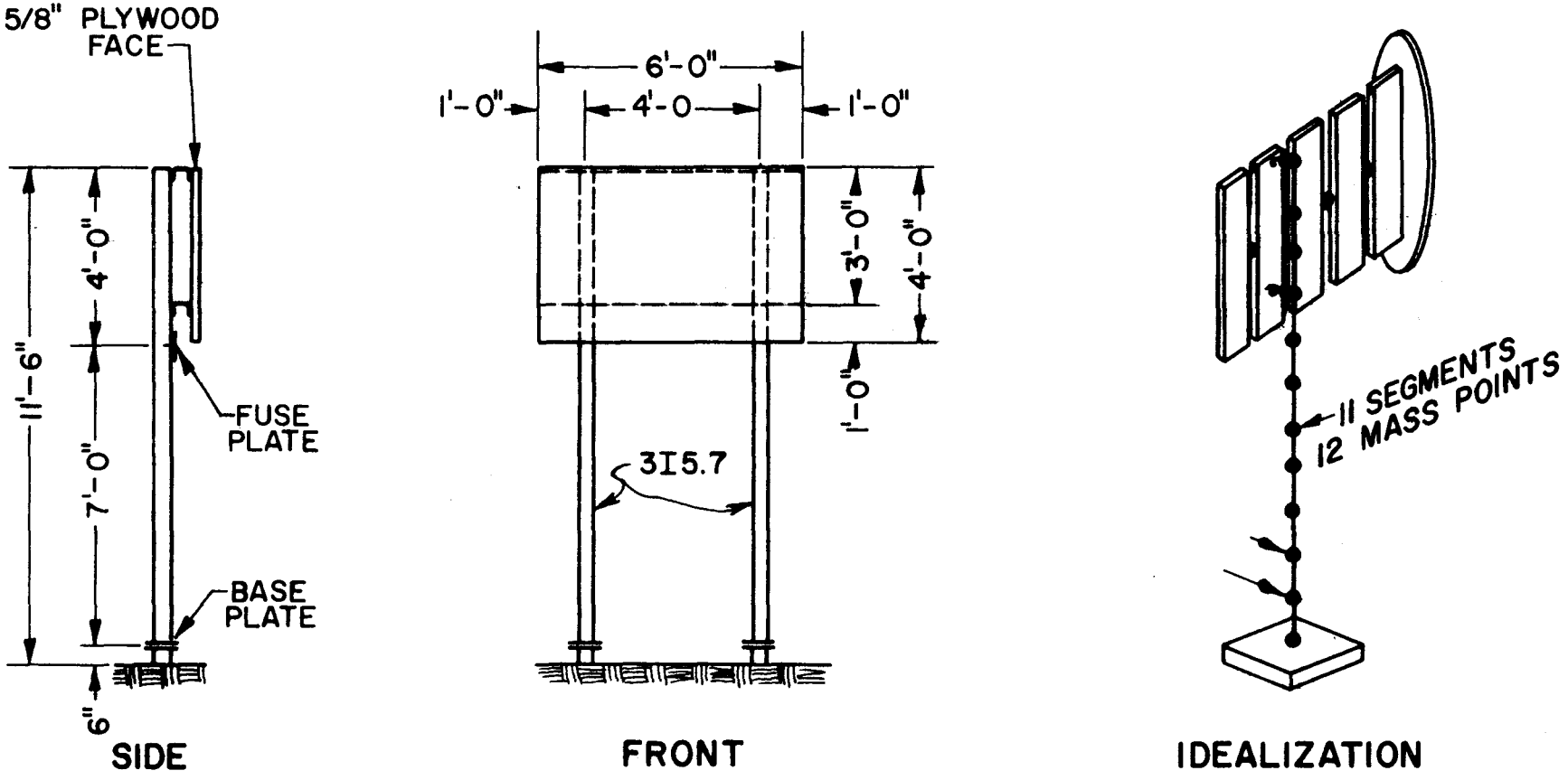

NOTE: SEE TABLE 4.3.1 FOR DETAILS

FIGURE 4.3.2 3I5.7 POST AND SIGN

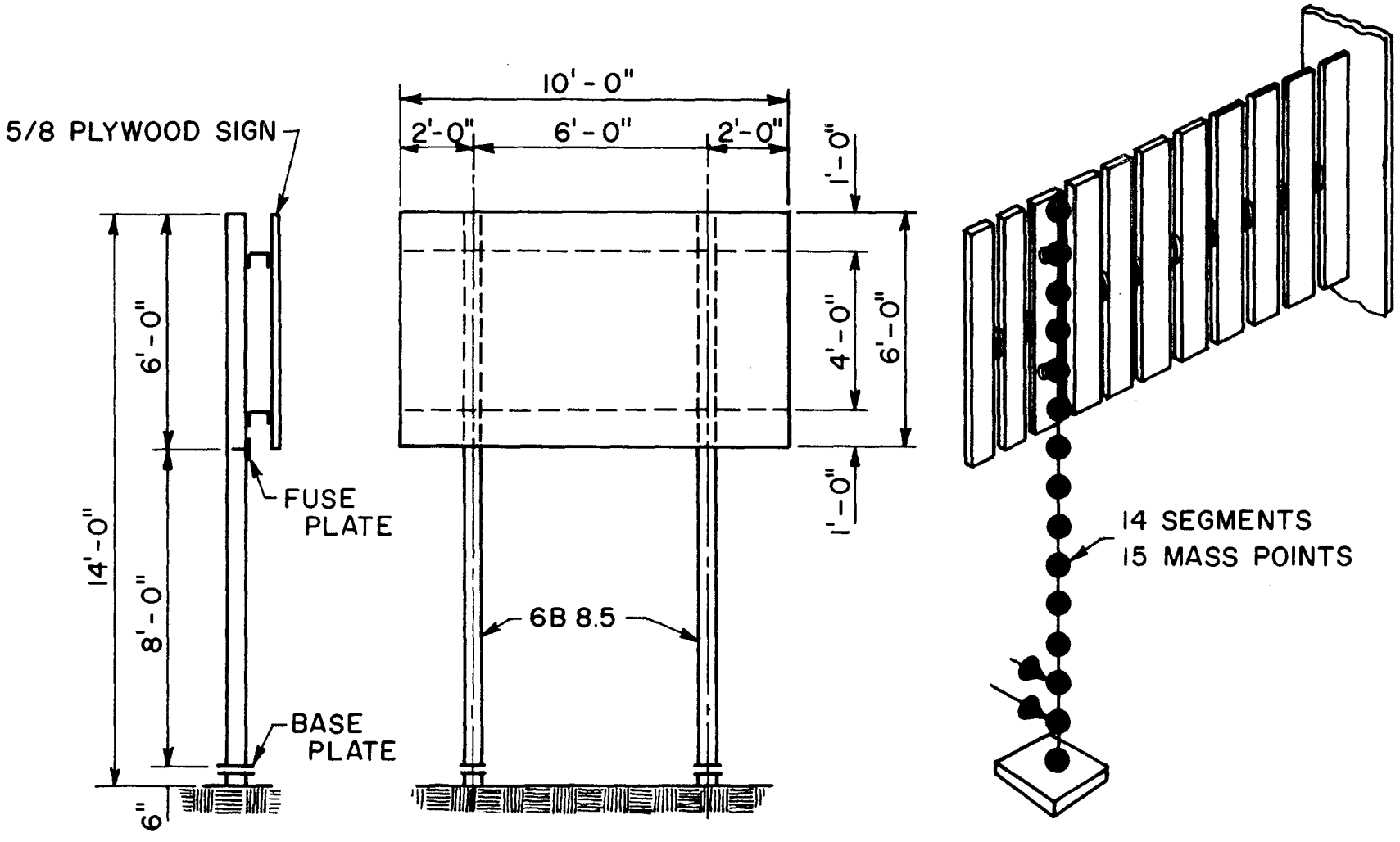

NOTE: SEE TABLE 4.3.1 FOR DETAILS

FIGURE 4.3.3 6B 8.5 POST AND SIGN

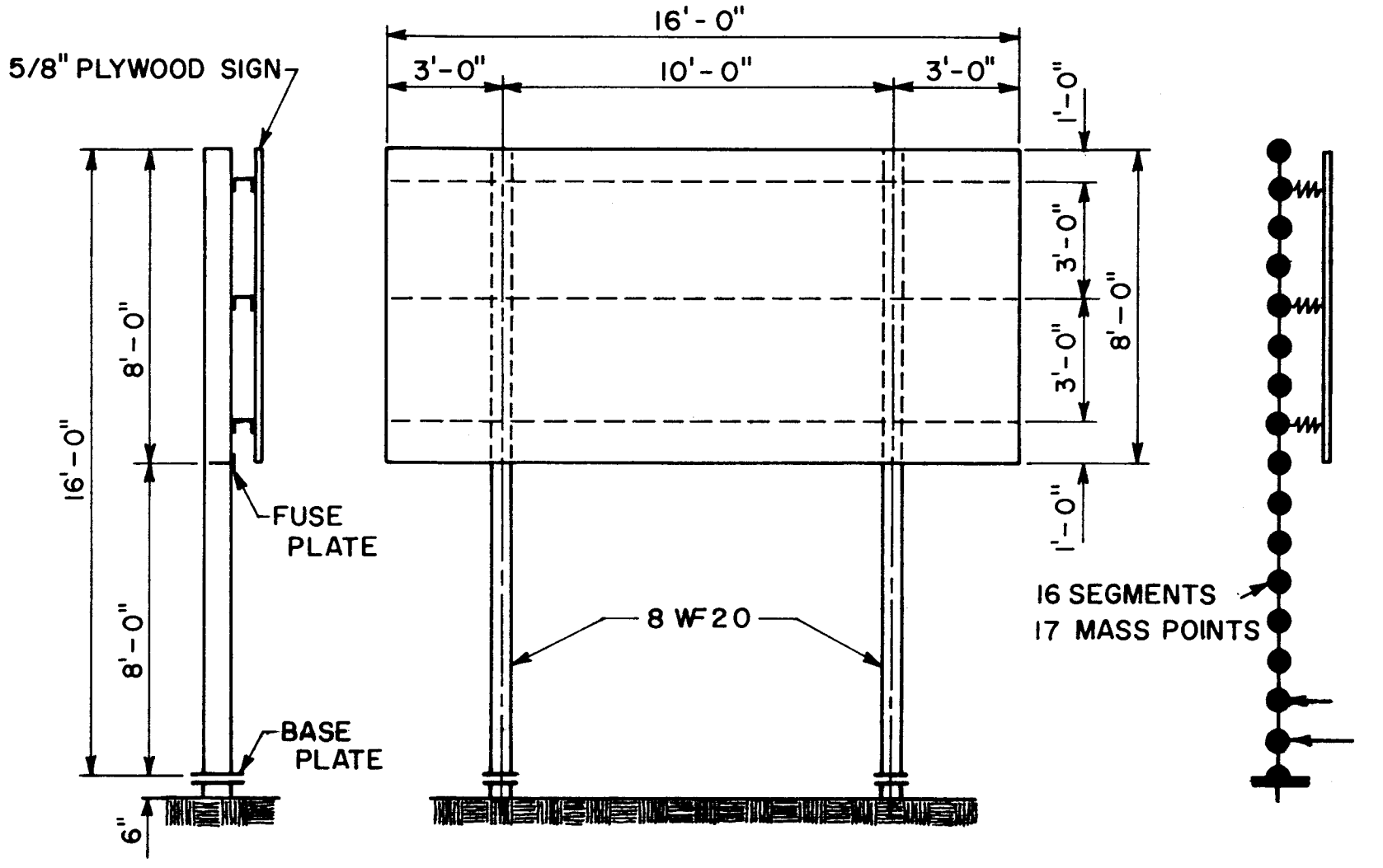

NOTE: SEE TABLE 4.3.1 FOR DETAILS

FIGURE 4.3.4 8 WF 20 POST AND SIGN

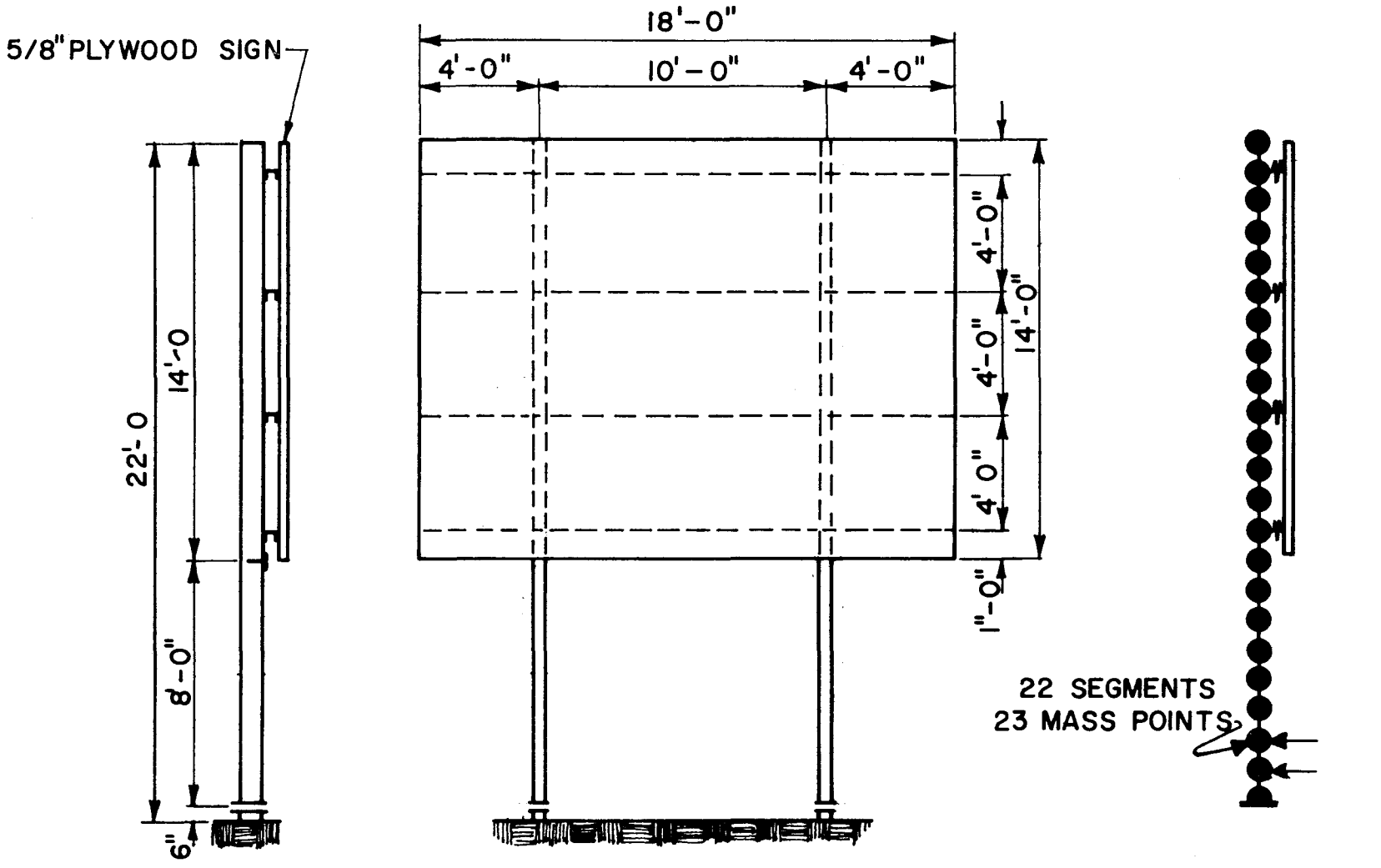

NOTE: SEE TABLE 4.3.1 FOR DETAILS

FIGURE 4.3.5 10 WF 25 POST AND SIGN

TABLE 4.3.1 FIXED PARAMETERS FOR STUDY SUPPORTS

SUPPORT SIZE	BASE PLATE WEIGHT (lb.)	INITIAL BASE* BOLT TENSION (lb.)	INITIAL FUSE PLATE TENSION (lb.)	WINDBEAM	BACKGROUND CONNECTION STIFFNESS (lb./ft.)	f(s) vs. SLIP REF. TO FIGURE PART III, CHAPTER IV
3I5.7	4.0	1,620	12,050	2-3Z2.33	30,000	Fig. 4.6.7
6B8.5	5.67	1,620	12,050	2-3Z2.33	30,000	Fig. 4.6.7
8WF20	10.51	2,250	28,400	3-3Z2.33	30,000	Fig. 4.6.8
10WF25	10.51	2,250	28,400	4-3Z2.33	30,000	Fig. 4.6.9

*f(s) vs. slip mean data curve from Part II, Figure 3.3.1

TABLE 4.3.2 VEHICLE PARAMETERS

VEHICLE WEIGHT (lbs.)	VEHICLE SPEEDS (mph)
1800	15, 40, 65
3600	15, 40, 65
4800	15, 40, 65

Description of problem runs. There were 114 separate problems run in this study. Table 4.3.3 describes the problems, lists the variables and the purpose of each problem. Note that problems 95 through 103 are for supports not included in the balance of the study.

4.4 Results

Summary of all problems. Table 4.4.1 is a summary of the results of the 114 problems solved in this study. Only the data used in constructing the tables and figures are included.

Effects of vehicle velocity and vehicle weight. Figure 4.4.1 through 4.4.4 show the effects of vehicle velocity and vehicle weight on the vehicle deceleration, passenger acceleration and change in vehicle velocity. Figure 4.4.5 through Figure 4.4.8 show the times at which critical events occurred (base release, loss of vehicle-post contact, fuse activation, i.e., when the fuse has slipped sufficiently to activate the "plastic hinge," and maximum fuse plate force).

In general the figures indicate that the vehicle deceleration and passenger acceleration increase as the initial vehicle velocity increases. For a specific initial vehicle velocity the change in velocity decreases as the vehicle becomes heavier. Differences in vehicle crush characteristics and support mass-to-stiffness ratios probably contribute significantly to the overlapping of the vehicle response curves for the 1800 lb. and 3600 lb. vehicles.

TABLE 4.3.3 LIST OF PARAMETER STUDY PROBLEMS

PROBLEM NUMBER	SUPPORT SIZE	VEHICLE WEIGHT (lb.)	VEHICLE VELOCITY (mph)	P U R P O S E
1- 9	3I5.7	1800 3600 4800	15, 40, 65	Study effects of vehicle weight and velocity.
10-18	6B8.5	1800 3600 4800	15, 40, 65	Study effects of vehicle weight and velocity.
19-27	8WF20	1800 3600 4800	15, 40, 65	Study effects of vehicle weight and velocity.
28-36	10WF25	1800 3600 4800	15, 40, 65	Study effects of vehicle weight and velocity.
37-42 69-71	3I5.7	1800 3600	40	Study effects of base bolt tension N' = 3,000, 6,000, 12,050 lbs.
43-48 72-74	6B8.5	1800 3600	40	Study effects of base bolt tension N' = 4,000, 8,000, 19,200 lbs.
49-54 75-77	8WF20	1800 3600	40	Study effects of base bolt tension N' = 6,000, 14,000, 28,400 lbs.
55-60 78-80	10WF25	1800 3600	40	Study effects of base bolt tension N' = 6,000, 14,000, 28,400 lbs.

TABLE 4.3.3 LIST OF PARAMETER STUDY PROBLEMS (Continued)

PROBLEM NUMBER	SUPPORT SIZE	VEHICLE WEIGHT (lb.)	VEHICLE VELOCITY (mph)	P U R P O S E
61-62	3I5.7	1800 3600	40	Study effects of base plate weight, W(1) = 8.0 lbs.
63-64	6B8.5	1800 3600	40	Study effects of base plate weight, W(1) = 11.34 lbs.
65-66	8WF20	1800 3600	40	Study effects of base plate weight, W(1) = 21.02 lbs.
67-68	10WF25	1800 3600	40	Study effects of base plate weight, W(1) = 21.02 lbs.
81-84	8WF20	3600	40	Study effects of background torsional stiffness $*\psi/\psi_{nominal}$ = 0, 1/2, 2, 4.
85-87	6B8.5	3600	40	Study effect of vehicle spring stiffnesses $**K/K_{nominal}$ = 1/2, 1, 2.
88-92	8WF20	3600	40	Study effects of initial fuse plate bolt tension N' = 3,550, 7,200, 14,200, 36,050, 47,250 lbs.
93-94	8WF20	3600	40	Study effects of background-to-post connection stiffness. K = 60,000, 90,000 lb./ft.
95-97	8WF30	1800 3600 4800	40	Study effects of support weight.

$*\psi_{nominal}$ = stiffness of 8' x 16' x 5/8" plywood background.

$**K_{nominal}$ = stiffness of vehicle springs for 1955 Ford, see Figure 8.3.2 of Part III.

TABLE 4.3.3 LIST OF PARAMETER STUDY PROBLEMS (Continued)

PROBLEM NUMBER	SUPPORT SIZE	VEHICLE WEIGHT (lb.)	VEHICLE VELOCITY (mph)	P U R P O S E
98-100	12WF30	1800 3600 4800	40	Study effects of support weight.
101-103	12WF45	1800 3600 4800	40	Study effects of support weight.
104-106	12WF58	1800 3600 4800	40	Study effects of support weight.
107-108	3I5.7	1800 3600	40	Study effects of base plate weight W(1) = 16.0 lb.
109-110	6B8.5	1800 3600	40	Study effects of base plate weight W(1) = 22.68 lb.
111-112	8WF20	1800 3600	40	Study effects of base plate weight W(1) = 42.04 lb.
113-114	10WF25	1800 3600	40	Study effects of base plate weight W(1) = 42.04 lb.

TABLE 4.4.1 SUMMARY OF PARAMETER STUDY RESULTS

Problem Number	Post Size	Vehicle Weight (lb.)	Vehicle Velocity (mph)	t_1 (mms.)*	t_2 (mms.)*	t_3 (mms.)*	t_4 (mms.)*	Vehicle Deceleration (g's)	Passenger Acceleration (g's)	Change in Vehicle Velocity (mph)	Maximum Connector Force (lb.)	Comments	Ang. Velocity Adequate **	Post Yielded***
1	3I5.7	1800	15	160	165	300+	---	6.40	9.05	14.53	4421		?	X
2	3I5.7	1800	40	55	63	66	63	8.59	8.44	6.31	1181			X
3	3I5.7	1800	65	34	43	44	42	10.79	7.00	4.94	1577			X
4	3I5.7	3600	15	41	46	209	183	4.71	3.15	2.23	7487	SEE		X
5	3I5.7	3600	40	17	25	33	27	6.39	2.14	1.45	4476	Fig. 4.3.2		X
6	3I5.7	3600	65	12	22	21	16	7.95	2.20	1.48	7832			X
7	3I5.7	4800	15	42	45	78	53	3.26	2.42	1.72	4755			X
8	3I5.7	4800	40	17	22	28	25	3.82	1.47	1.00	2347			X
9	3I5.7	4800	65	12	18	22	20	4.47	1.42	0.96	2809			X
10	6B8.5	1800	15	58	68	300+	---	3.31	3.59	2.74	3777		?	
11	6B8.5	1800	40	25	40	39	35	4.47	3.30	2.31	1918			
12	6B8.5	1800	65	18	35	29	26	5.80	3.89	2.69	1904			
13	6B8.5	3600	15	22	29	300+	---	2.04	1.05	0.72	6041	SEE	?	
14	6B8.5	3600	40	11	21	21	17	4.30	1.39	0.94	5221	Fig. 4.3.3		
15	6B8.5	3600	65	9	19	15	13	6.73	1.98	1.33	4744			
16	6B8.5	4800	15	20	26	300+	---	1.58	0.74	0.51	5851		?	
17	6B8.5	4800	40	11	19	20	17	2.60	0.96	0.65	4454			
18	6B8.5	4800	65	8	17	16	13	3.67	1.29	0.87	2095			
19	8WF20	1800	15	96	113	300+	---	5.06	7.30	7.07	5721		?	
20	8WF20	1800	40	40	65	63	51	7.07	7.83	5.84	5106			
21	8WF20	1800	65	29	53	46	39	11.32	9.69	6.97	4421	SEE		
22	8WF20	3600	15	34	43	300+	---	3.95	2.57	1.81	7066	Fig. 4.3.4	?	
23	8WF20	3600	40	17	31	39	26	7.95	3.66	2.49	7693			
24	8WF20	3600	65	12	28	24	19	11.59	5.05	3.43	5527			

TABLE 4.4.1 SUMMARY OF PARAMETER STUDY RESULTS
(Continued)

Problem Number	Post Size	Vehicle Weight (lb.)	Vehicle Velocity (mph)	t_1 (mms.)*	t_2 (mms.)*	t_3 (mms.)*	t_4 (mms.)*	Vehicle Deceleration (g's)	Passenger Acceleration (g's)	Change in Vehicle Velocity (mph)	Maximum Connector Force (lb.)	Comments	Ang. Velocity Adequate **	Post Yielded***
25	8WF20	4800	15	32	41	300+	---	2.58	1.87	1.31	8375		?	
26	8WF20	4800	40	18	31	35	27	4.51	2.58	1.76	5609			
27	8WF20	4800	65	14	27	26	21	6.36	3.41	2.32	5111			
28	10WF25	1800	15	125	140	300+	---	5.94	8.68	10.68	7322		?	
29	10WF25	1800	40	45	69	64	56	7.88	9.00	6.85	3512			
30	10WF25	1800	65	34	58	49	43	14.45	12.16	8.85	3369			
31	10WF25	3600	15	38	47	300+	---	4.77	3.22	2.29	8349	SEE	?	
32	10WF25	3600	40	20	33	33	26	9.53	4.78	3.27	7425	Fig. 4.3.5		
33	10WF25	3600	65	14	31	25	19	13.44	6.39	4.36	6648			
34	10WF25	4800	15	37	47	300+	---	3.04	2.47	1.76	7804		?	
35	10WF25	4800	40	22	35	37	30	5.57	3.57	2.46	3995			
36	10WF25	4800	65	17	30	28	23	9.93	4.82	3.30	5515			
37	3I5.7	1800	40	---	---	---	---	11.83	18.15	39.91	3954	N' = 6000	No	X
38	3I5.7	1800	40	---	---	---	---	11.85	18.21	39.91	4161	N' = 12050	No	X
39	3I5.7	3600	40	---	---	---	---	6.61	9.76	31.45	6032	N' = 6000		X
40	3I5.7	3600	40	---	---	---	---	6.64	9.76	31.46	6299	N' = 12050		X
41	3I5.7	4800	40	---	---	278	263	4.43	7.36	23.50	7044	N' = 6000		X
42	3I5.7	4800	40	---	---	---	---	4.43	7.19	23.61	5410	N' = 12050		X
43	6B8.5	1800	40	110	117	119	117	22.77	30.57	28.82	4287	N' = 8000		X
44	6B8.5	1800	40	---	---	---	---	22.84	35.81	39.91	4105	N' = 19200	No	X
45	6B8.5	3600	40	32	36	40	37	13.45	7.71	5.31	6414	N' = 8000		X
46	6B8.5	3600	40	---	---	---	---	14.69	25.81	39.91	8492	N' = 19200	No	X
47	6B8.5	4800	40	35	39	41	39	9.97	5.41	3.77	3612	N' = 8000		X
48	6B8.5	4800	40	---	---	45	41	12.12	20.98	39.90	9496	N' = 19200	No	X

TABLE 4.4.1 SUMMARY OF PARAMETER STUDY RESULTS
(Continued)

Problem Number	Post Size	Vehicle Weight (lb.)	Vehicle Velocity (mph)	t_1 (mms.)*	t_2 (mms.)*	t_3 (mms.)*	t_4 (mms.)*	Vehicle Deceleration (g's)	Passenger Acceleration (g's)	Change in Vehicle Velocity (mph)	Maximum Connector Force (lb.)	Comments	Ang. Velocity Adequate **	Post Yielded***
49	8WF20	1800	40	---	---	---	---	27.46	38.58	39.91	7064	N' = 14000	No	
50	8WF20	1800	40	---	---	---	---	27.66	38.63	39.93	816	N' = 28400	No	
51	8WF20	3600	40	41	48	51	45	20.31	14.56	10.24	9997	N' = 14000	?	
52	8WF20	3600	40	---	---	---	---	31.88	47.20	39.91	5175	N' = 28400	No	X
53	8WF20	4800	40	42	48	50	45	14.72	9.03	6.40	7884	N' = 14000		
54	8WF20	4800	40	64	69	72	68	25.92	23.11	17.25	7746	N' = 28400		X
55	10WF25	1800	40	98	112	111	107	25.65	29.69	27.15	9716	N' = 14000		
56	10WF25	1800	40	---	---	---	---	27.67	38.64	39.92	744	N' = 28400	No	
57	10WF25	3600	40	36	45	46	42	18.06	12.11	8.44	9455	N' = 14000		X
58	10WF25	3600	40	---	---	---	---	33.86	47.64	39.91	3743	N' = 28400	No	X
59	10WF25	4800	40	39	46	48	42	13.09	8.07	5.70	5775	N' = 14000		
60	10WF25	4800	40	70	75	79	74	29.51	28.63	21.82	8845	N' = 28400		X
61	3I5.7	1800	40	56	65	68	64	9.06	8.86	6.64	1826	W(1) = 8.0		X
62	3I5.7	3600	40	18	29	39	32	6.40	2.27	1.54	6193	W(1) = 8.0		X
63	6B8.5	1800	40	26	42	40	36	4.63	3.62	2.54	2363	W(1) = 11.34		
64	6B8.5	3600	40	12	22	22	18	4.63	1.59	1.08	4740	W(1) = 11.34		
65	8WF20	1800	40	40	67	67	53	7.22	8.31	6.26	4938	W(1) = 21.02		
66	8WF20	3600	40	17	32	300+	---	8.19	3.97	2.71	9592	W(1) = 21.02	?	
67	10WF25	1800	40	45	72	66	56	7.98	9.54	7.31	3549	W(1) = 21.02		
68	10WF25	3600	40	20	35	35	27	9.91	5.21	3.56	6784	W(1) = 21.02		
69	3I5.7	1800	40	63	70	74	72	11.36	10.64	8.17	2035	N' = 3000		X
70	3I5.7	3600	40	22	25	42	31	6.57	2.77	1.88	4801	N' = 3000		X
71	3I5.7	4800	40	20	24	32	28	4.28	1.84	1.25	3429	N' = 3000		X
72	6B8.5	1800	40	48	62	59	57	8.97	8.41	6.25	5252	N' = 4000		X

TABLE 4.4.1 SUMMARY OF PARAMETER STUDY RESULTS
(Continued)

Problem Number	Post Size	Vehicle Weight (lb.)	Vehicle Velocity (mph)	t_1 (mms.)*	t_2 (mms.)*	t_3 (mms.)*	t_4 (mms.)*	Vehicle Deceleration (g's)	Passenger Acceleration (g's)	Change in Vehicle Velocity (mph)	Maximum Connector Force (lb.)	Comments	Ang. Velocity Adequate **	Post Yielded***
73	6B8.5	3600	40	25	31	33	30	11.27	5.05	3.44	6192	N' = 4000		X
74	6B8.5	4800	40	20	26	26	24	4.64	2.13	1.45	5518	N' = 4000		
75	8WF20	1800	40	68	83	83	76	14.53	14.62	11.72	5204	N' = 6000		
76	8WF20	3600	40	21	32	38	28	9.78	4.70	3.20	7811	N' = 6000		
77	8WF20	4800	40	24	35	38	31	5.83	3.70	2.55	5236	N' = 6000		
78	10WF25	1800	40	69	85	84	76	15.31	15.72	12.74	5483	N' = 6000		
79	10WF25	3600	40	22	35	35	27	10.84	5.65	3.86	8174	N' = 6000		
80	10WF25	4800	40	27	39	40	33	6.51	4.50	3.13	6274	N' = 6000		
81	8WF20	3600	40	17	31	39	26	7.89	3.62	2.47	9796	$\lambda/\lambda_n = \frac{1}{2}$		
82	8WF20	3600	40	17	31	36	26	7.95	3.66	2.49	8063	$\lambda/\lambda_n = 2$		
83	8WF20	3600	40	17	32	34	25	7.96	3.66	2.49	8495	$\lambda/\lambda_n = 4$		
84	8WF20	3600	40	17	31	189	185	7.93	3.63	2.48	9918	$\lambda/\lambda_n = 0$		
85	8WF20	3600	40	22	43	48	33	5.98	3.83	2.65	6574	$K/K_n = \frac{1}{2}$		
86	8WF20	3600	40	17	31	39	26	7.95	3.66	2.49	7693	$K/K_n = 1$		
87	8WF20	3600	40	13	23	32	20	10.05	3.48	2.35	8677	$K/K_n = 2$		
88	8WF20	3600	40	17	30	30	24	8.03	3.61	2.45	4017	N' = 3550		
89	8WF20	3600	40	17	31	32	24	7.99	3.62	2.46	5473	N' = 14200		
90	8WF20	3600	40	17	31	31	24	8.02	3.61	2.46	4499	N' = 7200		
91	8WF20	3600	40	17	31	197	182	7.93	3.66	2.50	9529	N' = 36050		
92	8WF20	3600	40	17	32	300+	---	7.94	3.70	2.53	9978	N' = 47250	?	
93	8WF20	3600	40	17	31	39	26	8.00	3.69	2.51	7254	K = 60000		
94	8WF20	3600	40	17	31	38	26	8.03	3.70	2.52	9455	K = 90000		
95	8WF35	1800	40	47	76	69	58	8.42	10.45	8.18	3605		No	
96	8WF35	3600	40	20	37	35	27	10.45	5.91	4.07	6735			

TABLE 4.4.1 SUMMARY OF PARAMETER STUDY RESULTS
(Continued)

Problem Number	Post Size	Vehicle Weight (lb.)	Vehicle Velocity (mph)	t_1 (mms.)*	t_2 (mms.)*	t_3 (mms.)*	t_4 (mms.)*	Vehicle Deceleration (g's)	Passenger Acceleration (g's)	Change in Vehicle Velocity (mph)	Maximum Connector Force (lb.)	Comments	Ang. Velocity Adequate **	Post Yielded***
97	8WF35	4800	40	23	39	39	32	6.00	4.27	2.98	4381			
98	12WF40	1800	40	66	88	81	74	14.94	16.18	13.31	3663			
99	12WF40	3600	40	38	38	34	28	11.34	6.53	4.50	4816			
100	12WF40	4800	40	25	40	37	32	6.32	4.59	3.21	4868			
101	12WF45	1800	40	69	91	84	77	15.98	17.54	14.61	4455			
102	12WF45	3600	40	23	41	36	30	12.33	7.73	5.35	5564			
103	12WF45	4800	40	26	43	39	34	7.20	5.42	3.81	4738			
104	12WF58	1800	40	73	97	89	81	17.60	20.06	17.10	4093			
105	12WF58	3600	40	25	45	38	32	13.59	9.37	6.53	3618			
106	12WF58	4800	40	29	46	42	37	9.40	6.81	4.83	4910			
107	3I5.7	1800	40	58	68	76	67	9.81	9.57	7.28	5240	W(1) = 16.0		X
108	3I5.7	3600	40	18	35	65	46	6.54	2.59	1.78	7411	W(1) = 16.0		X
109	6B8.5	1800	40	26	47	44	38	4.90	4.21	2.98	1570	W(1) = 22.68		
110	6B8.5	3600	40	12	25	25	20	5.15	1.98	1.34	3606	W(1) = 22.68		
111	8WF20	1800	40	40	72		56	7.44	9.10	7.00	5778	W(1) = 42.04	?	
112	8WF20	3600	40	17	34		57	8.66	4.54	3.11	7990	W(1) = 42.04	?	
113	10WF25	1800	40	45		68	57	8.12		7.88	6414	W(1) = 42.04		
114	10WF25	3600	40	20	37	37	28	10.19	5.74	3.95	5580	W(1) = 42.04		

*t_1 = time of base release

t_2 = time of loss of vehicle contact

t_3 = time when fuse plate activates

t_4 = time when fuse force is maximum

**A blank indicates adequate angular velocity

***A blank indicates no yielding in the post

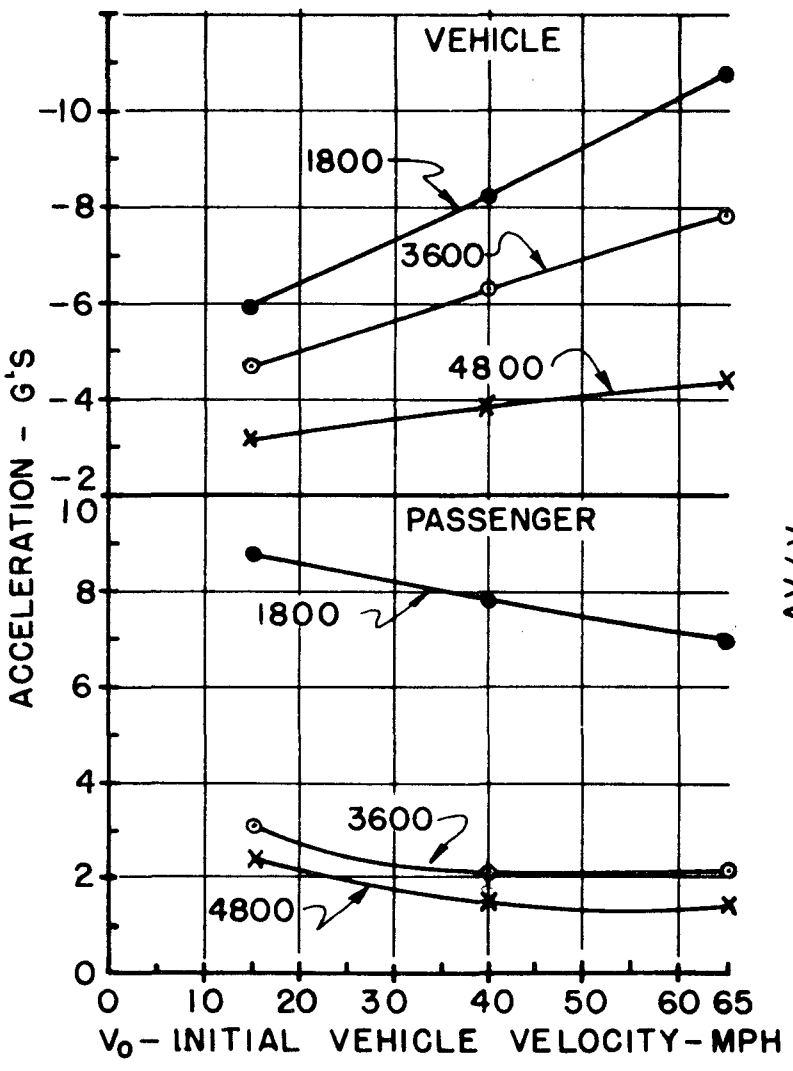

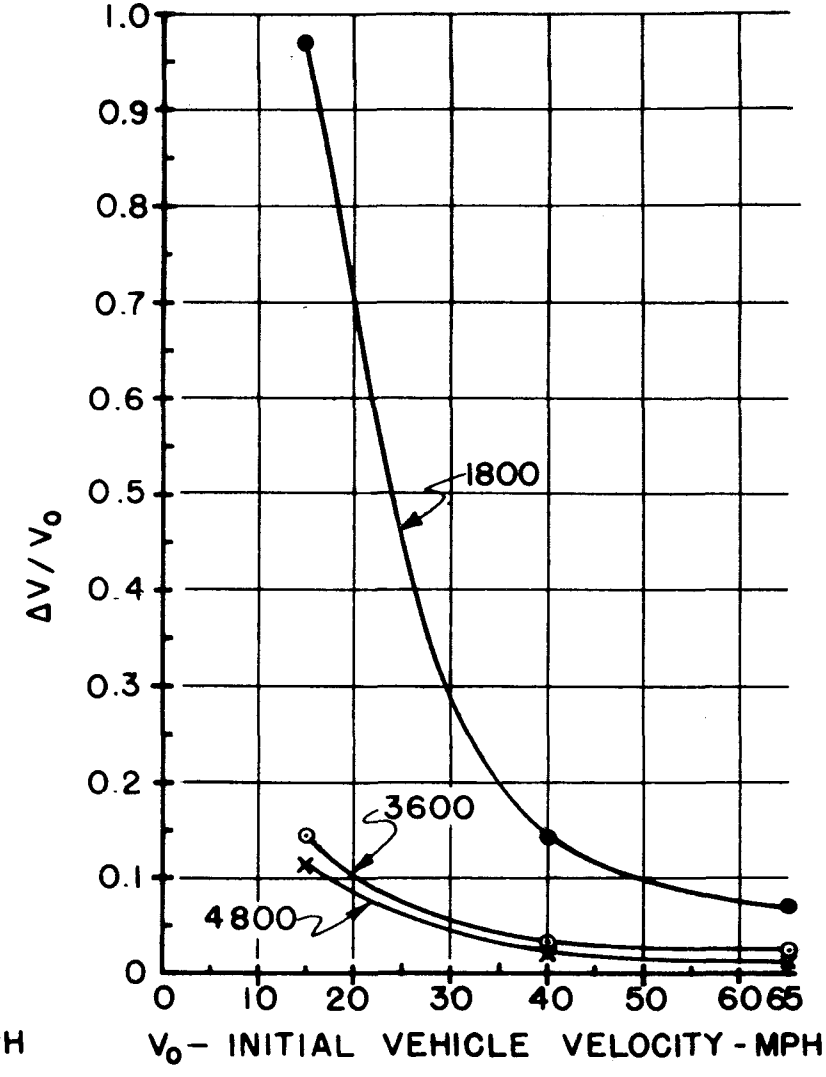

FIGURE 4.4.1 3I5.7 SUPPORT

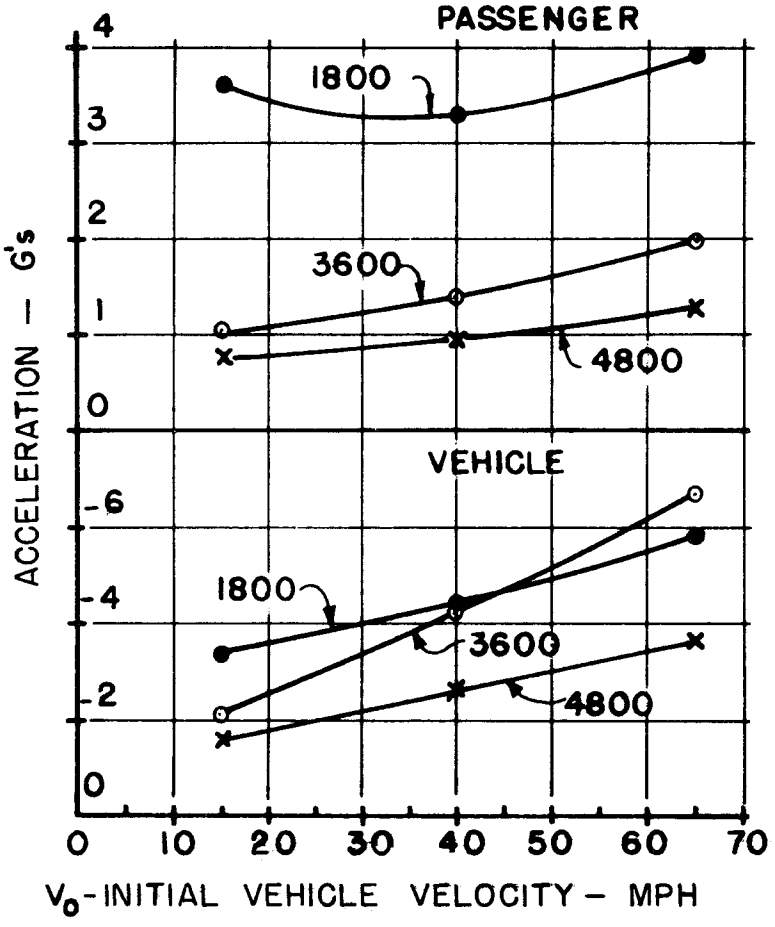

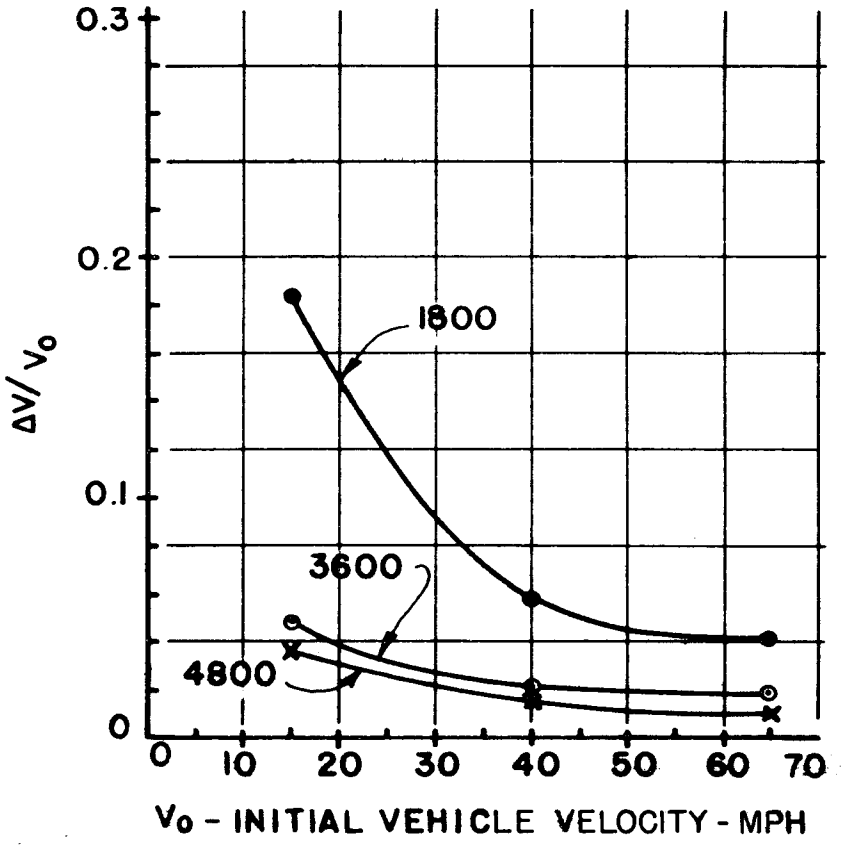

FIGURE 4.42 6B8.5 SUPPORT

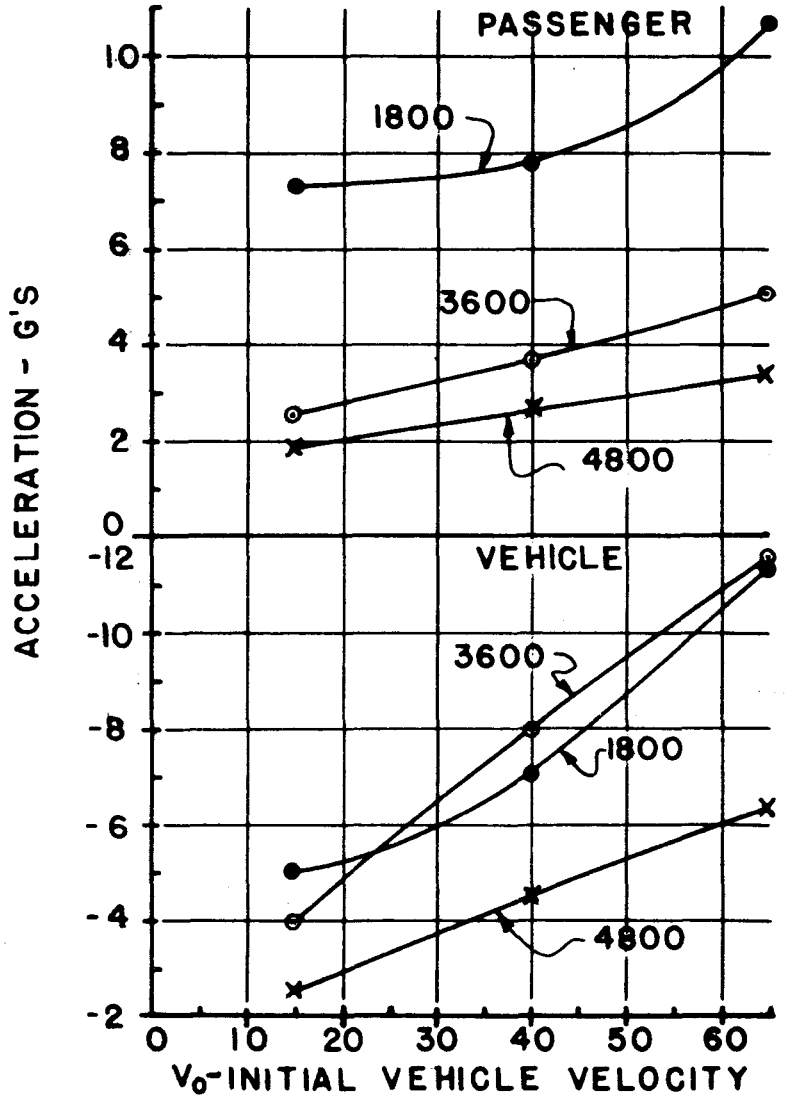

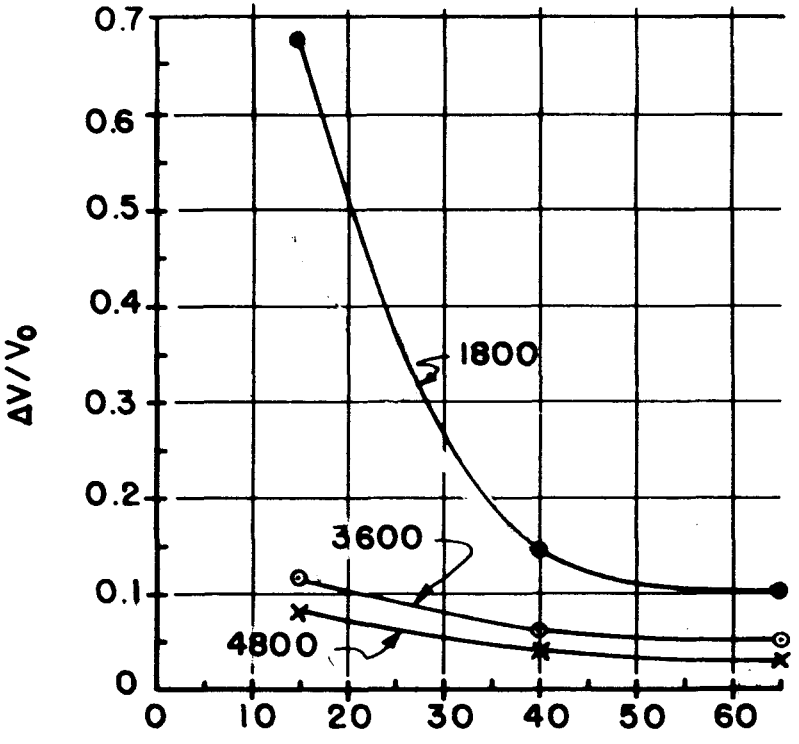

FIGURE 4.43 8WF 20 SUPPORT

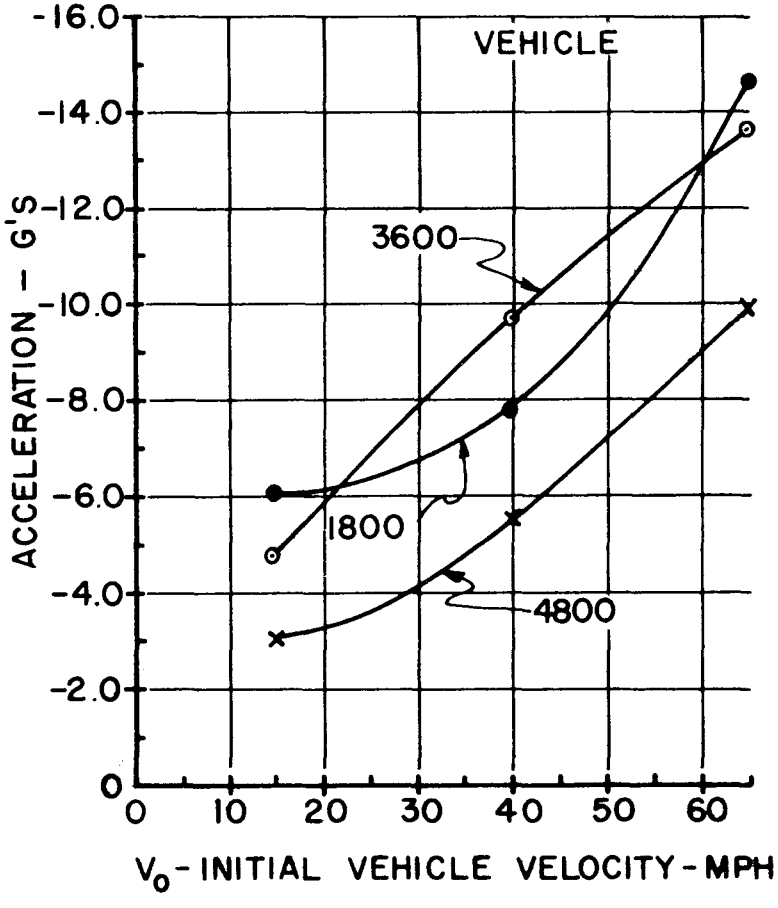

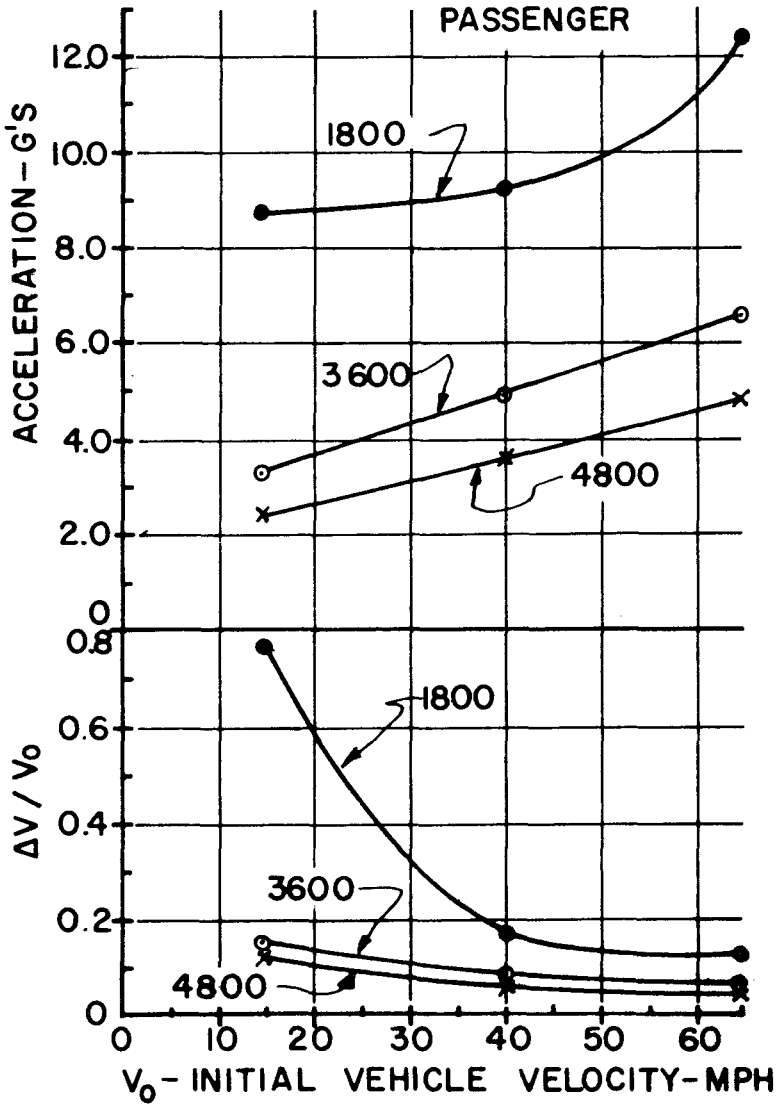

FIGURE 4.4.4 - 10WF25 SUPPORT

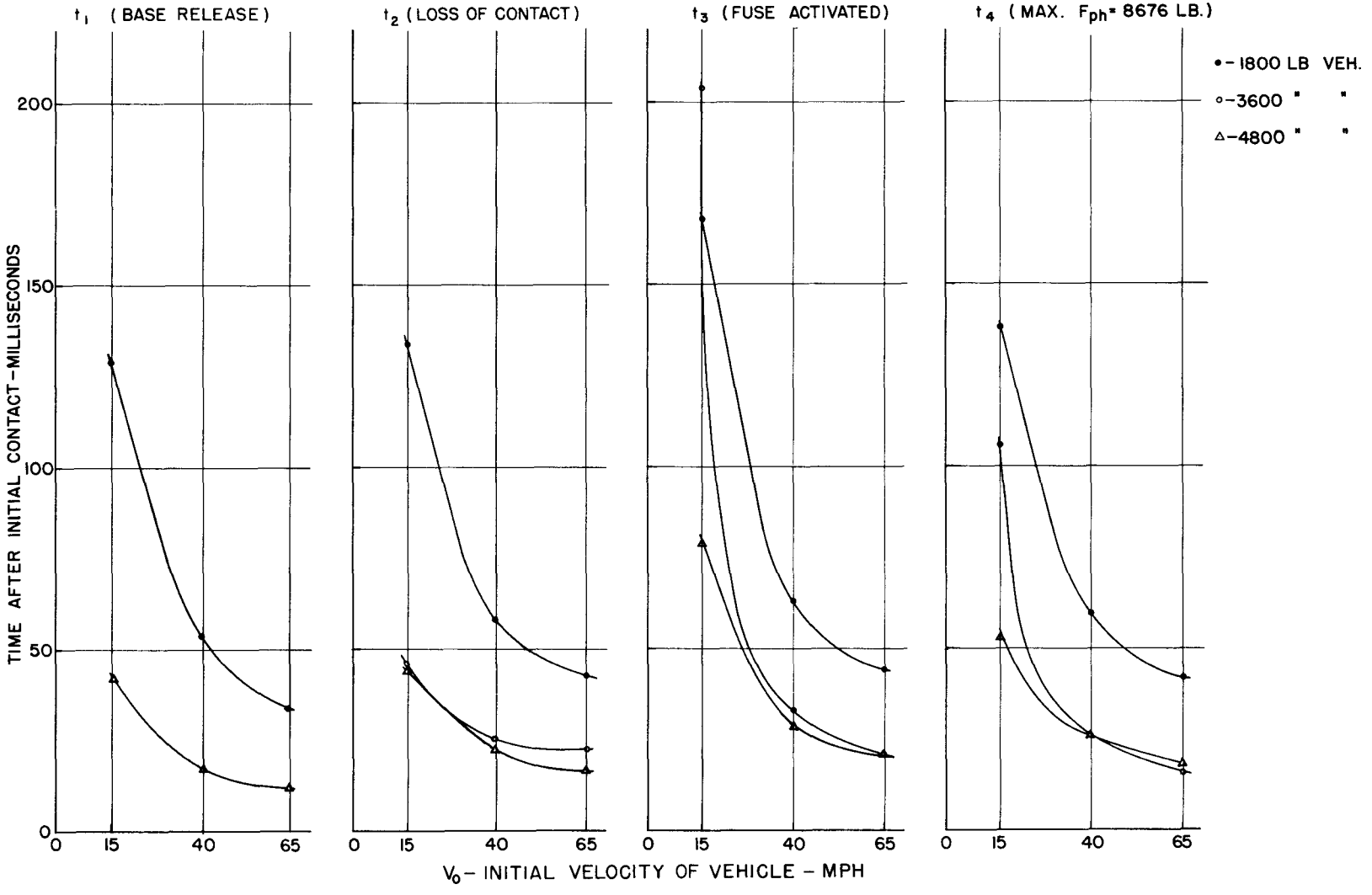

FIGURE 4.4.5 - TIME OF CRITICAL EVENTS (3I5.7)

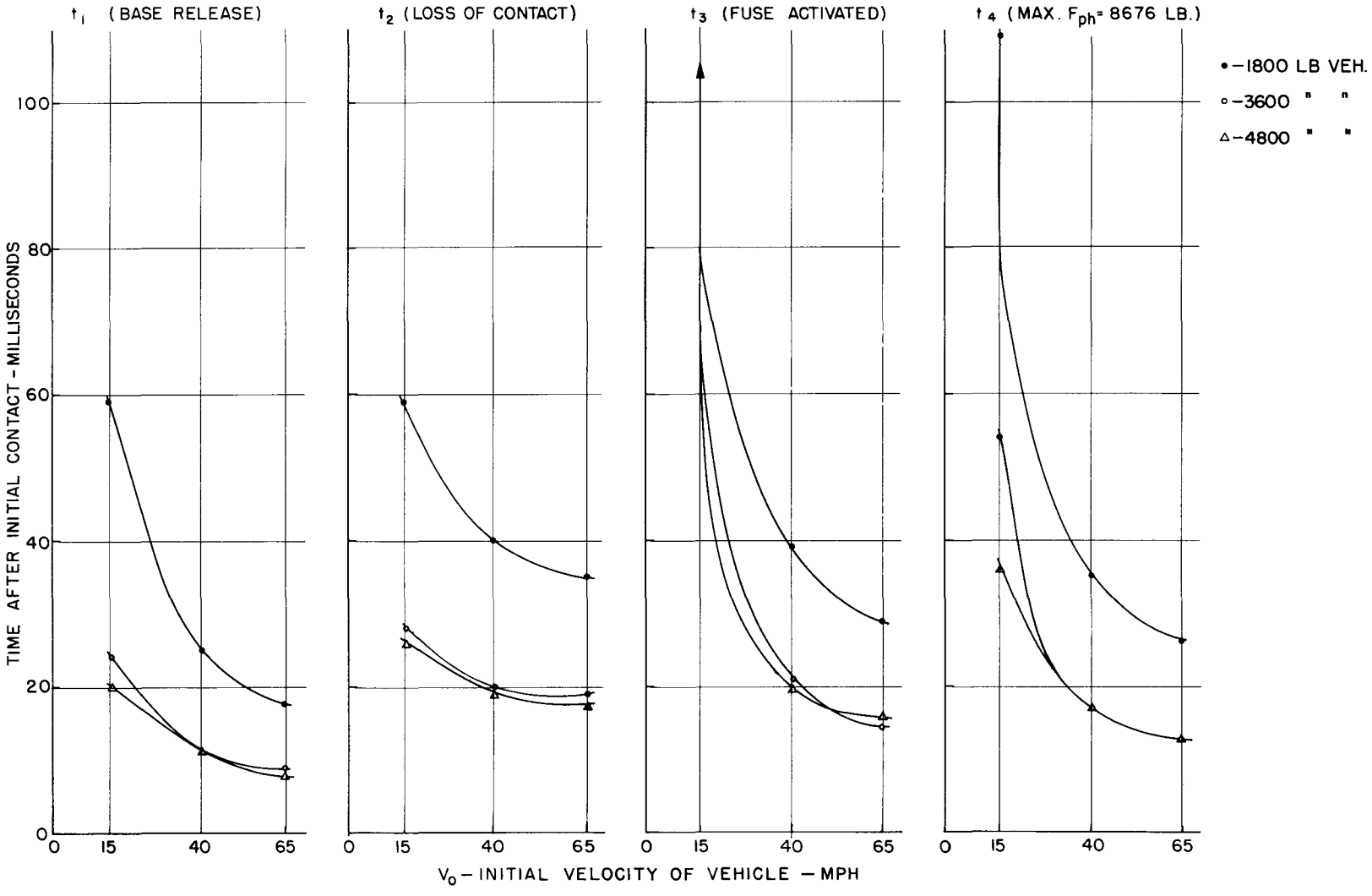

FIGURE 4.4.6 – TIME OF CRITICAL EVENTS (6B8.5)

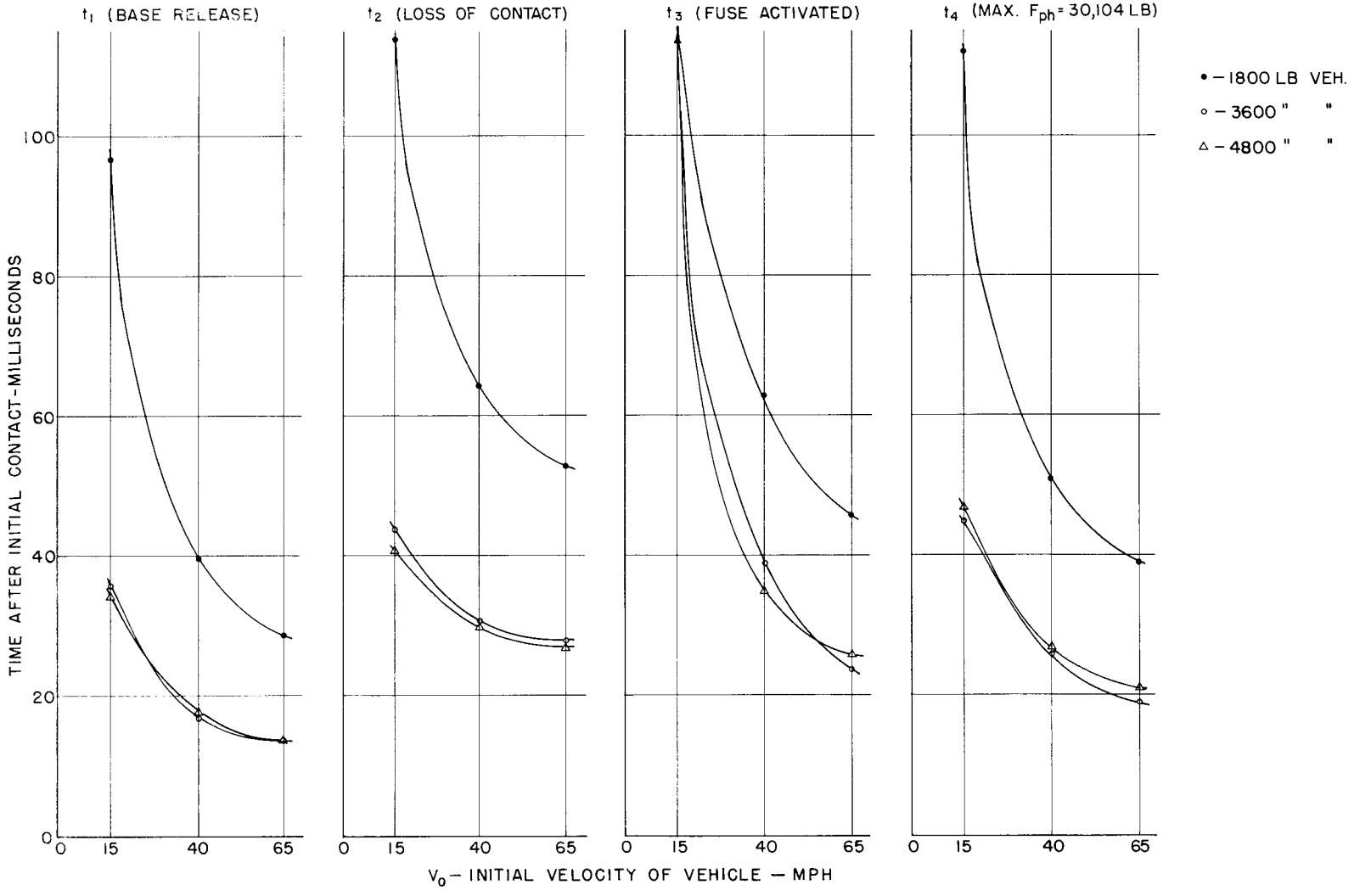

FIGURE 4.4.7 - TIME OF CRITICAL EVENTS (8WF20)

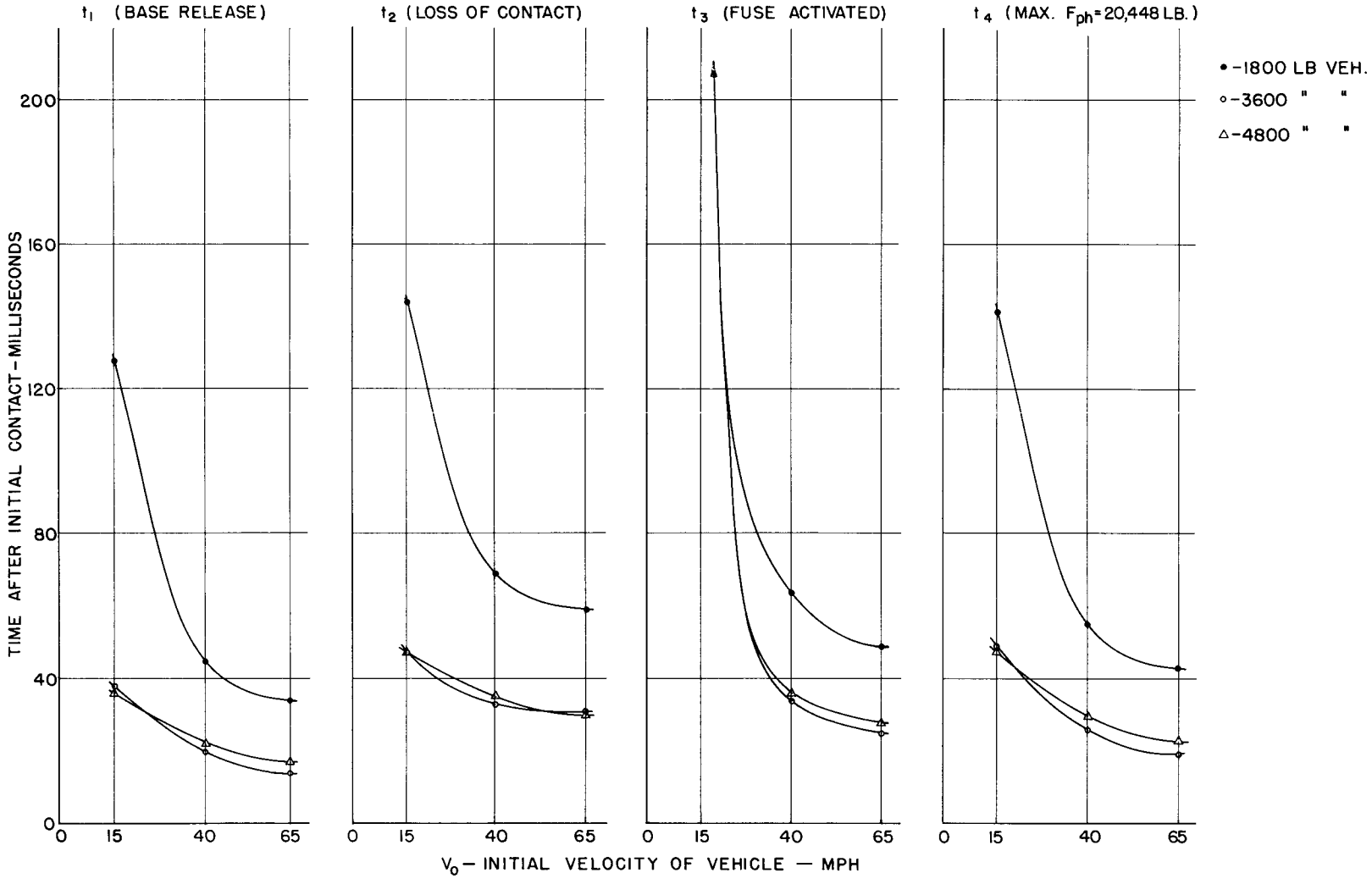

FIGURE 4.4.8 - TIME OF CRITICAL EVENTS (10WF25)

In Figure 4.4.1, for the 3I5.7 support, the trends of the data for the passenger acceleration are reversed to the general trends for the other three supports, i.e., the passenger acceleration decreases with increased initial vehicle velocity. This phenomena can be attributed to the inelastic behavior and attendant large deflections of the support post. A study of the detailed computer outputs for the problems covering collisions with the 3I5.7 support showed that the support yielded at the base and rotated in the direction of the vehicle movement about the plastic hinge thus formed (this behavior is not to be confused with the artificial "plastic hinge" in the upper portion of the support post). The vehicle thus tended to ride over the post before the base finally released. This inelastic action prolonged the time in which the vehicle was in contact with the post and hence affected the passenger response. An attempt was made to determine if the support post would clear the vehicle. This was accomplished by determining the angular velocity of post as it rotated about the "plastic hinge." It was assumed that if the post had sufficient angular velocity, when contact with the vehicle was lost, for the base to reach a maximum elevation above the ground of five feet, it would clear the vehicle. The last column in Table 4.4.1 indicates whether or not this condition was achieved. Note that in problem 1-36 in those cases when the fuse activated (t_3) in less than 300 milliseconds the criteria for safe operation was satisfied. In those problems in which t_3 is indicated as 300+ it is assumed that the "plastic hinge" did not form. Whether or not the post would

clear the vehicle in these cases is not known. It should be noted that all of these conditions occurred in collisions at the 15 mph speed.

In order to keep from misinterpreting the results presented here, it must be re-emphasized that the studies were conducted on operational sign supports and the parameters of each system have definite and different effects on the response. The following subsections will give the results of limited studies on the effects of the variations of the system parameters.

Effects of initial base bolt tension. Figure 4.4.9 through Figure 4.4.11 show the effects of the initial base bolt tension on the parameters of vehicle deceleration and velocity change.

The figures indicate that the light supports (3I5.7 and 6B8.5) are critically influenced by the initial bolt tension for collisions of all vehicles at 40 mph. Table 4.4.2 lists the critical values of bolt tension for each support which will cause vehicles impacting at 40 mph to be completely stopped. Table 4.4.3 shows the effect of initial base bolt tension on the acceleration of the simulated passenger and indicates that the severity of the collision, as measured by the passenger deceleration, increases with the support stiffness. The light supports yielded upon impact and hence absorbed a portion of the energy. For the heavier supports the stiffness of the support caused the major portion of the energy to be absorbed in vehicle crushing.

Base plate weight. Table 4.4.4 illustrates the influence of increased base plate weight on the system response for collision by an 1800 lb. vehicle at 40 mph. Table 4.4.5 is for the 3600 lb. vehicle at 40 mph. In both cases, for all supports the g's on the

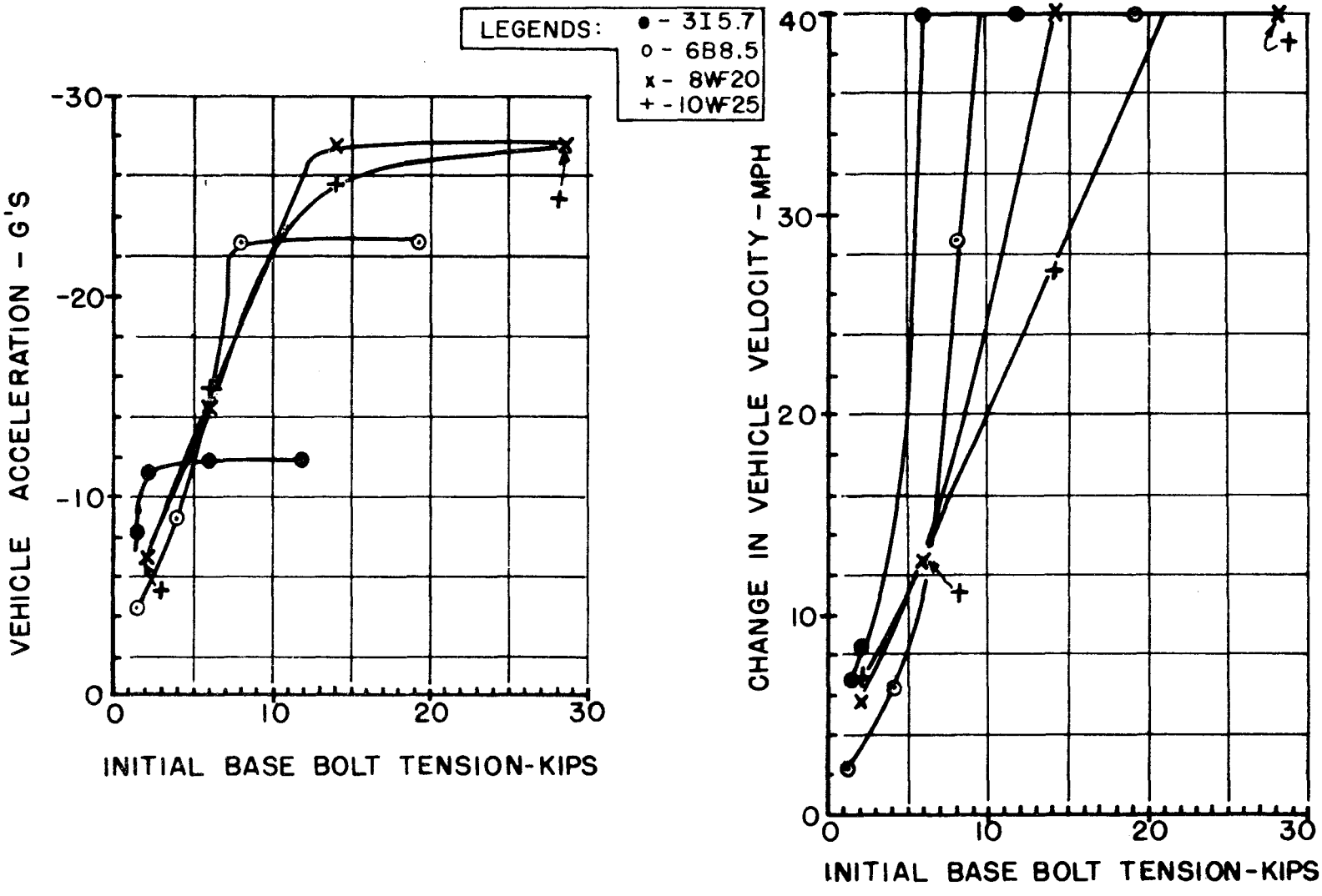

FIGURE 4.4.9 - 1800 LB VEHICLE, V_o = 40 MPH

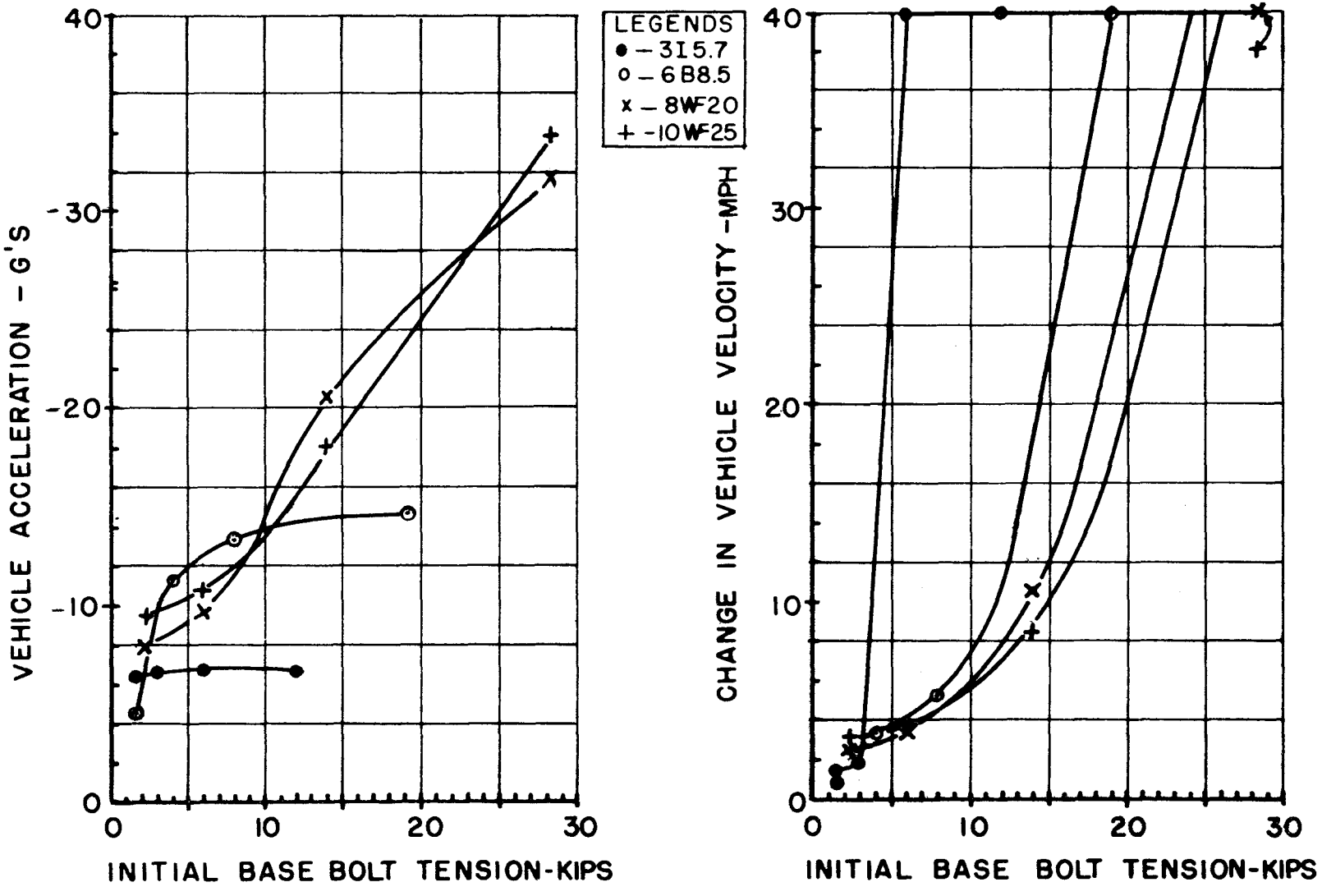

FIGURE 4.4.10 – 3600 LB VEHICLE, V_o = 40 MPH

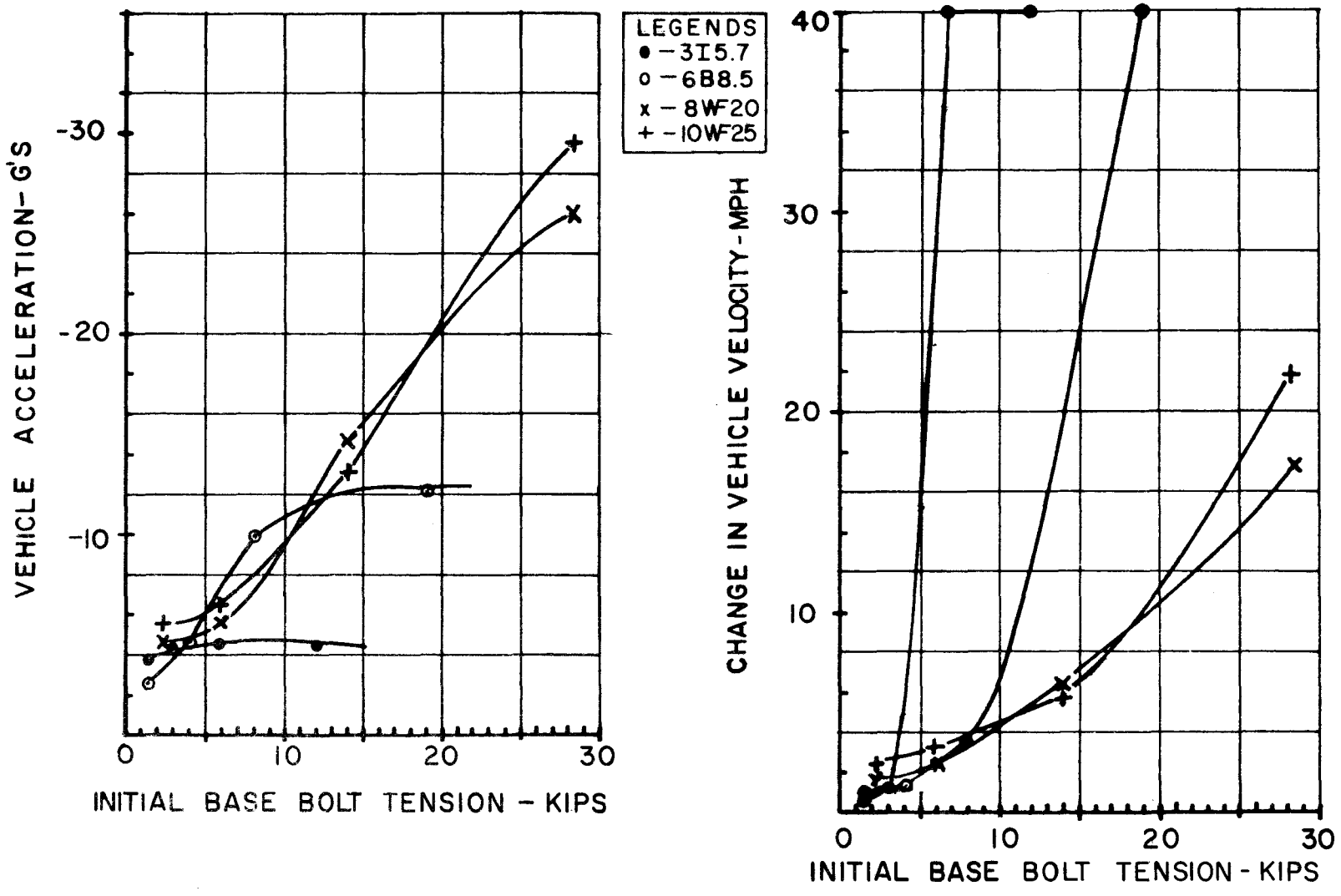

FIGURE 4.4.11-4800 LB VEHICLE V_o = 40 M.P.H.

TABLE 4.4.2 CRITICAL BASE BOLT TENSION TO STOP VEHICLE FOR 40 MPH COLLISION

SUPPORT	VEHICLE WEIGHT (lb.)	CRITICAL BOLT TENSION (lb.)
3I5.7	1800	6000
	3600	6000
	4800	6000
6B8.5	1800	10000
	3600	19000
	4800	19000
8WF20	1800	14000
	3600	29000
	4800	29000+
10WF25	1800	19000
	3600	29000
	4800	29000+

TABLE 4.4.3 EFFECT OF BASE BOLT TENSION ON SIMULATED PASSENGER ACCELERATION

SUPPORT	*VEHICLE WEIGHT (LB.)	PASSENGER ACCELERATION (g)			
		BOLT TENSION (LB.)			
		1620	3000	6000	12050
3I5.7	1800	8.44	10.64	18.15	18.24
	3600	2.14	2.77	9.76	9.76
	4800	1.47	1.84	7.36	7.19
		BOLT TENSION (LB.)			
		1620	4000	8000	19200
6B8.5	1800	3.30	8.41	30.57	35.81
	3600	1.39	5.05	7.77	25.81
	4800	0.96	2.13	5.41	10.98
		BOLT TENSION (LB.)			
		2250	6000	14000	28400
8WF20	1800	7.83	14.62	38.58	38.63
	3600	3.66	4.70	14.56	47.20
	4800	7.58	3.70	7.03	23.11
		BOLT TENSION (LB.)			
		2250	6000	14000	28400
10WF25	1800	9.15	15.72	29.69	38.64
	3600	4.88	5.65	12.11	47.64
	4800	3.57	4.50	8.07	78.63

*Vehicle input velocity = 40 mph.

TABLE 4.4.4 EFFECT OF BASE PLATE WEIGHT (1800 LB. VEHICLE, 40 MPH)

SUPPORT POST	WEIGHT OF BASE PLATE (lb.)	VEHICLE DECELERATION (g's)	PASSENGER ACCELERATION (g's)	VELOCITY CHANGE (mph)	$*t_1$ (sec.)	$*t_2$ (sec.)	$*t_3$ (sec.)	$*t_4$ (sec.)
3I5.7	4.0	8.59	8.44	5.81	0.053	0.060	0.063	0.060
	8.0	9.06	8.86	6.64	0.056	0.064	0.068	0.064
	16.0	9.81	9.57	7.28	.058	0.068	0.076	0.067
6B8.5	5.67	4.41	3.32	2.35	0.025	0.040	0.039	0.035
	11.34	4.63	3.62	2.54	0.026	0.042	0.040	0.036
	22.68	4.90	4.21	2.98	0.026	0.047	0.044	0.038
8WF20	10.51	7.03	7.83	5.84	0.041	0.065	0.063	0.052
	21.02	7.22	8.31	6.26	0.040	0.067	0.067	0.053
	42.04	7.44	9.10	7.00	.047	.072		0.066
10WF25	10.51	7.88	9.15	6.95	0.045	0.069	0.064	0.055
	21.02	7.98	9.54	7.31	0.045	0.072	0.066	0.056
	42.04	8.12		7.98	0.045		0.068	0.057

$*t_1$ = time of base release

t_2 = time of loss of vehicle contact

t_3 = time when fuse plate activates

t_4 = time when fuse force is maximum

TABLE 4.4.5 EFFECT OF BASE PLATE WEIGHT (3600 LB. VEHICLE, 40 MPH)

SUPPORT POST	WEIGHT OF BASE PLATE (lb.)	VEHICLE DECELERATION (g's)	PASSENGER ACCELERATION (g's)	VELOCITY CHANGE (mph)	$*t_1$ (sec.)	$*t_2$ (sec.)	$*t_3$ (sec.)	$*t_4$ (sec.)
3I5.7	4.0	6.38	2.15	1.45	.017	.025	.033	.026
	8.0	6.40	2.27	1.54	.018	0.028	.039	.032
	16.0	6.54	2.59	1.78	.018	0.035	.065	.054
6B8.5	5.67	3.88	1.39	0.94	0.011	0.020	0.021	0.017
	11.34	4.63	1.59	1.08	0.012	0.022	0.022	0.018
	22.68	5.15	1.98	1.34	0.012	0.025	0.024	0.020
8WF20	10.51	7.95	3.66	2.49	0.017	0.031	0.039	0.026
	21.02	8.19	3.96	2.71	0.017	0.032		0.022
	42.04	8.66	4.54	3.11	0.017	0.034		0.028
10WF25	10.51	9.65	4.88	3.33	0.020	0.033	0.034	0.026
	21.02	9.91	5.21	3.56	0.020	0.035	0.035	0.026
	42.04	10.19	5.74	3.95	0.020	0.037	0.037	0.028

$*t_1$ = time of base release

t_2 = time of loss of vehicle contact

t_3 = time when fuse plate activates

t_4 = time when fuse force is maximum

vehicle and simulated passenger increased with increased base plate weight. The vehicle velocity change increased in a similar manner. Note that the performance of the system, from a time-of-event standpoint, did not change appreciably.

Effect of sign background torsional stiffness. Table 4.4.6 gives the results of a limited study on the effect of the sign background stiffness. This study was conducted using the 8WF20 support. The torsional stiffness was varied from zero to four times the nominal value. The only significant effect was the time at which the fuse plate was activated. The ability of the fuse to activate is strongly influenced by the torsional stiffness of the sign background. It must offer enough resistance to develop the bending moment at the "plastic hinge."

Effect of vehicle stiffness. Table 4.4.7 illustrates the effect of vehicle crush characteristics on the response of the system. The study was conducted using the 3600 lb. vehicle at 40 mph impact velocity. It is obvious that the vehicle crush characteristics (reflecting the various construction features of passenger automobiles) have a very significant effect on the support response. Note that all system parameters were drastically influenced by the vehicle characteristics. This example dramatically illustrates the importance of having good vehicle data.

Effect of initial fuse plate bolt tension. Table 4.4.8 summarizes a study on the effect of the initial fuse plate bolt tension. The only significant influence is on t_3, the time at which the fuse is

TABLE 4.4.6 EFFECT OF SIGN BACKGROUND TORSIONAL STIFFNESS
(8WF20 SUPPORT, 8' x 16' BACKGROUND, 3600 LB. VEHICLE, 40 MPH)

$*\lambda/\lambda_{NOMINAL}$	VEHICLE DECELERATION (g's)	PASSENGER ACCELERATION (g's)	CHANGE IN VELOCITY (mph)	$**t_1$ (sec.)	$**t_2$ (sec.)	$**t_3$ (sec.)	$**t_4$ (sec.)
0.	7.93	3.63	2.48	0.017	0.031	0.189	0.185
0.5	7.93	3.63	2.48	0.017	0.031	0.039	0.026
1.0	7.95	3.66	2.49	0.017	0.031	0.039	0.026
2.0	7.95	3.66	2.49	0.017	0.032	0.036	0.026
4.0	7.96	3.66	2.49	0.017	0.031	0.034	0.025

$*\lambda_{NOMINAL}$ = torsional stiffness of 8' x 16' plywood panel

** t_1 = time of base release

t_2 = time of loss of vehicle contact

t_3 = time when fuse plate activates

t_4 = time when fuse force is maximum

TABLE 4.4.7 EFFECT OF VEHICLE STIFFNESS
(8WF20 SUPPORT, 8' x 16' BACKGROUND, 3600 LB. VEHICLE, 40 MPH)

$^{*}K/K_{NOMINAL}$	VELOCITY DECELERATION (g's)	PASSENGER ACCELERATION (g's)	CHANGE IN VELOCITY (mph)	$^{**}t_1$ (sec.)	$^{**}t_2$ (sec.)	$^{**}t_3$ (sec.)	$^{**}t_4$ (sec.)
0.5	5.98	3.83	2.65	0.022	0.043	0.048	0.033
1.0	7.95	3.66	2.49	0.017	0.031	0.039	0.026
2.0	10.05	3.48	2.35	0.013	0.022	0.032	0.020

$^{*}K_{NOMINAL}$ = stiffness of vehicle springs for 1955 Ford

$^{**}t_1$ = time of base release

t_2 = time of loss of vehicle contact

t_3 = time when fuse plate activates

t_4 = time when fuse force is maximum

TABLE 4.4.8 EFFECT OF INITIAL FUSE BOLT TENSION
(8WF20 SUPPORT, 8' x 16' BACKGROUND, 3600 LB. VEHICLE, 40 MPH)

INITIAL BOLT TENSION (lb.)	VEHICLE DECELERATION (g's)	PASSENGER ACCELERATION (g's)	CHANGE IN VELOCITY (mph)	$*t_1$ (sec.)	$*t_2$ (sec.)	$*t_3$ (sec.)	$*t_3$ (sec.)
3550	8.03	3.61	2.45	0.017	0.030	0.030	0.024
7200	8.02	3.61	2.46	0.017	0.030	0.031	0.024
14200	7.99	3.62	2.46	0.017	0.031	0.032	0.024
28400	7.95	3.66	2.49	0.017	0.031	0.039	0.026
36050	7.93	3.66	2.50	0.017	0.031		
47250	7.94	3.70	2.53	0.017	0.032		

$*t_1$ = time of base release

t_2 = time of loss of vehicle contact

t_3 = time when fuse plate activates

t_4 = time when fuse force is maximum

activated. This study illustrates the significance of the proper design of the fuse connection. Over design can result in a "plastic hinge" that will not form.

Effect of background-to-post connection stiffness. The connection of the sign background to the support post is idealized as a linear spring, the stiffness of which depends on the specific details of the connection. In this study the 8WF20 support and the 3600 lb. vehicle at 40 mph impact velocity were used. The tension and compression stiffness were varied as shown in Table 4.4.9. Note that no significant changes resulted. It was assumed, for these and all other problems in the parameter study, that connections were strong enough to develop the forces required.

Effects of support post weight. Four additional sign supports were included in the study to determine the system response trends. The background, base plate, and initial bolt tensions were identical to the 10WF25 support described in Figure 4.3.5 and Table 4.3.1. Only the support sign was varied.

Figure 4.4.12 gives the results of a 40 mph impact with three vehicles (1800 lb., 3600 lb., and 4800 lb.). Note that all supports operated satisfactorily. Data presented in Table 4.4.1 show the times at which critical events occurred. The deceleration of a particular weight of vehicle is observed to increase as the support becomes more massive. For any one particular post size the vehicle deceleration decreased, in general, with increased vehicle weight. The severity of the collision can be measured by the acceleration of simulated passenger and the vehicle velocity change.

TABLE 4.4.9 EFFECT OF BACKGROUND-TO-POST CONNECTION STIFFNESS
(8WF20 SUPPORT, 8' x 16' BACKGROUND, 3600 LB. VEHICLE, 40 MPH)

STIFFNESS OF CONNECTION (lb./ft.)	CONNECTION COMPRESSION FACTOR	VEHICLE DECELERATION (g's)	PASSENGER ACCELERATION (g's)	CHANGE IN VELOCITY (mph)	$*t_1$ (sec.)	$*t_2$ (sec.)	$*t_3$ (sec.)	$*t_4$ (sec.)
30,000	3.00	7.95	3.66	2.49	0.017	0.031	0.039	0.026
60,000	2.00	8.00	3.69	2.51	0.017	0.031	0.039	0.026
90,000	1.50	8.03	3.70	2.52	0.017	0.031	0.038	0.026

$*t_1$ = time of base release

t_2 = time of loss of vehicle contact

t_3 = time when fuse plate activates

t_4 = time when fuse force is maximum

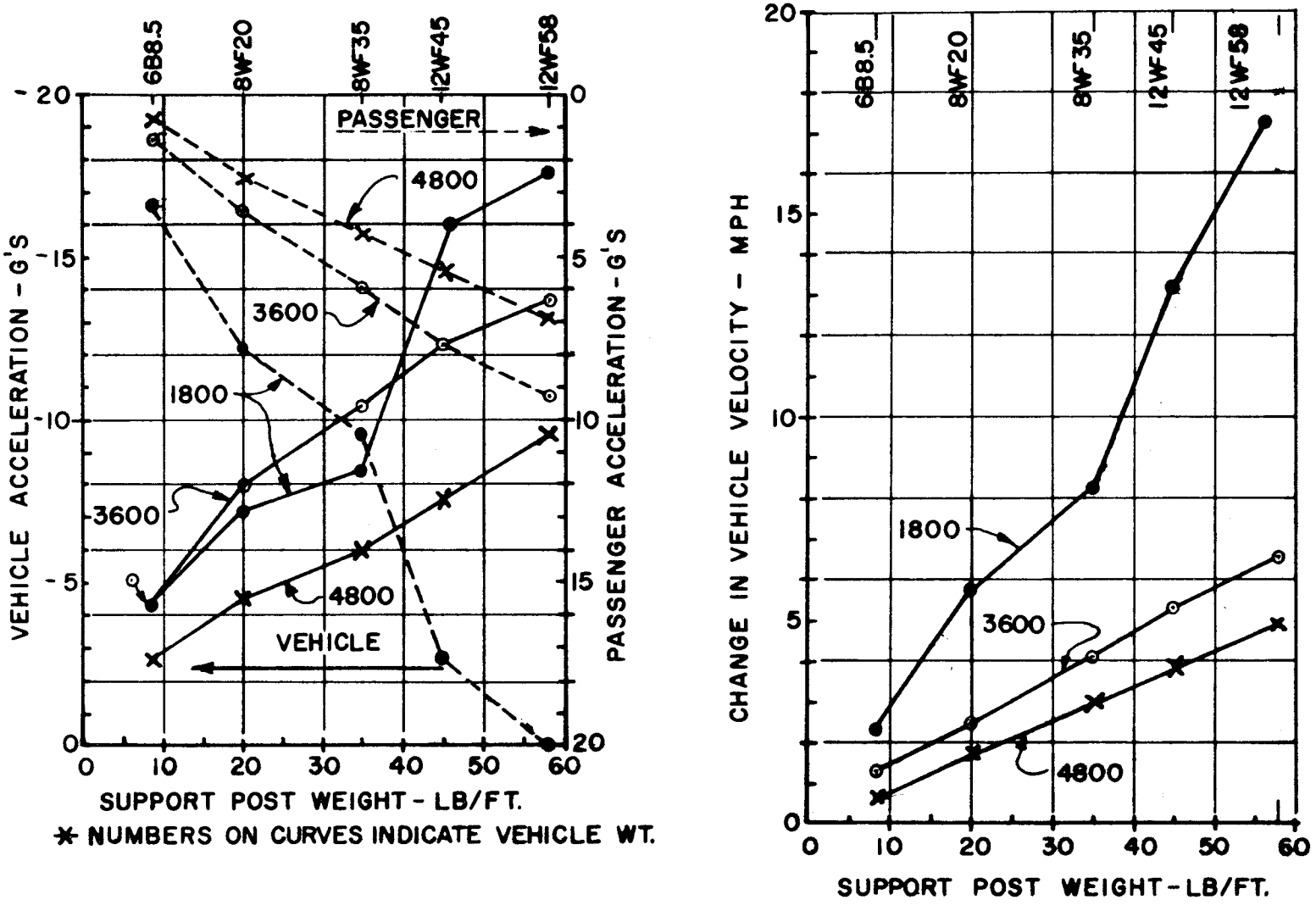

FIGURE 4.4.12 - EFFECTS OF SUPPORT WEIGHT (40 MPH COLLISION VELOCITY)

Note that the data curves are not smooth and that there is an overlap of the 1800 lb. and 3600 lb. vehicle response curves. This is probably due to the influence of the different vehicle spring stiffnesses and different mass-to-stiffness ratios of the supports.

4.5 Conclusions

The following general conclusions can be drawn based on the results of the studies presented in Section 4.4.

The sign background. The torsional stiffness of the sign background affects the time at which the fuse is activated. The background must have sufficient torsional stiffness to supply the restraint necessary to develop the "plastic hinge" without large angular deformation of the background. If the stiffness of the background is small (less than half that of the backgrounds tested) the conceptual function of the "plastic hinge" is not realized and it would seem reasonable to eliminate it. The study indicated that in those problems in which the fuse was activated, the sign rotated between a minimum of 0.3 degrees and a maximum of 6.0 degrees. In general, the sign background should have a stiffness (T/ψ) of 100 ft.-lb./degree for a rotation of six degrees.

Background-to-post connection. The stiffness of the background-to-post connection appears to have little influence on the support, vehicle and passenger response. The connections must have sufficient strength to transmit the forces required to develop the "plastic hinge." It was observed that the force in the connection increased as the stiffness was made larger. The maximum tensile force observed in the studies was approximately 10,000 lbs.

Initial fuse plate bolt tension. The initial tension in the fuse plate bolts determines when the fuse will activate. Turn-of-nut tightening methods appear to be satisfactory if the connection is not over-designed for wind load and the background-to-post connection has sufficient strength

to transmit the forces necessary for the development of the "plastic hinge." In using the turn-of-nut method, the bolt size should be limited to 3/4 in. diameter.

If the fuse plate must be over-designed (an over-design might be necessary because of the limited bolt sizes available) the connection strength and sign background stiffness must be increased to compensate. In the design of the fuse plate, it is desirable to keep the depth of the slot to a minimum so that the fuse will activate with a small amount of slip.

Initial base plate bolt tension. The base bolt tension is probably the most critical single factor for the safe operation of the "break-away" sign support. The study indicates that light supports (3I5.7 and 6B8.5) are influenced more by initial bolt tension than the larger supports (8WF20 and 10WF25). It is suggested that values of bolt tension not exceed those used in the study by 50%.

The vehicle. The studies indicate that the crush characteristics of the vehicle can have a significant effect on the response of the system. This is one reason why the conclusions drawn from the parameter study can only reflect general trends. It also dramatizes the very real need for contemporary vehicle data. At the present time such information is not available.

The support post. The maximum size of support is dictated by the allowable vehicle and passenger response. It appears from the limited study reported in Section 4.4, that a 45 lb./ft. post is the limit of practical post size. This conclusion is based on the 1800 lb. vehicle collision. All vehicles failed to completely activate the "plastic

hinge" on all supports at 15 mph although this fact alone is not to be considered to invalidate the concept. The g levels on the vehicle and passenger at the lower speeds are not sufficient to cause serious mechanical or physical damage.

It was found that the weight of the base plate had very little effect on the system response. This conclusion is valid only within practical limitations. Certainly if the base plate weight were increased tenfold there would be a significant effect. For the normal increase in weight expected, this conclusion will be valid. It must be pointed out that rigidity of the base plates is very important to the operation of the base and to the theory developed to explain it. If significant changes are made in the design of the base, the force-slip characteristics should be re-evaluated by laboratory test.

CHAPTER 5

RECOMMENDATIONS

The following recommendations are made based on experience gained through research, through technical discussions with the Technical Subcommittee of the Policy Committee, and through accident records from collisions with sign support structures on interstate highways.

5.1 "Break-Away" Supports

The following recommendations are made for "break-away" type sign supports:

1. The results of the parameter study (Section 4.4) indicate that the maximum post size should be limited to 45 lb./ft. sections.

2. The base plates should be proportioned to resist the bending moment due to wind load. They should be designed using recognized material stress allowables. The weight of the plate attached to the upper post should be as near to the values recommended in Table 5.1.1 as is practical. The base bolts should be designed to transmit the wind moment assuming the bolts are not pretensioned. A small amount of pretensioning is required to prevent the upper post from "walking" off the foundation under oscillating wind loads. Table 5.1.1 shows the recommended minimum and maximum bolt tensions and torques for galvanized A325 bolts. The maximum values should not be exceeded if the conceptual behavior of the base is to be achieved.

3. The moment capacity for the fuse connection of the "plastic

TABLE 5.1.1 RECOMMENDED RANGE OF BASE PLATE VARIABLES

SUPPORT SIZE (lb./ft.)	BASE PLATE WEIGHT (lb.)	BOLT DIAMETER (in.)	TORQUE RANGE (in./lb.)	TENSION RANGE (lb.)
0 - 8	8.0	1/2	200 - 300	920 - 1380
9 - 20	12.0	5/8	450 - 680	1740 - 2600
10 - 30	21.0	3/4	750 - 1060	2400 - 3600
30 +	21.0	7/8	850 - 1280	2400 - 3600
30 +	21.0	1	950 - 1420	2400 - 3600

hinge" is determined by the maximum wind load moment at the fuse. The moment capacity of the fuse is determined by Eq. (2.9.3).

$$M = mnN'f(s)r \tag{5.5.1}$$

where M = maximum wind load bending moment at the fuse

n = number of bolts crossing the slip plane

m = number of faying surfaces per bolt

N' = initial bolt tension

f(s) = coefficient of friction of the faying surfaces

r = depth of post section (back to back of flanges)

The required initial tension in the bolt is

$$N' = \frac{M}{mnf(s)r} \tag{5.5.2}$$

The coefficient of f(s) for hot dipped galvanized steel posts, plates, and washers ranges from 0.17 to 0.26 with 0.21 being a representative value (see Part II, Section 4.6).

The required bolt tension can be achieved by the use of a calibrated torque wrench. Table 3.3.1 of Part III can be used to determine the bolt torque for values of N'. If the ASTM turn-of-nut method is used, the bolt size whose proof load is nearest to the value of N', as calculated from Eq. (5.5.2), should be chosen. If a bolt is chosen whose proof load exceeds the calculated N' by 50% (this may occur in certain instances when the designer is forced to use available A325 or A490 bolt sizes) the background-to-post connections should be

proportionately strengthened and the torsional stiffness of the background increased.

The thickness of the fuse plate should not exceed the thickness of the post flange.

4. The sign background can be made of plywood, aluminum, steel or other suitable panels spliced securely together and, when necessary, stiffened with wind beams to form a structurally stiff plate. The torsional stiffness, (T/ψ), of the backgrounds investigated in this report can be calculated from Eq. (5.6.1) or Eq. (5.6.2) (see Part III, Section 5.6) depending on the type of background. The torsional stiffness should be sufficient to activate the fuse and develop the "plastic hinge." It is recommended that the torsional stiffness of the sign background be not less than 100 ft.-lb./degree (5730 ft.-lb./radian).

5. Accident records have indicated that clamped background-to-post connections presently in use are inadequate. Whether this inadequacy is inherent in the design of the connection or caused by over-designed fuse connections is not known. The complexity of the dynamics of the problem make such a determination difficult. The studies of this report indicate, however, that when strong connections are provided the fuse will be activated and the "plastic hinge" will form for all but low speed collisions (15 mph or less). Full-scale crash tests have indicated that direct bolting provides a good connection. A combination of bolting and clamping may be the solution to obtaining a reliable connection. The study presented in Section 4.4 indicates that the maximum fuse force that can be anticipated for the

support configurations considered is 10,000 lb. This force is not necessarily the force in a single connection, but is the maximum force at a single connection point.

REFERENCES

1. Crandall, S. H., Engineering Analysis, McGraw-Hill Book Co. Inc., New York, N. Y., 1965, p. 158.

2. Rogers, G. L., Dynamics of Framed Structures, John Wiley & Sons, Inc., New York, N. Y., 1959, p. 75.

3. Olson, R. M., "Instrumentation and Photographic Techniques for Determining Displacement, Velocity Change, and Deceleration of Vehicles with Break-Away Sign Structures," Research Report 68-3, Sign Support Structures, Texas Transportation Institute, September, 1966.

4. Severy, D. M. and Mathewson, J. H., "Automobile-Barrier Impacts," Highway Research Board Bulletin 91, 1954, p. 61.

5. Fredericks, R. H., "Automobile Crash Research," paper presented at the SAE Detroit Section Meeting, November 12, 1962.

6. Severy, D. M. and Mathewson, J. H., "Automobile-Barrier and Rear End Collisions Perfromance," SAE Preprint 31A, 1958.

7. Rowan, N. J., Olson, R. M., Edwards, T. C., Gaddis, A. M. and Williams, T. G., "Impact Behavior of Sign Supports-II," Staff Progress Report 68-2, Texas Transportation Institute, College Station, Texas, September, 1965, p. 21.

8. Samson, C. H., Rowan, N. J., Olson, R. M. and Tidwell, D. R., "Impact Behavior of Sign Supports," A Research Report 68-1, Texas Transportation Institute, College Station, Texas, March, 1965, p. 41.

9. "Specifications for Structural Joints Using ASTM A325 or A490 Bolts," Approved by the Research Council on Riveted and Bolted Structural Joints of the Engineering Foundation, Industrial Fasteners Institute, Cleveland, Ohio, March, 1964, p. 7.

PART III

LABORATORY INVESTIGATIONS, DATA AQUISITION, DATA ANALYSIS, CRASH TESTS, AND CASE STUDIES OF ACTUAL ROADSIDE SIGN INSTALLATIONS

TABLE OF CONTENTS

CHAPTER		PAGE
1.	INTRODUCTION	1:1
2.	STATIC TESTS OF BREAK-AWAY BASE	2:3
	2.1 Objective	2:3
	2.2 Types of Tests	2:3
	2.3 Testing Philosophy	2:5
	2.4 Test Procedure	2:6
	2.5 Results	2:6
	2.6 Conclusions	2:18
3.	TORQUE-TENSILE LOAD PROPERTIES OF ASTM A325 BOLTS	3:24
	3.1 Objective	3:24
	3.2 Test Procedure	3:24
	3.3 Results	3:24
4.	STATIC FUSE PLATE TESTS	4:30
	4.1 Objective	4:30
	4.2 Test Specimen	4:30
	4.3 Types of Tests	4:32
	4.4 Data Reduction	4:32
	4.5 Test Procedure	4:34
	4.6 Results	4:34
	4.7 Behavior of Mild Steel at Low Temperatures	4:41
5.	ROTATIONAL STIFFNESS OF SELECTED SIGN BACKGROUNDS	5:47
	5.1 Objective	5:47
	5.2 Test Fixture	5:47
	5.3 Test Specimens	5:47
	5.4 Test Procedure	5:52
	5.5 Results	5:54
	5.6 Theoretical Representation of Torsional Stiffness	5:58
6.	DATA ACQUISITION	6:62
	6.1 Principles of Instrumentation	6:62
	6.2 Criteria of Instrumentation	6:62
	6.3 Electronic Instrumentation	6:62
	6.4 Photographic Instrumentation	6:80

CHAPTER		PAGE
7.	METHODS OF DATA ANALYSIS	7:83
	7.1 Vehicle Accelerometer Analysis	7:83
	Data reduction	7:83
	Data analysis	7:86
	7.2 Techniques of High-Speed Film Reduction	7:87
	Motion analyzer	7:87
	Time correlation	7:87
	Datum references	7:89
	Time and displacement data	7:89
	Procedure for penetration data analysis time parameter	7:91
	Procedure for penetration data analysis distance parameter	7:93
	Procedure for obtaining velocity information from electronic data	7:94
	7.3 Determination of Vehicle Velocity	7:94
	7.4 Conclusion	7:95
8.	FULL-SCALE CRASH TESTS	8:97
	8.1 Purpose of Tests	8:97
	8.2 Fixed Barrier Penetration Data	8:97
	8.3 Determination of Force-Deformation Characteristics for Vehicle Used in the Fixed Barrier Tests	8:108
	8.4 Summary of Sign Support Crash Tests	8:121
	8.5 Description of Test 446-5	8:122
	8.6 Description of Test 446-7	8:130
	8.7 Description of Test 446-8	8:138
	8.8 Description of Test 446-9	8:146
	8.9 Description of Test 446-10	8:154
9.	LOCATION AND INSTALLATIONS OF ROADSIDE SIGNS	9:162
	9.1 Introduction	9:162
	9.2 Case Studies	9:163
	REFERENCES	174
	APPENDIX	A:176

LIST OF FIGURES

FIGURE		PAGE
2.2.1	Static Base Plate Test	2:4
2.5.1	Slip vs. Applied Load, Direct Shear Test	2:8
2.5.2	Applied Load vs. Bolt Load, Direct Shear	2:9
2.5.3	Applied Load vs. Bolt Load, Direct Shear	2:10
2.5.4	Actual Values of Coefficient of Friction, Direct Shear	2:12
2.5.5	Theoretical Coefficient of Friction, Direct Shear	2:14
2.5.6	Slip vs. Applied Load, Eccentric Load	2:15
2.5.7	Bolt Load vs. Applied Load, Eccentric Load	2:16
2.5.8	Bolt Load vs. Applied Load, Eccentric Load	2:17
2.5.9	Actual Values of Coefficient of Friction, Eccentric Load	2:19
2.5.10	Theoretical Values of Coefficient of Friction, Eccentric Load	2:20
2.5.11	Actual Values of Coefficient of Friction, All Tests	2:21
2.5.12	Theoretical Values of Coefficient of Friction, All Tests	2:22
3.2.1	Test Set-Up for Torque-Tensile Test	3:25
3.3.1	Torque-Tensile Data	3:26
4.2.1	Fuse Plate Specimen	4:31
4.3.1	Test Fixture for Tensile Test of Slotted Steel Fuse Plate	4:33
4.6.1	Slotted Plate Tensile Tests (6B8.5)	4:35
4.6.2	Slotted Plate Tensile Tests (6B8.5)	4:36

FIGURE		PAGE
4.6.3	Slotted Plate Tensile Tests (8WF17)	4:37
4.6.4	Slotted Plate Tensile Tests (8WF17)	4:38
4.6.5	Slotted Plate Tensile Tests (10WF25)	4:39
4.6.6	Slotted Plate Tensile Tests (10WF25)	4:40
4.6.7	Coefficient of Friction vs. Slip (6B8.5)	4:42
4.6.8	Coefficient of Friction vs. Slip (8WF17)	4:43
4.6.9	Coefficient of Friction vs. Slip (10WF25)	4:44
5.2.1	Test Fixture for Sign Background Torsion Tests	5:48
5.3.1	Test I, Plywood Background	5:49
5.3.2	Test II, Aluminum Panels	5:50
5.3.3	Test III, Laminated Aluminum Paper Honeycomb Panel	5:51
5.4.1	Test Set-Up for Measuring Rotation	5:53
5.5.1	Torque-Rotation for Specimen I	5:55
5.5.2	Torque-Rotation for Specimen II	5:56
5.5.3	Torque-Rotation for Specimen III	5:57
5.6.1	Comparison of Theory With Torsion Tests	5:60
6.3.1	Instrumentation Trailer	6:63
6.3.2	Block Diagram Showing Placement of Target Sign Instrumentation	6:66
6.3.3	Recorders and Amplifiers	6:68
6.3.4	Accelerometers	6:69
6.3.5	Block Diagram Showing Placement of Statham and Endevco Accelerometers on Crash Vehicle	6:70
6.3.6	(a) Tapeswitch Mounting (b) Backboard Showing Clock	6:73 6:73

FIGURE		PAGE
6.3.7	Wands for Velocity Determination	6:75
6.3.8	Strain Gaged Fuse Plate	6:76
6.3.9	(a) Strainsert Bolt (b) Flashbulb Switches	6:77 6:77
6.3.10	Linear Potentiometer	6:79
6.4.1	Camera Field of View	6:81
7.1.1	Crash Vehicle Accelerometer Analysis by Graphical Integration	7:84
7.1.2	Digital Data Reduction System	7:85
7.2.1	Film Motion Analyzer	7:88
7.2.2	Displacement-Time Plot, Test 446-5	7:92
8.2.1	Sequence Photographs of Fixed Barrier Crash Series	8:99
8.2.2	Sequence Photographs of Fixed Barrier Crash Series	8:100
8.2.3	Sequence Photographs of Fixed Barrier Crash Series	8:101
8.2.4	Photographs of Vehicles at Conclusion of Each Fixed Barrier Test	8:104
8.2.5	Before and After Views of Vehicles in Fixed Barrier Series	8:105
8.2.6	Before and After Views of Vehicles in Fixed Barrier Series	8:106
8.2.7	Observed Penetration and Rebound in Fixed Barrier Crash Tests	8:107
8.3.1	Curve Fitting Technique for Force-Deformation of Vehicles in Fixed Barrier Tests	8:110
8.3.2	Test 446-1, 1955 Ford 4-Door Sedan	8:112
8.3.3	Test 446-2, 1959 Simca 4-Door Sedan	8:113
8.3.4	Test 446-3, 1960 Corvair Coupe	8:114

FIGURE		PAGE
8.3.5	Test 446-4, 1954 Cadillac 4-Door Sedan	8:115
8.3.6	Test 446-6, Series 3000 White Truck	8:116
8.3.7	Test 446-2, 1959 Simca, Force-Deformation Comparison	8:117
8.3.8	Test 446-3, 1960 Corvair, Force-Deformation Comparison	8:118
8.3.9	Test 446-6, Series 3000 White Truck, Force-Deformation Comparison	8:119
8.5.1	Test 446-5	8:123
8.5.2	Sequence Photographs of Test 446-5	8:125
8.5.3	Test 446-5, Test Vehicle Damage	8:127
8.5.4	Test 446-5, Support Damage	8:129
8.6.1	Test 446-7	8:131
8.6.2	Sequence Photographs of Test 446-7	8:133
8.6.3	Test 446-7, Test Vehicle Damage	8:135
8.6.4	Test 446-7, Support Damage	8:137
8.7.1	Test 446-8	8:139
8.7.2	Sequence Photographs of Test 446-8	8:141
8.7.3	Test 446-8, Test Vehicle Damage	8:143
8.7.4	Test 446-8, Support Damage	8:145
8.8.1	Test 446-9	8:147
8.8.2	Sequence Photographs of Test 446-9	8:149
8.8.3	Test 446-9, Test Vehicle Damage	8:151
8.8.4	Test 446-9, Support Damage	8:153
8.9.1	Test 446-10	8:155
8.9.2	Sequence Photographs of Test 446-10	8:157

FIGURE		PAGE
8.9.3	Test 446-10, Test Vehicle Damage	8:159
8.9.4	Test 446-10, Support Damage	8:161
9.2.1	Case Study 1 - Sign Support Location on I.H. 10	9:164
9.2.2	Case Study 2 - Sign Support Location on I.H. 10	9:165
9.2.3	Case Study 3 - Sign Support Location on I.H. 10	9:166
9.2.4	Case Study 4 - Sign Support Location on I.H. 10	9:167
9.2.5	Case Study 5 - Sign Support Location on I.H. 10	9:168
9.2.6	Case Study 6 - Sign Support Location on I.H. 10	9:169
9.2.7	Case Study 7 - Sign Support Location on I.H. 45	9:170

APPENDIX

1.	Visicorder Record, Tests 446-2 and 446-3	A:177
2.	Visicorder Record, Tests 446-5	A:178
3.	Visicorder Record, Test 446-6	A:189
4.	Visicorder Record, Test 446-7	A:180
5.	Visicorder Record, Tests 446-8 and 446-9	A:181
6.	Visicorder Record, Test 446-10	A:182

LIST OF TABLES

TABLE		PAGE
2.4.1	Equipment and Instruments Used in Base Tests	2:7
3.3.1	Values of K_T in $N' = K_T \tau$	3:29
4.2.1	Fuse Plate Specimens	4:31
4.6.1	Strength of Slotted Steel Plate Bolted Connection (Mechanical Fuse)	4:45
6.3.1	Electronic Instrumentation	6:64
6.3.2	Galvanometers Employed	6:72
6.4.1	Photographic Instrumentation	6:82
7.2.1	Comparison of Elapsed Time	7:88
7.2.2	Reference Marks for High-Speed Film Reduction	7:90
7.3.1	Crash Vehicle Velocity Prior to Impact and After Collision	7:96
8.1.1	Full-Scale Crash Tests	8:98
8.2.1	Fixed Barrier Crash Test Summary	8:103
8.3.1	Comparison of Computations of Energy Absorbed	8:120
8.4.1	Sign Support Crash Tests	8:121

CHAPTER 1

INTRODUCTION

Part III describes and presents the results of all tests conducted in support of the research. Laboratory tests were conducted on the following "break-away" sign support components: 1) the slip base, 2) the fuse plate of the "plastic hinge," (3) the sign background, and 4) the base plate bolts. In addition to the laboratory testing of components, ten full-scale crash tests were conducted. These were as follows: 1) one test on a full-scale "break-away" support, 2) three tests on a deforming A-frame, 3) one test of an aluminum truss support, and 4) five tests involving the collision of five different types of automobiles with a fixed barrier.

The purpose of these tests was twofold. In order to correlate and verify the mathematical model, the characteristics of the various mechanical features of the "break-away" concept were required. The laboratory tests were planned to provide specific information on the components of the sign support that were crash tested. This approach assured that good data were available for the simulation. Input data for other size support posts could be extrapolated from the test data. These data were then used to provide input information for the parameter study.

The fixed barrier tests were conducted to obtain basic information on the force-deformation and other crash characteristics of various types of automobiles.

All laboratory tests of component parts were tested under slowly applied loads. It was felt that data obtained in this manner would give the researcher basic information on the behavior characteristics. This basic static information could be used as input for the mathematical model. If the results obtained in this manner correlated well with the full-scale crash tests, the static information could be accepted as representative of the behavior of the component parts under dynamic loads. As pointed out in Section 3.5 of Part II., this was the case and dynamic tests were not required.

Three of the full-scale crash tests were conducted to determine the behavior of two other types of sign supports (different concepts than the "break-away" support). The remaining crash test was conducted to determine the effects of design modifications to one of the concepts.

C H A P T E R 2

STATIC TESTS OF BREAK-AWAY BASE

2.1 Objective

One of the variables which influences the behavior of the "break-away" sign support is the resistance of the base to slip under both statically and dynamically applied loads. The base must be able to resist wind loads but retain its basic function of slipping under dynamically applied loads.

The objective of this series of tests was to determine the applied force-slip characteristics of a galvanized base for an 8WF20 support post.

2.2 Types of Tests

Figure 2.2.1 shows the details of the base component tested in this series. Also shown are the two types of tests conducted; a direct shear test and an eccentric load test. The direct shear test gave basic information on the applied force-slip characteristics for the base with the effects of externally applied moments minimized (a slight eccentricity was introduced by the manner of loading). The eccentric load test produced a condition in which slip occurred under applied moment and shear. The results of these tests not only supplied basic applied force-slip data, but also yielded information for the verification of the hypothesis of base behavior developed in Section 2.10 of Part II.

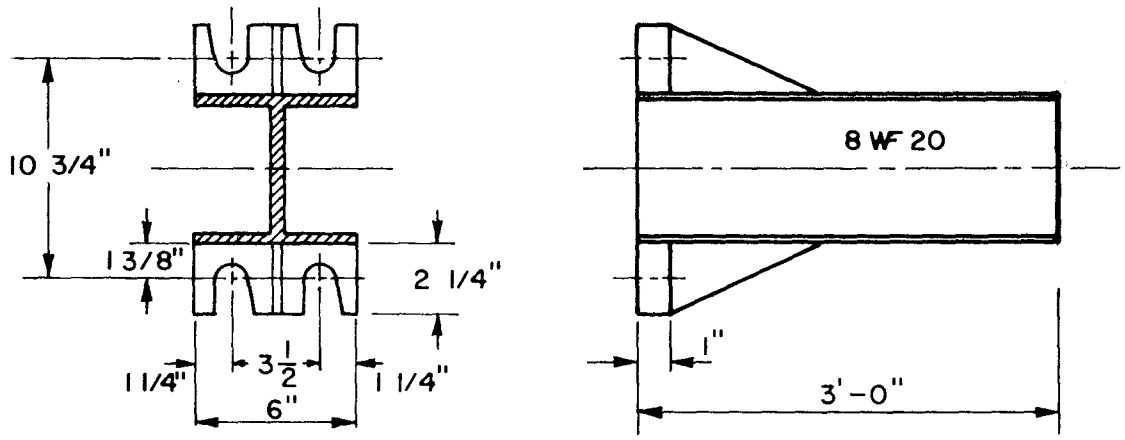

BASE DETAIL

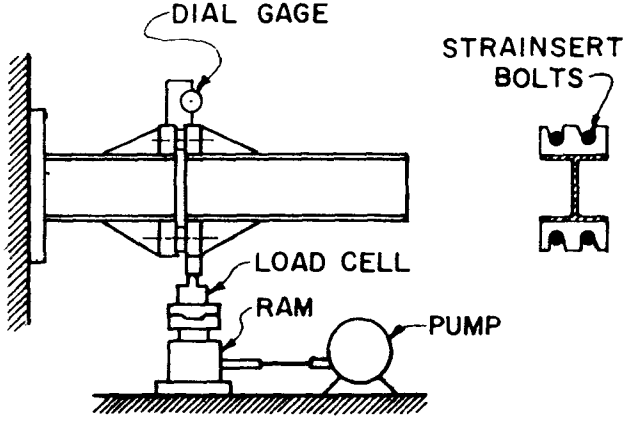

DIRECT SHEAR TEST

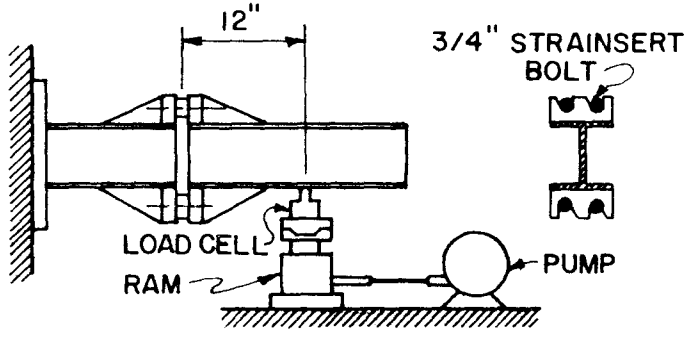

ECCENTRIC LOAD TEST

FIGURE 2.2.1 STATIC BASE PLATE TEST

2.3 Testing Philosophy

For either type loading, the base resistance can be expressed as:

$$F = n\, f(s) \sum_{i=1}^{i=m} T_i$$

where

F = applied load

$f(s)$ = coefficient of friction

m = number of bolts crossing the slip plane

n = number of faying surfaces per bolt

T_i = the tension in each bolt

For the base tested $m = 4$ and $n = 2$ and

$$F = 2f(s) \sum_{i=1}^{i=4} T_i$$

Therefore

$$f(s) = \frac{F}{2 \sum_{i=1}^{i=4} T_i}$$

For any value of slip, s, the applied load and the clamping force in the bolt could be measured. Therefore, a functional relation between slip and coefficient of friction for any applied load and clamping force could be obtained.

2.4 Test Procedure

Table 2.4.1 lists the type of equipment employed in these tests. In each series of tests, four initial bolt torques were used; 750 in.-lb., 1500 in.-lb., 2250 in.-lb., and 3000 in.-lb. The test procedure was as follows:

(1) Torque all bolts to prescribed initial torque with a torque wrench,

(2) apply load in 1000 lb. increments,

(3) simultaneously read the applied load, the slip, and the load in the two instrumented bolts, and

(4) continue reading and recording at 1000 lb. increments noting the occurrence of significant events, such as maximum load and slip.

2.5 Results

Figure 2.5.1 shows the slip vs. applied load for the direct shear tests. Figure 2.5.2 is a plot of the tension in the bottom bolt (see sketch in figure) vs. the applied load, and Figure 2.5.3 shows the tension in the top bolt vs. the applied load. Figure 2.5.1 shows that the slip at maximum applied load increases with initial bolt torque. Note in Figure 2.5.2 that the tension in the bottom bolt increases when the applied load reaches the knee of the load vs. slip curve (the point in Figure 2.5.1 where the slip first becomes significant). The tension in the top bolt (see Figure 2.5.3) has the same trend but is not as pronounced. This indicates that the canting of the bottom bolt induces a tension which increases the bolt force and hence increases

TABLE 2.4.1 EQUIPMENT AND INSTRUMENTS USED IN BASE TESTS

DESCRIPTION	MANUFACTURER	RANGE
Tatnall Load Cell	Budd Co.	0 - 100,000 lb.
Dial Indicator (0.001 in.)	Federal Inst. Co.	0 - 1.0 in.
Instrumented Bolts (3/4" in diameter galvanized A325 bolts).	Strainsert Co.	0 - 21,000 lb.
Hydraulic Ram	Simplex	0 - 200,000 lb.
Electric Pump	Soiltest	Variable Speed

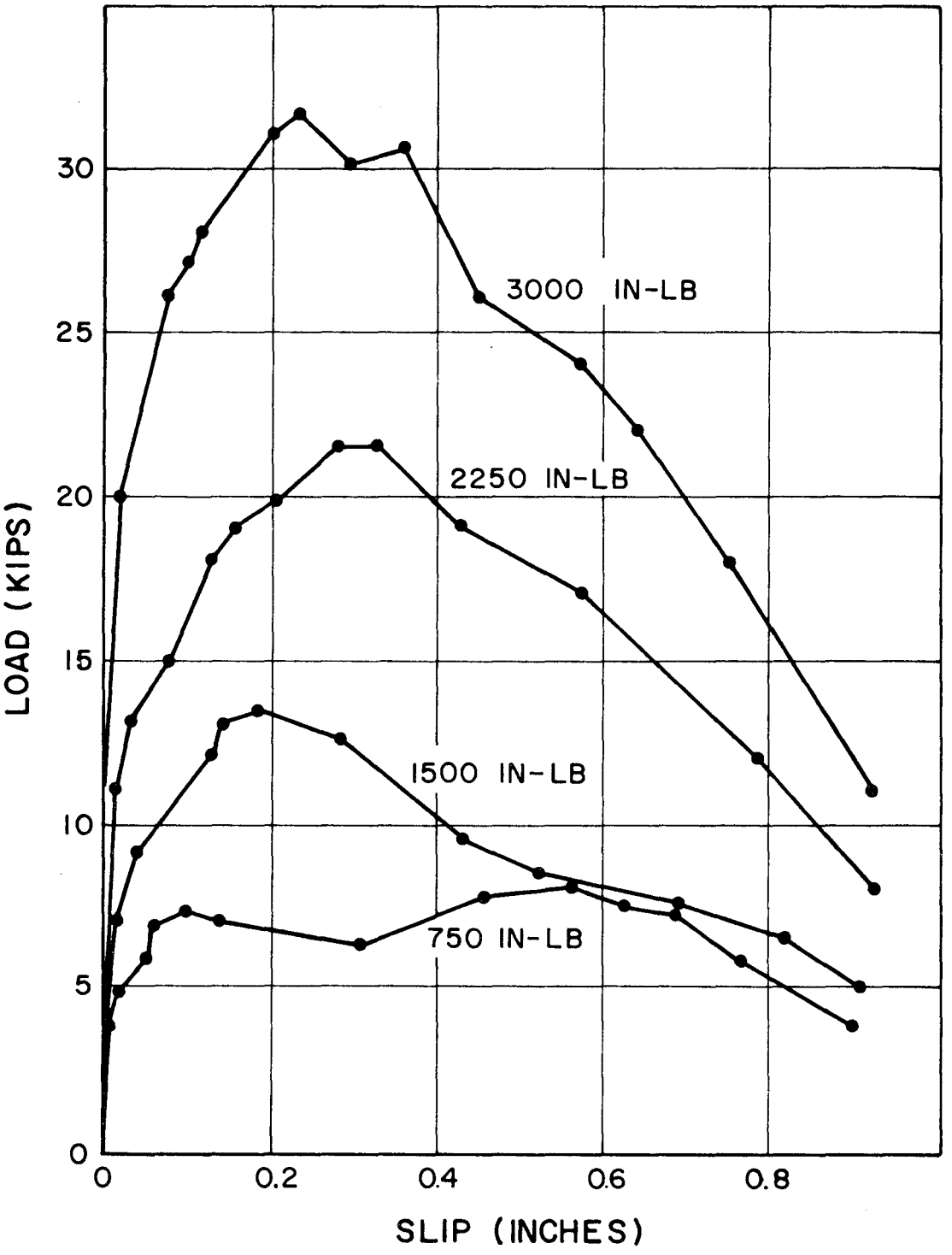

FIGURE 2.5.1 SLIP VS. APPLIED LOAD, DIRECT SHEAR TEST

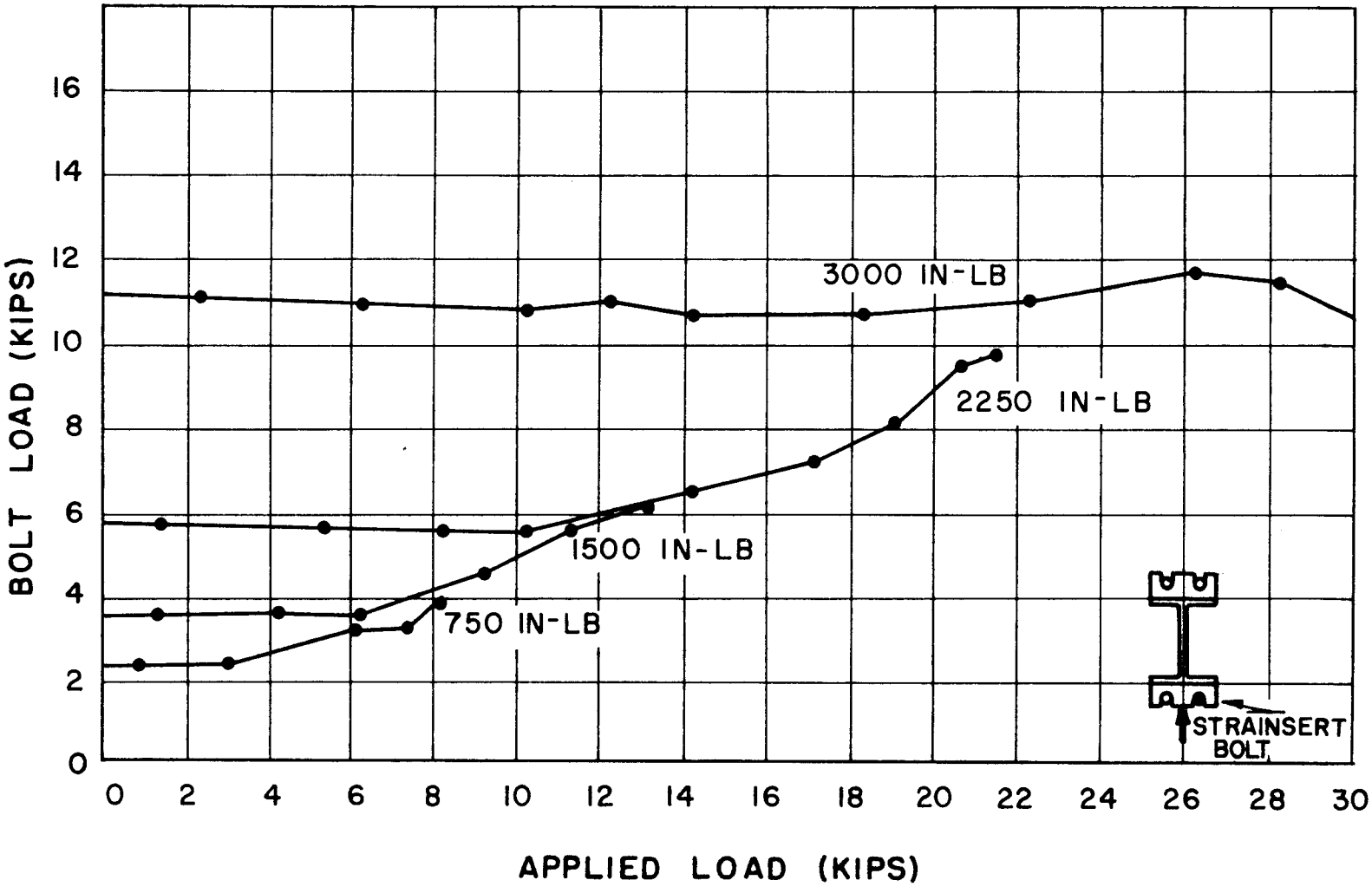

FIGURE 2.5.2 APPLIED LOAD VS. BOLT LOAD, DIRECT SHEAR

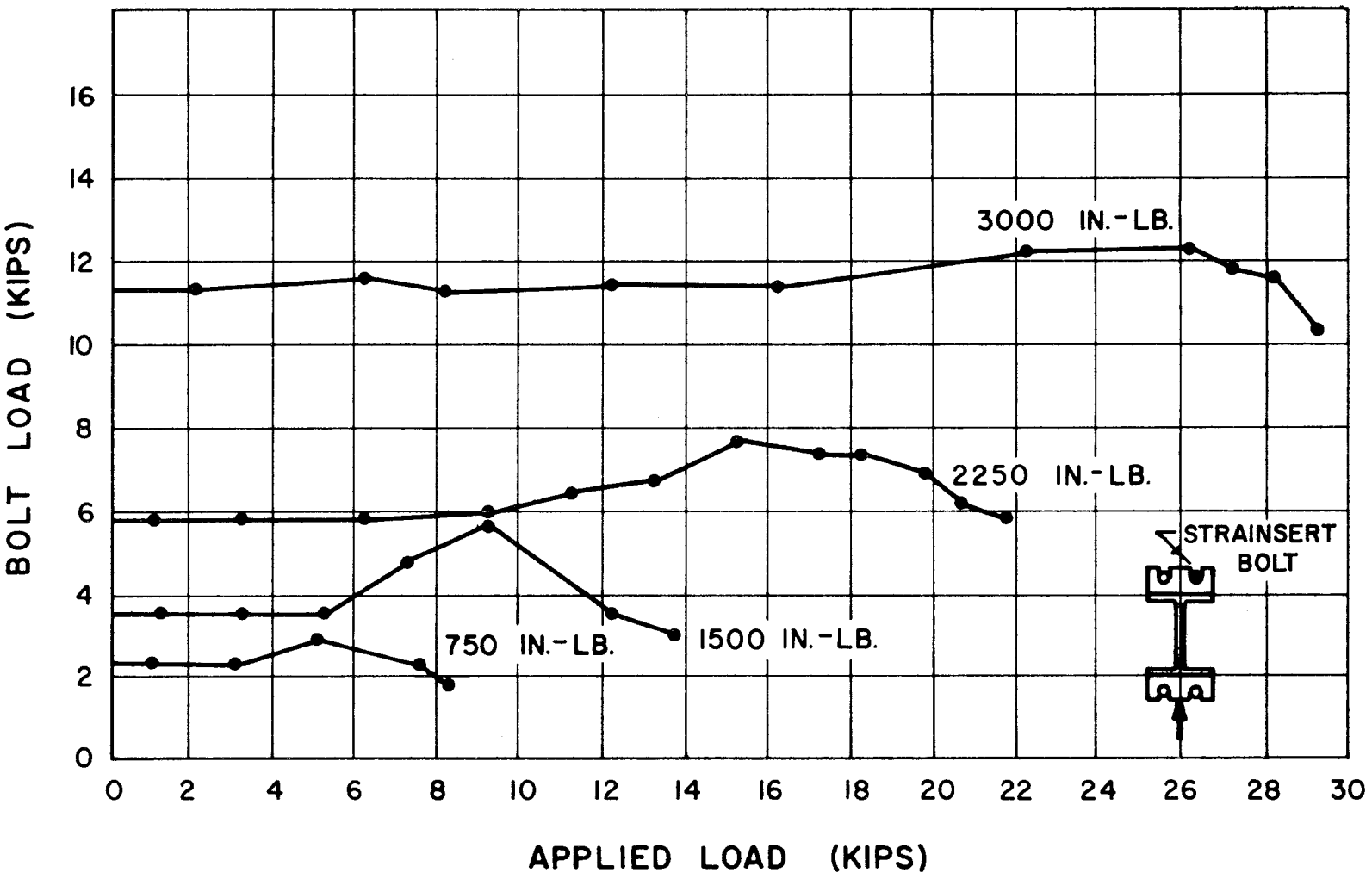

FIGURE 2.5.3 APPLIED LOAD VS. BOLT LOAD, DIRECT SHEAR TEST

the clamping force causing the resistance to increase. Figure 2.5.4 shows the calculated values of coefficient of friction plotted versus slip. These values were calculated using the measured values of T (the bolt tension).

$$f(s) = \frac{F}{2 \sum_{i=1}^{i=4} T_i}$$

Since only two bolts were instrumented, the formula must be modified

$$f(s) = \frac{F}{4 \sum_{i=1}^{i=2} T_i} = \frac{F}{4(T_t + T_b)}$$

where

T_t = load in top bolt

T_b = load in bottom bolt

Note in Figure 2.5.4 that the coefficient of friction is essentially constant after the slip at maximum applied load is reached. This method of calculating the coefficient of friction takes into account the increase in bolt tension due to canting and thus gives the results expected for Coulomb friction.

In order to provide data that would be applicable for the hypothesis developed in Section 2.10 of Part II, a second method of interpreting the test results was used. The resistance can be

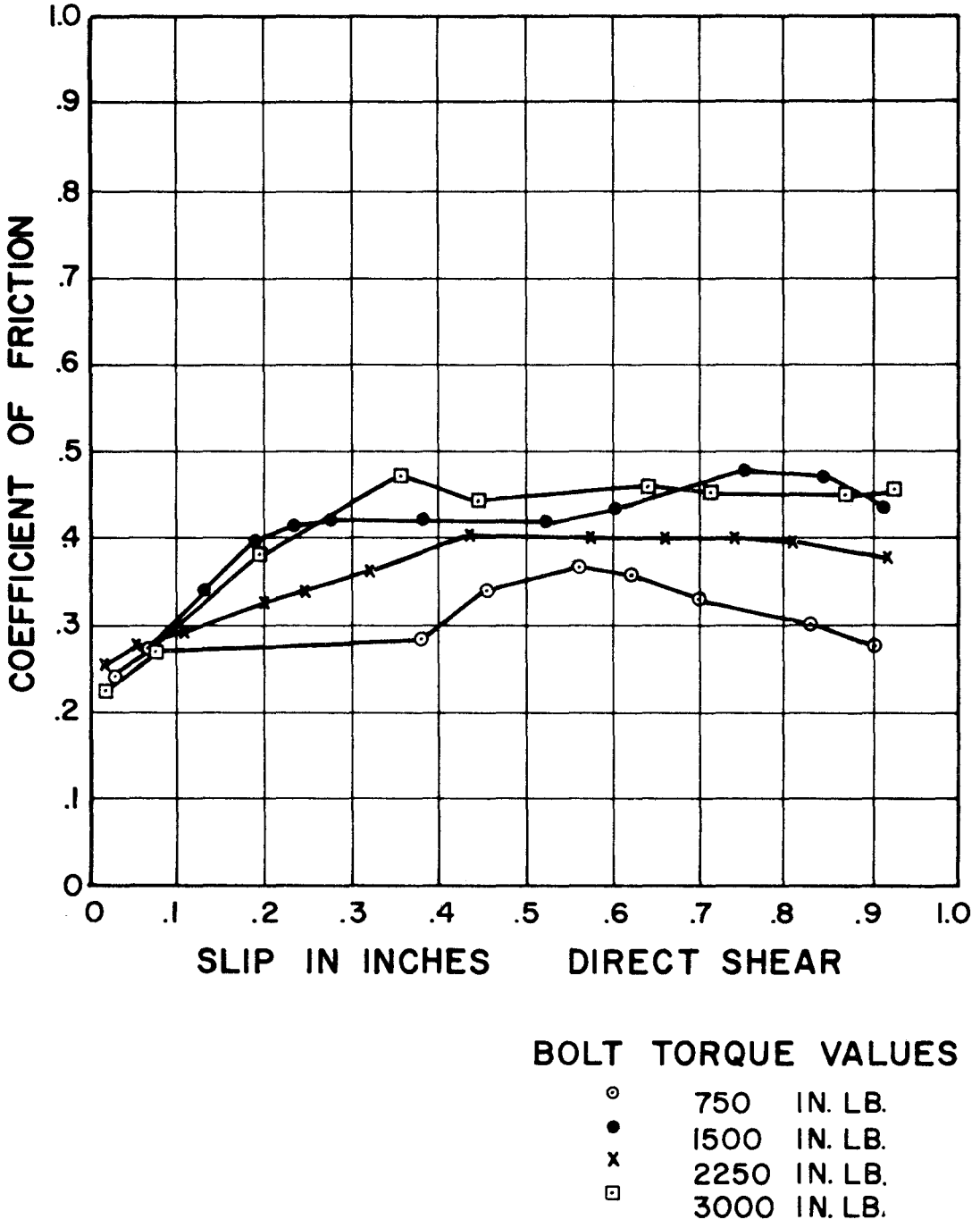

FIGURE 2.5.4 ACTUAL VALUES OF COEFFICIENT OF FRICTION, DIRECT SHEAR

expressed as:

$$F = mn\ f(s)\ N'$$

where

N' = initial bolt tension which is assumed to be an invariant.

With $m = 4$ and $n = 2$

$$F = 8f(s)\ N'$$

and

$$f(s) = \frac{F}{8N'}$$

The values of the coefficient of friction calculated in this manner are presented in Figure 2.5.5, and are termed Theoretical Values. Note that in this case, the coefficient of friction is not constant since it must reflect the changes in bolt tension due to bolt canting.

Figure 2.5.6 shows the slip vs. applied load for the eccentric load tests. Figure 2.5.7 is a plot of the tension in the bottom bolt vs. the applied load, and Figure 2.5.8 shows the tension in the top bolt vs. the applied load. In Figure 2.5.6 the slip at maximum load decreases with increased initial bolt torque; the decrease being essentially in reverse order of the increase in the direct shear tests (see Figure 2.5.1). Again note that the tension in the bottom bolt begins to increase at the knee of the slip vs. applied load curve. It is felt that in this case the canting is not as significant as in the direct shear case. This can be supported by referring to the dotted theoretical line in Figure 2.5.7. This line represents the tension

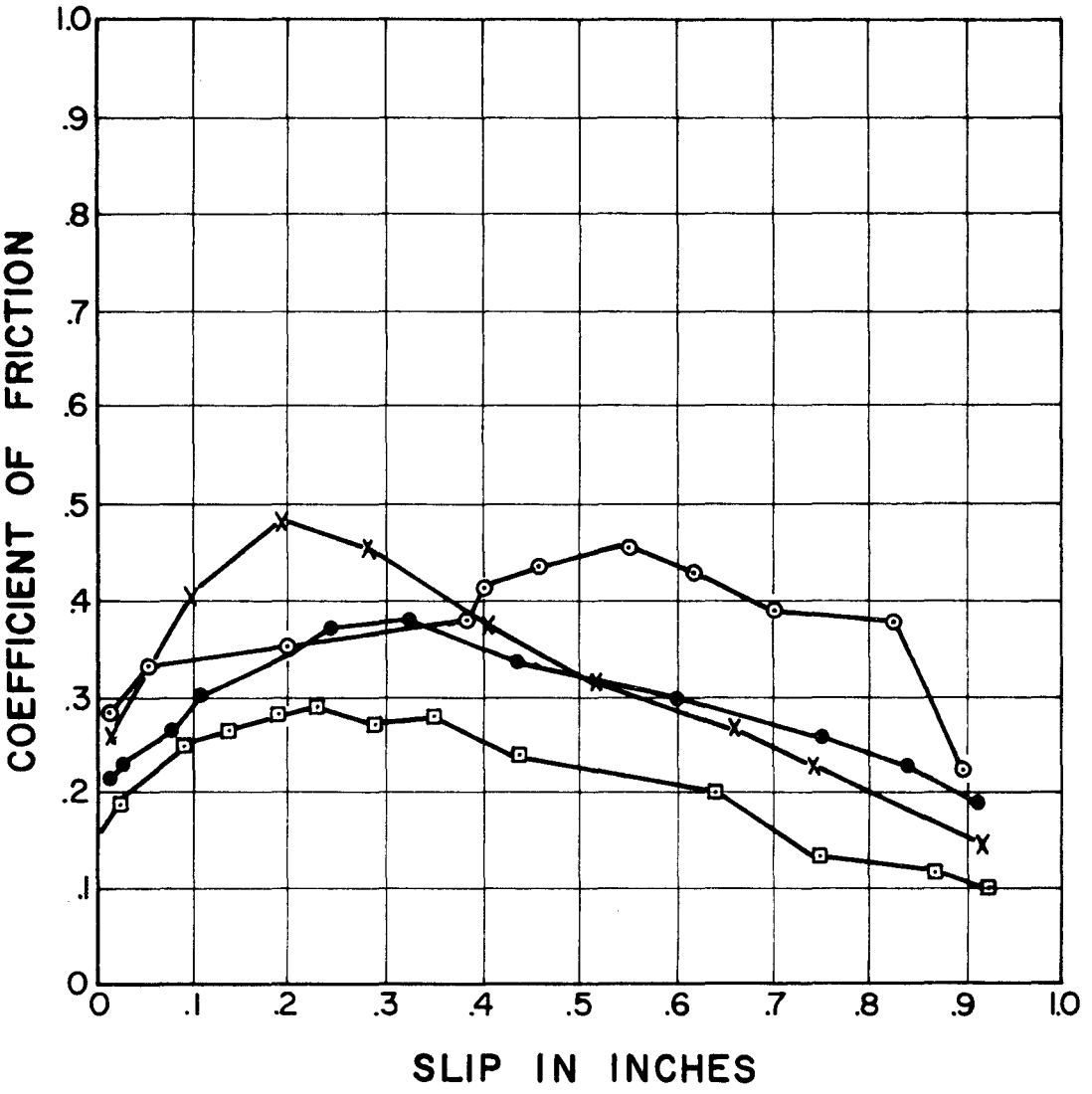

FIGURE 2.5.5 THEORETICAL COEFFICIENT OF FRICTION, DIRECT SHEAR

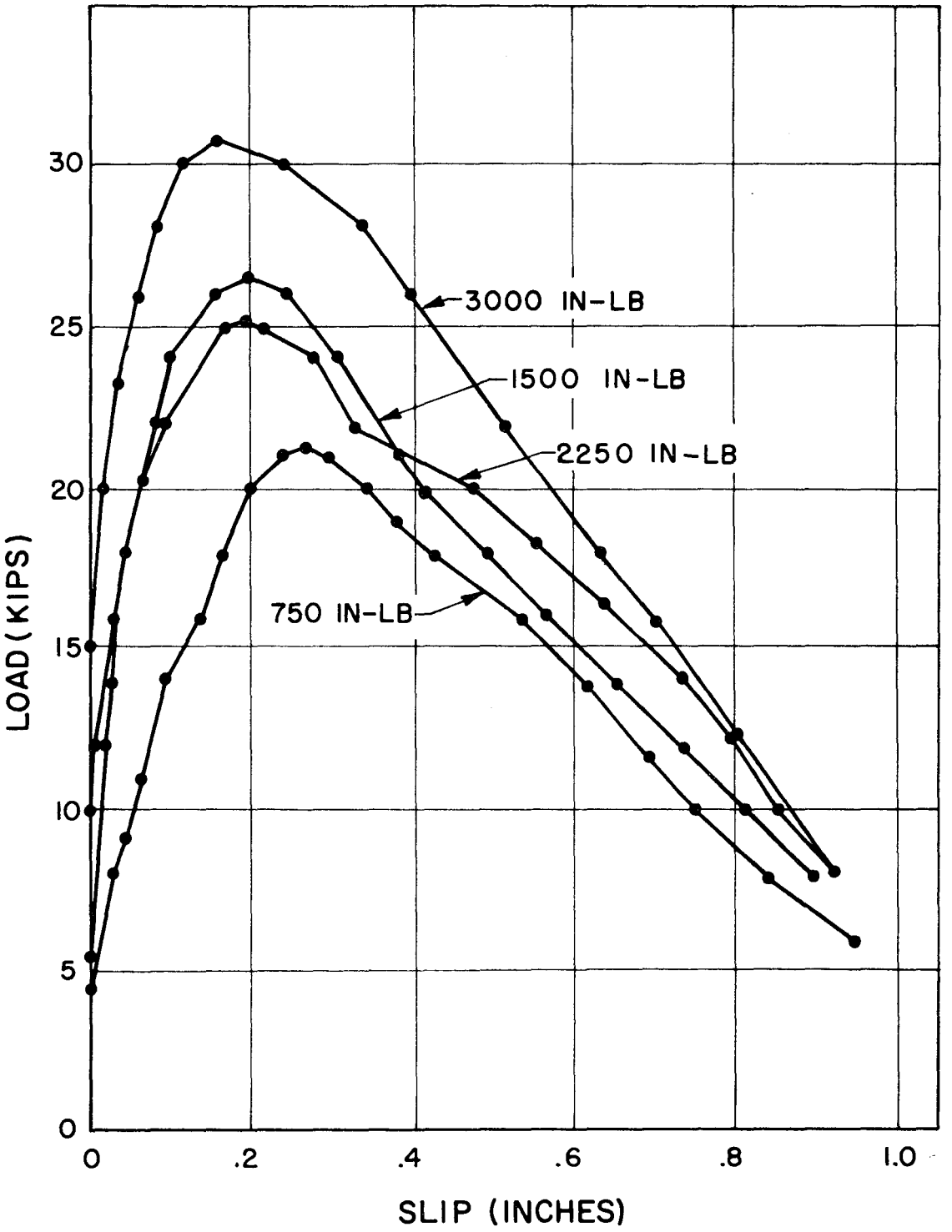

FIGURE 2.5.6. SLIP VS. APPLIED LOAD, ECCENTRIC LOAD

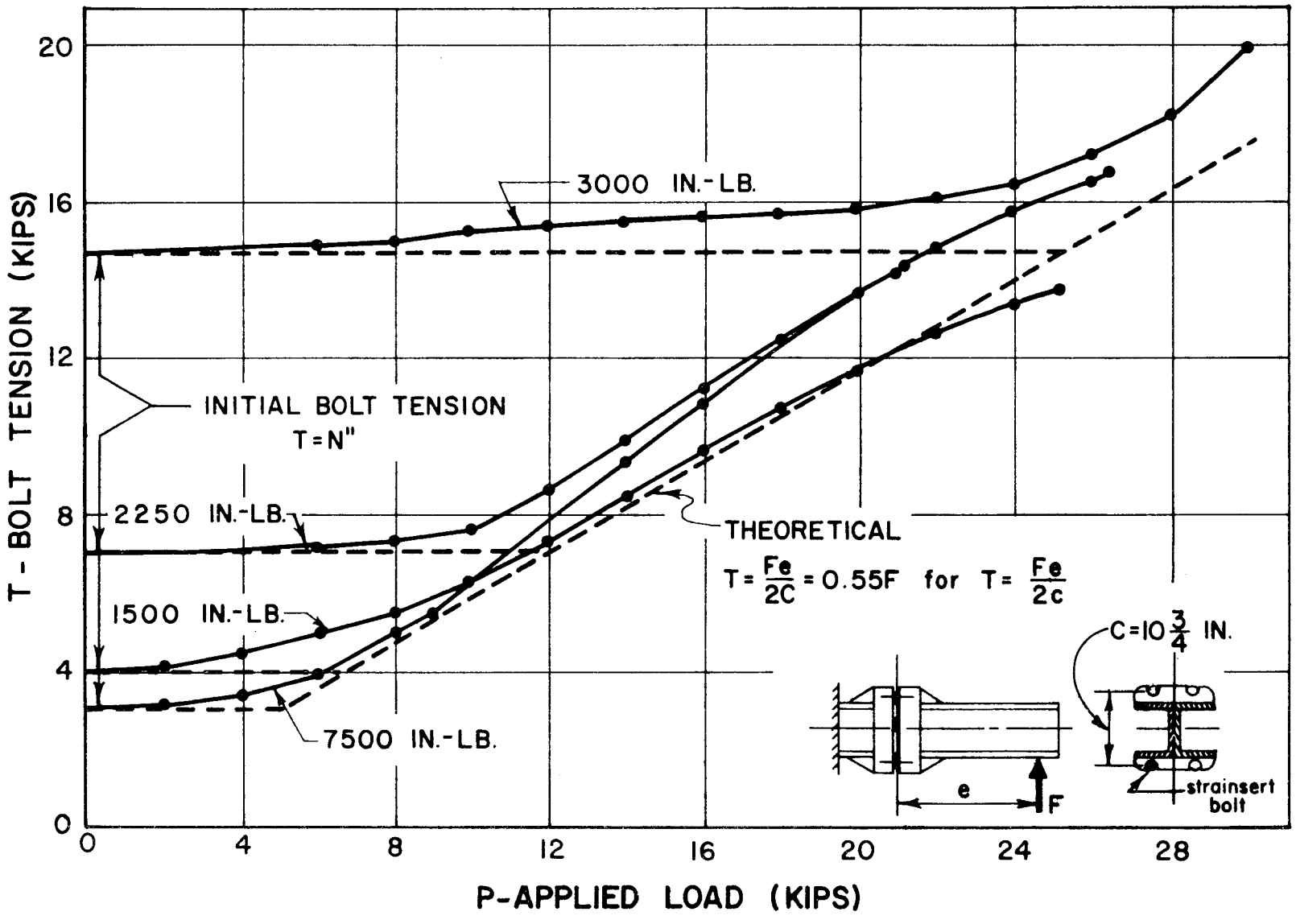

FIGURE 2.5.7 BOLT LOAD VS. APPLIED LOAD, ECCENTRIC LOAD

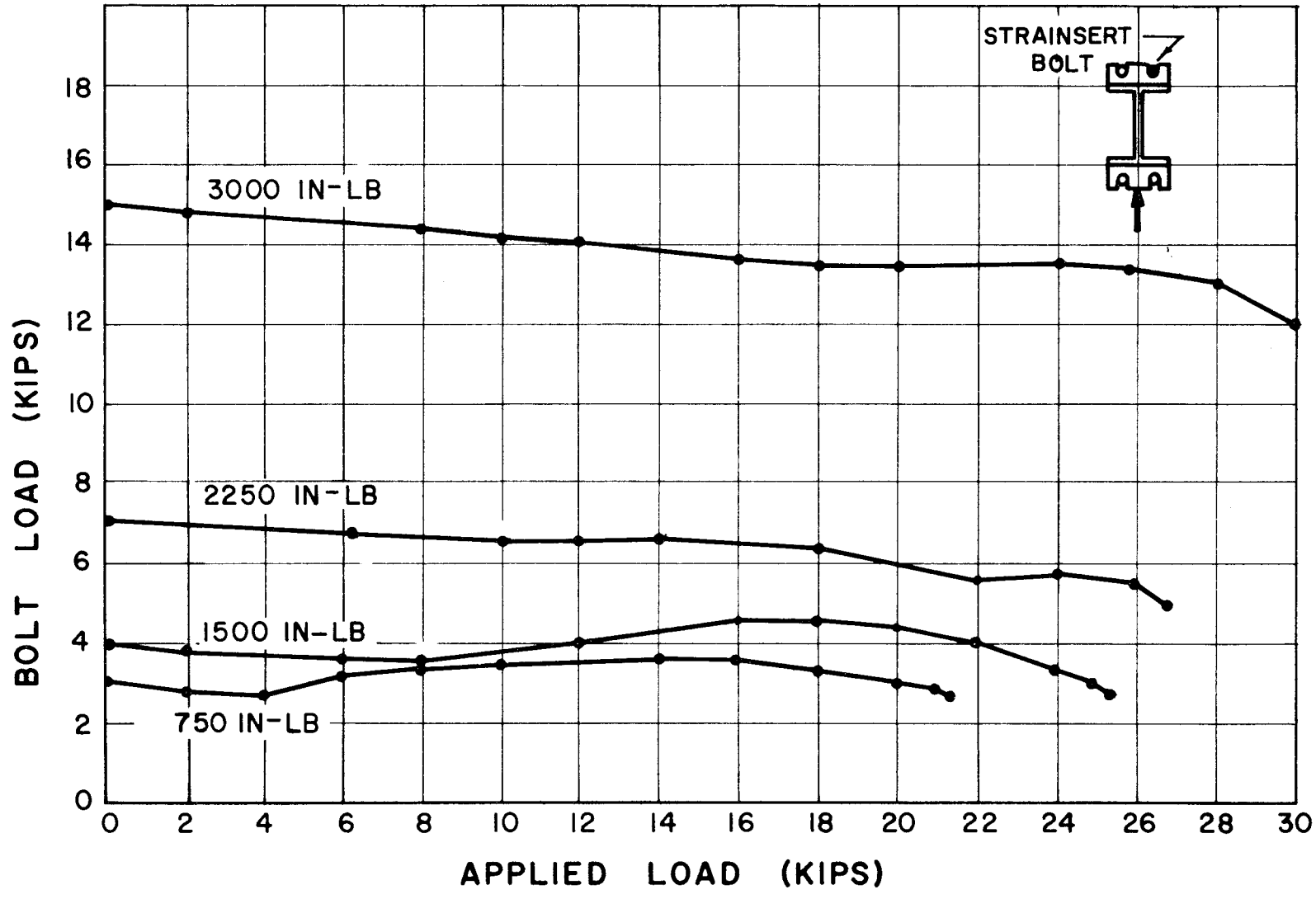

FIGURE 2.5.8 BOLT LOAD VS. APPLIED LOAD, ECCENTRIC LOAD

in the bolt which forms a part of the couple to balance the external moment Fe. Therefore

$$M = Fe = 2Tc \text{ or } T = \frac{Fe}{2c}$$

It can be seen that the actual data points fall close to this line. The point where the horizontal dashed line (line representing N', the initial bolt tension) intersects the diagonal dashed line (line for $T = \frac{Fe}{2c}$) is the point where the preload in the bolt is exceeded. The bottom bolts carry no significant increased load until this preload is exceeded. Slight variations are apparent however, due to the elasticity of the system. Note in Figure 2.5.8 that the force in the top bolt remains essentially constant up to peak load.

Figure 2.5.9 is a plot of the Actual Values of the coefficient of friction vs. the slip. As in the case of the Actual Values for Direct Shear, the coefficient is again essentially constant after slip at maximum applied load has been reached. Figure 2.5.10 shows the Theoretical Values of the coefficient of friction vs. the slip. In this case, the coefficient decreases slightly with increased slip.

Figure 2.5.11 is a composite plot of the Actual Values for all tests. The upper bound being $f(s) \simeq 0.45$ and the lower bound being $f(s) \simeq 0.28$. Figure 2.5.12 is a composite plot of the Theoretical Values for all tests. The upper bound being $f(s) \simeq 0.35$ and the lower bound being $f(s) \simeq 0.24$.

2.6 Conclusions

It can be concluded that a satisfactory representation of the

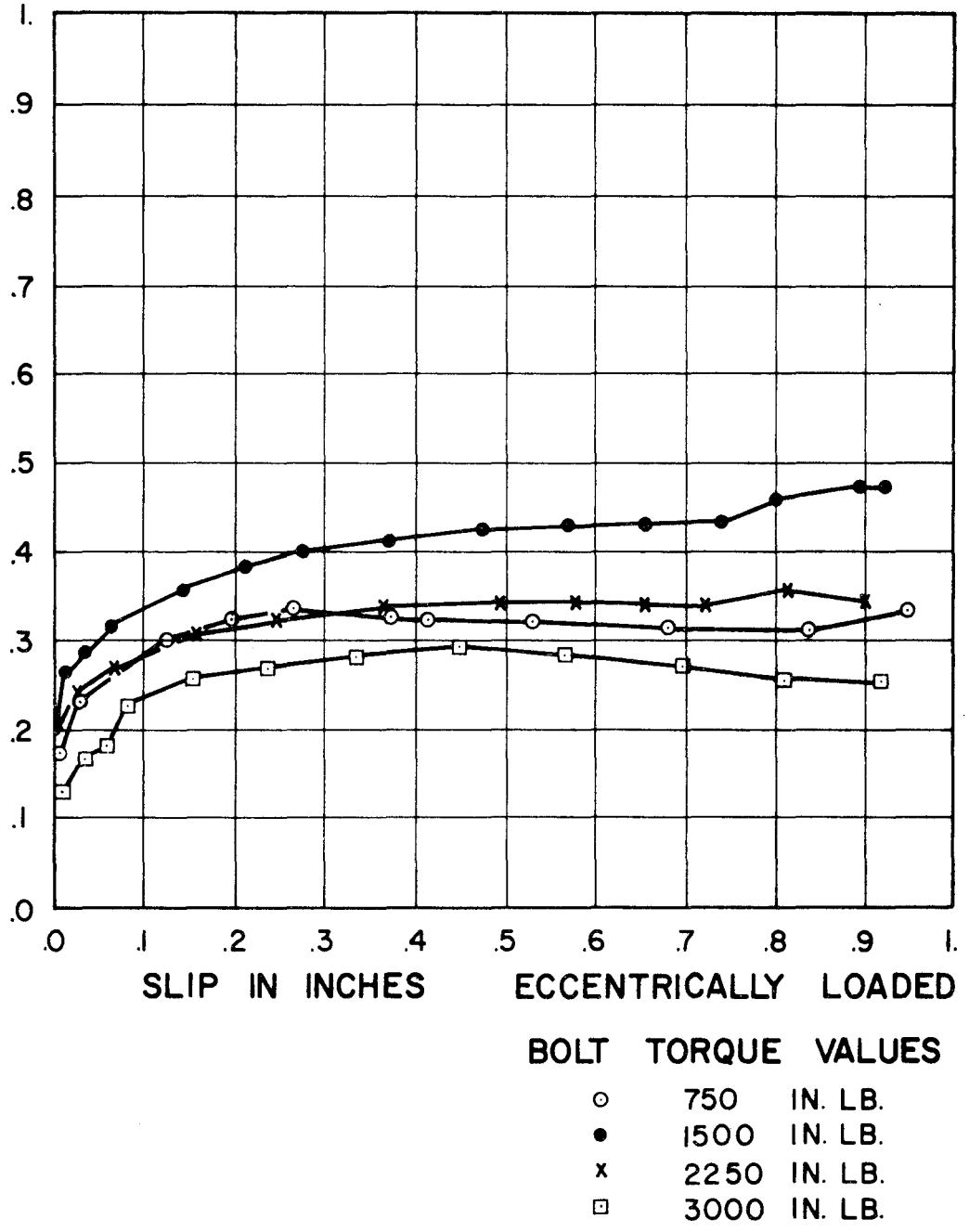

FIGURE 2.5.9 ACTUAL VALUES OF COEFFICIENT OF FRICTION, ECCENTRIC LOAD

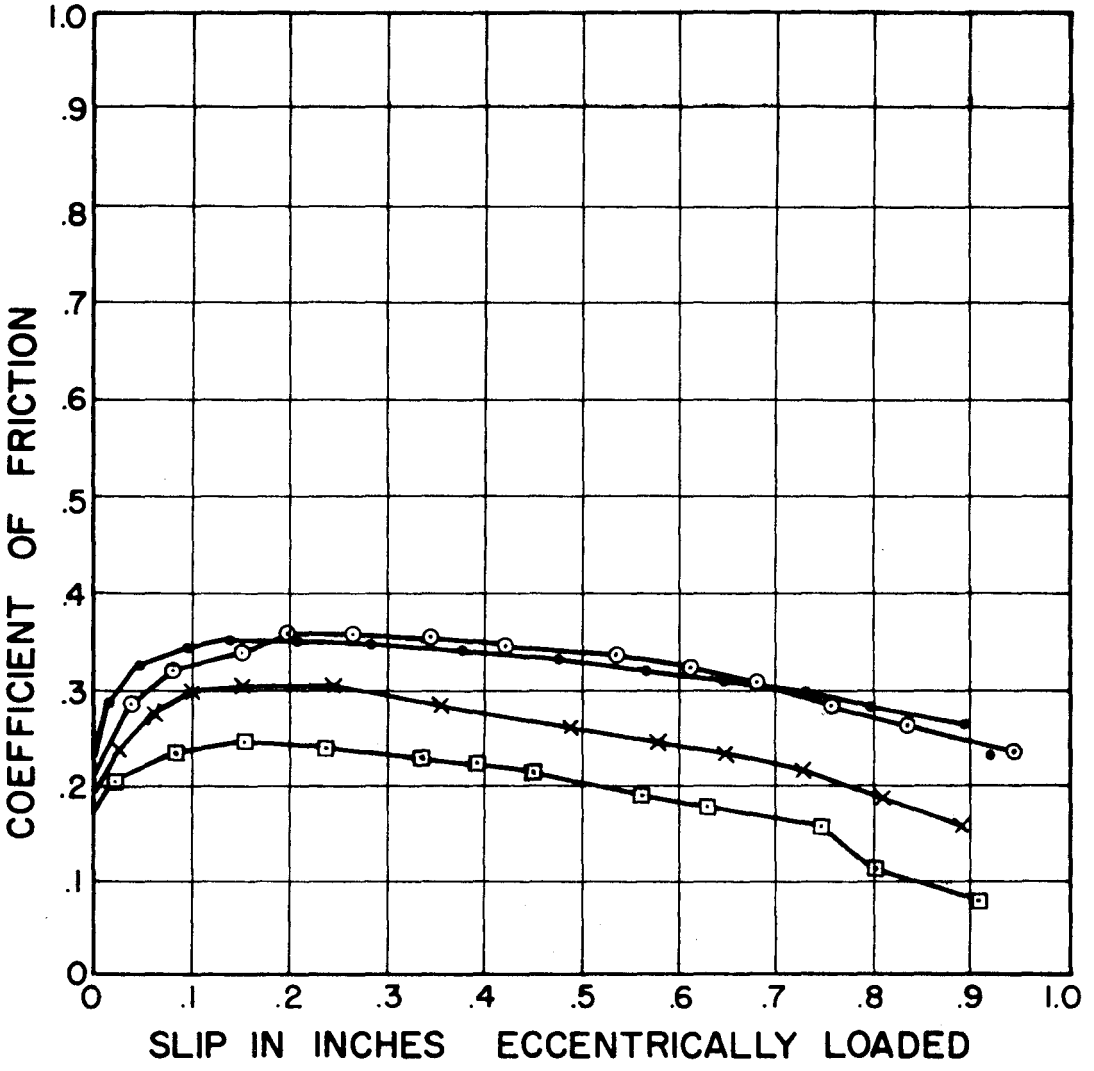

FIGURE 2.5.10 THEORETICAL VALUES OF COEFFICIENT OF FRICTION, ECCENTRIC LOAD

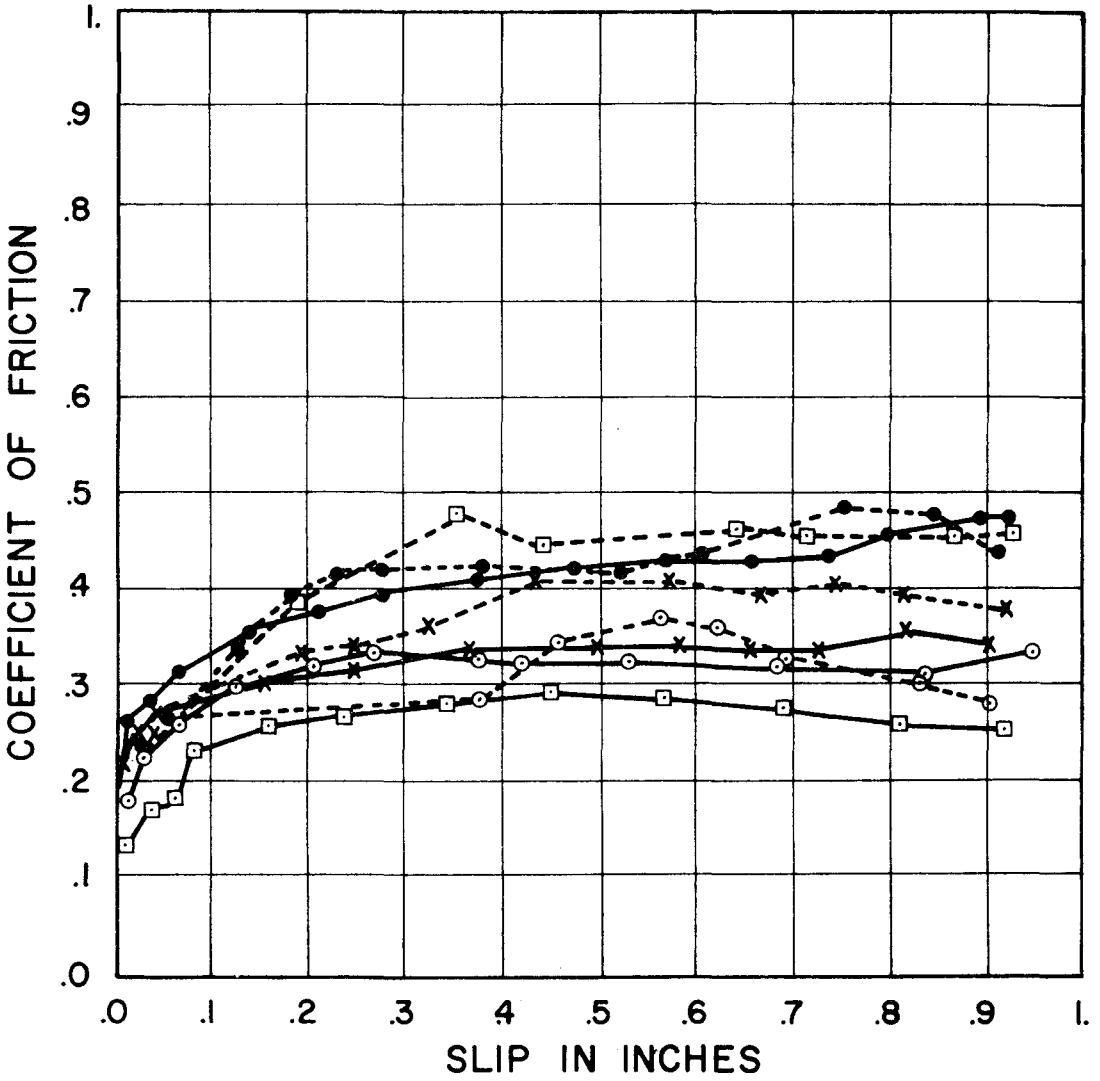

DIRECT SHEAR

BOLT TORQUE

⊙ 750 IN. LB.
● 1500 IN. LB.
x 2250 IN. LB.
⊡ 3000 IN LB.

ECCENTRICALLY LOADED

BOLT TORQUE VALUES

⊙ 750 IN. LB.
● 1500 IN. LB.
x 2250 IN. LB.
⊡ 3000 IN. LB.

FIGURE 2.5.11 ACTUAL VALUES OF COEFFICIENT OF FRICTION, ALL TESTS

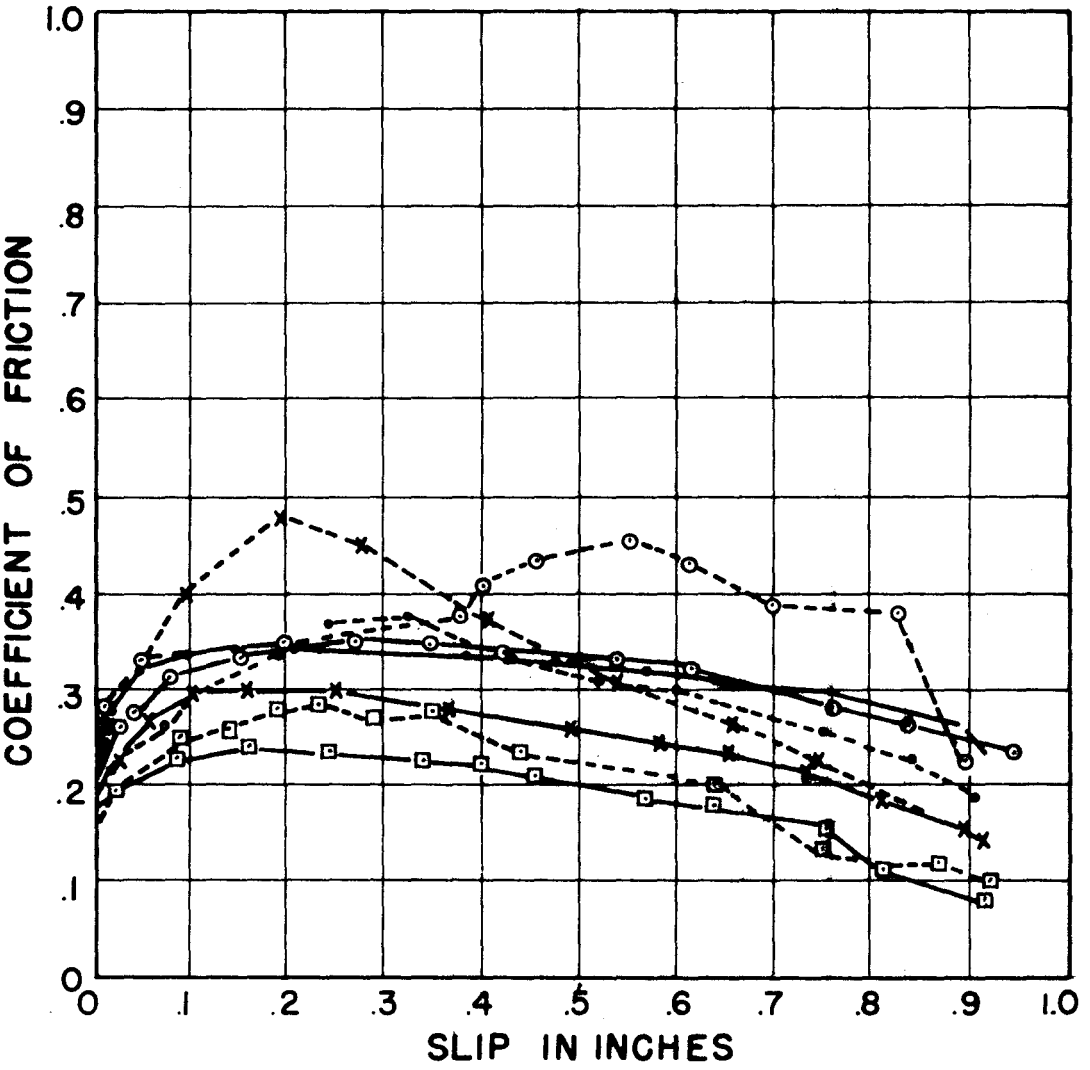

FIGURE 2.5.12 THEORETICAL VALUES OF COEFFICIENT OF FRICTION, ALL TESTS

base behavior under applied load can be obtained with the hypothesis presented in Section 2.10 of Part II, provided an empirical functional relation between slip and coefficient of friction is used. These tests also indicate that satisfactory slip data can be obtained from direct shear tests and applied to bases subject to moment and shear.

C H A P T E R 3

TORQUE-TENSILE LOAD PROPERTIES OF ASTM A325 BOLTS

3.1 Objective

The object of these tests was to determine the tensile force produced in an ASTM A325 bolt when used in a typical "break-away" base. The data obtained from tests will be used to extrapolate to other bolt sizes.

3.2 Test Procedure

A test consisted of torqueing a galvanized 3/4 inch A325 bolt mounted in the base plates for an 8WF20 post, see Figure 3.2.1. Torqueing was done with a torque wrench with a dial reading to the nearest 1 ft.-lb. This wrench was calibrated by the Texas Highway Department before use. The bolt was torqued several times to a value above the maximum attained in the test in order to condition the washer faces and the threads on the nut and bolt. The bolt was instrumented internally to measure axial strains (manufactured by the Strainsert Co.). The bolt was dead load calibrated before use. Four separate torqueing cycles were run with a separate individual manning the torque wrench for each cycle.

3.3 Results

Figure 3.3.1 gives the results of the four tests. Note that each set of data describes a linear relation between bolt torques and bolt tension. The average straight line through the data is described

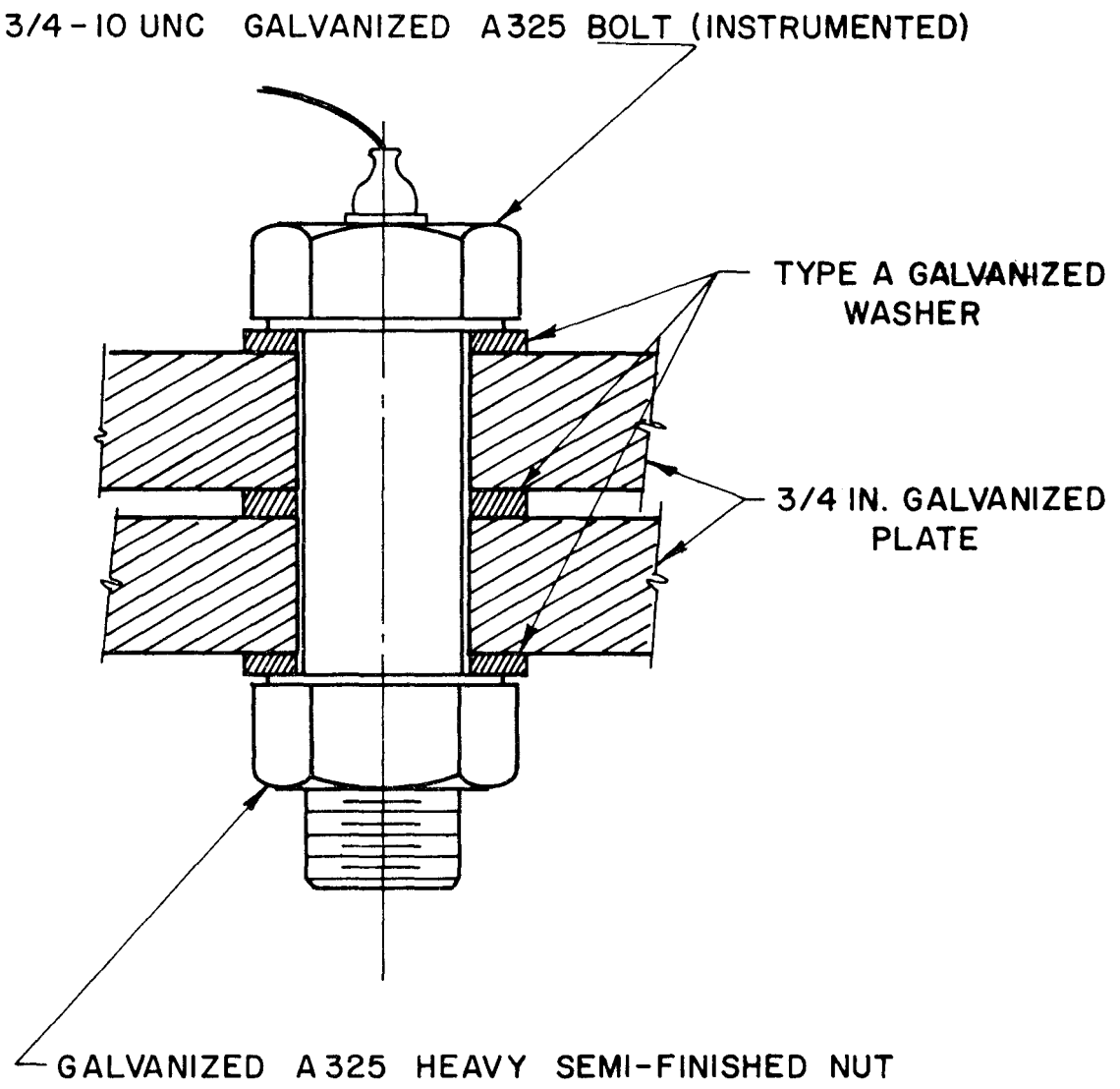

FIGURE 3.2.1 TEST SET-UP FOR TORQUE-TENSILE TEST

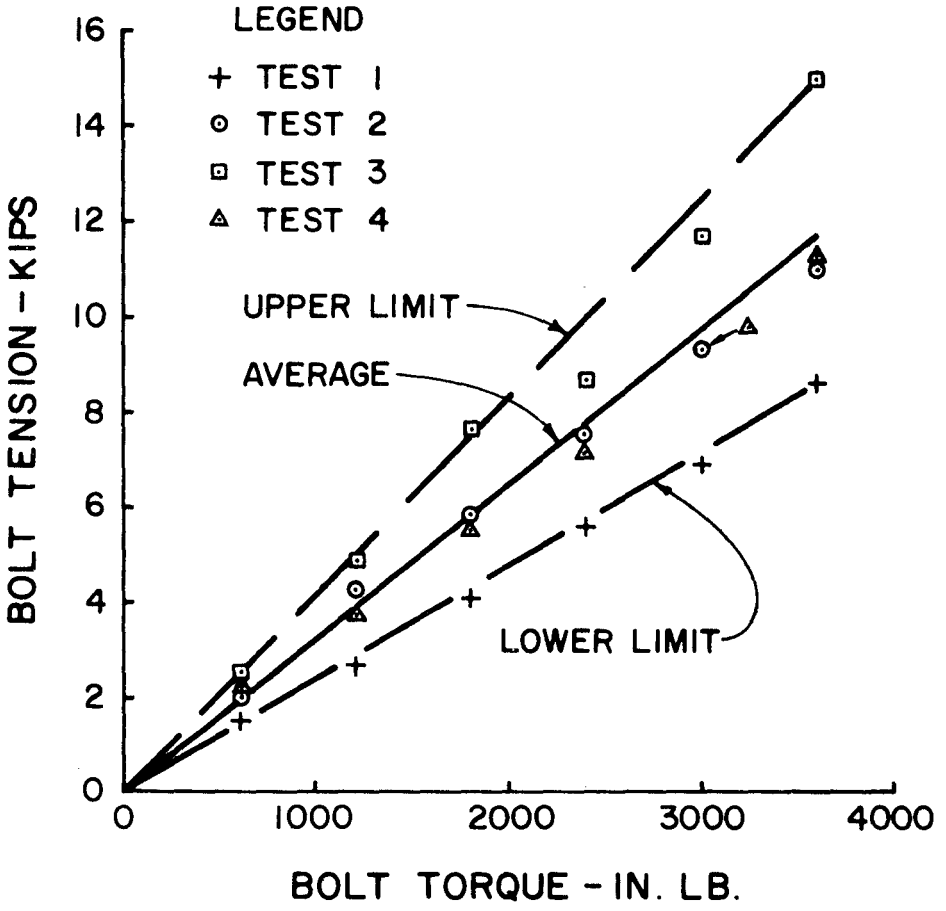

FIGURE 3.3.1 TORQUE-TENSILE DATA

by

$$N' = 3.185\ \tau$$

where

N' = force in bolt, lbs.

τ = torque on bolt, in.-lb.

This can be written as

$$N' = K_T \tau$$

where K_T = torque factor[1] and is expressed by

$$K_T = \frac{1}{\frac{p}{2\pi} + \frac{f_1(PD)}{1.734} + \frac{f_2\ (D + b)}{4}} \qquad (3.3.1)$$

where

p = pitch of threads, inch.

PD = pitch diameter, in.

D = outside thread diameter, in.

b = washer face diameter (taken as width across flats).

f_1 = coefficient of friction between threads

f_2 = coefficient of friction at washer face

It is assumed $f_1 = f_2$, which is reasonable, since all surfaces were galvanized. Equation (3.3.1) becomes

$$K_T = \frac{1}{\frac{p}{2\pi} + f_1 \left[\frac{PD}{1.734} + \frac{(D + b)}{4}\right]} \qquad (3.3.2)$$

and

$$f_1 = \frac{\frac{1}{K_T} - \frac{p}{2\pi}}{\frac{PD}{1.734} + \frac{(D + b)}{4}} \qquad (3.3.3)$$

For an A325 3/4-10 UNC bolt

D = 0.75 in.

PD = 0.685 in.

b = 1.25 in.

p = 1/10 = 0.10 threads/in.

$$f_1 = \frac{\frac{1}{3.185} - \frac{0.1}{2\pi}}{\frac{0.685}{1.734} + \frac{(2.00)}{4}} = 0.333$$

Values for K_T for other size bolts can be found using Equation (3.3.1) and the above value of f_1. Table 3.3.1 gives a summary for other bolt sizes.

TABLE 3.3.1 VALUES OF K_T IN $N' = K_T \tau$*

BOLT SIZE	K_T
1/2 - 13 UNC	4.940
5/8 - 11 UNC	3.870
3/4 - 10 UNC	3.185
7/8 - 9 UNC	2.783
1 - 8 UNC	2.472
1 1/8 - 7 UNC	2.162
1 1/4 - 7 UNC	1.980

*N' in lbs. and τ in in./lbs. For ASTM A325 galvanized bolts tested as shown in Figure 3.2.1.

C H A P T E R 4

STATIC FUSE PLATE TESTS

The first design drawings issued by the Texas Highway Department specified a cast iron fuse plate at the "plastic hinge." Several field failures of the fuse under wind load led the department engineers to seek an alternate fuse plate. A new design of a mechanical fuse fabricated from ASTM A441 steel was proposed. This fuse was designed to slip rather than fracture. Subsequent development led to the slotted steel fuse plate currently being used on the "break-away" sign support post. The tests and results presented in this chapter were conducted under the sponsorship of the Texas Highway Department in cooperation with the Bureau of Public Roads.[2]

4.1 Objective

The objective of these tests was to determine the maximum load capacity and the coefficient of friction - slip data of the slotted steel fuse plate when subjected to a tensile load. The bolting of the plates in these tests was in accordance with the ASTM turn-of-nut method of tightening.[3] This criteria assures that the bolt has been tensioned to its proof load. Effects of rebolting and weathering on the load capacity were also an objective.

4.2 Test Specimens

Representative fuse plates were chosen from the support sizes used in the Texas design (December 1965). Figure 4.2.1 shows the plate sizes used.

TABLE 4.2.1 FUSE PLATE SPECIMENS

NOTE: See Figure 4.2.1 for nomenclature

POST SIZE	SPECIMEN NUMBER	TEST SERIES	BOLT SIZE (in.)	C (in.)	D (in.)	E (in.)	F (in.)	G (in.)	H (in.)	J (in.)	d_1 (in.)	t_1 (in.)
6B8.5	1-5	A&B	$\frac{5}{8}$	$\frac{7}{8}$	$2\frac{1}{4}$	4	$\frac{5}{8}$	$2\frac{3}{4}$	1	$4\frac{3}{8}$	$\frac{11}{16}$	$\frac{3}{8}$
8WF17	1-5	A&B	$\frac{7}{8}$	$1\frac{1}{4}$	$2\frac{3}{4}$	$5\frac{1}{4}$	$\frac{7}{8}$	$3\frac{1}{4}$	$1\frac{1}{4}$	$5\frac{3}{8}$	$\frac{15}{16}$	$\frac{1}{2}$
	1-2	A&B	1	$1\frac{1}{2}$	$2\frac{3}{4}$	$5\frac{3}{4}$	1	$3\frac{1}{4}$	$1\frac{1}{4}$	$5\frac{1}{2}$	$1\frac{1}{16}$	$\frac{3}{4}$
10WF25	3-5	A	1	$1\frac{1}{2}$	$2\frac{3}{4}$	$5\frac{3}{4}$	1	$3\frac{1}{4}$	$1\frac{1}{4}$	$5\frac{1}{2}$	$1\frac{1}{16}$	$\frac{3}{4}$
	4	B	1	$1\frac{1}{2}$	$2\frac{3}{4}$	$5\frac{3}{4}$	1	$3\frac{1}{4}$	$1\frac{1}{4}$	$5\frac{1}{2}$	$1\frac{1}{16}$	$\frac{5}{8}$
	5	B	1	$1\frac{1}{2}$	$2\frac{3}{4}$	$5\frac{3}{4}$	1	$3\frac{1}{4}$	$1\frac{1}{4}$	$5\frac{1}{2}$	$1\frac{1}{16}$	$\frac{3}{8}$

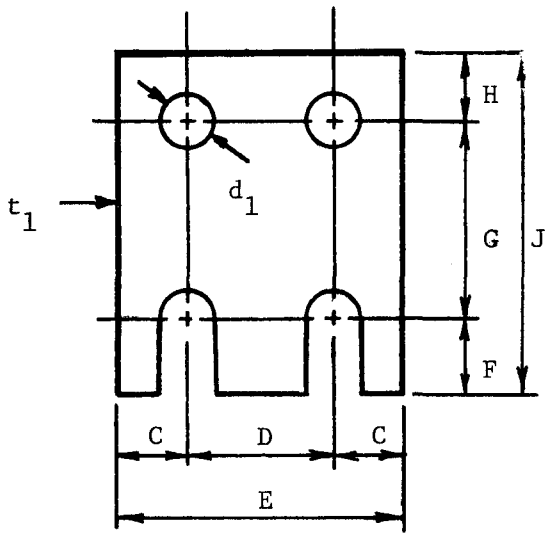

NOTE: SEE TABLE 4.2.1 FOR VALUES

FIGURE 4.2.1 FUSE PLATE SPECIMENS

4.3 Types of Tests

Three series of tensile tests were conducted. Series A tests used five identical specimens. The plates in these tests were galvanized and in a new condition. New galvanized bolts were used on each test and tightened by the turn-of-nut method. These tests simulated a first application of load condition. Series B tests used the same five specimens and bolts used in the Series A test (except in the Series B tests on the 10WF25 post) in this case, however, the bolts were retightened. This simulated a rebolting after re-erection following a collision.

Series C tests were conducted with specimens identical to those used in Series A tests. In this case, however, the whole test assembly (see Figure 4.3.1) was weathered for one year before testing.

4.4 Data Reduction

The fuse plate resistance can be expressed as

$$F = mnf(s)N'$$

where

m = number of bolts crossing the slip plane

n = number of friction faces per bolt

f(s) = coefficient of friction

N' = load in the bolt, in this case assumed to be at the bolt proof load.

With m = 2 and n = 2

$$f(s) = \frac{F}{4N'}$$

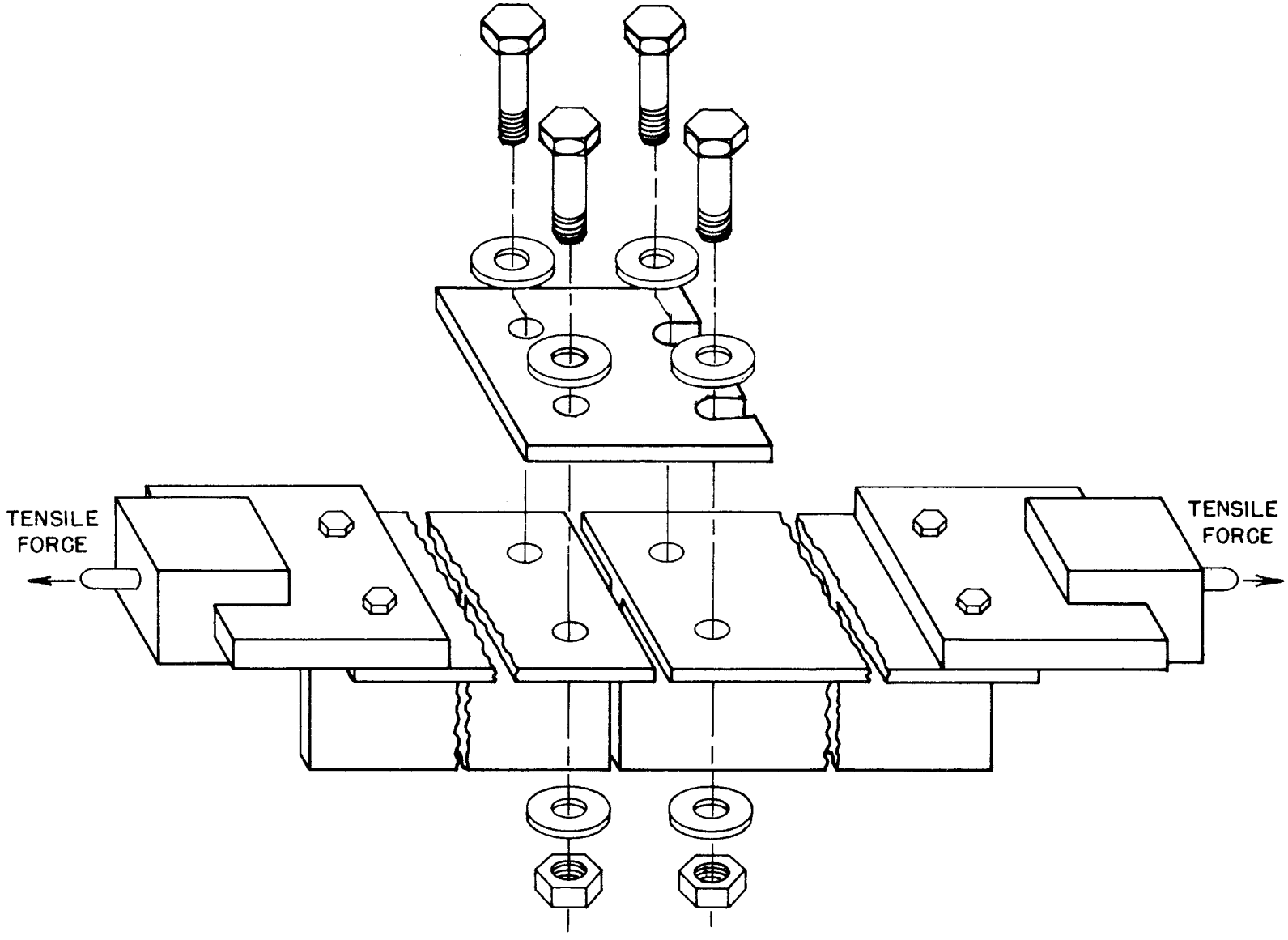

FIGURE 4.3.1 TEST FIXTURE FOR TENSILE TEST OF SLOTTED STEEL FUSE PLATE

For any value of slip, s, the applied load is known, yielding the apparent coefficient of friction for that slip.

4.5 Test Procedure

The equipment employed in these tests was as follows:

(1) Baldwin-Southwark-Emery 120,000 lb. capacity testing machine.

(2) 6" dividers and 12" scale (0.01" graduation).

(3) Test fixture (see Figure 4.3.1).

The typical test procedure was as follows:

(1) Tighten bolt by the turn-of-nut method.

(2) Place fixture in tensile grips of the testing machine with open end of the slots facing upward and mark 2" gage length on edge of T-section.

(3) Apply load at constant strain rate and take slip reading with dividers using the previously marked gage length.

4.6 Results

Series A and B tests. Figure 4.6.1 through Figure 4.6.6 show the data for the five specimens in Series A and Series B tests (four specimens in Series B for 10WF25 post). Observation of the test specimens after testing revealed that the contact surfaces were galled and that the bolt holes in the plate and the flange of the post section were elongated. Rebolting of once-used specimens increased the maximum capacity of the joint in every case. This would tend to indicate an increase in the coefficient of friction, but probably is due more

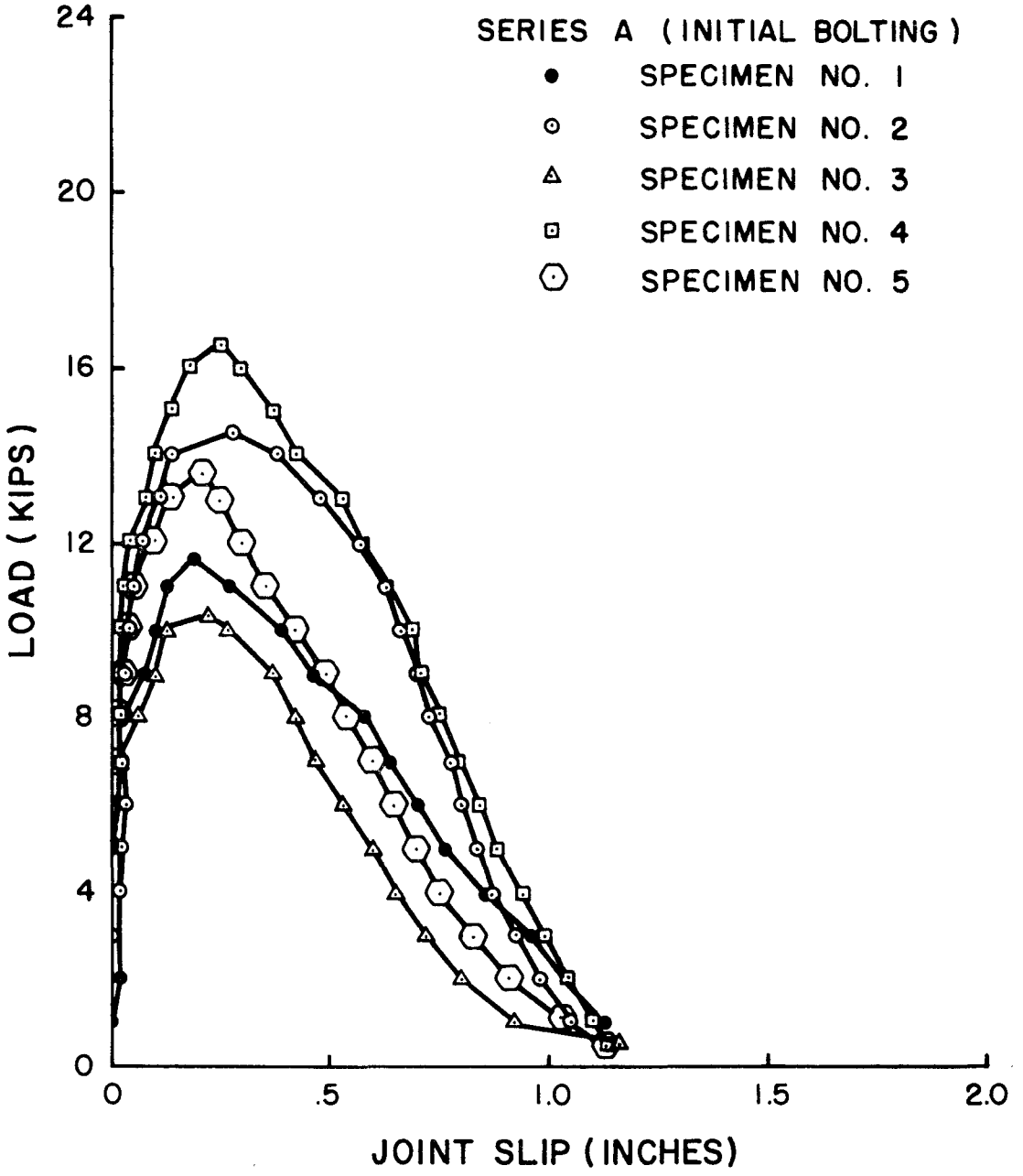

FIGURE 4.6.1 SLOTTED PLATE TENSILE TESTS (6 B 8.5)

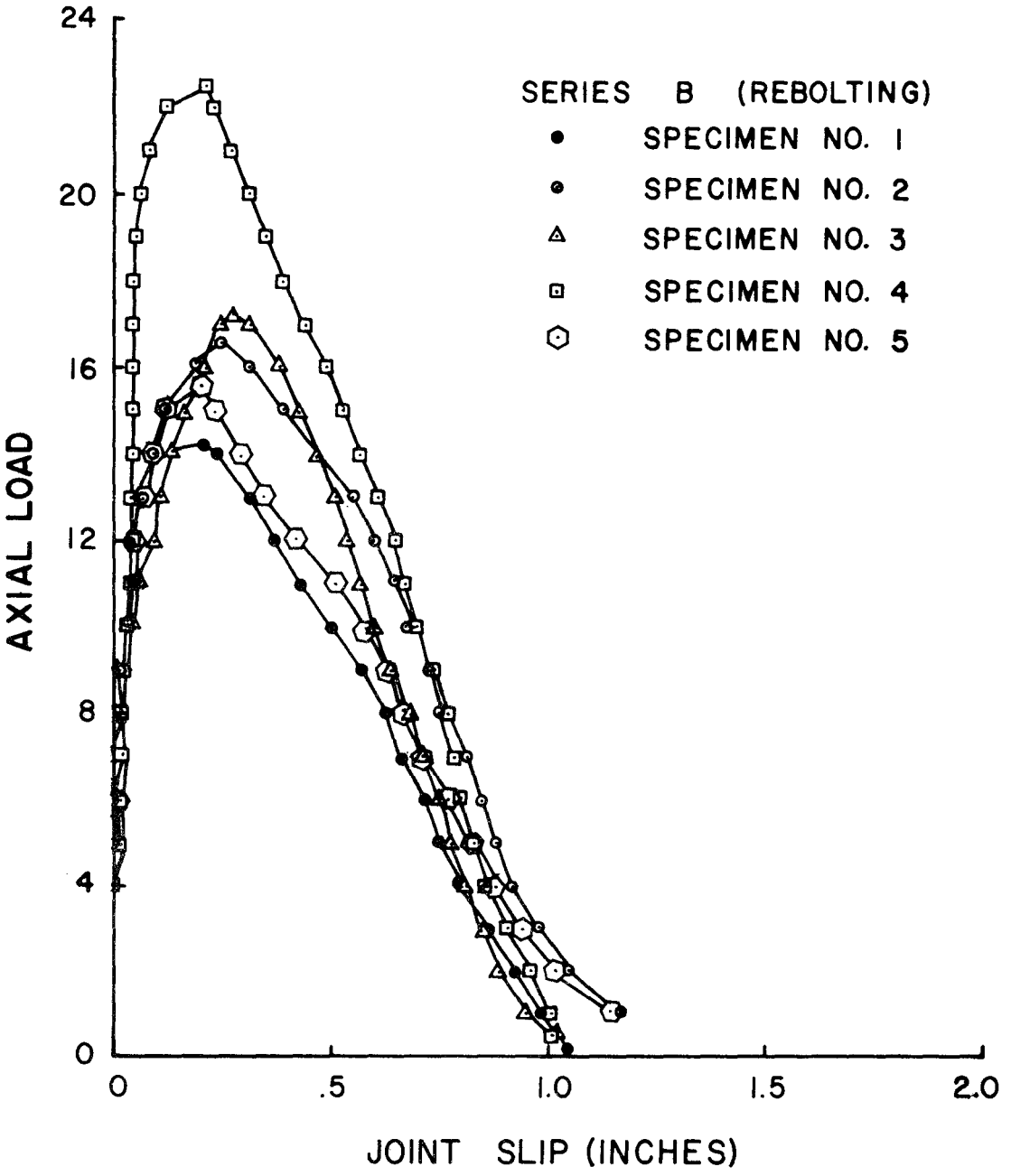

FIGURE 4.6.2 SLOTTED PLATE TENSILE TESTS (6 B 8.5)

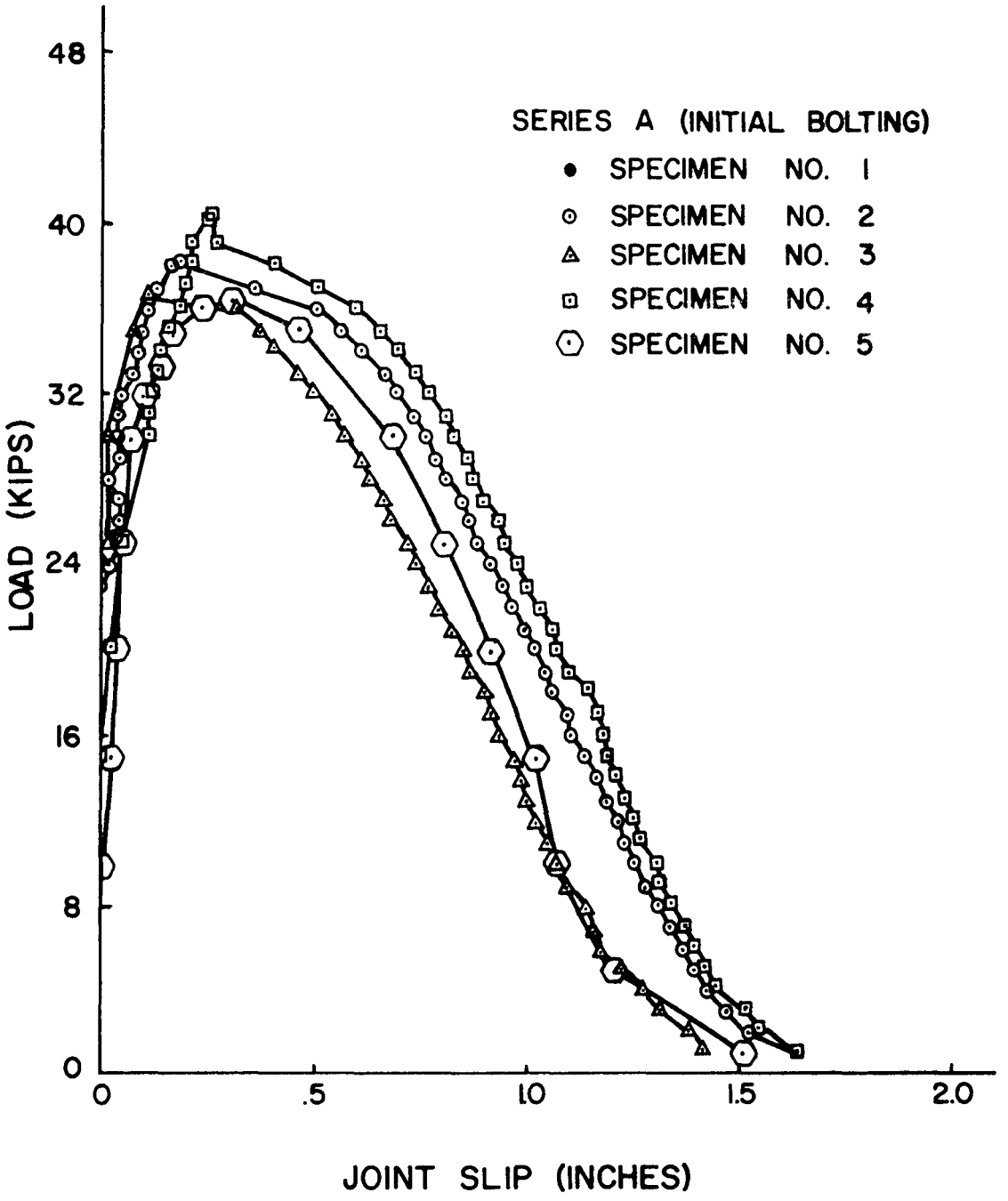

FIGURE 4.6.3 SLOTTED PLATE TENSILE TESTS (8 WF 17)

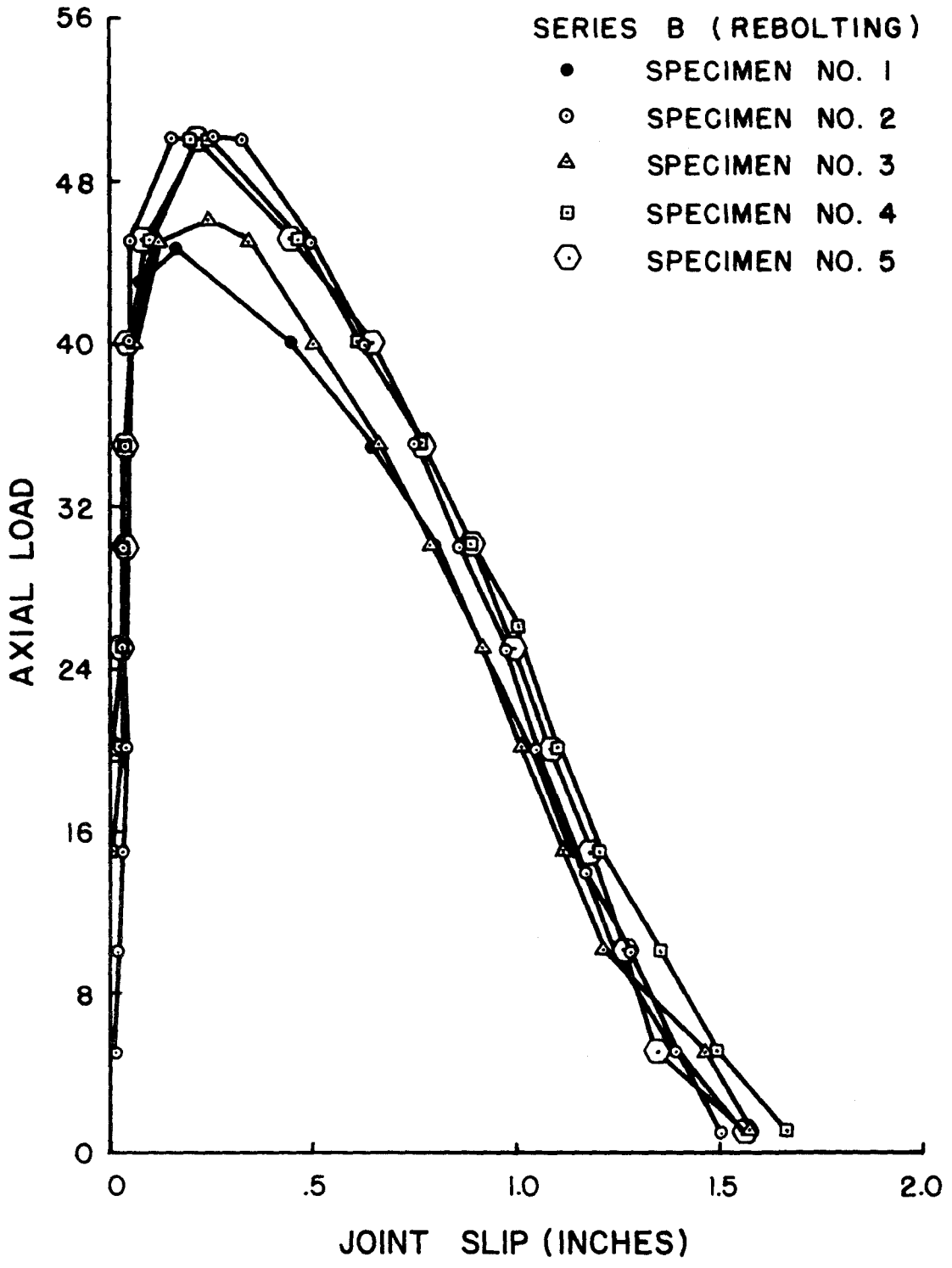

FIGURE 4.6.4 SLOTTED PLATE TENSILE TESTS (8 WF 17)

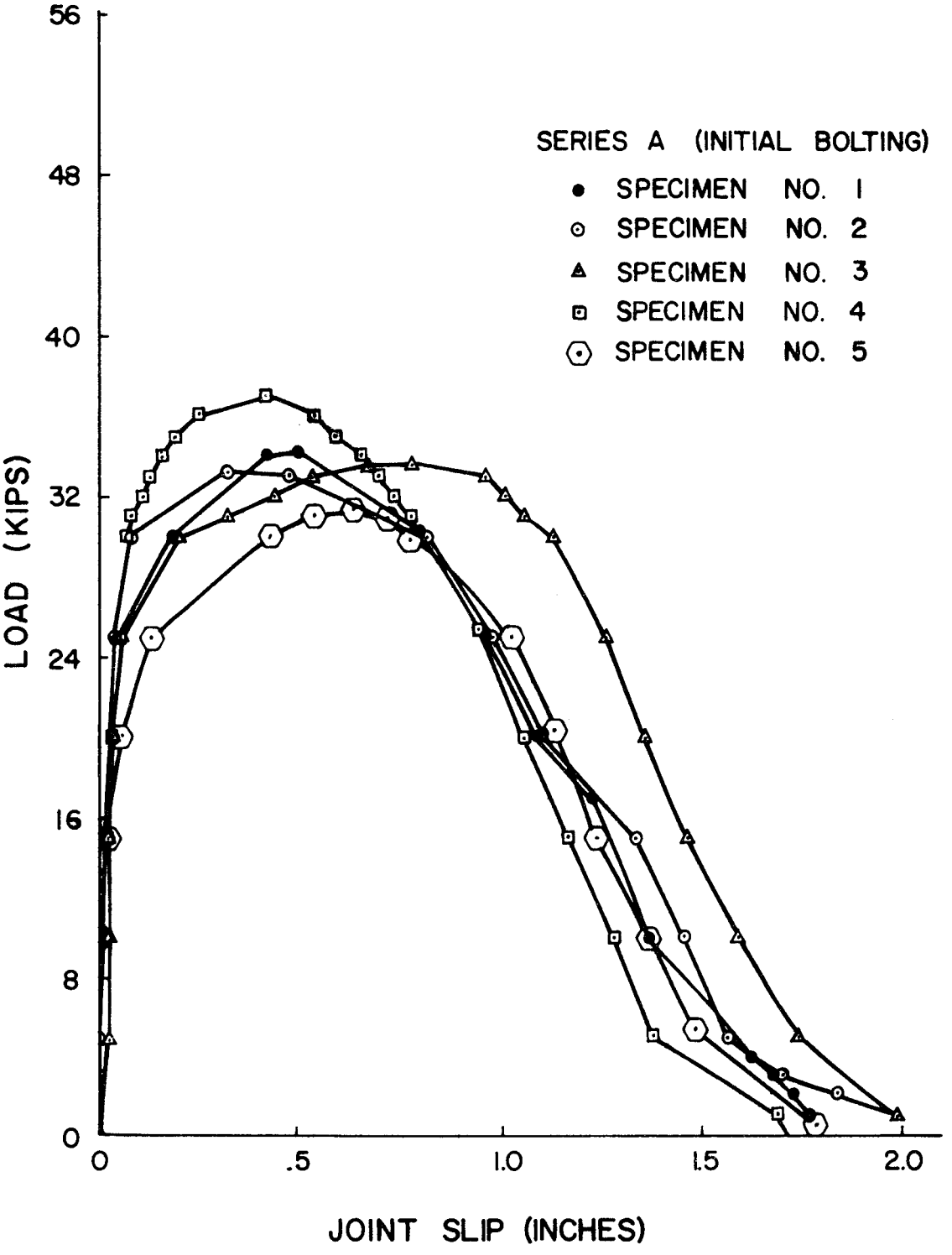

FIGURE 4.6.5 SLOTTED PLATE TENSILE TESTS (10 WF 25)

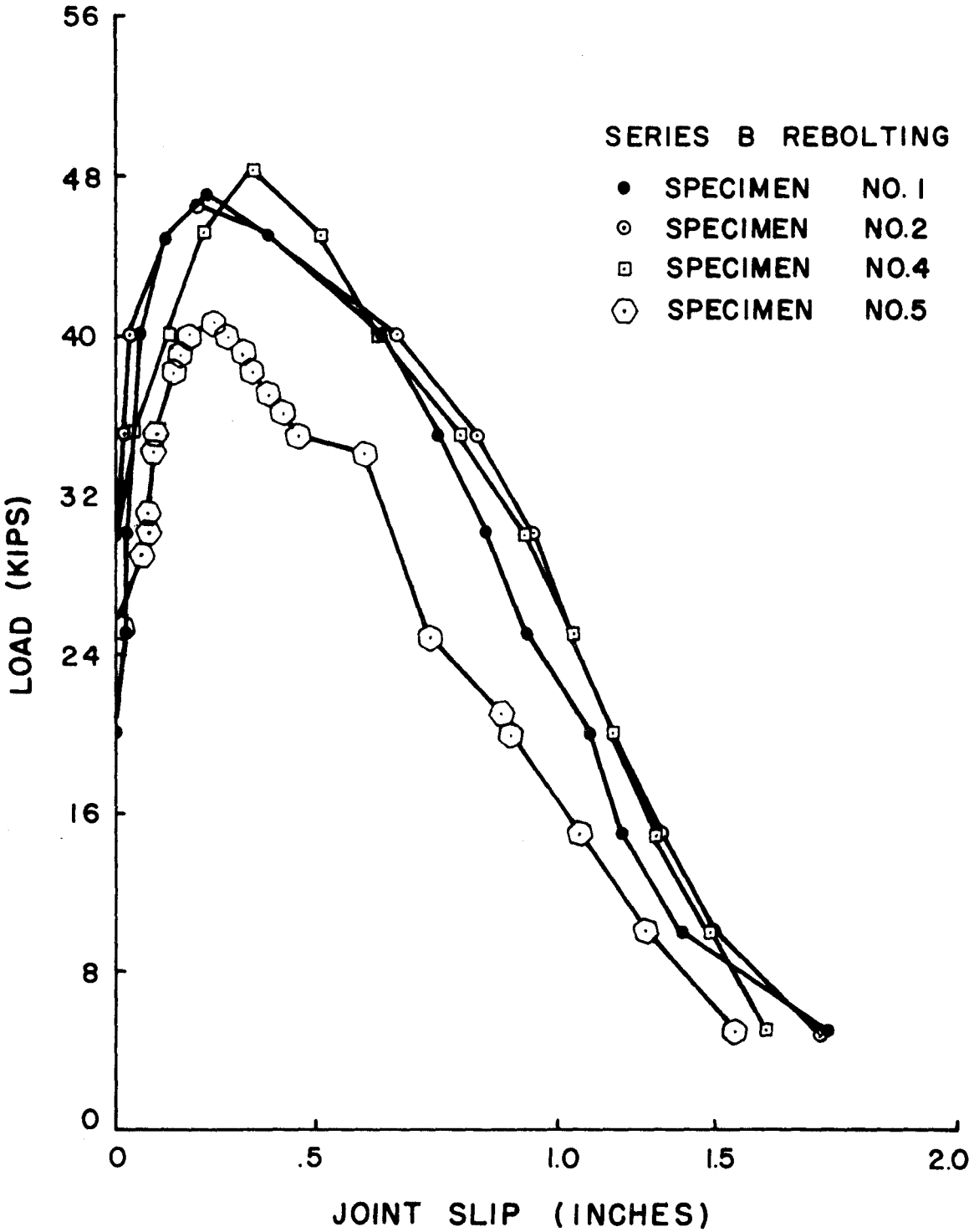

FIGURE 4.6.6 SLOTTED PLATE TENSILE TESTS (10 WF 25)

to the increased bolt force due to the diminishing of creep effects in the zinc layers, i.e., the zinc layers were previously compressed by the first torqueing. Figure 4.6.7, Figure 4.6.8 and Figure 4.6.9 show the upper and lower bound curves for the calculated values of the coefficient of friction.

Subsequently, the question of effects of weathering on bolted friction connections was raised. On April 15, 1966, five additional specimens were bolted together and placed out-of-doors subject to climatic conditions. On April 17, 1967, these specimens were tested and the maximum load for each specimen is shown in Table 4.6.1. The average value of maximum load for the five "weathered" specimens was 41.8 kips.

The average force required to pull the connections apart following exposure to the weather appears to be approximately 11% greater than the initial bolted connections and 14% less than the rebolted connections.

Based upon this limited number of specimens it appears that weathering does not appreciably affect the strength of the galvanized slotted steel plate bolted connection.

Recommendations for slotted steel fuse plate connections are contained in Section 3.3, Part I of this report.

4.7 Behavior of Mild Steel at Low Temperatures

Tensile tests are normally performed at ambient temperature, thus the mechanical properties of mild steel reflect the behavior of the material at approximately +70°F. It is known that as the temperature decreases the tensile strength and yield strength increase whereas the percent elongation decreases. For mild steel the ultimate strength increases from 60 ksi at 70°F to 120 ksi at -200"F, while the percent elongation decreases

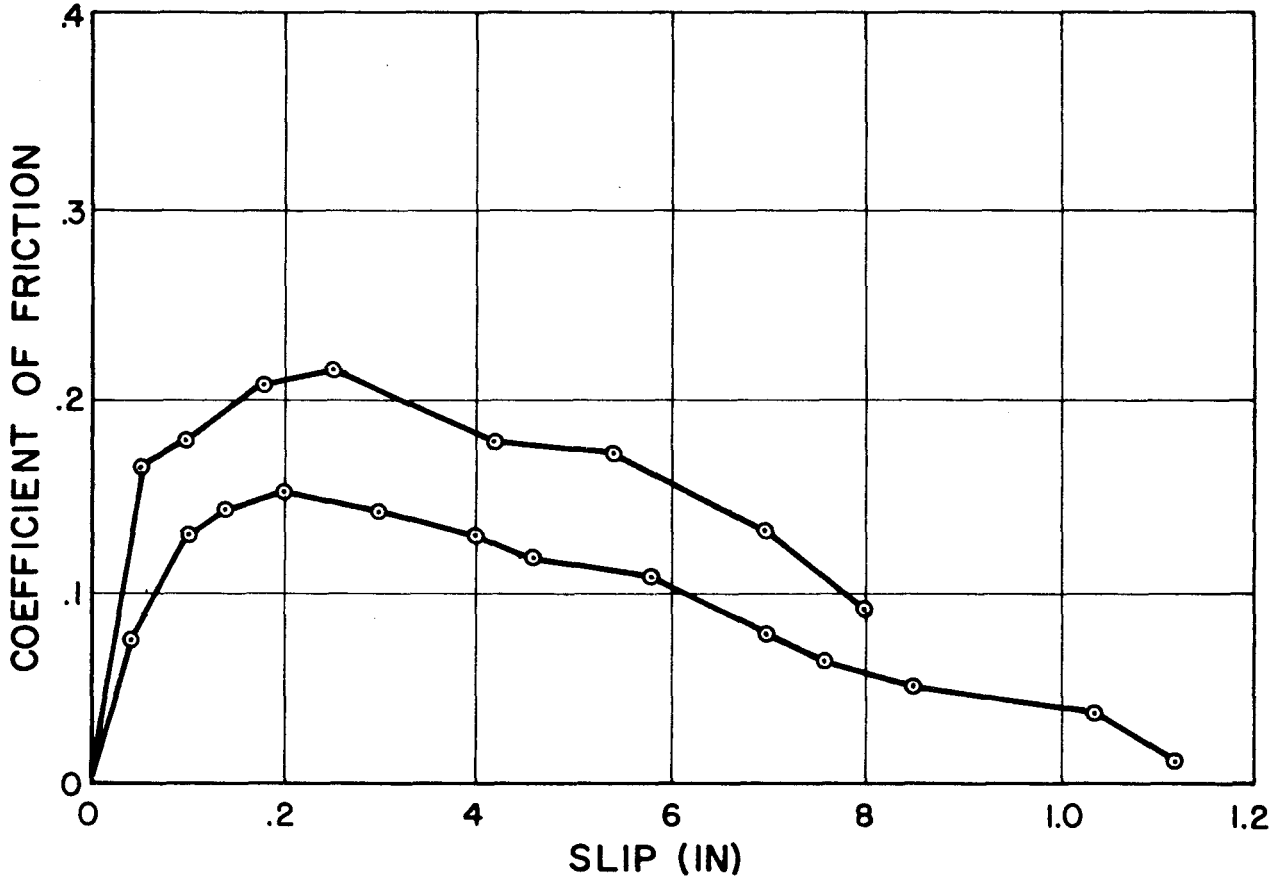

FIGURE 4.6.7 COEFFICIENT OF FRICTION VS. SLIP

(6 B 8.5)

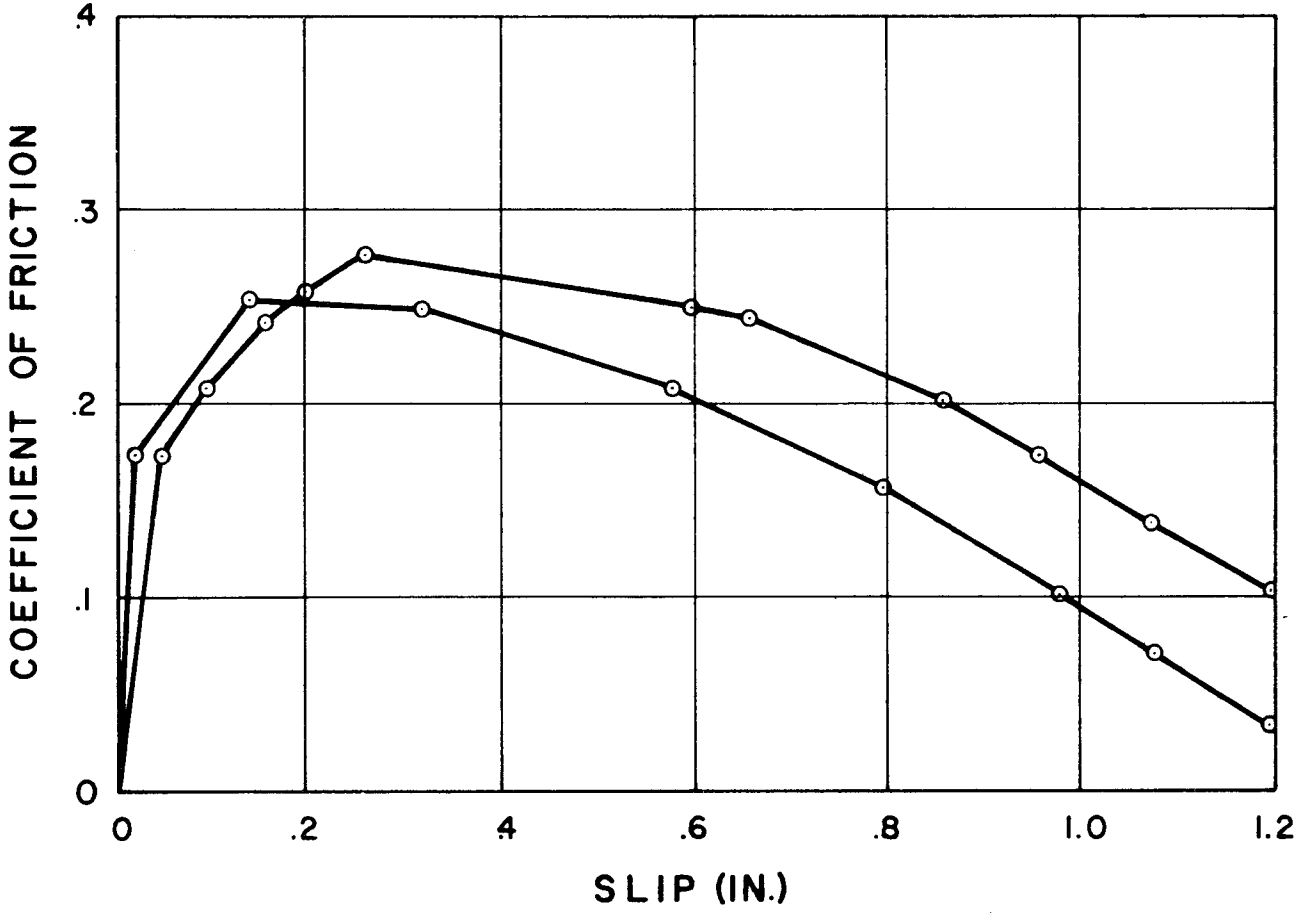

FIGURE 4.6.8 COEFFICIENT OF FRICTION VS. SLIP

(8 WF 17)

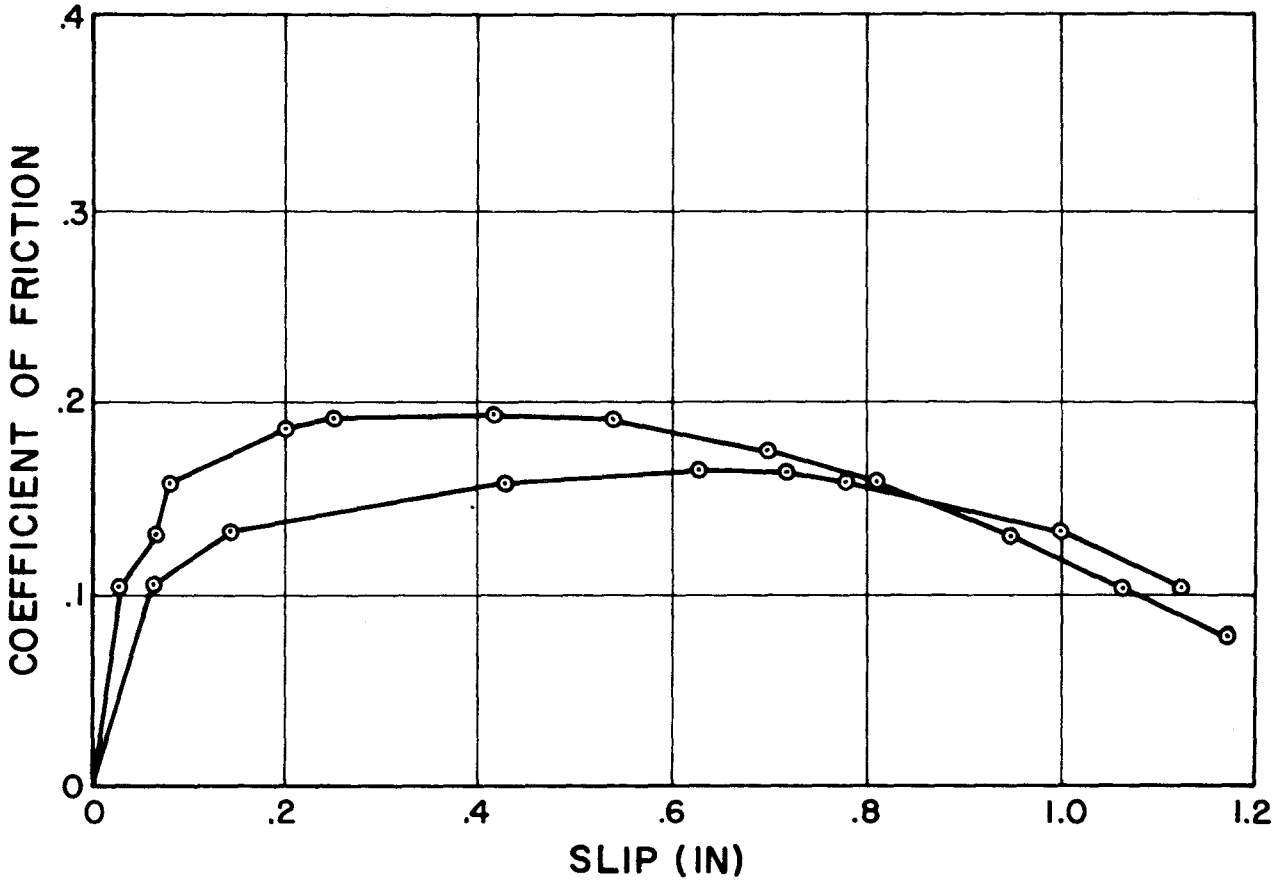

FIGURE 4.6.9 COEFFICIENT OF FRICTION VS. SLIP
(10 WF 25)

TABLE 4.6.1 STRENGTH OF SLOTTED STEEL PLATE BOLTED CONNECTION (MECHANICAL FUSE)*

MAXIMUM LOAD ATTAINED IN TENSILE TEST

SPECIMEN NUMBER	(SERIES A) INITIAL BOLTING (kips)	(SERIES B) REBOLTED CONNECTION (kips)	(SERIES C) "WEATHERED" CONNECTION (kips)
1	38.0	44.4	35.7
2	38.1	51.2	46.0
3	36.4	46.6	43.0
4	40.2	50.2	42.5
5	36.3	49.9	41.9
AVERAGE	37.8	48.5	41.8

*Plate for 8WF17 (see Table 4.2.1) Specimens 1-5

from 30% to 5%; these quantities are approximate but indicate the range of behavior.[4] It is also well-known that impact (or high strain rate), shape, thickness, and rolling technique of a structural part, notches and other irregularities, all tend to embrittle a normally ductile material.

The ductile to brittle transition for a statically loaded notched specimen occurs at a temperature below -200"F when the yield stress is in excess of 80 ksi.[5] This conclusion is based upon the results of investigations on a mild steel conducted by the U. S. Navy. At the present time it appears that temperatures in the neighborhood of -50°F will produce no significant change in the behavior of the slotted steel fuse plate under static loads.

CHAPTER 5

ROTATIONAL STIFFNESS OF SELECTED SIGN BACKGROUNDS

5.1 Objective

The rotational stiffness of the sign background is important because it contributes rotational stiffness to the support post above the "plastic hinge." The time, after impact, at which the fuse plate activates is significantly influenced by the torsional stiffness of the sign background.

In order to gain insight into the ranges of stiffness presented by various background materials, static torsional tests of three full-scale backgrounds were initiated.

5.2 Test Fixture

Figure 5.2.1 shows the test fixture used to conduct the tests. The sign background (complete with windbeam) was attached with standard connections (see specific detail drawing for each test) to the fixed and rotating beam. The spacing between the fixed and the rotating beam varied to be consistent with the post spacing for the specific backgrounds tested. Torque was applied to the background by loading the rotating beam eccentrically. The pivot point was located as near as possible to the longitudinal center of gravity.

5.3 Test Specimens

Three test specimens were used. Figure 5.3.1 shows the specimen for Test I, Figure 5.3.2 the specimen for Test II, and Figure 5.3.3

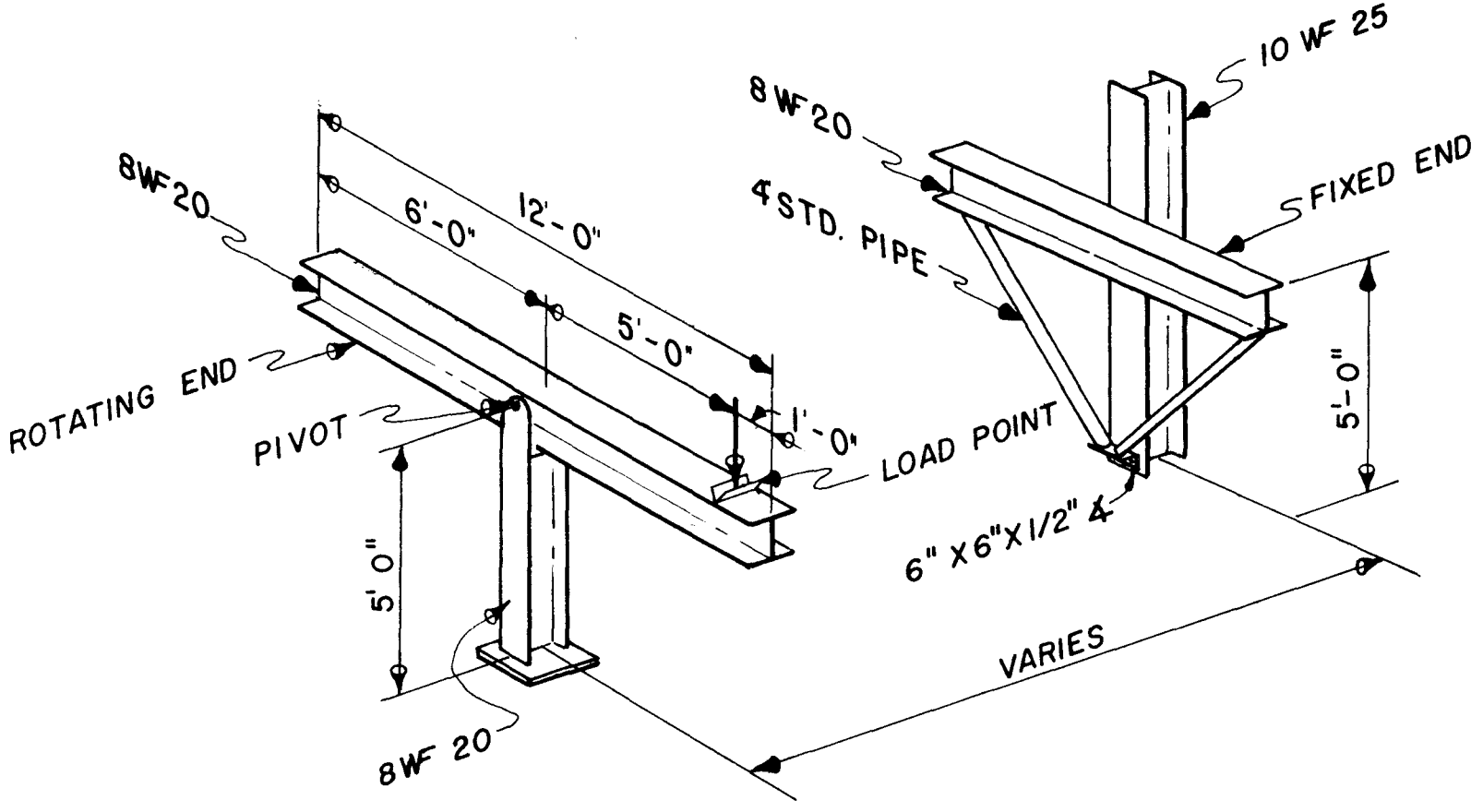

FIGURE 5.2.1 TEST FIXTURE FOR SIGN BACKGROUND TORSION TESTS

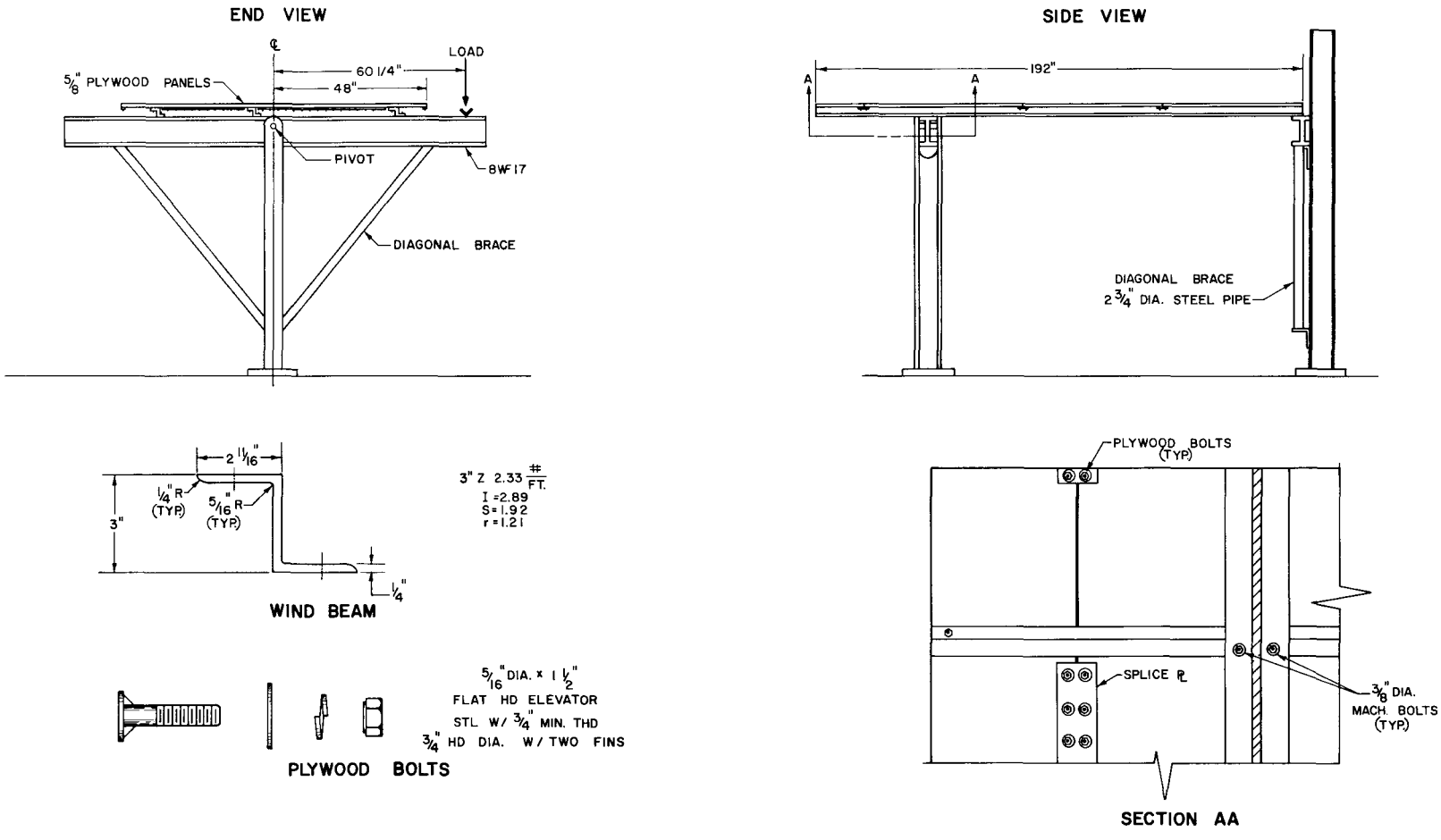

TEST I PLYWOOD BACKGROUND

FIGURE 5.3.1

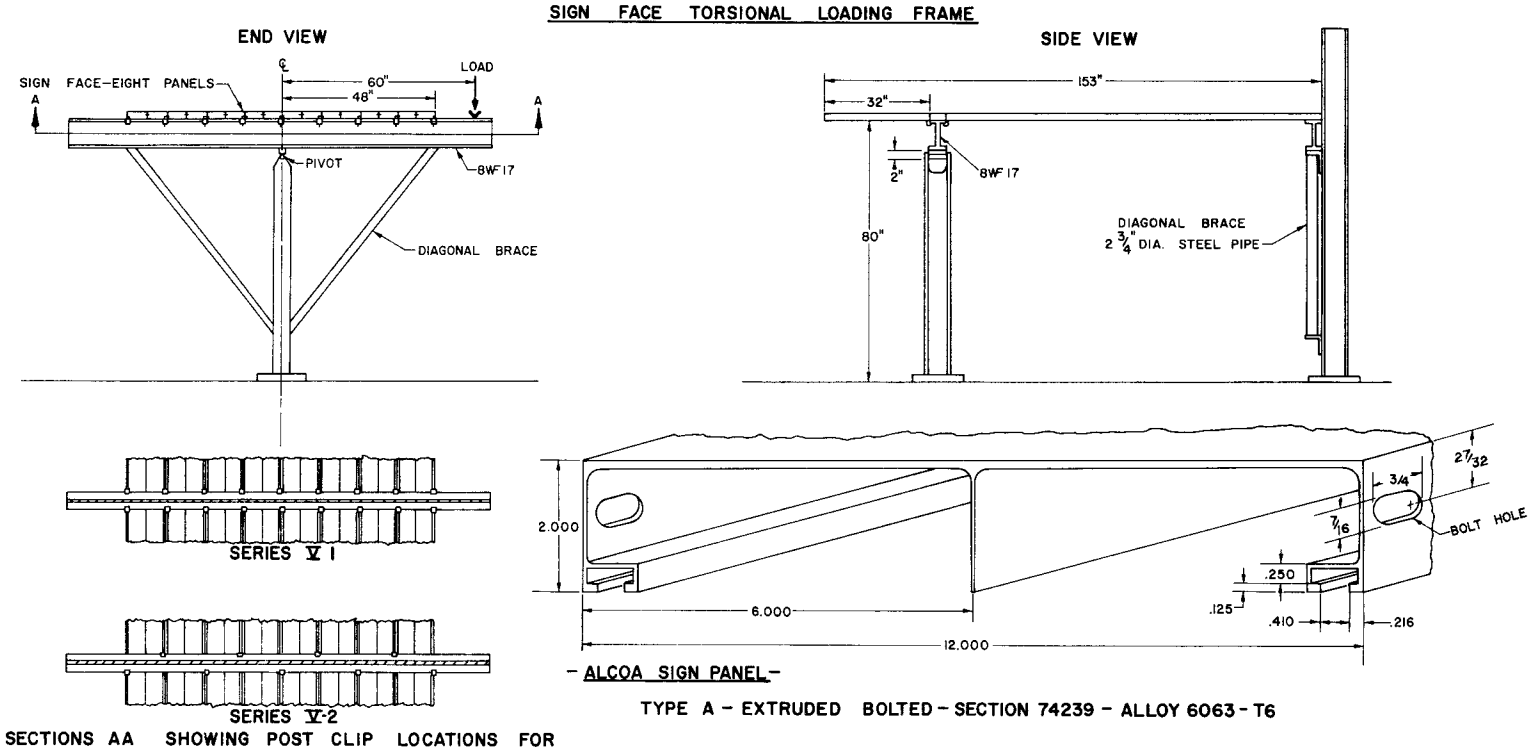

TEST II ALUMINUM PANELS

FIGURE 5.3.2

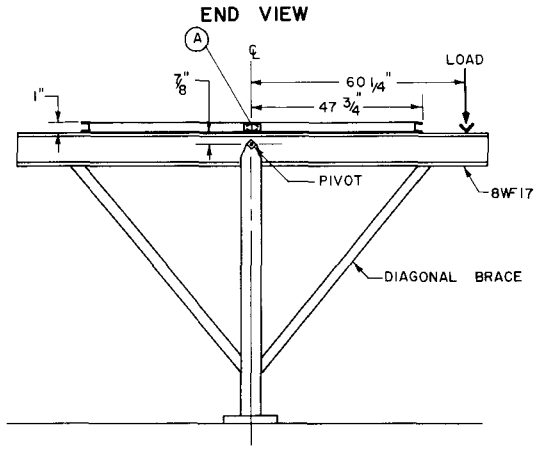

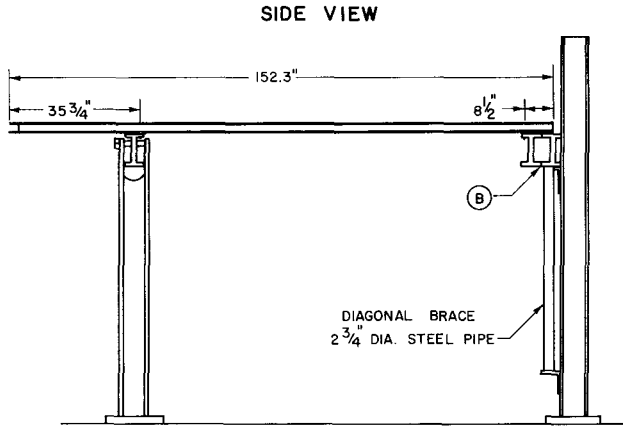

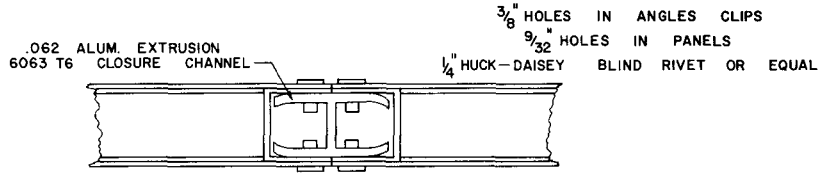

VIEW (A)

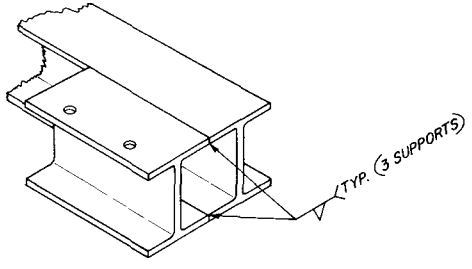

VIEW (B)

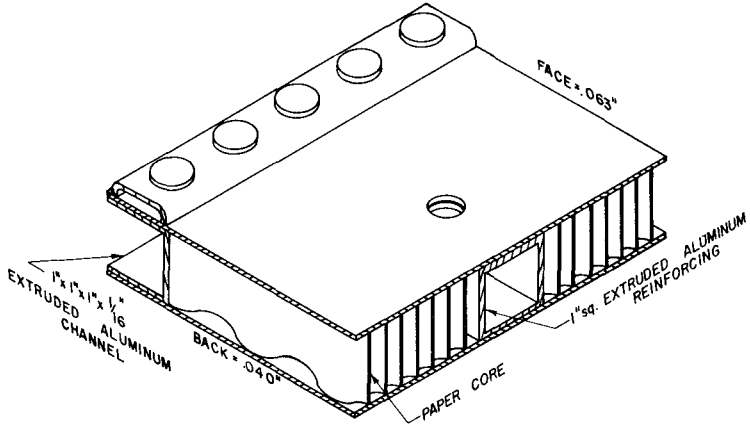

LAMINATED PANEL DETAIL

TEST III LAMINATED ALUMINUM PAPER HONEYCOMB PANEL

FIGURE 5.3.3

the specimen for Test III. All specimens were standard backgrounds currently in use on roadside signs.

5.4 Test Procedure

The torque was applied to the rotating beam by applying 50 lb. weights to a loading yoke placed 5' - 0" from the fulcrum. With this arrangement, torque could be varied in 250 ft.-lb. increments. The rotation of the background was calculated by measuring the deflection of a target placed on the rotating beam. Deflection measurements were made with a cathetometer. This device is capable of making measurements to the nearest 0.1 millimeter. Figure 5.4.1 shows the test set-up for measuring the rotating beam deflection.

The test procedure was as follows:

(1) Attach sign background to fixed and rotating beam.

(2) Attach loading yoke and counterbalance the rotating beam so that there is no torque on the sign background.

(3) Take no torque deflection reading on the target attached to the rotating beam.

(4) Add 50 lb. weights to loading yoke and take deflection reading, read again when deflection has stabilized (about 2 1/2 minutes).

(5) Load to maximum rotation or maximum load, which ever occurs first.

(6) Unload in 50 lb. increments.

(7) Take no torque deflection reading for permanent set determination.

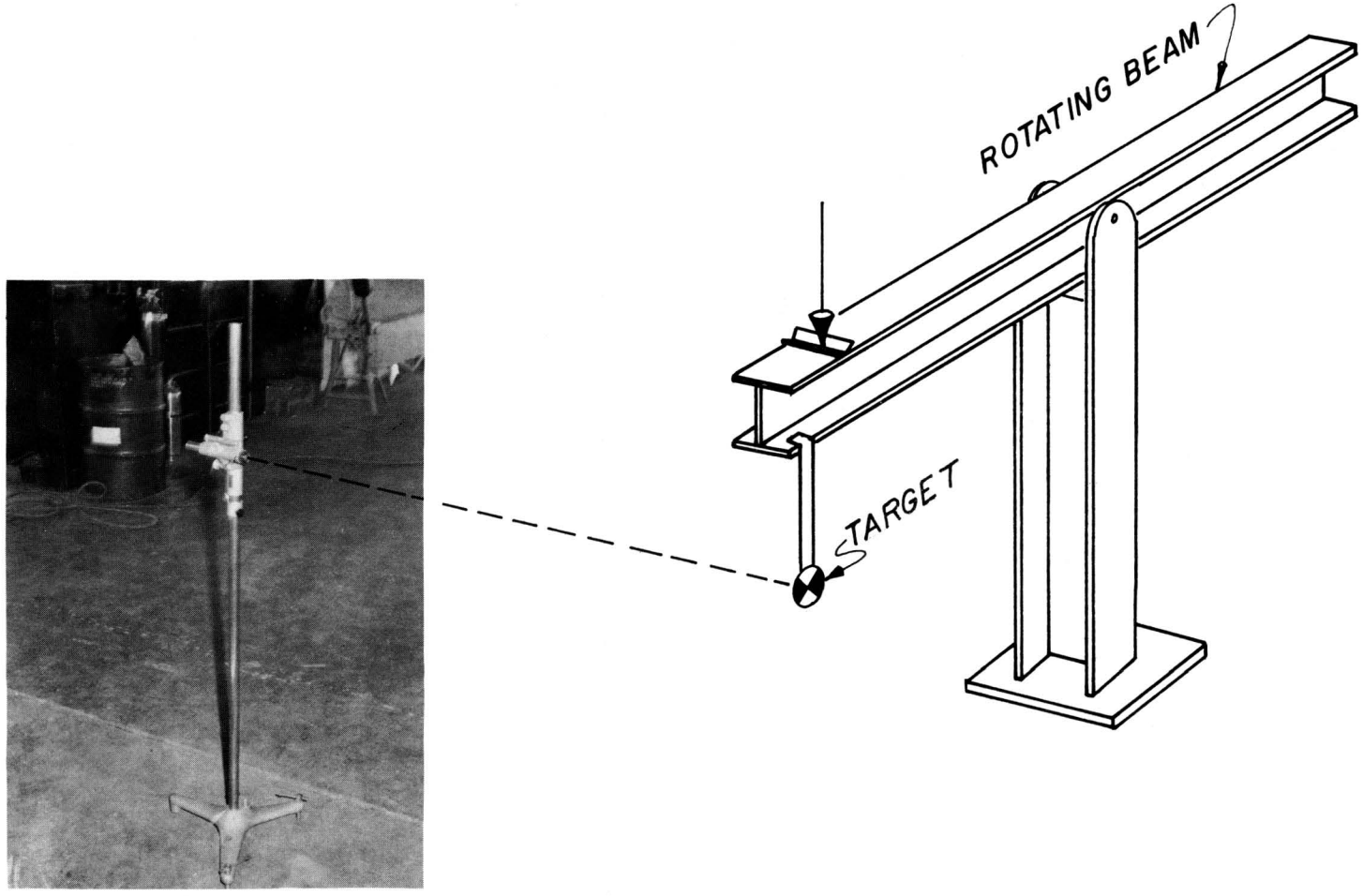

CATHETOMETER

FIGURE 5.4.1 TEST SET-UP FOR MEASURING ROTATION

5.5 Results

Figure 5.5.1 is a torque-rotation curve showing the reduced data for Specimen I (plywood background). Note that the behavior is not linear, indicating some inelastic action was present. Examination of the plywood sign face revealed that the plywood bolts (used to connect the windbeam) had deformed the wood adjacent to the hole. This yielding in the sign had caused a permanent set of 2.6° in the background.

Figure 5.5.2 is a plot of the torque-rotation data for Specimen II (extruded aluminum panel). Two curves are plotted. One curve is data for a test in which each extruded windbeam was clamped on both sides of the fixed and rotating beam. The other curve is the result when the background was clamped on each extruded windbeam on alternate sides of the fixed and rotating beam (see Figure 5.3.2 for clamping details). Comparison of the data shows that the alternate clamping reduced the torsional stiffness slightly. This reduction is not significant, however, and would influence the activation of the fuse plate only slightly. However, the background-to-post connection strength would be half in this case. Note that there was no significant creep in this test as indicated by the continuity of the curves. Examination of the background after testing showed no apparent material distress.

Figure 5.5.3 is the torque-rotation curve for Specimen III (aluminum sandwich panel). Note that this background behaved in a near elastic manner exhibiting a small amount of creep at the higher torques. There was a permanent deformation of 1.6 degrees after the

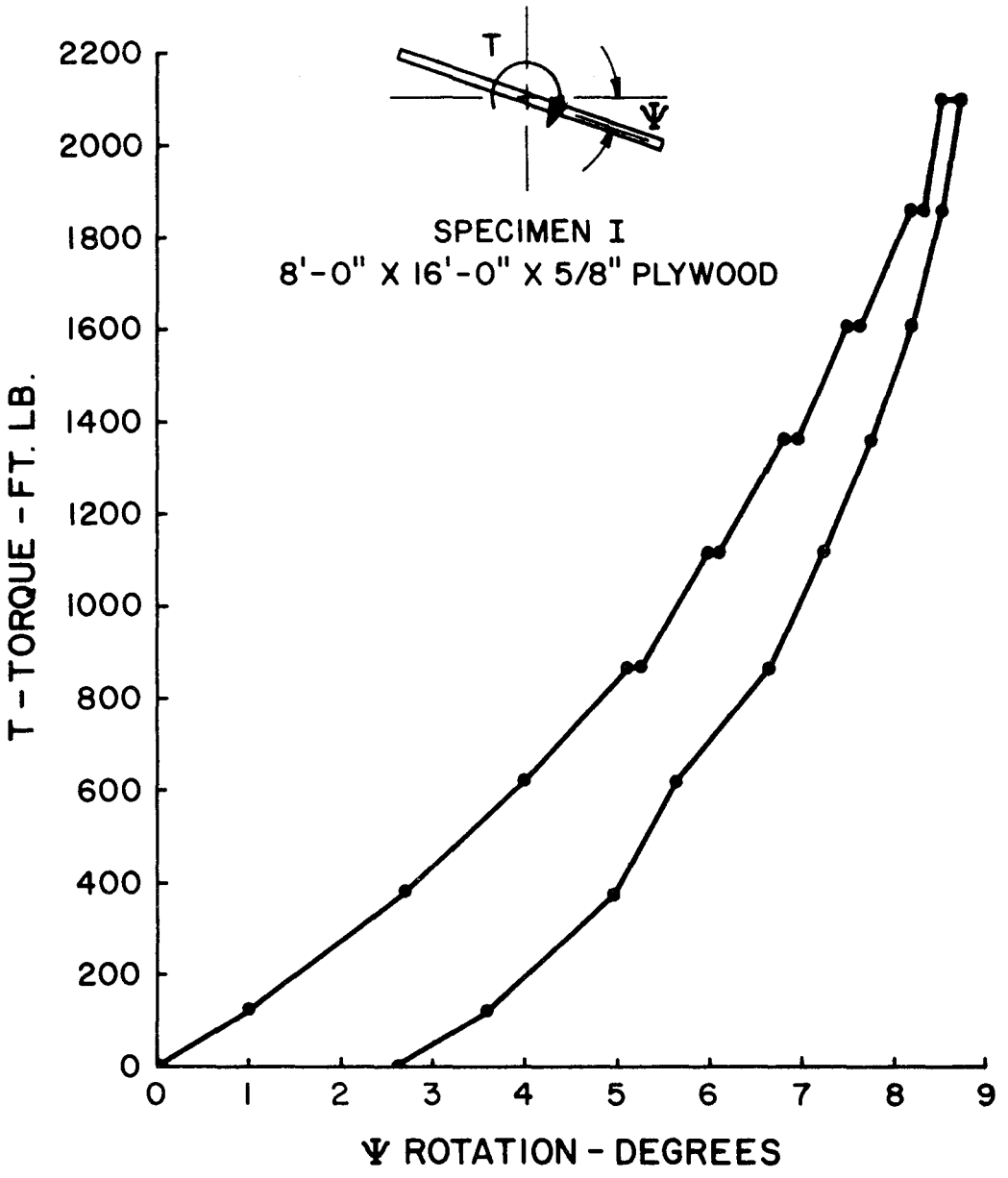

FIGURE 5.5.1 TORQUE-ROTATION FOR SPECIMEN I

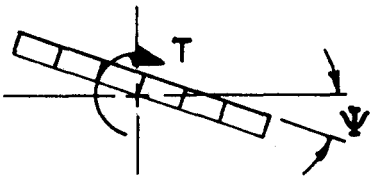

SPECIMEN NO. II
EXTRUDED ALUM. PANEL

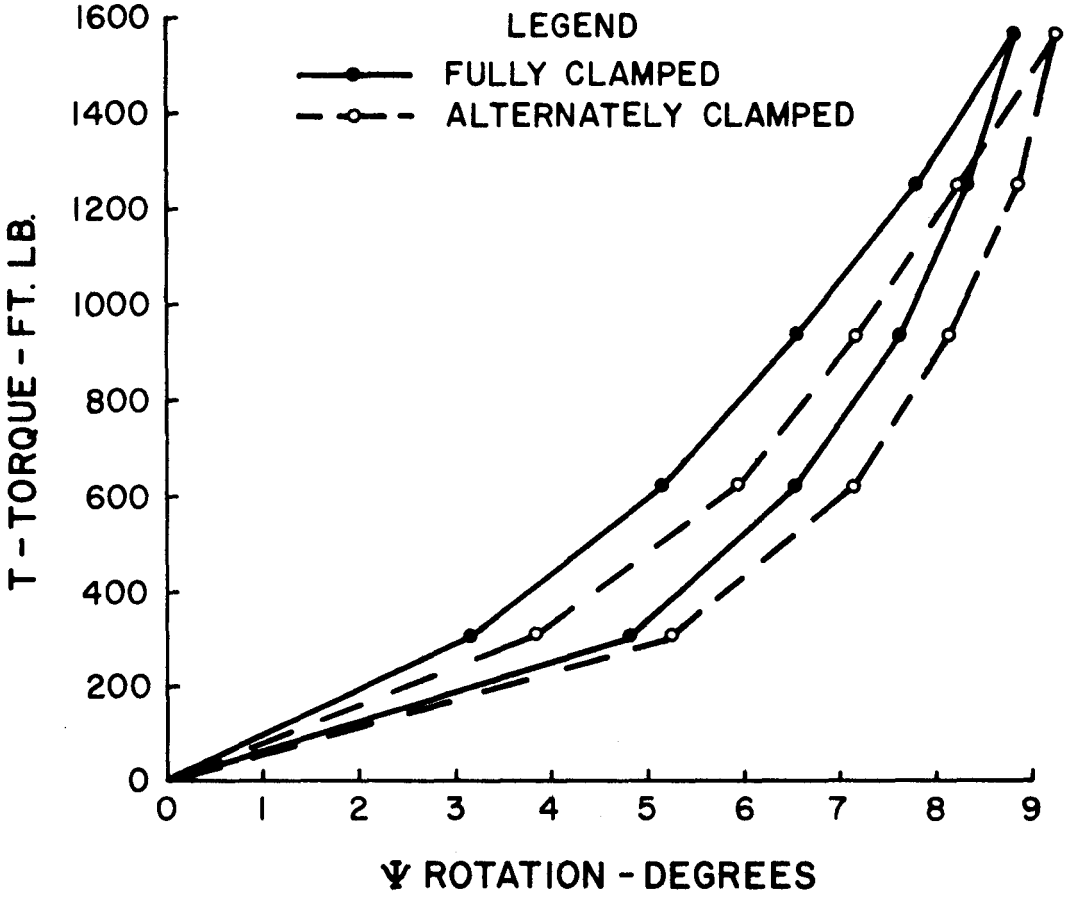

FIGURE 5.5.2 TORQUE-ROTATION FOR SPECIMEN II

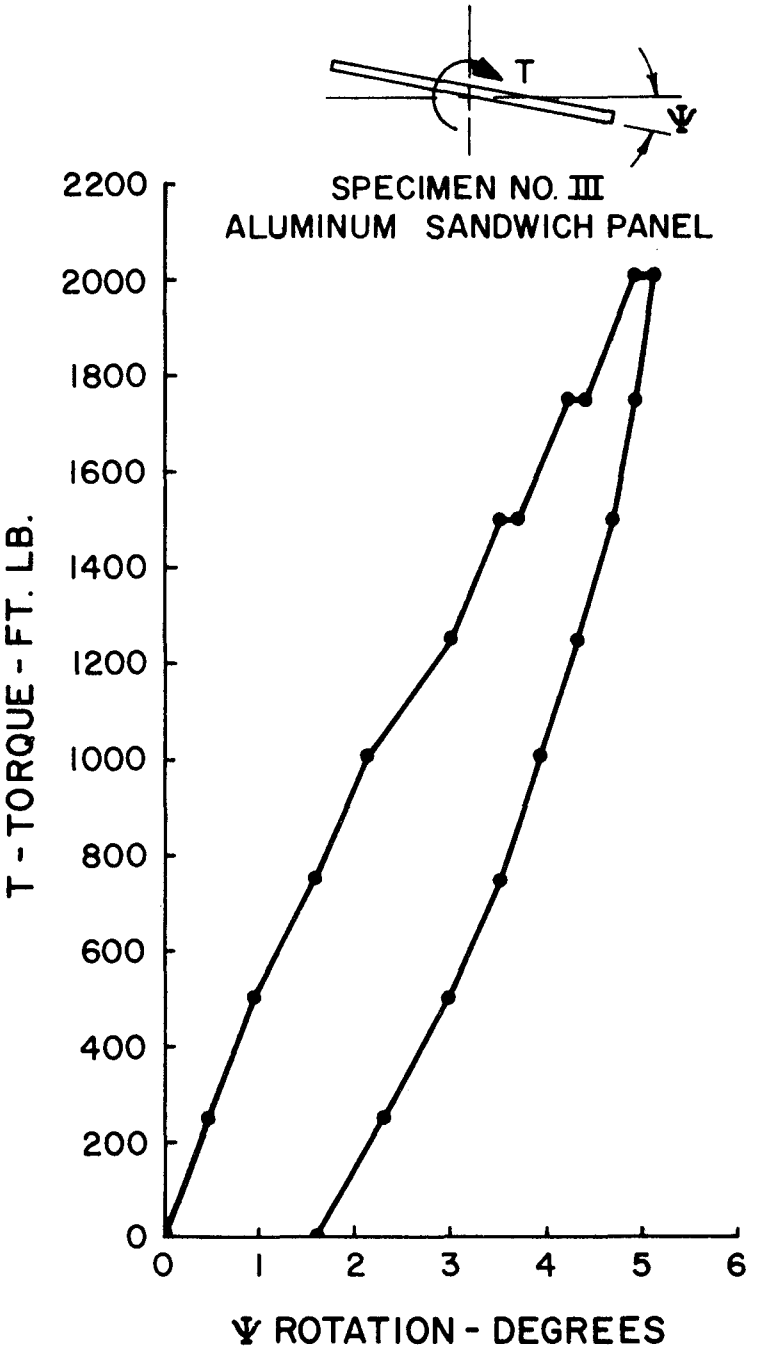

FIGURE 5.5.3 TORQUE-ROTATION FOR SPECIMEN III

removal of the torque. Examination of this background revealed considerable distortion of the tubular center reinforcement which probably contributed significantly to the permanent set.

5.6 Theoretical Representation of Torsional Stiffness

The sign background in torsion can be considered as a viscoelastic plate restrained from warping in two parallel planes. This problem alone would present a very difficult rigorous analysis. It is further complicated by inelastic effects, boundary conditions imposed by the attachment details, and in the case of some backgrounds, orthotropic properties. A rigorous analysis is beyond the scope of this investigation.

Since the object of the tests was to gain insight into the ranges of stiffness presented by various backgrounds, existing theory on the torsion of thin plates and tubes will be applied to obtain design equations.

For Specimen I and II (plywood panel and extruded aluminum panel) the theory presented by Timoshenko and Goodier,[6] for the torsion of a bar in which one cross section remains plane, fits the experimental data well for rotations up to six degrees. Equation (5.6.1) expresses the torsional stiffness for a homogenous elastic plate.

$$\frac{T}{\psi} = \frac{2}{3} G ab^3 \frac{1}{[L - \frac{a}{12}\sqrt{10E/G}]} \qquad (5.6.1)$$

where

$\frac{T}{\psi}$ = torsional stiffness, (ft. lb./radian)

μ = poisson's ratio

G = shear modulus, $\frac{E}{2(1 + \mu)}$, (psf.)

a = plate depth, (ft.)

b = plate thickness, (ft.)

L = plate length between supports, (ft.)

E = modulus of elasticity, (psf)

Figure 5.6.1 shows the comparison of Equation (5.6.1) with the experimental values for Specimen I and II. Note that the torsional stiffness of the windbeam (either extruded or attached) has been neglected.

Specimen III, the aluminum honeycomb panel, can be considered as a thin tube with three cells. Timoshenko and Goodier[7] give the following relation for the torsion of thin tubes.

$$\frac{T}{\psi} = \frac{2\, a^2 b^2\, Gt}{(b + a)L} \qquad (5.6.2)$$

where

$\frac{T}{\psi}$ = torsional stiffness, (ft.lb./radian)

a = panel depth, (ft.)

b = panel thickness, (ft.)

t = face thickness, (ft.)

L = panel length, (ft.)

G = shear modulus of face material, (psf)

Figure 5.6.1 shows the comparison of Equation (5.6.2) with the experimental data for Specimen III. Equation (5.6.2) neglects the torsional stiffness added by the longitudinal stiffness.

The comparison shown in Figure 5.6.1 indicates that Equation (5.6.1)

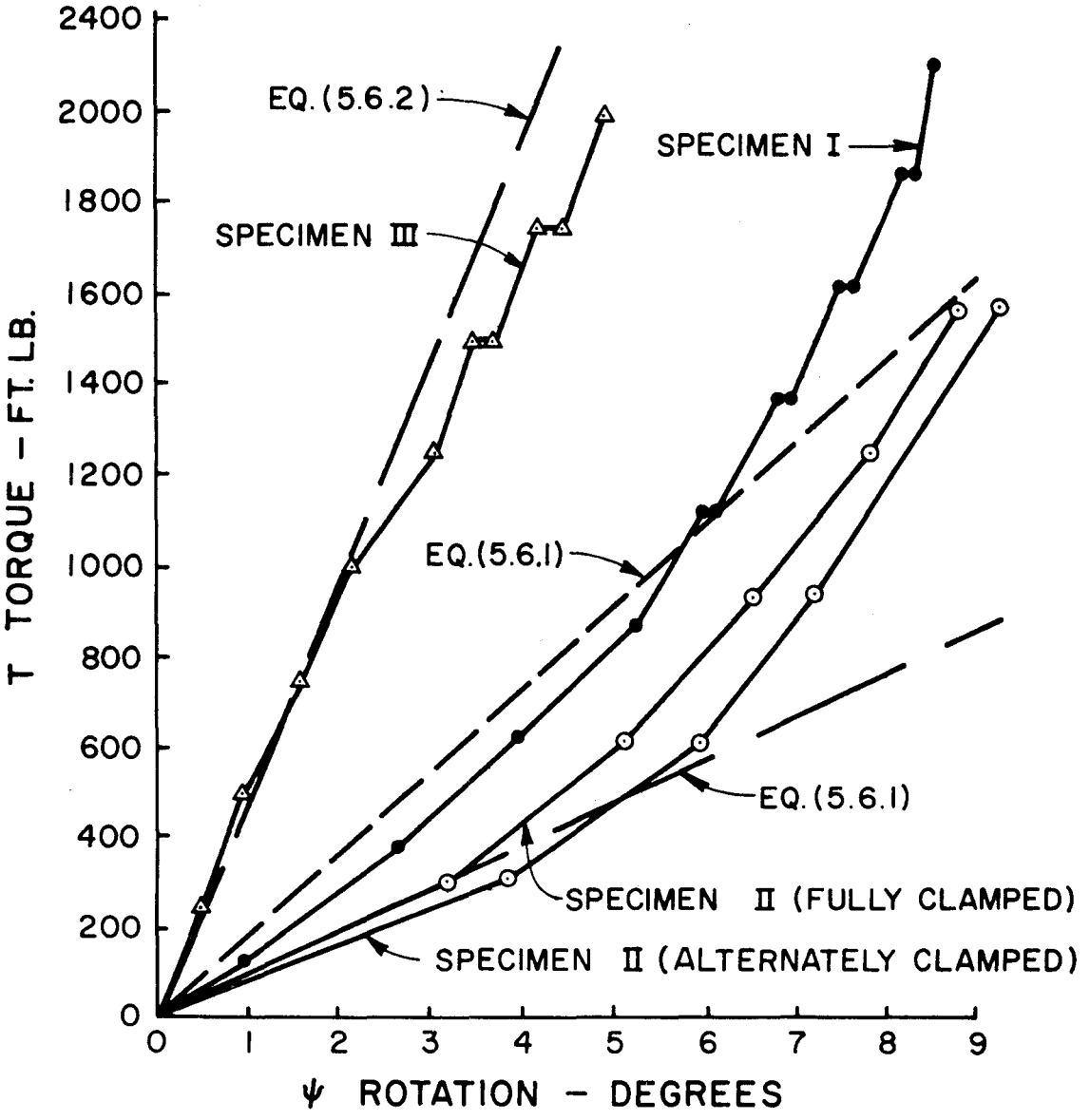

FIGURE 5.6.1 COMPARISON OF THEORY WITH TORSION TESTS

and Equation (5.6.2) can be used to represent the torsional stiffness of the sign backgrounds tested for angles of rotation up to six degrees. For angles greater than six degrees, Equation (5.6.1) should be modified as follows:

$$\frac{T}{\psi} = \frac{2}{3} G ab^3 \frac{1}{[L - \frac{a}{12}\sqrt{10E/G}]} - \frac{(\psi - 6)}{2}$$

C H A P T E R 6

DATA ACQUISITION

6.1 Principles of Instrumentation

Instrumentation employed in crash tests in this study was planned to provide corroborative information. Previous research[8] has indicated that signals from accelerometers mounted on the frame of a crash vehicle are susceptible of analysis, and films obtained with high-speed cameras provide a continuous visual record of a collision incident. During the course of the current investigation, it was found that the information obtained from these separate data acquisition systems can be successfully compared. Discussion of these comparisons are contained in Chapters 7 and 8.

6.2 Criteria of Instrumentation

Three criteria were established for selection of instrumentation.

(1) A device would provide data susceptible of analysis.

(2) Supplementary instrumentation would be installed whenever possible to provide redundancy in event of malfunction of a device.

(3) Certain installations would be made to ascertain feasibility of such installations for further testing.

6.3 Electronic Instrumentation

The electronic equipment is housed in a mobile instrumentation laboratory, shown in Figure 6.3.1. Typical information acquired electronically is listed in Table 6.3.1, and Figure 6.3.2 is a sketch of installations on test sign supports.

Two Honeywell Model 1508 recording oscillographs were used to

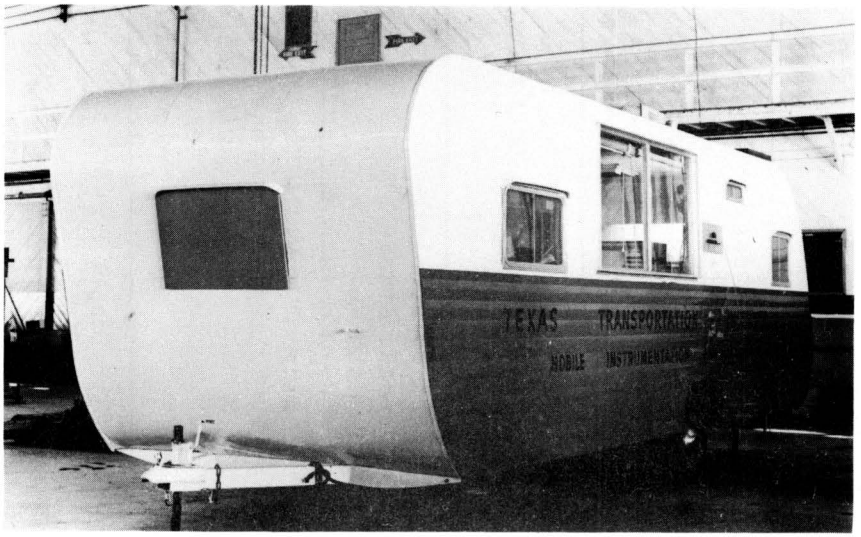

MOBILE INSTRUMENTATION TRAILER

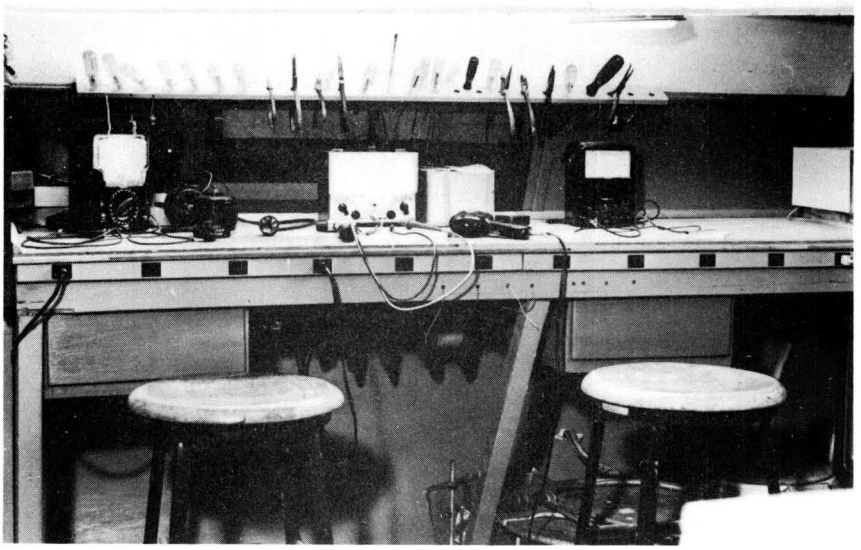

WORKBENCH IN TRAILER

FIGURE 6.3.1 INSTRUMENTATION TRAILER

TABLE 6.3.1 ELECTRONIC INSTRUMENTATION

TESTS 446-2 Through 10

DEVICE	DESCRIPTION	LOCATION	TO PROVIDE	COMMENTS
Piezoelectric Accelerometer	ENDEVCO Model 2211C with Model 2614B Amplifier	Mounted on left main frame member behind the driver's seat	Deceleration data of crash vehicle	Two used on all tests except one on Test #2, none on Test #3
Strain Gage Accelerometer	STATHAM Model A69TC	Mounted on left main frame member behind the driver's seat	Deceleration data of crash vehicle	Two used on all tests except one on Test #2
Recording Oscillograph	HONEYWELL VISICORDER Model 1508	Instrument trailer, 100 feet from target	Record of accelerometer and strain gage data	
Velocity Switches	TAPESWITCH, INC., Type "Roadswitch"	Placed in the path of the crash vehicle	Velocity of vehicle prior to impact	Two and sometimes three sets of switches at different locations along path
Impact Switch	TAPESWITCH, INC., Type "Roadswitch"	Attached to target	Time of impact by recording a mark on recording paper and flashing a bulb for high-speed film	

TABLE 6.3.1 ELECTRONIC INSTRUMENTATION, Continued

DEVICE	DESCRIPTION	LOCATION	TO PROVIDE	COMMENTS
Strainsert Bolts	STRAINSERT, INC., Type BL81,	Used to attach support to stub (four bolts used)	Force in bolts during collision incident	Test 446-5 only
Strain Gages	BUDD Type C6-121-R2VC-120	On support post, see Figure 6.3.2	Three gages used to provide: 1) Bending data 2) Force on fuse plate 3) Force on rear flange	Test 446-5 only
Linear Potentiometer	Slide-wire Type by PACIFIC SCIENTIFIC	Attached to stub of support post, see Figure 6.3.2	Time variable displacement of target	Test 446-5 only
Strain Gages	BUDD Type C6-121-R2TC-120	On diagonal strut, see Figure 6.3.2	Force on member	Tests 446-7 and 446-8

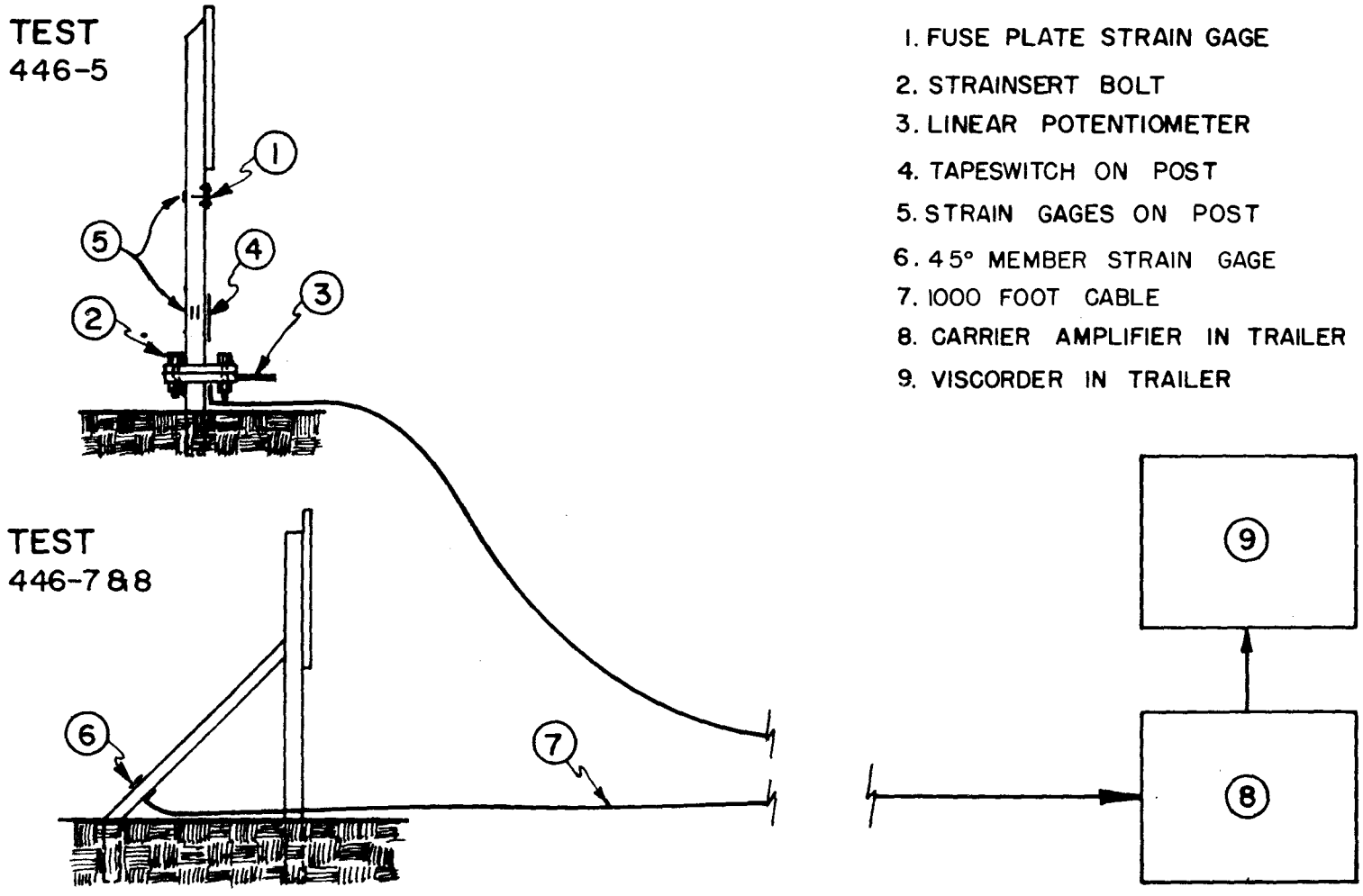

9:99

BLOCK DIAGRAM SHOWING PLACEMENT OF TARGET SIGN INSTRUMENTATION

FIGURE 6.3.2

record all information which was collected from the instruments. Each Visicorder contains 12 galvanometers into which the signals were fed. The galvanometers reflect a beam of visible light from a mercury lamp onto light-sensitive recording paper; this set of instruments is shown in Figure 6.3.3. The paper travels at a speed of 120 inches per second, giving an operating time of ten seconds for a 100 foot roll. The actual crash test takes place within a second, but the recorder must be turned on two to three seconds before impact to insure proper recorder speed at the time of impact. Time lines, used for analysis, are also placed on the paper by a timing light at a rate of 100 lines per second.

Honeywell Model 119B1 carrier amplifiers were used to excite strain gage accelerometers, strain gages and other two- and four-arm bridge devices. The transducers are excited with a five volt peak-to-peak signal at a frequency of 5000 Hz.

The accelerometers used on vehicle crash tests are basically two types: (1) Statham Model A69TC accelerometers, resistive wheatstone bridge type, and (2) Endevco Model 2211C piezoelectric accelerometers; these devices are illustrated in Figure 6.3.4. The accelerometers were mounted on the vehicle by means of a steel mounting block which was welded to the frame at a point about nine feet rearward of the front bumper on the driver's side of the vehicle (see Figure 6.3.5). This location was chosen since it is near the point where the seat belt is fastened to the floor of the vehicle in the standard size sedans. On the compact vehicles, a similar location was chosen. The Statham and Endevco accelerometers are supplied with a calibration factor

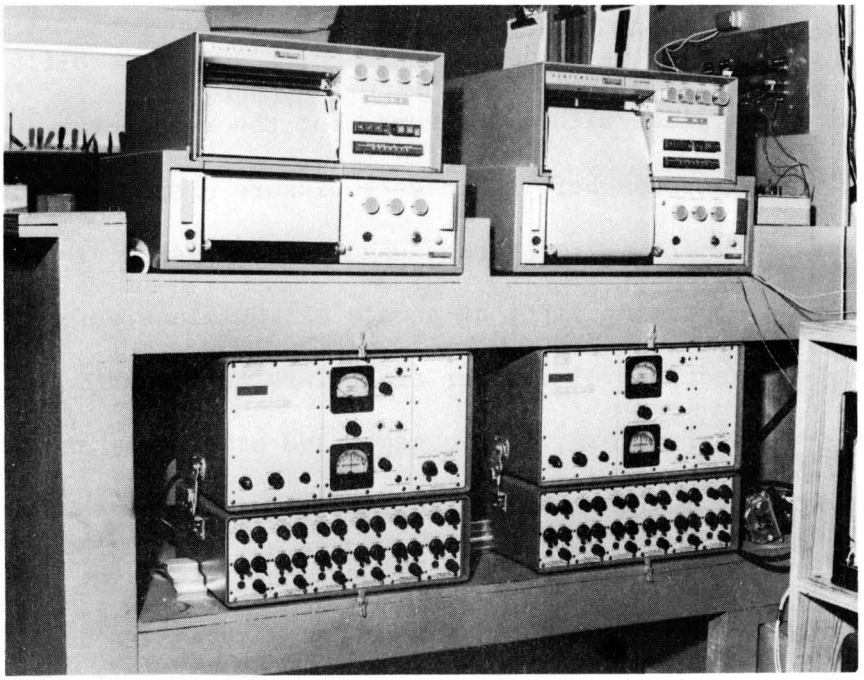

RECORDER AND AMPLIFIER SET-UP

FIGURE 6.3.3 RECORDERS AND AMPLIFIERS

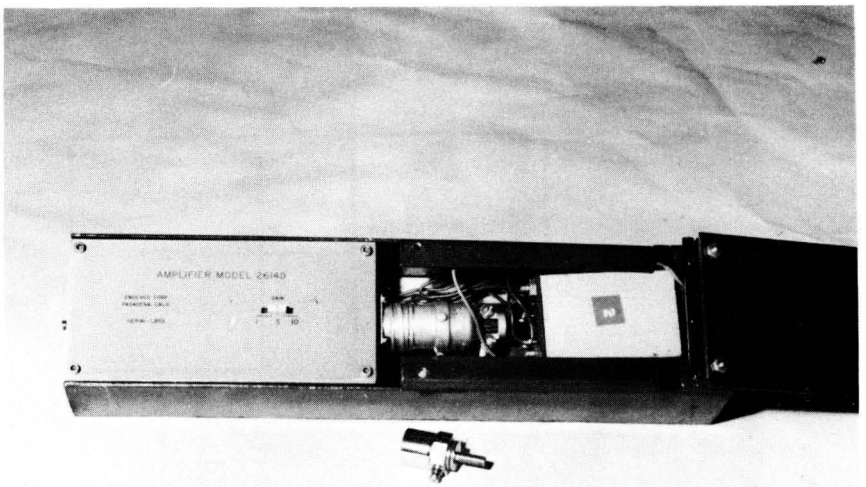

ENDEVCO ACCELEROMETER
AND AMPLIFIER

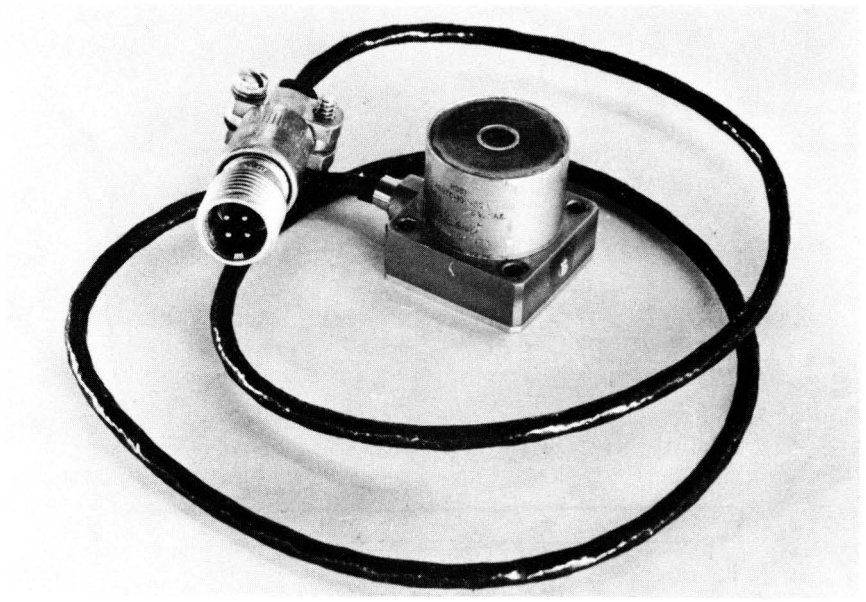

STATHAM ACCELEROMETER

FIGURE 6.3.4 ACCELEROMETERS

1. ACCELEROMETERS AT SEAT BELT SECURING POINT
2. ENDEVCO AMPLIFIERS LOCATED IN TRUNK
3. 1000 FOOT CABLE
4. CARRIER AMPLIFIER IN TRAILER
5. VISICORDERS IN TRAILER

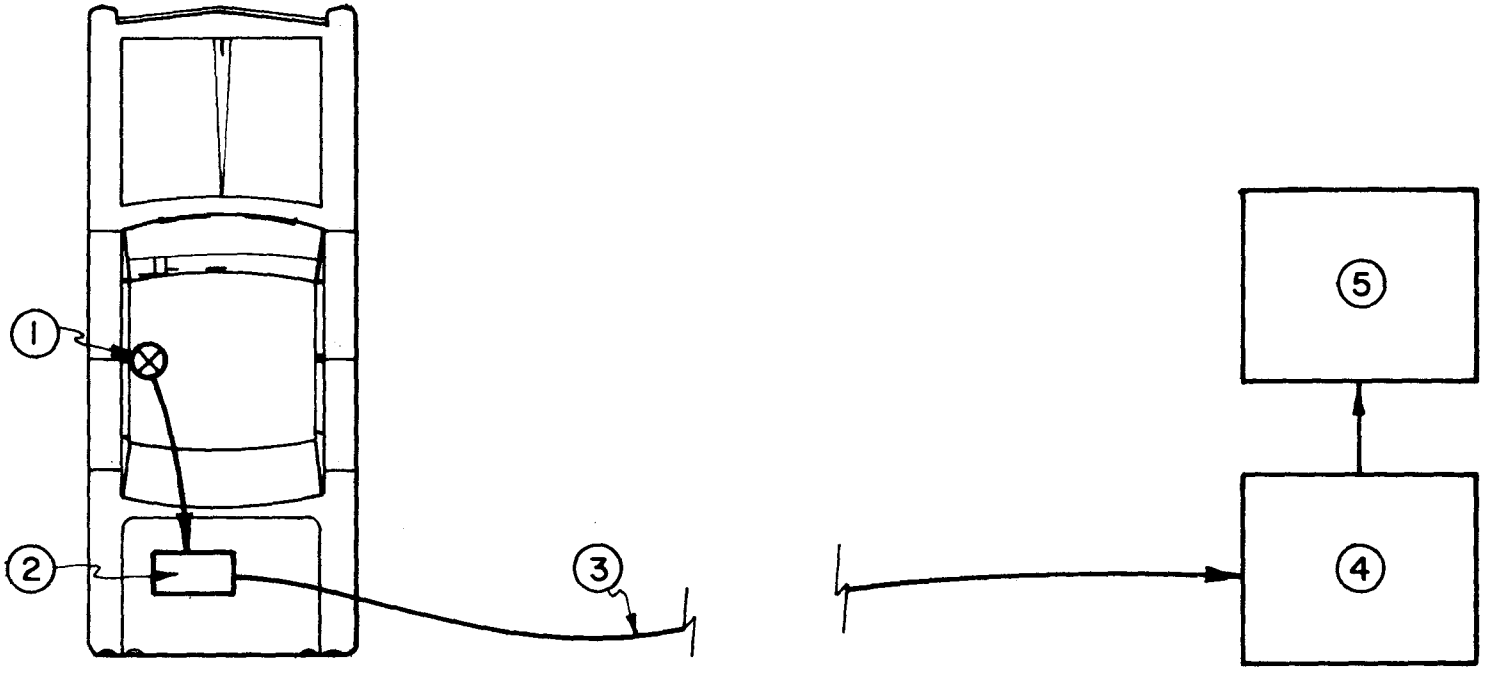

BLOCK DIAGRAM SHOWING PLACEMENT OF STATHAM AND ENDEVCO ACCELEROMETERS ON CRASH VEHICLE

FIGURE 6.3.5

which permits convenient calibration of the instruments.

These devices are used to gather deceleration data from which, by means of an iteration process, velocity and displacement data is acquired. This information is then compared with high-speed film data. Comparison of the two records has been satisfactory. However, correlation of accelerometer data from two similar tests seemed to be in agreement until the frequency response of the galvonometer is taken into account; some galvonometers had a response up to 60 Hz, others responded to frequencies up to 250 Hz. By including the additional bandwidth on one accelerometer but not on the other, repetition of results is not possible. This problem has been alleviated by using more consistency in galvonometer selection. Table 6.3.2 lists the galvonometers employed in the individual tests.

The radar speed meter used to record vehicle speed in earlier tests, conducted for the Texas Highway Department,[9] was replaced by electrical tape switches, manufactured by the Tapeswitch Corporation of America, in an effort to increase accuracy. The tape switches were placed in pairs three feet apart in the path of the crash vehicle; an installation of these switches is shown in Figure 6.3.6 (a). The automobile tire activates the switches upon passing over them. The switch pairs were generally placed in the following locations: (1) one pair 30 feet before impact, (2) one pair four feet before impact, and (3) one pair 12 feet after impact, if the vehicle was expected to travel beyond the target. The signal from the switches was recorded on the Visicorders along with the other data.

TABLE 6.3.2 GALVANOMETERS EMPLOYED*

TEST NO.	ENDEVCO #1	ENDEVCO #2	STATHAM #4	STATHAM #5
446-1	(N O D A T A R E C O R D F O R T H I S T E S T)			
446-2	M100-120	NONE USED	M400-120	NONE USED
446-3	NONE USED	NONE USED	M100-120A	M400-120
446-4	M400-120	M100-120A	M400-350	M100-120A
446-5	M400-120	M400-120	M400-350	M100-120A
446-6	M400-120	M400-120	M400-350	M100-120A
446-7	M400-120	M400-120	M400-350	M100-120A
446-8	M400-120	M400-120	M400-350	M100-120A
446-9	M400-120	M400-120	M400-350	M100-120A
446-10	M100-120	NONE USED	M100-120	NONE USED

* All Honeywell Microminature Galvanometers

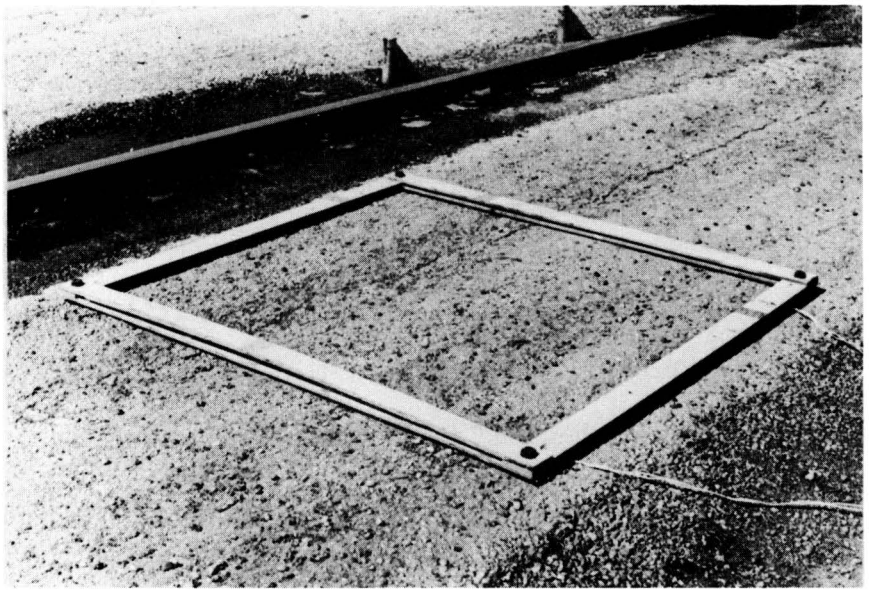

TAPESWITCH MOUNTING
(a)

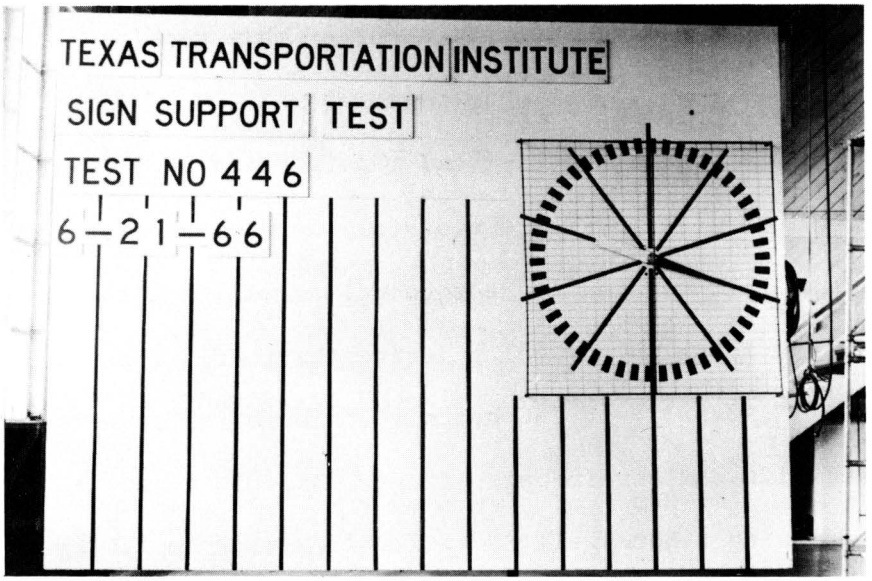

BACKBOARD SHOWING CLOCK
(b)

FIGURE 6.3.6

In Test 446-10 another method was tried for velocity determination. The tape switches were replaced by a set of contact switches (see Figure 6.3.7). This figure shows a block diagram of the electrical wiring. This method is simply another switch arrangement, one contact being on the vehicle and the other at a fixed position on the ground.

The centi-revolution clock employed in earlier tests,[10] used as an auxiliary timer for high-speed film analysis, has been modified by enlarging the clock face, thereby improving definition and legibility. The clock was calibrated regularly by stroboscopic light technique. The modified timer and backboard are shown in Figure 6.3.6(b).

On Test 446-5, a pair of 90° Rosette strain gages were attached to the fuse plate on the target post. They were calibrated to measure force on the fuse plate. The placement of this gage is illustrated in Figure 6.3.8.

Instrumented bolts (Model BL81) manufactured by the Strainsert Company, illustrated in Figure 6.3.9(a), were used to attain the proper initial base bolt tension (by torqueing) as well as to measure the change in the force in the bolts during the test. These bolts were standard ASTM A325 3/4-10 UNC bolts which were instrumented internally with a full 120 ohm strain gage bridge. Signals from the bolt were amplified, using a Honeywell Model 119B1 Carrier Amplifier, and supplied to the recording oscillograph. The bolts were dead load calibrated before and after each test.

In addition to the tape switches used for velocity determination,

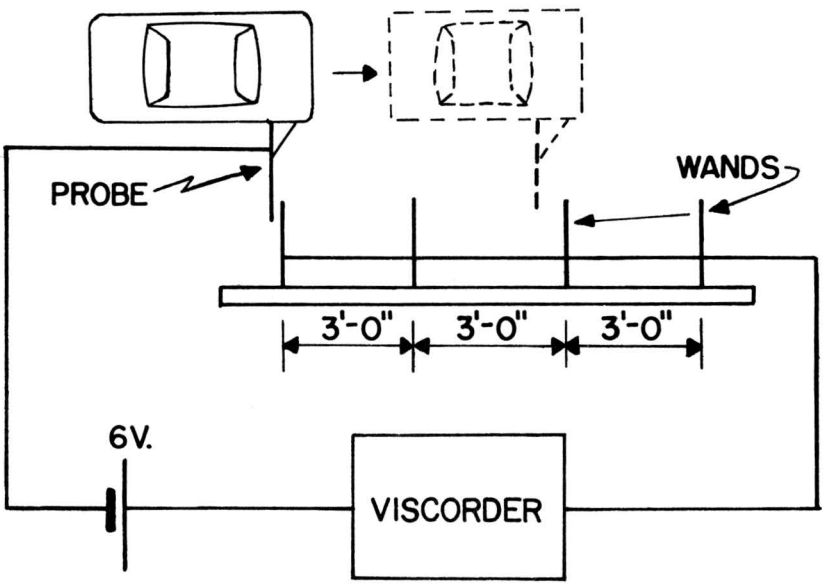

BLOCK DIAGRAM OF WANDS

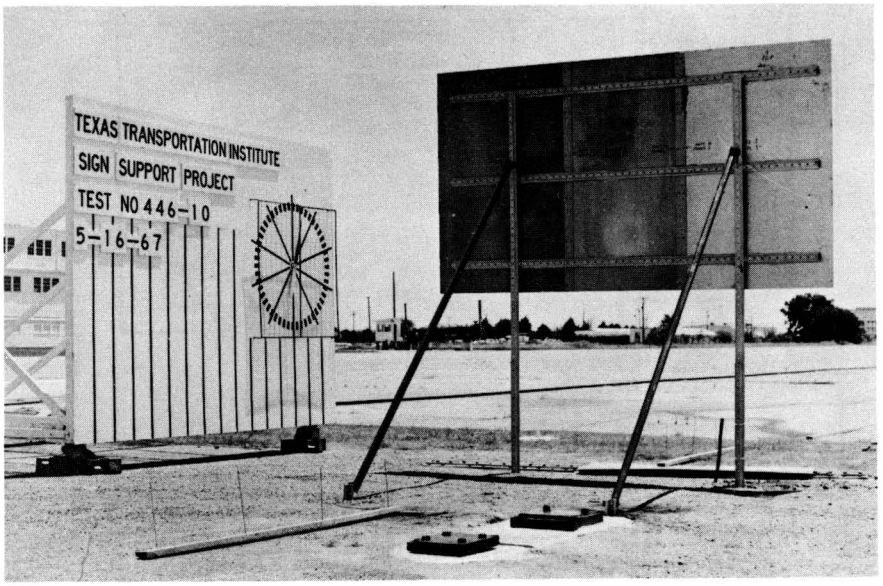

FIGURE 6.3.7 WANDS FOR VELOCITY DETERMINATION

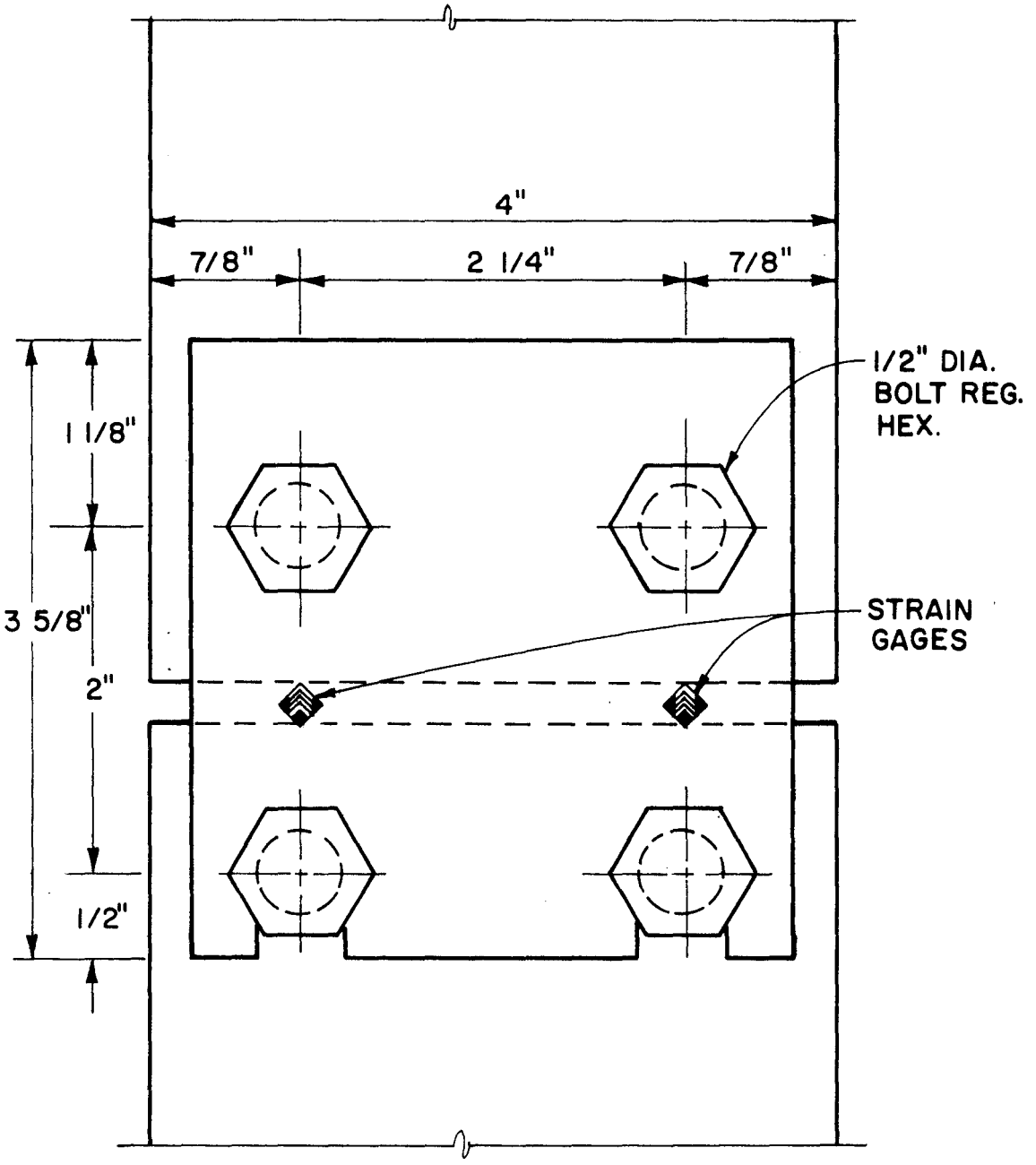

FIGURE 6.3.8 STRAIN GAGED FUSE PLATE

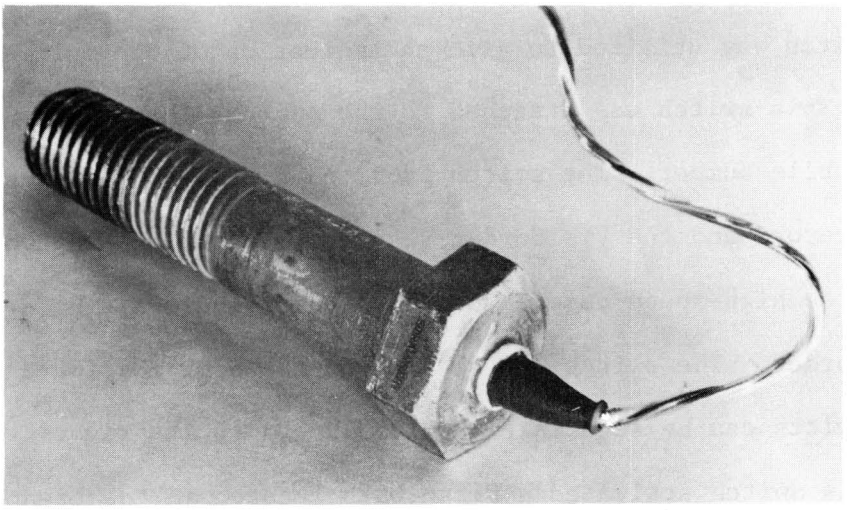

STRAINSERT BOLT
(a)

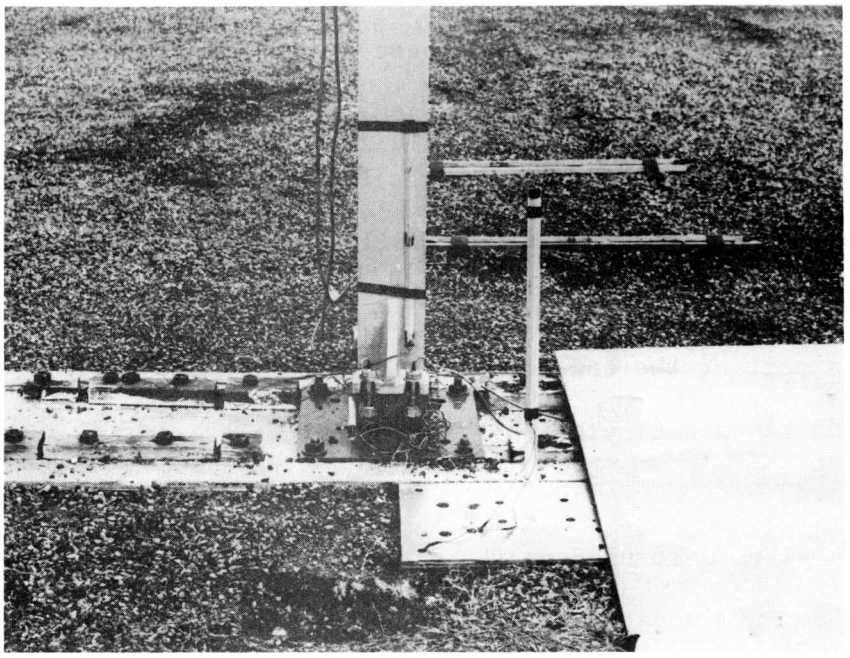

FLASHBULB SWITCHES
(b)

FIGURE 6.3.9

a tape switch was utilized to give an indication of the initial time of contact. This switch was attached to the post in the area contacted by the automobile bumper. The switch provided a time correlation between the film record and the Visicorder record by actuating a flash bulb aimed at the high-speed camera and simultaneously recording a mark on the Visicorder. The switch can be seen on the post in Figure 6.3.9 (b). Another switch can be seen in Figure 6.3.9 (b) to the right front of the post. This switch activated a flash bulb located in the trench in the center foreground. This bulb illuminated the underside of the vehicle and base of the post.

A linear potentiometer, see Figure 6.3.10, was used in Test 446-5 to measure the displacement of the base plate. The potentiometer was fixed to the foundation (immovable base plate) with the slide attached to the base plate of the target post. This information was transmitted to the Visicorder. This instrument failed to operate during the test. Examination of the high-speed film record showed that the instrument was struck by a part of the tow mechanism attached to the vehicle. In the two previous tests employing this same instrument, satisfactory results were obtained.[11]

Strain gages were used on the diagonal brace on Tests 446-7 and 446-8. A four-arm Wheatstone bridge configuration was used and the bridge was calibrated in tension. The arms of the bridge were made up of two 90° Rosette gages. The indicated strain was 2.6 times the actual strain. The force measured did not account for bending moment and therefore was of little value since an undetermined amount of bending moment was experienced.

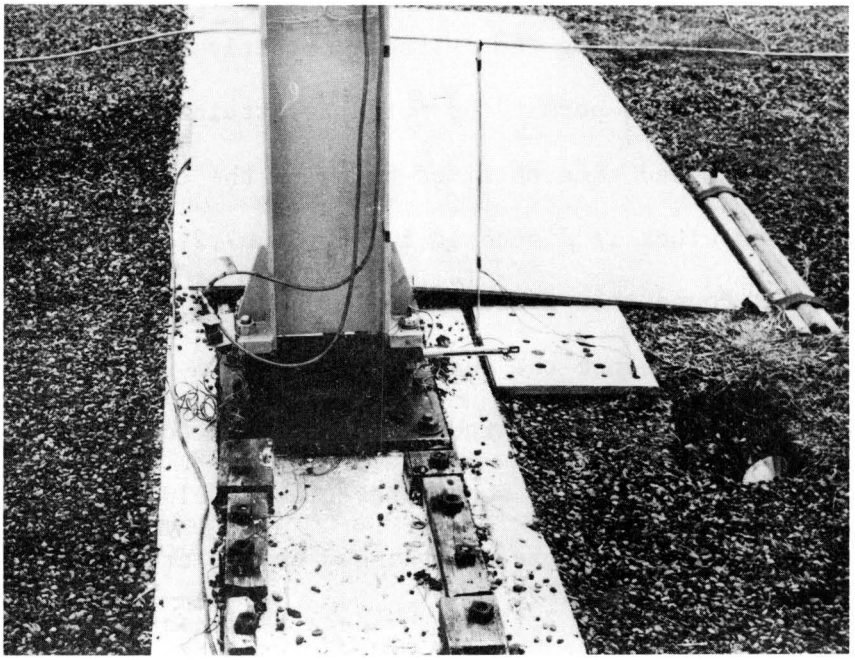

FIGURE 6.3.10 LINEAR POTENTIOMETER

6.4 Photographic Instrumentation

High-speed cameras were used as the basic instrument for recording the history of a collision incident. Films obtained with such equipment provide a continuous visual record of the incident which can be examined one frame at a time. Each camera can be operated at nearly constant speed by selecting the voltage correctly and allowing adequate time prior to impact to permit the motor to attain the desired speed. Correlation of elapsed time obtained by using the camera speed and the centi-revolution clock is discussed in Section 7.2, Part III of this report. It was found that mounting the high-speed cameras on a sturdy base would greatly enhance the quality of the film record.

Distance references were established adjacent to the test component as seen in Figure 6.4.1 which shows the camera field of view; in addition, reference marks were established on the crash vehicle. These reference marks (see Table 7.2.2) provide a permanent record of distance on the high-speed film. Thus, time and displacement data can be obtained by examination of the high-speed film record.

Other cameras were employed to obtain general views of the collision incident. Table 6.4.1 contains a list of the cameras used in this investigation.

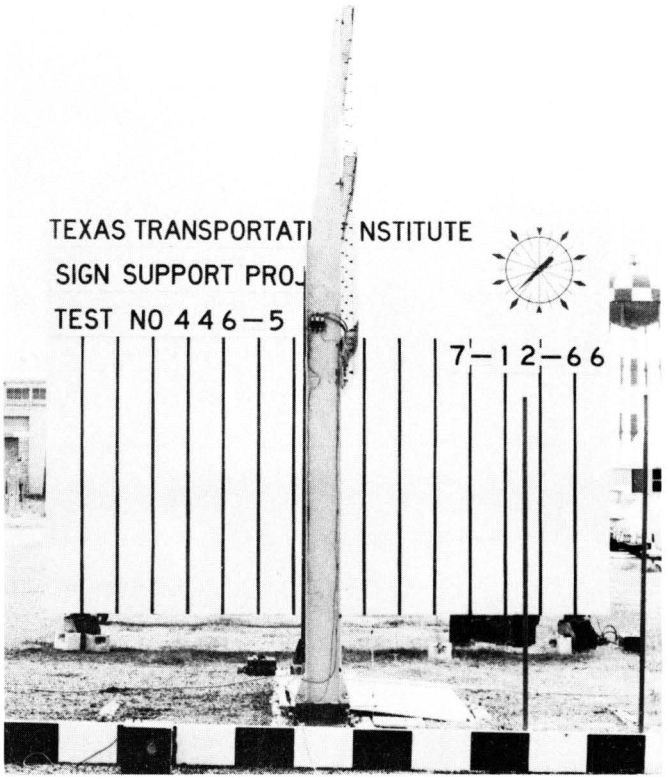

FIGURE 6.4.1 CAMERA FIELD OF VIEW

TABLE 6.4.1 PHOTOGRAPHIC INSTRUMENTATION

ITEM	DEVICE	DESCRIPTION	LOCATION	TO PROVIDE
1	High-speed motion picture camera	Wollensak, Fastax, WF-3T, 50 mm lens, 16 mm Ekta-chrome ER Type 7257 film, with high-speed (2R 3000) perforations, 1000 frames per second	Approximately 100 feet from impact point, line of sight perpendicular to path of crash vehicle	Crash vehicle time-displacement data
2	High-speed motion picture camera	Wollensak, Fastax, WF-3T, 35 mm lens, 16 mm Ekta-chrome ER Type 7257 film, with high-speed (2R 3000) perforations, 1000 frames per second	As described in Item 1 above.	Crash vehicle time-displacement data; back-up for Camera 1 with wider field
3	Motion picture camera with higher standard speed	Kodak Cine Special II, 16 mm Ektachrome Commer-cial Type 7255 film, with No. 85 conversion filter, 64 frames per second	Near high-speed camera location described above.	General views of crash test used for copying purposes.
4	Standard speed motion picture camera	Bolex H-16 Rex 4, 16 mm Ektachrome Commercial Type 7255 film, 24 frames per second	Near high-speed camera location described above	General views of crash test; panned shots
5	Standard speed motion picture camera	Bell & Howell 70 HR, 16 mm Ektachrome Commercial Type 7255 film, 24 frames per second	On boom of lift truck near high-speed camera location described above	General overhead views of crash test

C H A P T E R 7

METHODS OF DATA ANALYSIS

7.1 Vehicle Accelerometer Analysis

An accelerometer was installed on the crash vehicle as described previously. Changes in acceleration with respect to time were recorded on photographic paper by means of the Visicorder. The signal transmitted from the accelerometer to a galvanometer produced a trace on light-sensitive paper. The oscillating trace thus produced is a record of the acceleration history of the accelerometer as a function of time. The configuration of this trace is idealized in Figure 7.1.1(a). Changes in vehicle velocity and displacement can be computed by employing a process of successive integration.

Data reduction. Data is reduced by transforming the analog record, from the oscillographic trace to a digital record. The digitizing is done manually with the aid of the Gerber Digital Data Reduction System, shown in Figure 7.1.2. The system operation uses a set of x-y position cross-hairs to locate a point on the trace. The x-y reference axes can be set by the operator to coincide with reference axes of the trace being analyzed. Each point chosen by the operator is digitized (values measured from the reference axes) by pushing a button. The data is displayed visually and automatically punched on a data processing card. Data can be digitized by two methods: (1) by measuring the peaks and nulls (acceleration values) and the corresponding times, and (2) by measuring acceleration values at a predetermined interval on the time axis. Method 1 has proved satisfactory on trace records with high

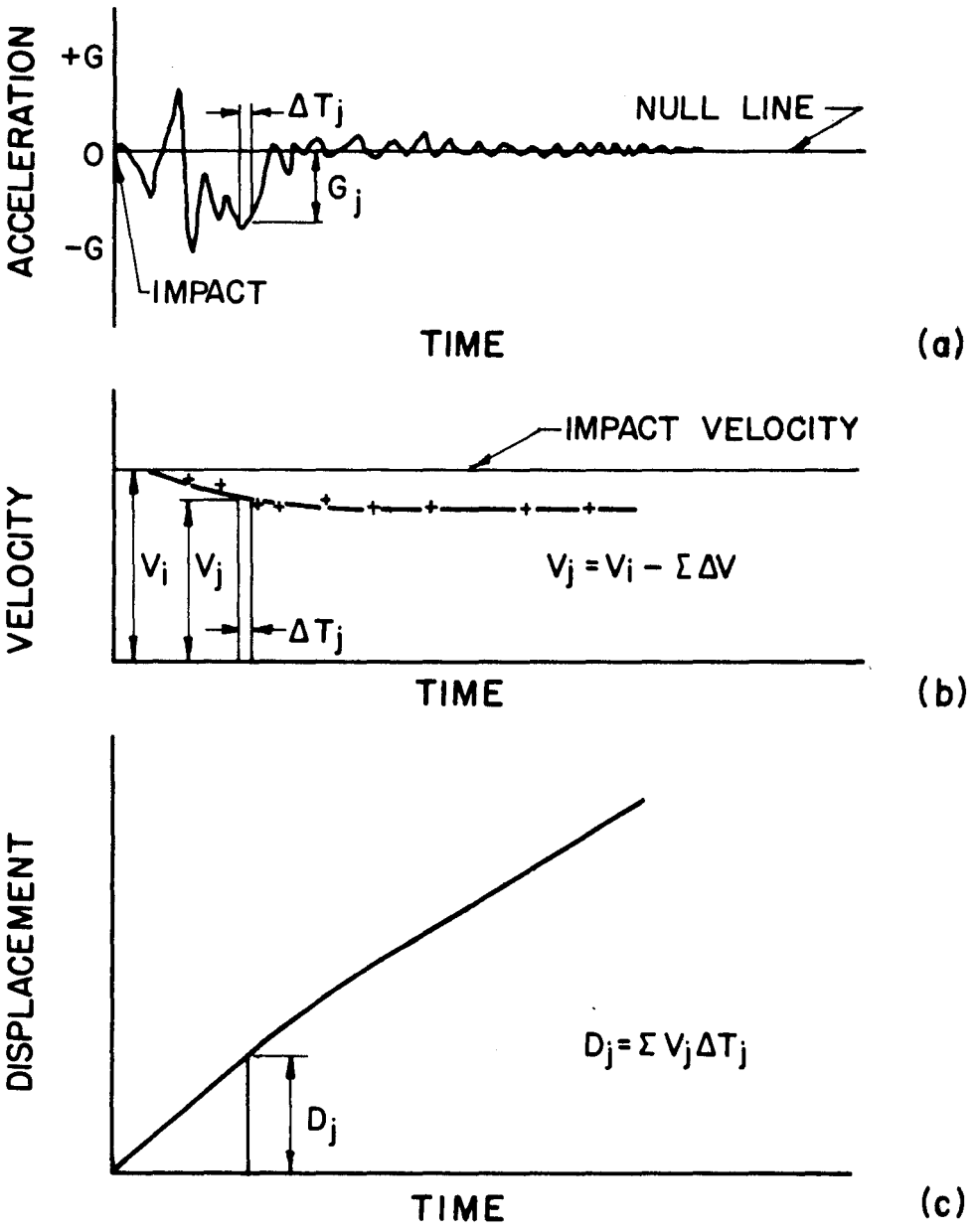

FIGURE 7.1.1 CRASH VEHICLE ACCELEROMETER ANALYSIS BY GRAPHICAL INTEGRATION

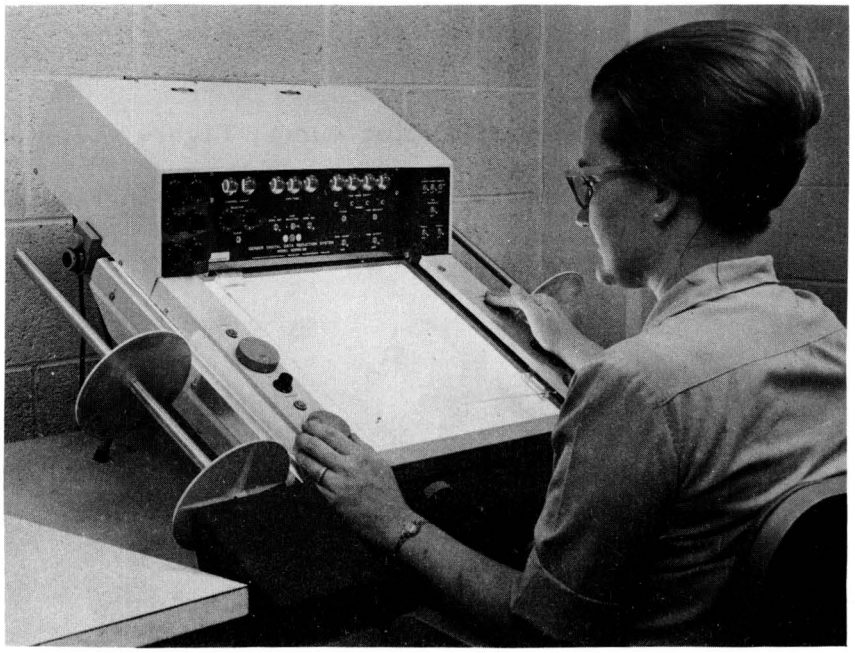

FIGURE 7.1.2 DIGITAL DATA REDUCTION SYSTEM

frequency response galvanometers. Method 2 must be used when low frequency galvanometers are employed.

Data analysis. The analysis of the accelerometer data consists of determining the change in vehicle velocity and the vehicle displacement.

The area under the acceleration-time curve, Figure 7.7.1(a), yields the change in velocity as a function of time as shown in Figure 7.1.1(b). This may be stated

$$\Delta V = \sum_{a}^{b} G_j \quad \Delta T_j$$

where

ΔV = the velocity increment

G_j = the acceleration value at time j

ΔT_j = the time increment

The velocity at any time is

$$V_b = V_a - \Delta V$$

For the data analysis in this report, V_i is the vehicle velocity at impact obtained by other means (film records or switch data).

By a similar process of graphical integration, incremental areas under the velocity-time curve are summed to produce the displacement-time curve shown in Figure 7.1.1(c). All computations are made using the IBM 7094 digital computer.

7.2 Techniques of High-Speed Film Reduction

Motion analyzer. The primary source of data for the highway sign support research is the film record taken by high-speed motion picture cameras; this record of the event makes possible a methodical and detailed analysis of the sequence of action, frame by frame. The instrument used in the visual data analysis of the photographic record is a Vanguard Motion Analyzer, a model M-16CD projection head mounted on a model A-11D projection case as shown in Figure 7.2.1. This instrument, equipped with a frame counter, permits horizontal and vertical measurements on an enlarged, rear projected image of the film. A centi-revolution clock is visible in the projected image providing one means of measuring elapsed time during a collision incident. A second source of time data is provided by the constant speed motor on the high-speed camera.

Time correlation. A synchronous electric motor clock operates at nearly constant speed (rated at 1800 revolutions per minute) during the period of each crash test. Operating speed of the clock is checked by stroboscopic light techniques, and varies from rated speed by approximately ten percent. The high speed camera must be started at a predetermined time prior to impact; the elapsed time interval, dependent upon impact velocity of the vehicle, permits the camera motor to attain nearly constant speed (rated at 1000 frames per second). A light signal is transcribed on the film record which permits a check on the camera speed during a collision incident. This speed varies by approximately four percent from the rated value. Thus each of the time sources has a variation in its rated speed. To determine the agreement between the two

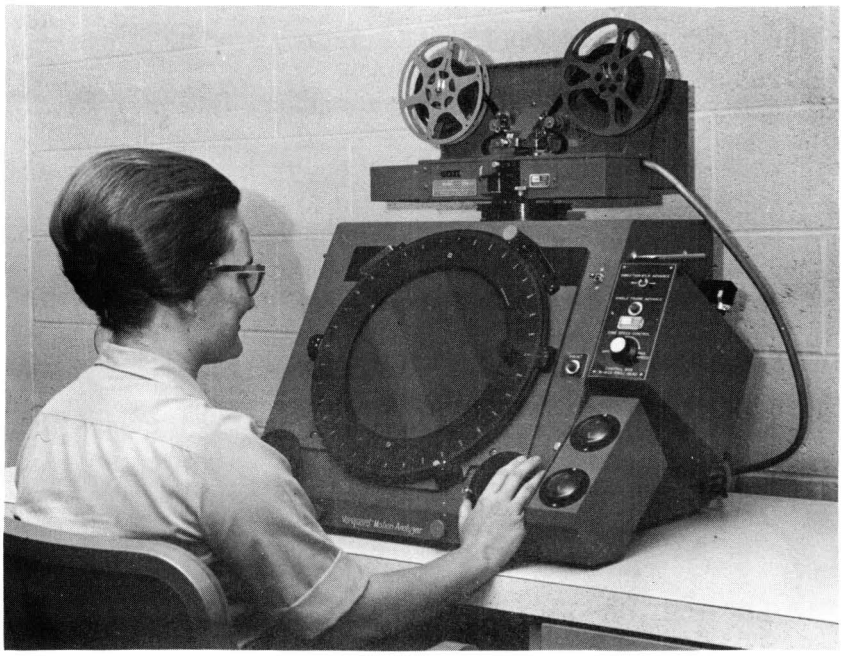

FIGURE 7.2.1 FILM MOTION ANALYZER

TABLE 7.2.1 COMPARISON OF ELAPSED TIME

Test Number	Camera Frame Count (See Note)	Elapsed Clock Time (milliseconds)	Difference (milliseconds)	Remarks
446-1	100	99.70	-0.30	1800 rpm clock motor
446-2	100	92.60	-7.40	1800 rpm clock motor
446-3	100	96.36	-3.64	1800 rpm clock motor
446-4	100	98.47	-1.53	1800 rpm clock motor
446-5	100	146.29	+46.29	1800 rpm clock motor
446-6	100	99.34	-0.66	1800 rpm clock motor
446-7	100	105.56	+5.56	1725 rpm clock motor
446-8	100	112.04	+12.04	1725 rpm clock motor
446-9	100	114.20	+14.20	1725 rpm clock motor
446-10	100	114.56	+14.56	1725 rpm clock motor

Note: Using the rated speed of 1000 frames per second, the values in this column are in milliseconds.

time sources, and to eliminate any gross errors in operation, the film record is scanned frame by frame. The clock reading and frame count are recorded and compared. When the clock and the camera are properly operated, the two records coincide. The differences between the two time sources are indicated in Table 7.2.1; and with the exception of Test 446-5, the agreement is satisfactory. The poor agreement between the two values in this test was probably caused by an improper setting of the voltage input to the camera motor.

It is noted in the table that two clock motors were employed in these studies. The second motor was installed in order to employ a larger clock hand and face to improve the data reduction. This motor, while adequate, has not produced as good agreement as the original motor. However, as will be discussed later the information obtained from these instruments has been in remarkable agreement.

Datum references. Fixed reference marks are established to provide length or distance measurements during a collision incident. These marks, listed in Table 7.2.2, appear in the camera field of view.

Time and displacement data. One source of velocity data is from the film record. After the time and displacement data are collected and plotted, the slope of the curve indicates the vehicle velocity at any selected time. A stadia board, divided into three inch increments, mounted on the side of the test vehicle is the length reference, and is read using the range poles in the foreground as fixed reference lines. The following method is used in this calculation:

(1) The film is advanced until the car comes into the range with one of the reference lines.

TABLE 7.2.2 REFERENCE MARKS FOR HIGH SPEED FILM REDUCTION

ITEM	DEVICE	DESCRIPTION	LOCATION	TO PROVIDE
1	Stadia reference board	2" x 6" x 12' - 0" pine board with black and white spaces in alternate 12" increments	Adjacent to impact area	A fixed horizontal length reference
2	Stadia markers (reference targets)	6" x 16-gage sheet metal painted with 3" x 3" diamond-shaped black triangles on white background	One side of crash vehicle	Length reference for analysis of high-speed motion picture
3	Range poles	3/4" x 8' - 0" pipe poles painted red	Adjacent to stadia reference board	Fixed reference points
4	Backboard	16' - 0" x 12' - 0" plywood mounted on wood truss frame	Approximately 20' from impact point parallel with path of crash vehicle	Background for photographs and pertinent test information
5	Centi-revolution clock	Clock face divided into 100 intervals, clock hand attached to 1800 RPM synchronous electric motor	Mounted on backboard	Time reference for analysis of high-speed motion picture film
6	Flashbulb	Press 25 bulb in blackened reflector	In front of stadia reference board	Instant of impact reference cue

(2) The film is advanced frame by frame with readings being made on the three inch increment marks. In some cases a judgment must be made as to which frame is the one closest to this set amount of movement of the vehicle. These readings continue until there is (1) in the case of break-away sign bases, the vehicle moves out of the field of view, or (2) in the case of a fixed barrier, to the point that rebound of the automobile is completed.

(3) The differences in frame counts multiplied by the time per frame will give the time interval involved for the car to move forward three inches. This time is cumulated and plotted versus the accumulated or progressive displacement of the automobile. A sample curve is shown in Figure 7.2.2.

(4) The "time-zero" or impact point and loss of contact between vehicle and support post are shown on the curve. The displacement divided by elapsed time determine the velocity of the automobile at impact and after the incident is completed.

Procedure for penetration data analysis time parameter. For the fixed barrier tests, the following procedure was used to determine critical times during the penetration of the barrier:

(1) The film is advanced to the determined "time-zero" or impact and the frame number recorded.

(2) Using the range pole as fixed reference, the film is then advanced, slowly at first and then frame by frame, to the point that rebound action is evident. This frame number is recorded as the time of maximum penetration.

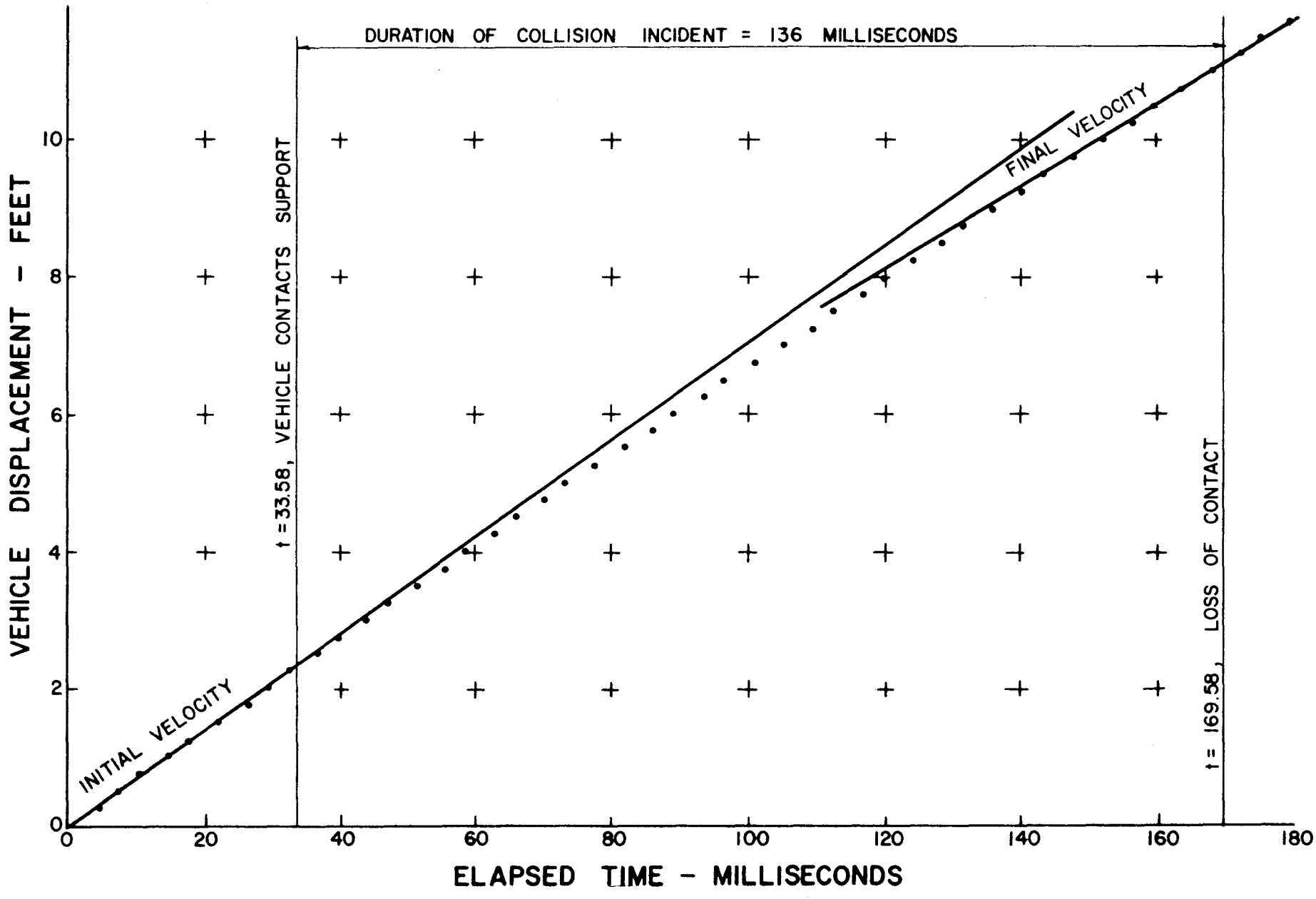

FIGURE 7.2.2 DISPLACEMENT-TIME PLOT, TEST 446-5

(3) Again the film is advanced until no further movement of the car can be detected; this frame number is recorded as the time of final penetration.

(4) The estimated time per frame multiplied by the number of frames from impact to maximum penetration gives the actual time lapse involved; a similar calculation is made for the time from impact to final penetration. The difference between these two calculated figures is the time of rebound.

Procedure for penetration data analysis distance parameter. For the fixed barrier tests, the following procedure was used to determine the penetration of the barrier:

(1) The film is advanced to the determined "time-zero" or impact. The point of the range pole's alignment with the stadia markers on the side of the automobile is read and recorded as the initial reading.

(2) The film is advanced to the point that rebound action is evident, and the reading of the range pole's alignment with the stadia marker is read and recorded as the maximum penetration.

(3) Again the film is advanced until no further movement of the car can be detected; this time the reading is recorded as the final penetration.

(4) The net amounts of maximum and final penetration are the differences between the initial reading and each of the other two readings. The amount of rebound is the difference between these two net penetration figures. Results of these analyses will be discussed in Chapter 8.

Procedure for obtaining velocity information from electronic data. As a wheel of the vehicle passes over a switch (or in the case of wands, contact is made) the switch is closed and a discontinuity is recorded on the oscillogram. The recording oscillograph operating at 120 in./sec., provides a time base. The switches are mounted in pairs three feet apart, using this fixed distance and obtaining a measurement between discontinuities on the oscillogram the vehicle velocity can be easily computed. This computation provides another means of determining vehicle velocity at a selected time during the collision incident.

7.3 Determination of Vehicle Velocity

Displacement and time data for each crash test are recorded from the high-speed film plotted graphically. The average velocity of the crash vehicle at an arbitrary time during the event is defined as the slope of the displacement-time curve at the arbitrary instant of time.

A second method of recording velocity on the oscillographic record has been discussed previously. The tapeswitch and wand devices provide a corroborative check on the film analysis. In the fixed barrier series, two sets of tapeswitches were used; (1) at the end of the guide rail to indicate the velocity of the crash vehicle at the time it was released from the two cable, and (2) immediately in front of the fixed barrier to show the rate at which the vehicle was moving immediately prior to impacting the barrier. In tests of sign supports, an additional set of switches was mounted on the ground behind the sign support. When activated, the responses from the tapeswitches were recorded simultaneously on a continuous

trace recording oscillograph, with the responses from an impact switch located on the post, the latter switch providing a reference on the trace to indicate impact or "time zero."

Comparison of the information obtained from these two sources is contained in Table 7.3.1, in which impact velocity and final velocity are shown. In addition, the difference between these two velocities is tabulated and compared with the change in velocity as computed by integration of the vehicle accelerometer trace. The agreement between the three techniques of data analysis is quite satisfactory, and provides a means of comparing the changes in velocity of the crash vehicle in the several tests.

7.4 Conclusions

It should be noted that in the fixed barrier tests a variety of malfunctions resulted in failure of the electronic devices. In Test 446-1, a power failure occurred; in Test 446-2, the light car hit the barrier off-center, gained and the oscillogram was not susceptible of rational analysis; in Test 446-4, the amplifier became disconnected. Such unfortunate occurrences are a hazard in barrier tests. The malfunction of one system, however, emphasizes the merit of having redundancy in instrumentation.

TABLE 7.3.1 CRASH VEHICLE VELOCITY PRIOR TO IMPACT AND AFTER COLLISION

TEST NO.	IMPACT VELOCITY (fps)		FINAL VELOCITY (fps)		CHANGE IN VELOCITY (fps)		
	FILM	SWITCH	FILM	SWITCH	FILM	SWITCH	COMPUTED*
446-1	63.6		0	N.A.	63.6	N.A.	No Data
446-2	66.6	65.5	0	N.A.	66.6	N.A.	Bad Data
446-3	66.2	66.7	0	N.A.	66.2	N.A.	62.0
446-4	64.7		0	N.A.	64.7	N.A.	No Data
446-5	69.4	66.8	63.6	60.0	5.8	6.8	4.8
446-6	59.0	58.0	0	N.A.	59.0	N.A.	63.2
446-7	64.1	64.2	57.9	No Data	6.2	N.A.	5.8
446-8	62.8	67.8	57.9	62.6	4.9	5.2	5.5
446-9	64.9	67.9	56.2	58.8	8.7	9.1	5.7
446-10	63.6	68.6	54.6	59.0	9.0	9.6	10.6

*Computed by integration technique from accelerometer records. (See Appendix)

CHAPTER 8

FULL-SCALE CRASH TESTS

Ten full-scale crash tests were conducted; five were fixed barrier impacts, and five were controlled collisions with three different concepts of break-away sign support structures.

8.1 Purpose of Tests

Table 8.1.1 lists and classifies all ten tests conducted. The purpose of each test is included in the table.

8.2 Fixed Barrier Penetration Data

The series of fixed barrier tests provided data concerning the impact behavior of vehicles in collisions with a rigidly fixed 8WF20 support post. The film records of these controlled collisions provide a means of quantitatively measuring the extent of damage to the automobile, damage that would in turn affect the passengers. The damage is expressed in terms of the distance which the fixed barrier penetrated the vehicles and the time required for this penetration. The high-speed film records show the apparent forward movement (post penetration) of the vehicle, the apparent backward movement (rebound) of the vehicle, and the final rest position of the vehicle. Figures 8.2.1, 8.2.2 and 8.2.3 contain typical sequence photographs from the high-speed film showing the penetration behavior. Five vehicles were tested, ranging in weight from 2060 pounds to 7960 pounds. The critical events shown are:

Time, t_1: Bumper touches barrier (seconds)

TABLE 8.1.1 FULL-SCALE CRASH TESTS

TEST NO.	TEST DESCRIPTION	PURPOSE OF TEST
446-1	Fixed Barrier	To determine typical medium weight passenger car impact characteristics.
446-2	Fixed Barrier	To determine typical front engine compact passenger car impact characteristics.
446-3	Fixed Barrier	To determine typical rear engine compact passenger impact characteristics.
446-4	Fixed Barrier	To determine typical large weight passenger car impact characteristics.
446-5	Break-Away Base Cantilever Sign Support	To determine the behavior of slotted steel fuse plate installed by turn-of-nut method; to provide correlation data.
446-6	Fixed Barrier	To determine typical cab-over-engine truck impact characteristics.
446-7	Deforming Steel A-Frame Sign Support with Drilled Shaft Foundation	To Observe the behavior of this type support.
446-8	Deforming Steel A-Frame Sign Support with Driven Support Foundation	To compare behavior with same type support with different foundation.
446-9	Fracture Joint Aluminum A-Frame Sign Support	To observe the behavior of this type support.
446-10	Modified Deforming Steel A-Frame Sign Support with Driven Support Foundation	To observe the effect of modification of support post.

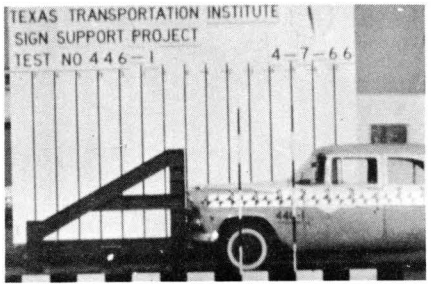

$t_1 = 0.000$

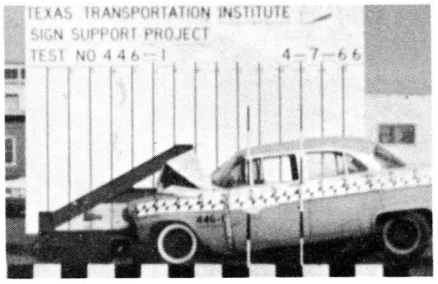

$t_2 = 0.142$

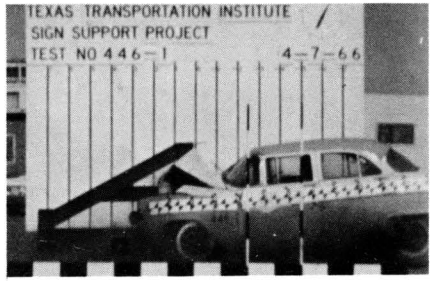

$t_3 = 0.502$

TEST 446-1

8:99

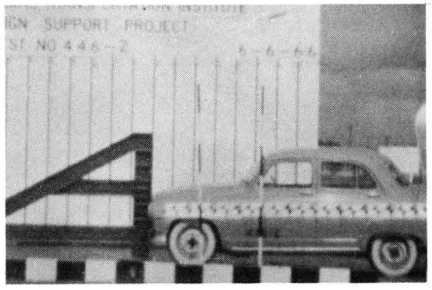

$t_1 = 0.000$

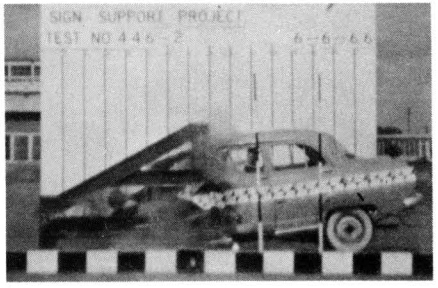

$t_2 = 0.131$

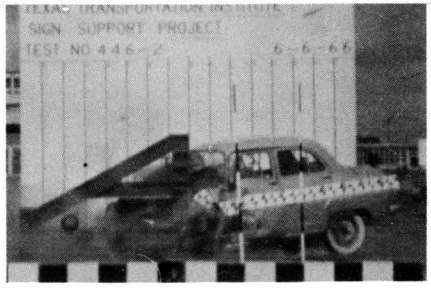

$t_3 = 0.338$

TEST 446-2

FIGURE 8.2.1 SEQUENCE PHOTOGRAPHS OF FIXED BARRIER CRASH SERIES

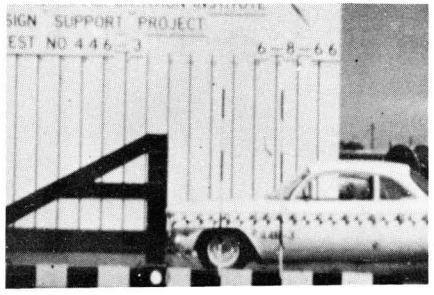

$t_1 = 0.000$

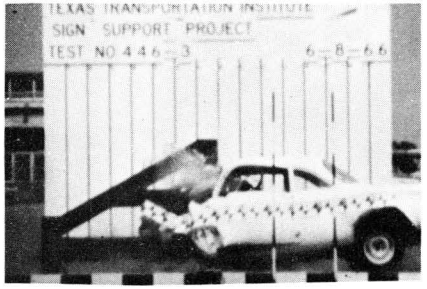

$t_2 = 0.144$

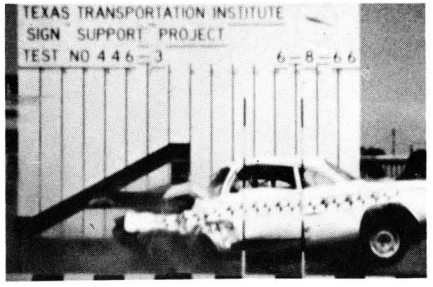

$t_3 = 0.435$

TEST 446-3

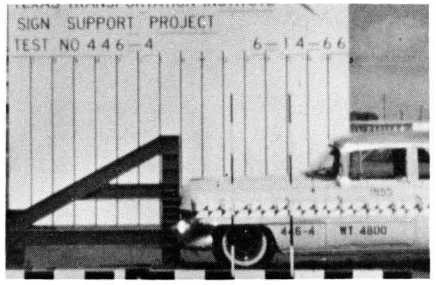

$t_1 = 0.000$

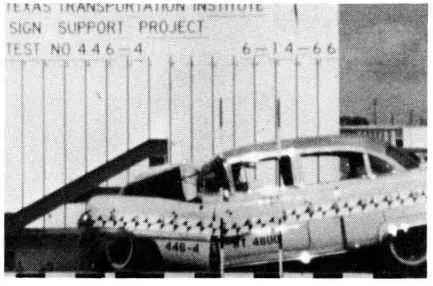

$t_2 = 0.105$

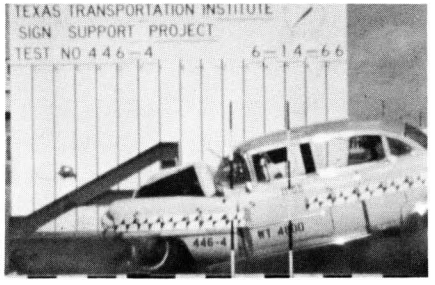

$t_3 = 0.351$

TEST 446-4

8:100

FIGURE 8.2.2 SEQUENCE PHOTOGRAPHS OF FIXED BARRIER CRASH SERIES

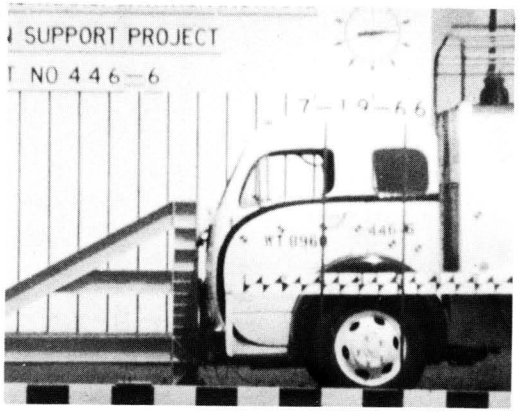

t_1 =0.000

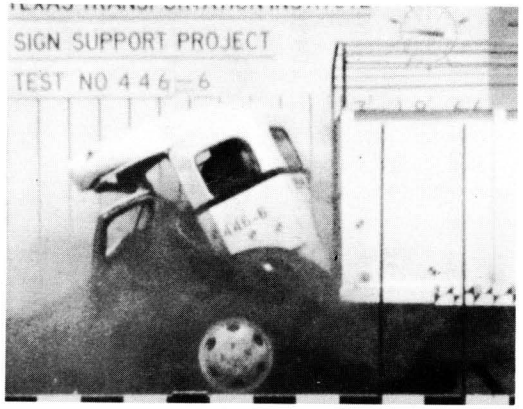

t_2=0.149

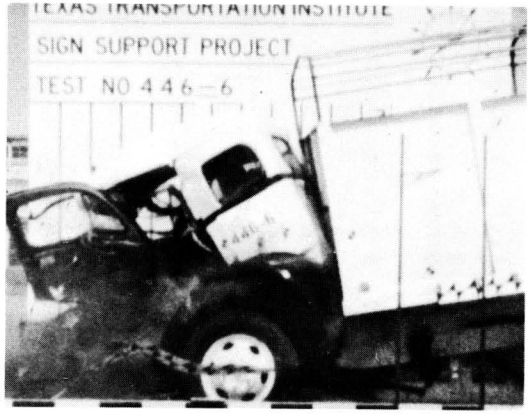

t_3=0.930

TEST 446-6

FIGURE 8.2.3 SEQUENCE PHOTOGRAPH OF FIXED BARRIER CRASH SERIES

Time, t_2 = Maximum penetration by the post, seconds

Time, t_3 = Final penetration by the post, seconds

The distances of penetration and time intervals for each collision in the fixed barrier series were observed and are recorded in Table 8.2.1. This table gives pertinent information concerning each test in the series, including physical data for each of the test vehicles and the estimated velocity of the automobile at the time of impact with the barrier as taken from the high-speed film data. Figure 8.2.4 contains photographs showing each of the vehicles at the conclusion of each crash test. Figures 8.2.5 and 8.2.6 show before-and-after photographs which illustrate the damage to the vehicles.

Figure 8.2.7 shows graphically the data presented in Table 8.2.1. It appears that, except for the Corvair with an engine in the rear, there is an inverse linear relationship between the weight of the crash vehicle and the observed rebound of the automobile after impact. Although there was no engine in the front of the Corvair, it was observed that there was an inflated tire which was not fastened to the flooring. This tire was ruptured by the impact, and the rim on which it was mounted showed significant permanent deformation; the amount of force absorbed by this spare tire could not be determined. Each test vehicle, except the Simca, struck the fixed barrier near the center of the grill. The Simca struck the barrier some 15 inches left of center on the driver's side of the car.

The relationship between vehicle weight and maximum and final penetration is not as clearly observed as is the rebound-weight

TABLE 8.2.1 FIXED BARRIER CRASH TEST SUMMARY

TEST NO.	TEST DATE	YEAR, MAKE & TYPE AUTOMOBILE	WEIGHT OF VEHICLE (lbs.)	VELOCITY AT IMPACT * (fps)	MAXIMUM POST PENETRATION (ft.)	(sec.)	FINAL POST PENETRATION (ft.)	(sec.)	TOTAL REBOUND (ft.)	(sec.)
446-1	4-7-66	1955 Ford 4-Door Sedan	3380	63.6	3.71	.142	2.83	.502	0.88	.360
446-2	6-6-66	1959 Simca 4-Door Sedan	2060	66.6	4.25	.131	3.25	.338	1.00	.207
446-3	6-8-66	1960 Corvair 2-Door Sedan	2320	66.2	5.25	.144	3.75	.435	1.50	.291
446-4	6-14-66	1954 Cadillac 4-Door Sedan	4800	64.7	4.50	.105	3.75	.351	0.75	.246
446-6	7-19-66	Series 3000 White Truck	7960	59.0	5.00	.149	4.50	.930	0.50	.781

*By analysis of high-speed film.

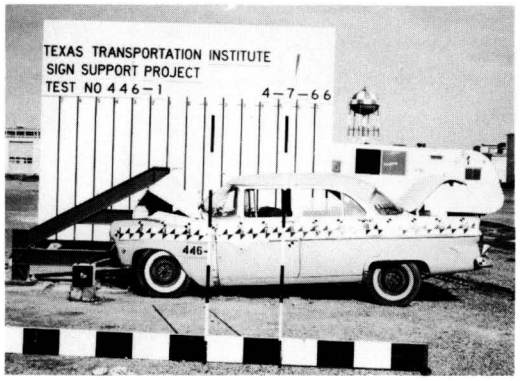

446-1

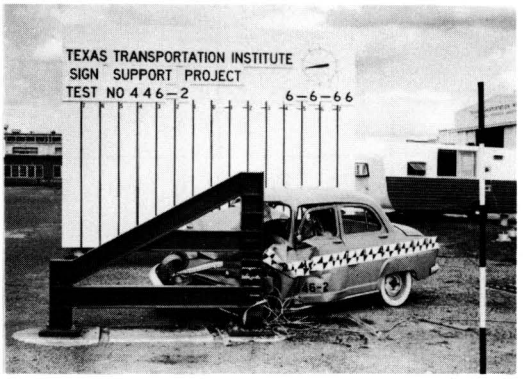

446-2

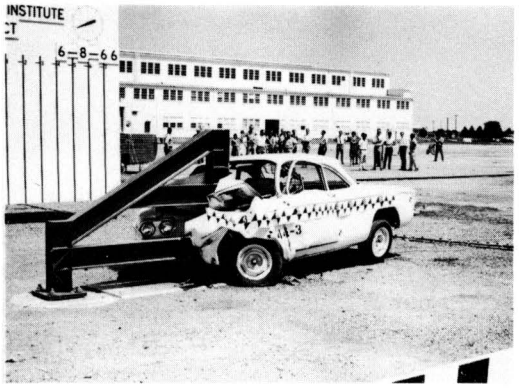

446-3

446-4

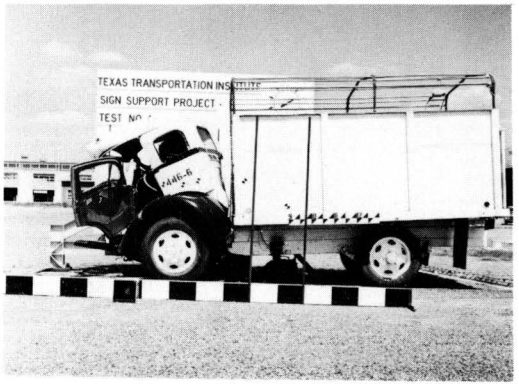

446-6

FIGURE 8.2.4 PHOTOGRAPHS OF VEHICLES AT CONCLUSION OF EACH FIXED BARRIER TEST

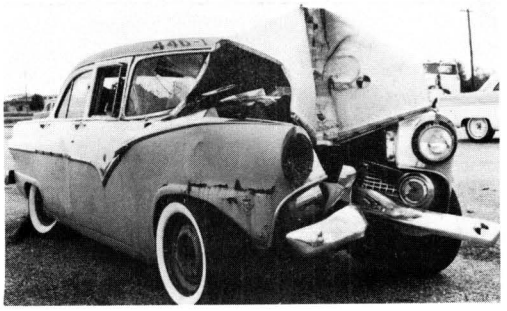

446-1

446-2

446-3

FIGURE 8.2.5 BEFORE AND AFTER VIEWS OF VEHICLES IN FIXED BARRIER SERIES

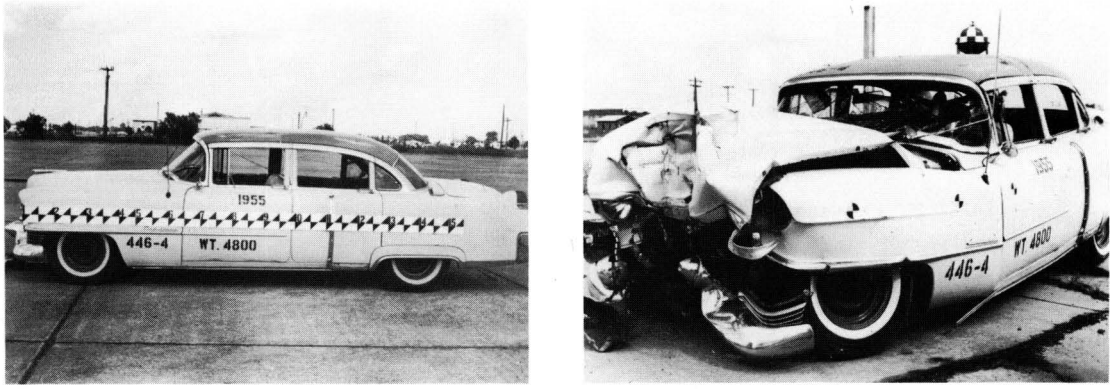

446-4

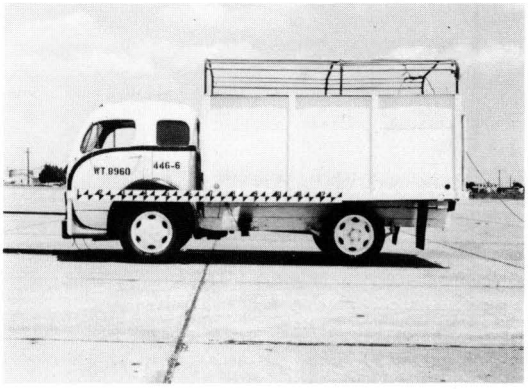

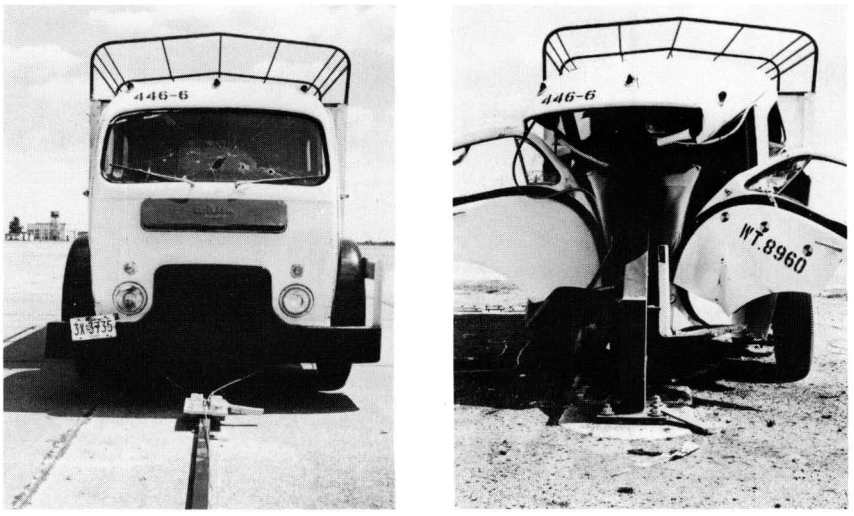

446-6

FIGURE 8.2.6 BEFORE AND AFTER VIEWS OF VEHICLES IN FIXED BARRIER SERIES

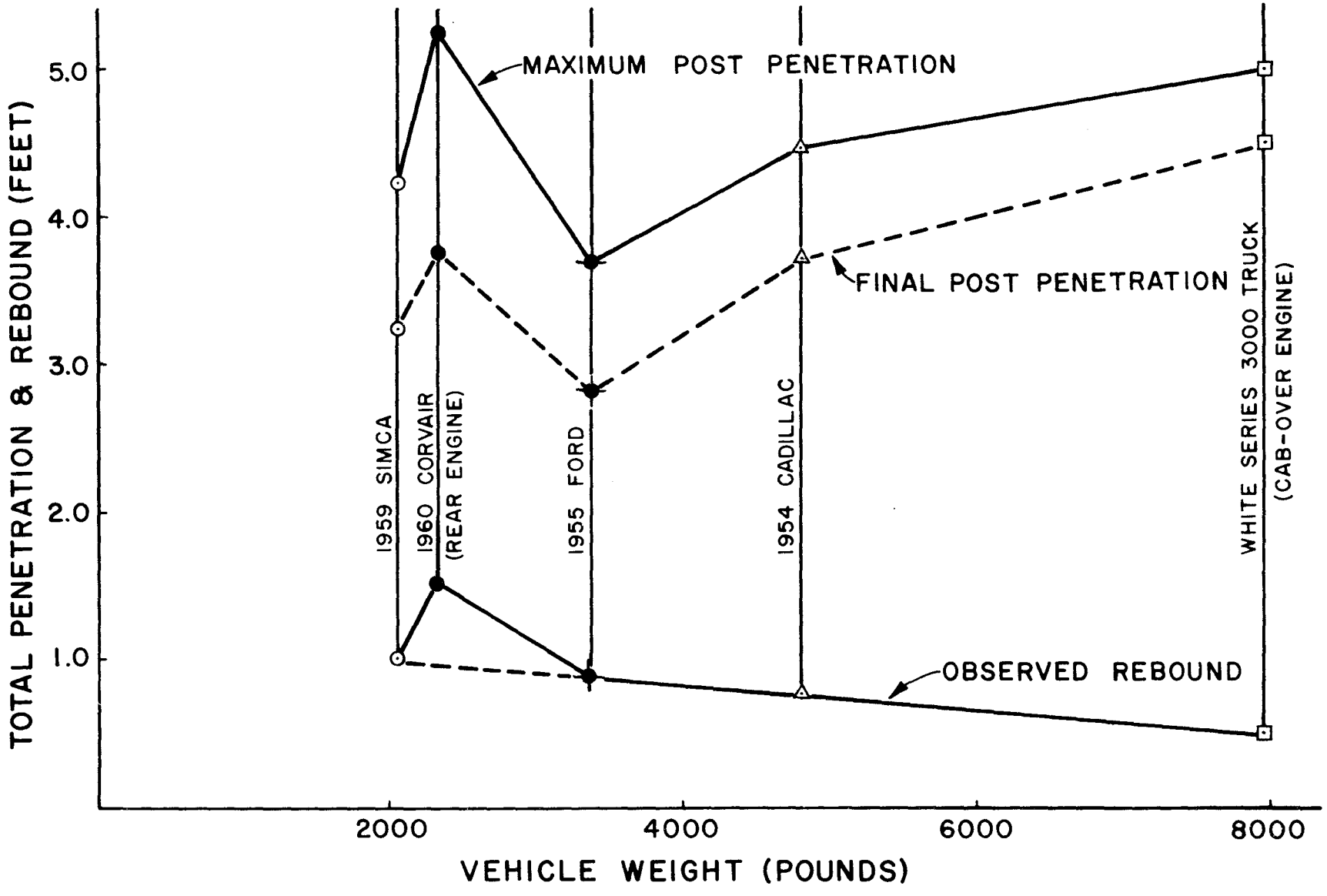

FIGURE 8.2.7 OBSERVED PENETRATION & REBOUND IN FIXED BARRIER CRASH TESTS

relationship. It is apparent that, except for the Corvair, the total penetration increases with increase in weight. Again it should be noted that the Simca did not strike the barrier on center; thus the high penetration can be rationalized on this basis, since the engine was not involved in the penetration as was the case in the other collisions. These fixed barrier crash tests provide information concerning post penetration which had not heretofore been published. Some investigators have conducted wall barrier tests in which the crushing was distributed over the width of the front of the vehicle,[12,13,14] and others have performed full-scale tests in which only a portion of the vehicle was crushed.[15,16] The latter studies involved bridge rails and guard rails.

8.3 Determination of Force-Deformation Characteristics for Vehicles Used in the Fixed Barrier Tests

Two methods were used to determine the force-deformation characteristics of the vehicles used on the fixed barrier tests. It must be recognized that the data developed from these tests is representative of the type automobiles used. Changes in construction in post-1960 automobiles would most surely produce different results. However, the information gained does reflect the range of values to be expected. The test procedures, methods of instrumentation and data reduction techniques developed should be valuable to future researchers.

The first method of data reduction uses the time-displacement information taken from the high-speed motion picture records. This technique uses a multiple regression curve fitting technique to fit

the best least square polynomial to the time-displacement data. The method of using a fitted curve to develop force-deformation information can be explained by reference to Figure 8.3.1.

In Figure 8.3.1 (a), a best least square polynomial is fitted to the time-displacement data points on a data reference axis (x - t). The origin of this axis is chosen such that enough points in the constant velocity period (before impact) are present to force the fitted curve to approximate the straight line relation between displacement and time in this period. The best fit polynomial is any fourth order, or higher, polynomial which fits the data and whose first time derivative at t'_o (the instant of impact) approximates the velocity at impact. The polynomial chosen is then transferred to the impact event axis (x' - t') whose origin is at time t_o (the instant of impact on the data reference axis (x - t). The acceleration (deceleration) is determined by taking the second time derivative of the polynomial and plotting it against time on the impact event axis as shown on Figure 8.3.1 (b). The force on the vehicle is calculated at any time as

$$F = \ddot{x}'(t) \frac{\text{Vehicle Weight}}{g}$$

where g is the acceleration due to gravity. In this calculation of force, it is assumed that the vehicle is a rigid body. Forces calculated in this manner reflect only the resultant force needed to give the mass center of the vehicle the response dictated by the impact, i.e., this is the force required to give the vehicle the observed time-displacement behavior. For this reason, the time force relation

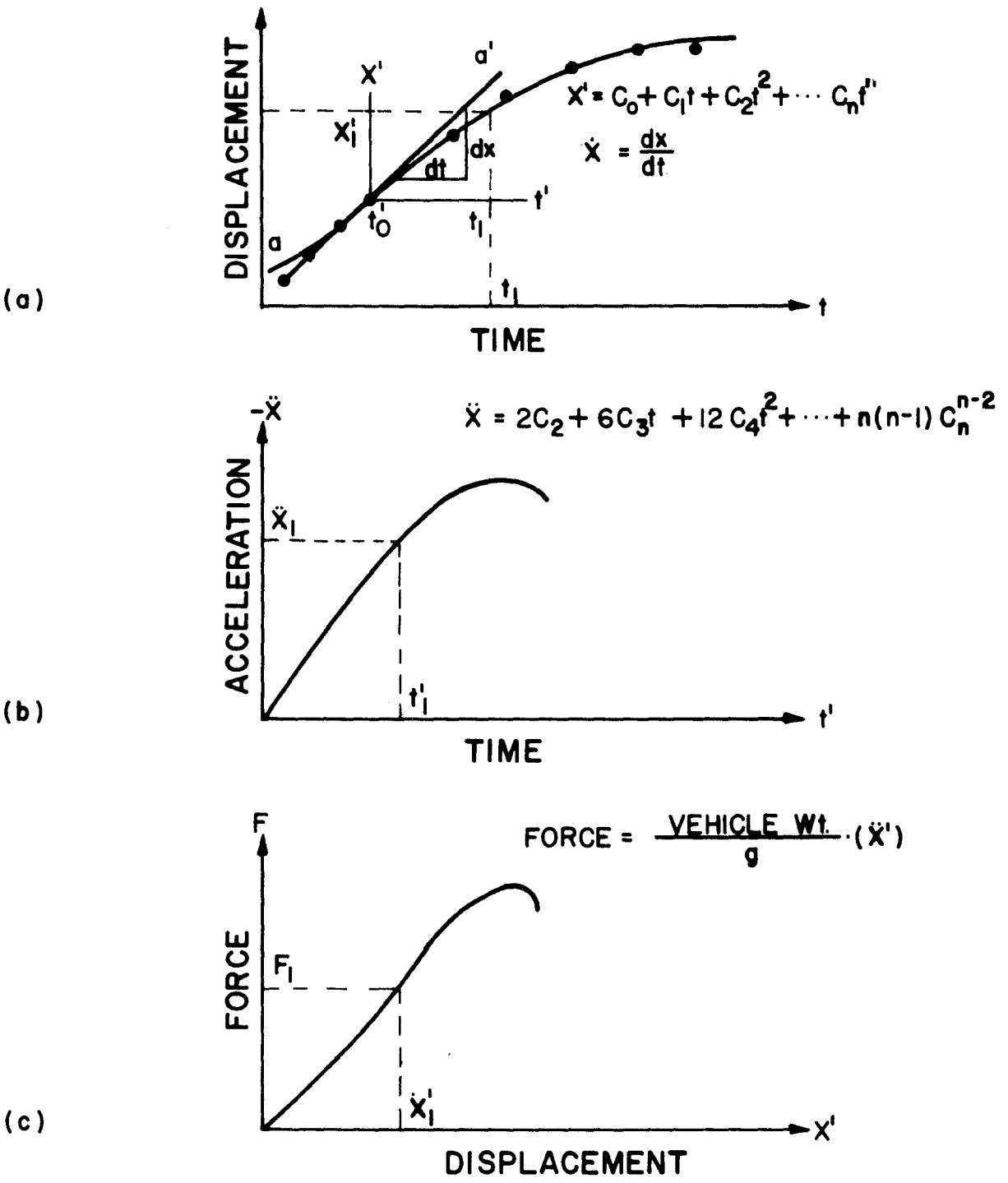

FIGURE 8.3.1 CURVE FITTING TECHNIQUE FOR FORCE-DEFORMATION OF VEHICLES IN FIXED BARRIER TESTS

will be smooth and will not reflect spikes or other discontinuities.

The force-displacement curve shown in Figure 8.3.1 (c) is generated by plotting force and displacement for the same point in time. This is illustrated by the dotted lines for x'_1, $\ddot{x}'_1$, F_1 for time t'_1. Figure 8.3.2 through Figure 8.3.6 show the results of this method of analysis for the fixed barrier tests.

The second method of data reduction for determining the force-deformation characteristics of the vehicle makes use of the vehicle accelerometer trace. Section 7.1 explained the method of arriving at time-displacement data by double integration of the accelerometer trace. The force at any time is

$$F = \ddot{x}(t) \frac{\text{Vehicle Weight}}{g}$$

as in the first method. By picking force and displacement for a particular point in time, a force-displacement curve can be constructed. Figures 8.3.2 through Figure 8.3.9 show the force-displacement curves constructed for Tests 446-2, 446-3 and 446-6. Two curves are presented for the data from the accelerometers, one for each of two different galvanometers used in recording. The force-deformation curve obtained by method 1, from the film analysis, is shown for comparison. To get a better perspective on the comparison of the two methods, the area under the curves, the energy absorbed in three feet of penetration, was calculated. Table 8.3.1 shows the energy values computed by each method.

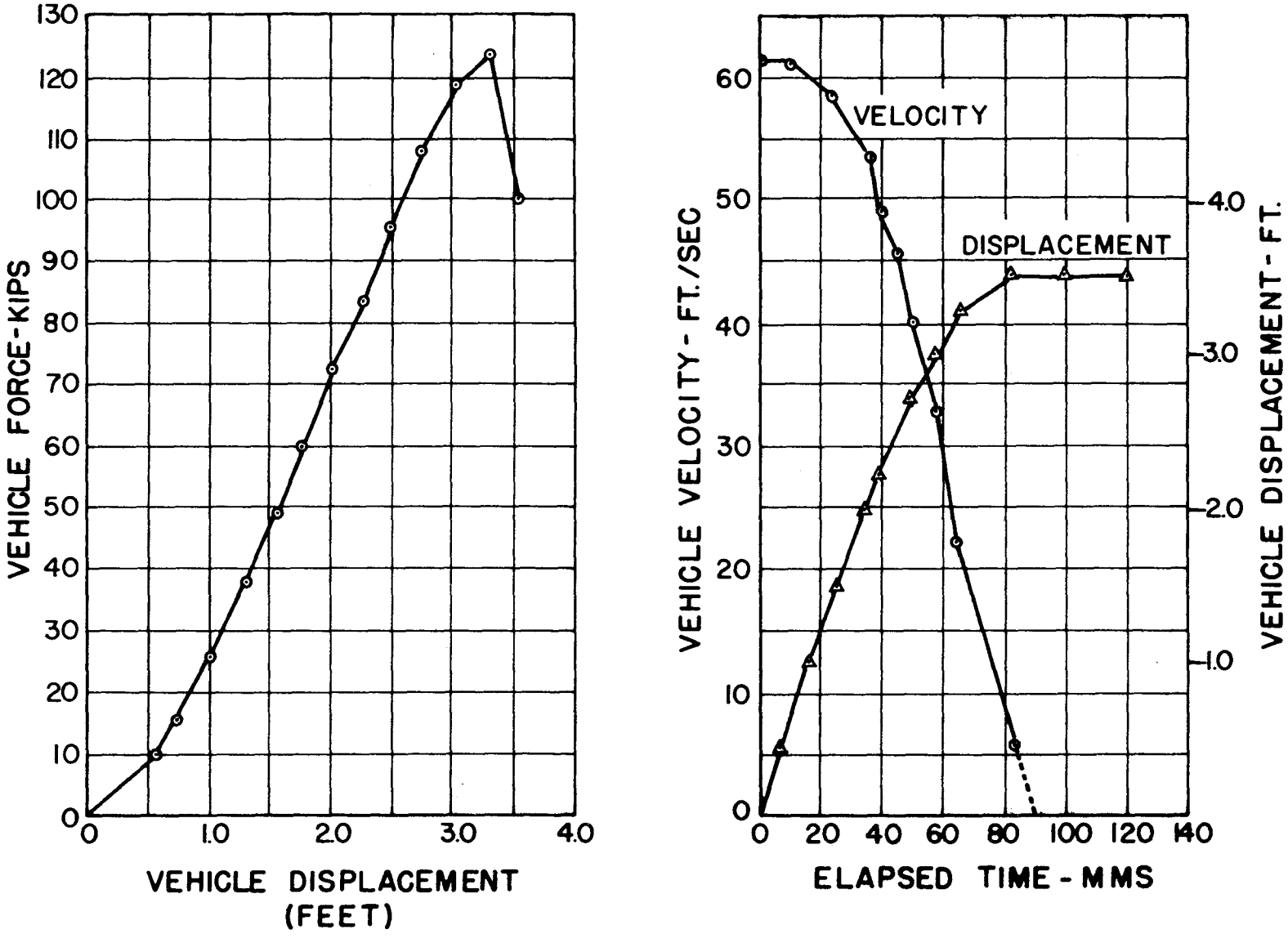

FIGURE 8.3.2 TEST 446-1, 1955 FORD 4-DOOR SEDAN

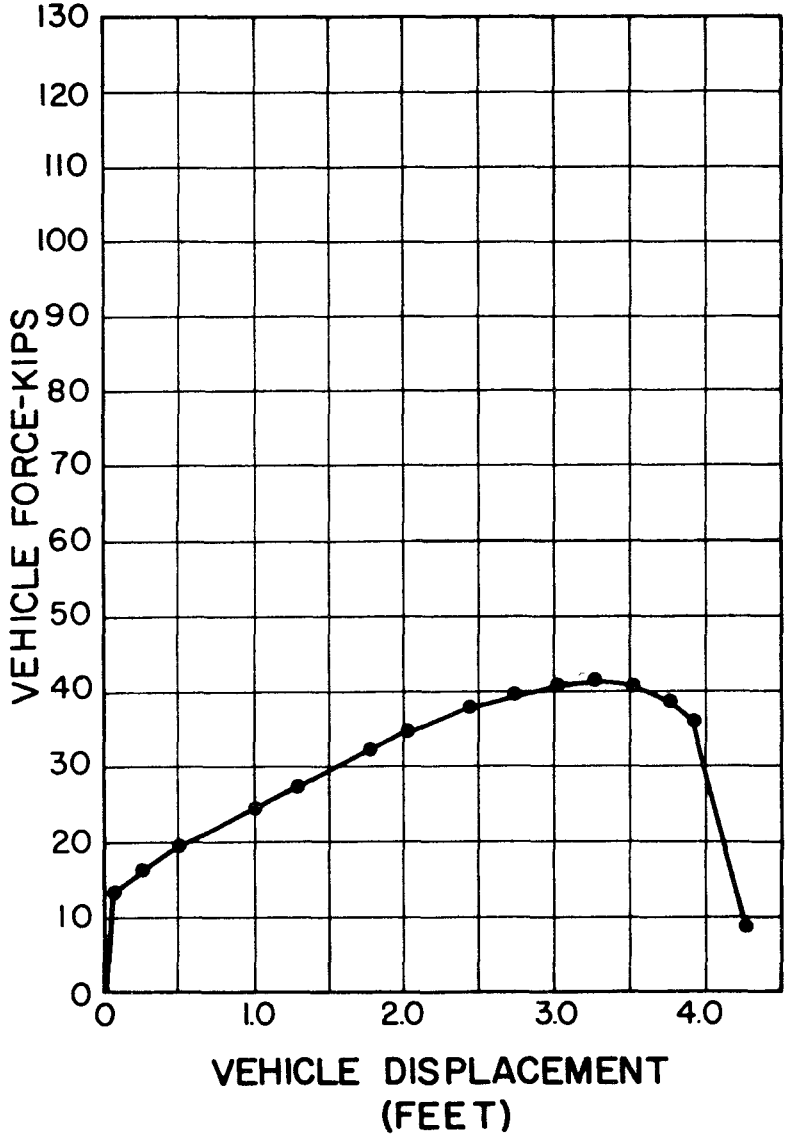

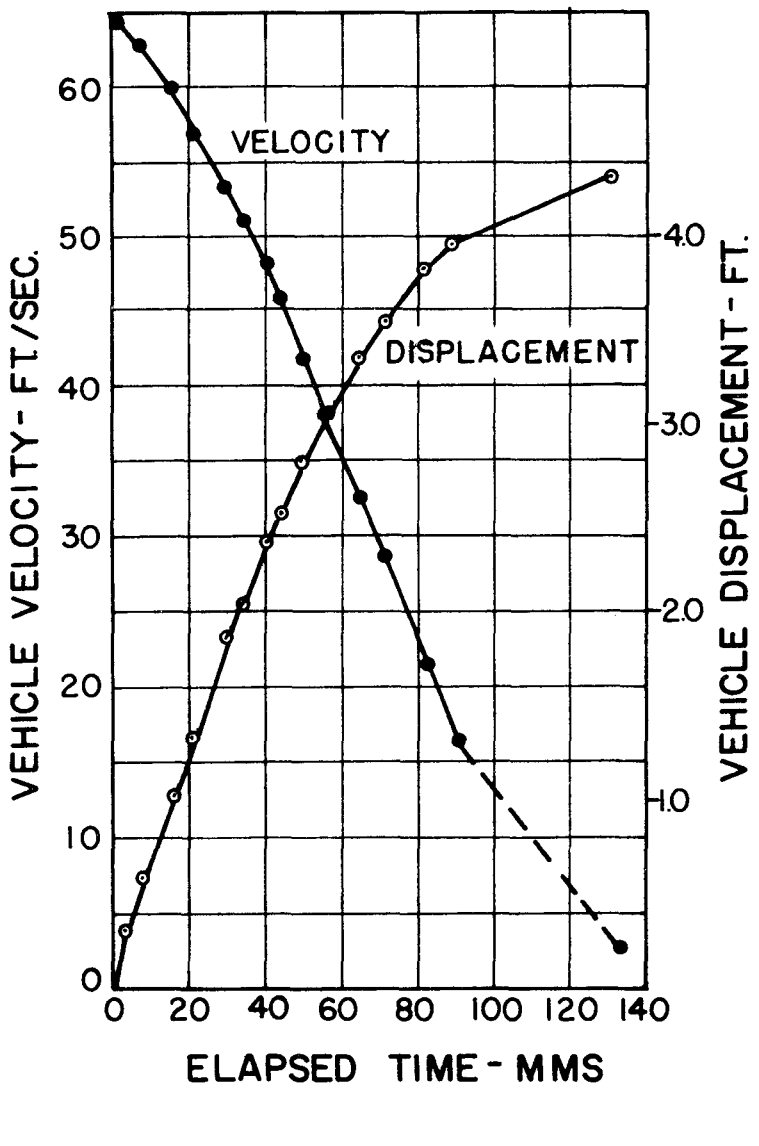

FIGURE 8.3.3 TEST 446-2, 1959 SIMCA 4-DOOR SEDAN

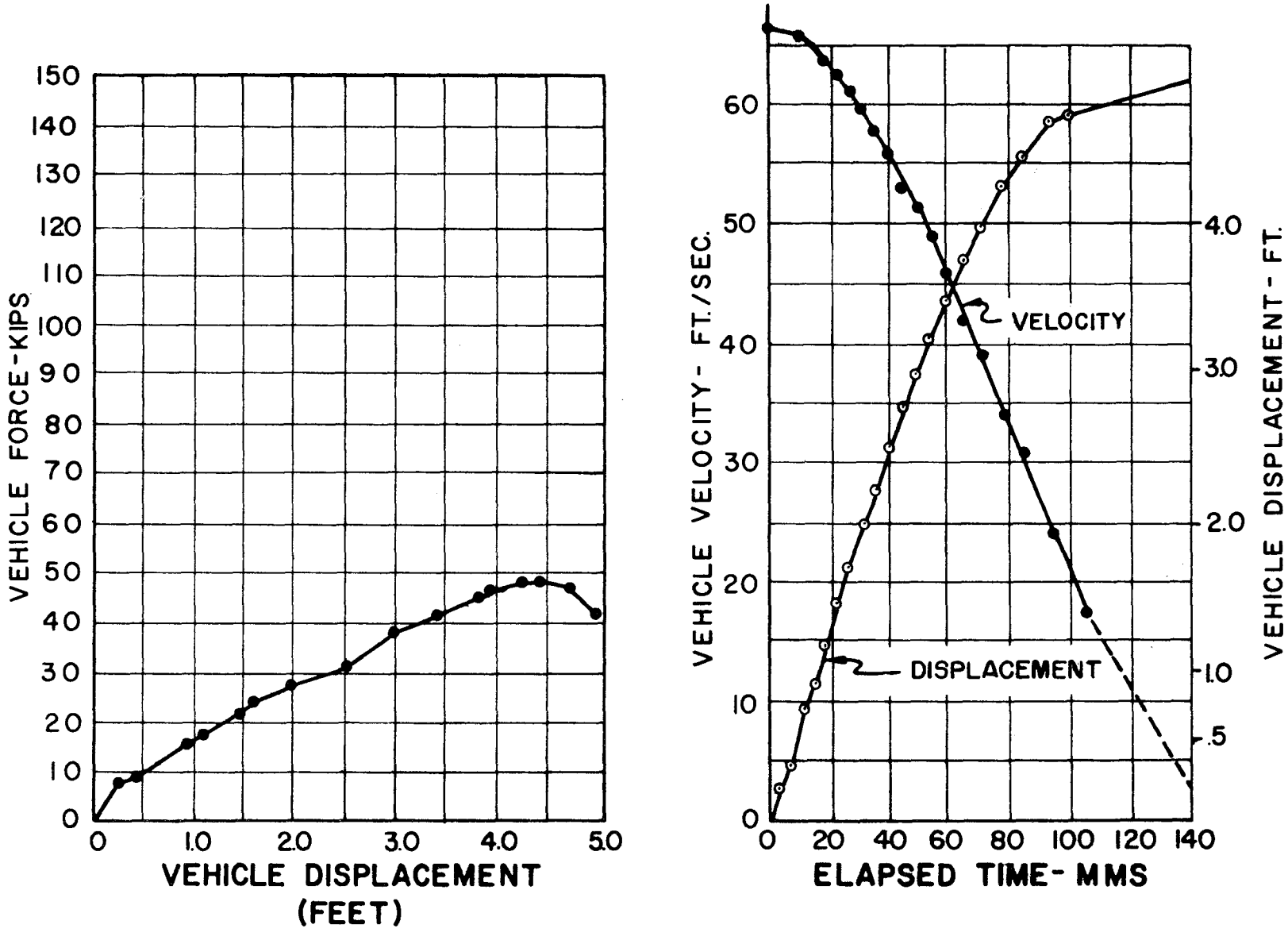

FIGURE 8.3.4 TEST 446-3, 1960 CORVAIR COUPE

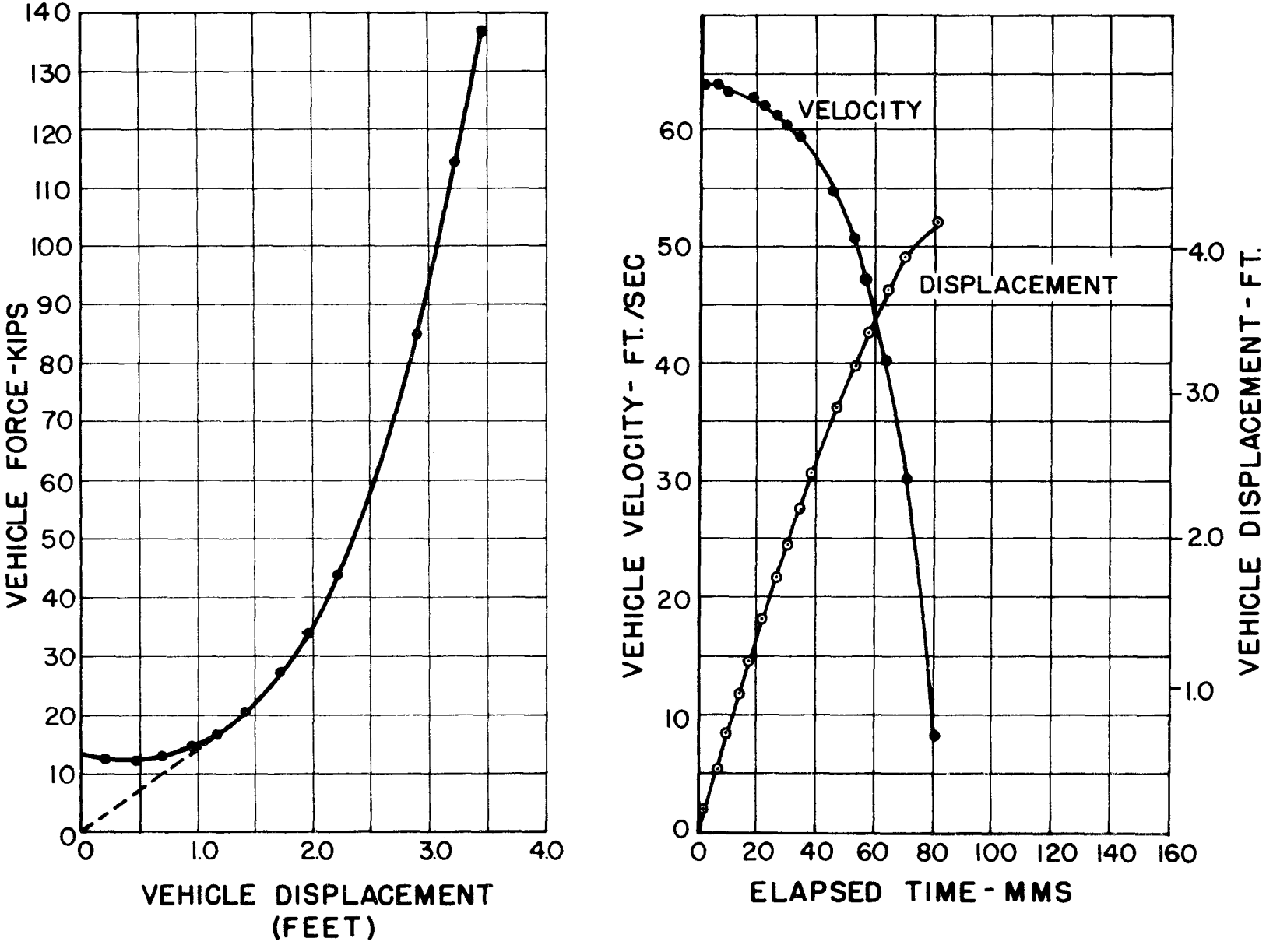

FIGURE 8.3.5 TEST 446-4, 1954 CADILLAC 4-DOOR SEDAN

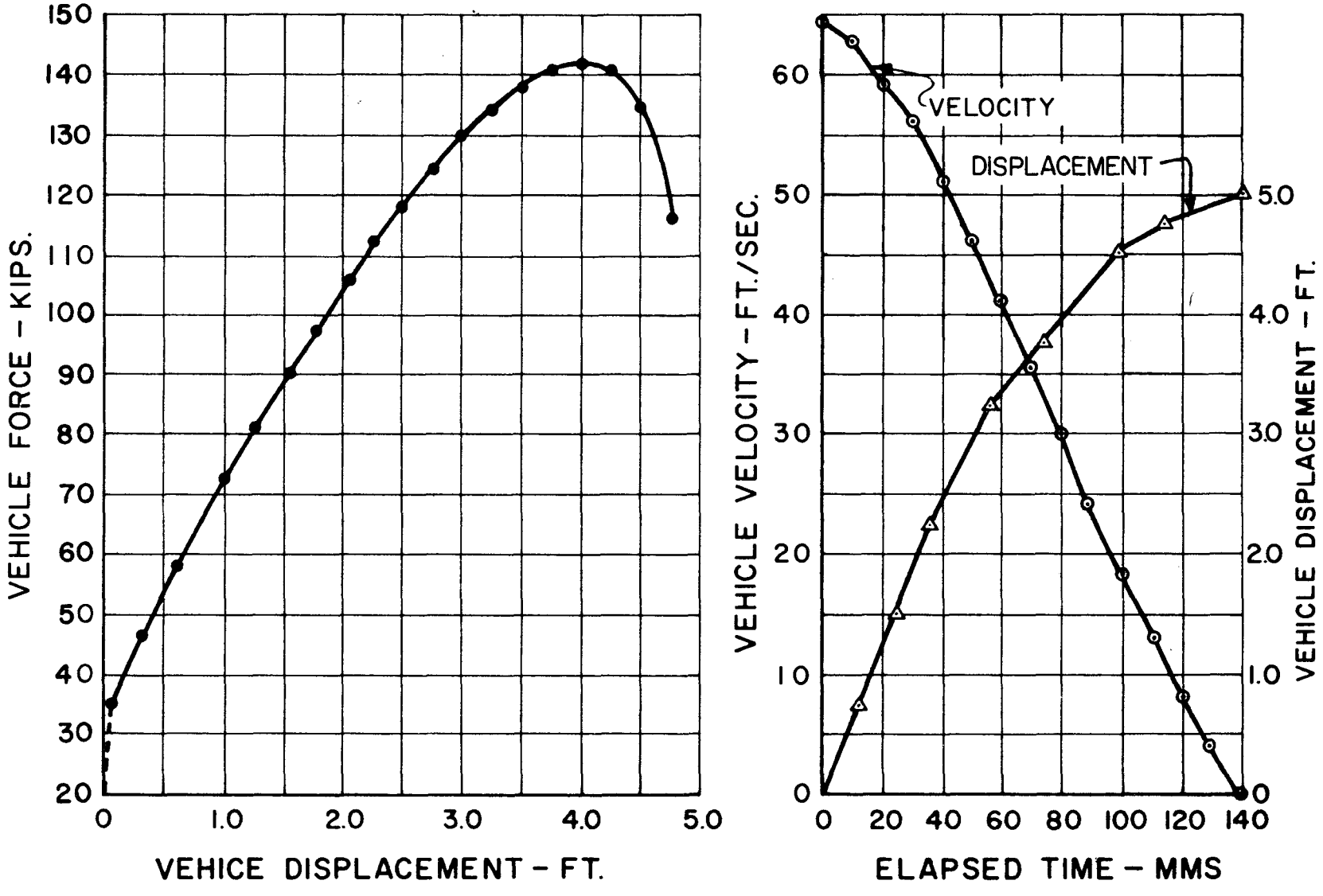

FIGURE 8.3.6 TEST 446-6, SERIES 3000 WHITE TRUCK

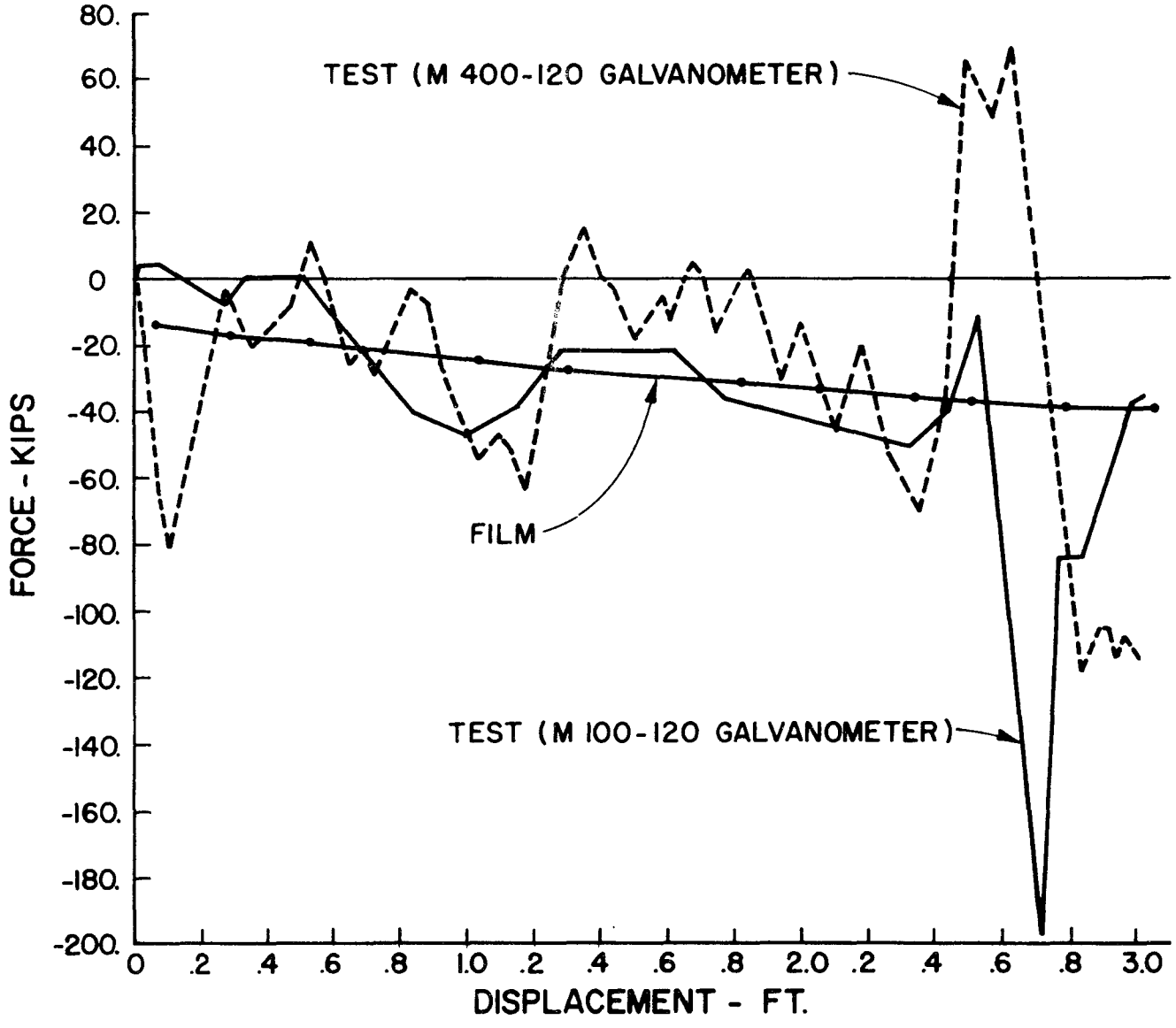

FIGURE 8.3.7 — TEST 446-2, 1959 SIMCA, FORCE-DEFORMATION COMPARISON

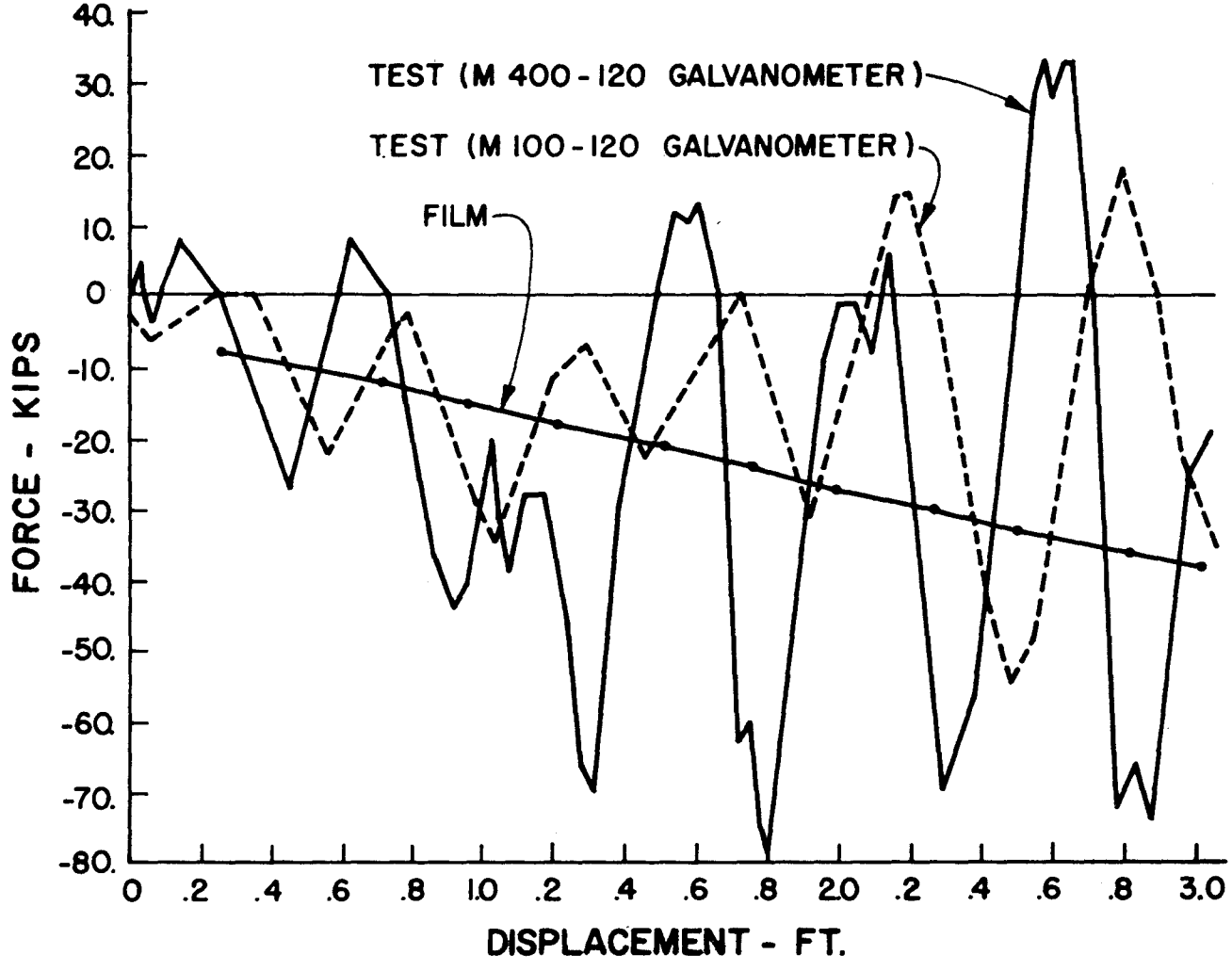

FIGURE 8.3.8 – TEST 446-3, 1960 CORVAIR, FORCE-DEFORMATION COMPARISON

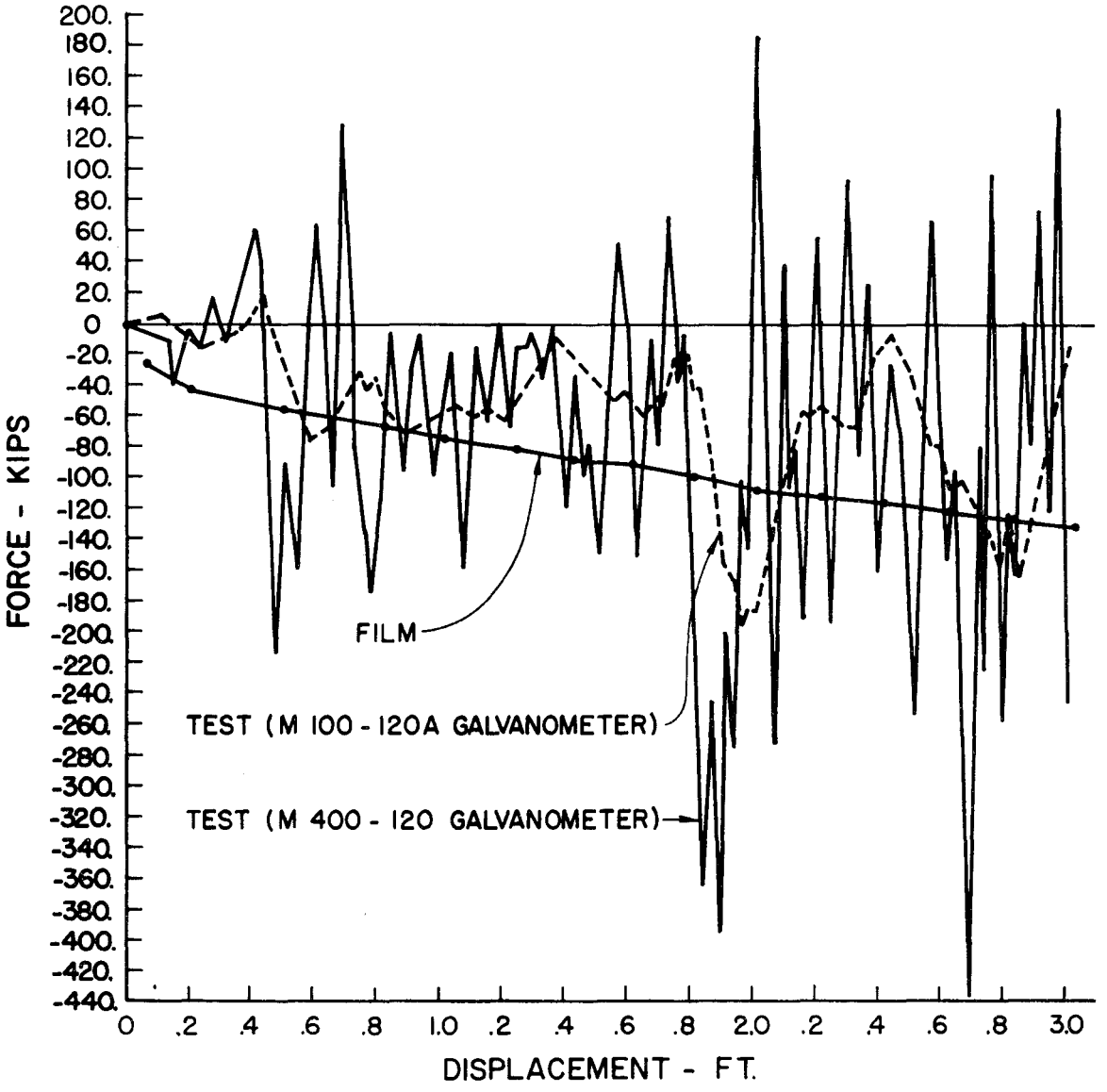

FIGURE 8.3.9. TEST 446-6, SERIES 3000 WHITE TRUCK, FORCE - DEFORMATION COMPARISON

TABLE 8.3.1 COMPARISON OF COMPUTATIONS OF ENERGY ABSORBED

TEST NUMBER	Energy in 3 Feet of Penetration (ft./lbs.)	
	Method 1 (FROM HIGH-SPEED FILM DATA)	Method 2 (FROM VEHICLE ACCELEROMETER TRACE)
446-2	87,512	112,099 (M400-120) 75,560 (M100-120)
446-3	64,491	66,416 (M400-120) 40,844 (M100-120)
446-6	507,900	461,350 (M100-120A) 517,400 (M400-120)

8.4 Summary of Sign Support Crash Tests

Five full-scale crash tests of sign supports were conducted to provide information concerning the behavior of selected sign support configurations and to observe the vehicle damage. A summary of the sign support crash tests follows:

TABLE 8.4.1 SIGN SUPPORT CRASH TESTS

TEST NO.	SIGN SUPPORT DESCRIPTION	CRASH VEHICLES	
		DESCRIPTION	WEIGHT (lbs.)
446-5	Break-away base steel cantilever support	1955 Ford four door sedan	3500
446-7	Deformable steel A-frame support, concrete foundation	1955 Ford two door sedan	3480
446-8	Deformable steel A-frame support, posts driven into natural ground	1955 Ford two door sedan	3460
446-9	Fracture joint aluminum A-frame support	1955 Ford four door sedan	3580
446-10	Modified deformable steel A-frame support, posts driven into natural ground	1955 Ford four door sedan	3300

Prints of the oscillographic records obtained for each test are contained in the Appendix to this report.

8.5 Description of Test 446-5

Type of Sign Support:	Break-Away Base Cantilever Support
Construction Details:	(See Figure 8.5.1)
Sign Face:	8' x 16' x 5/8" plywood
Support Posts:	2-8WF20 (A441, hot dip galvanized)
Windbeams:	3-3Z2.33 (6061-T6 aluminum)
Mechanical Fuse:	4 7/8" x 5 1/4" x 9/16" slotted plates (A441 steel)
Fuse Plate Connection:	4-7/8" diameter A325 bolts. Initial tension in each bolt = 36,000 lb., estimated by turn-of-nut method.

Crash Vehicle: A 1955 Ford four door sedan, weighing 3500 pounds, was employed in this test.

Crash Vehicle Instrumentation: Two Endevco accelerometers and two Statham accelerometers, as described in Table 6.3.1, were mounted on steel blocks welded to the vehicle frame. An amplifier and power source were contained in the trunk of the vehicle. The accelerometer signals were transmitted to a recording oscillograph by a 1000 foot shielded cable (Belden 8775).

Post Instrumentation: Four Strainsert bolts, as described in Table 6.3.1, were used to connect the break-away base. Strain gages were attached to the support post, as described in Table 6.3.1, and a linear potentiometer was mounted on the stub of the break-away base.

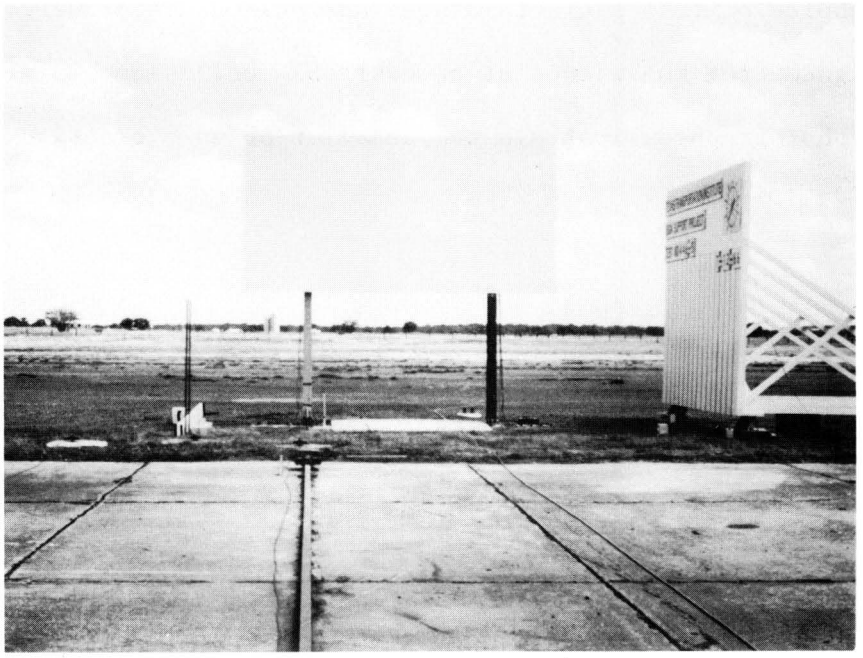

FIGURE 8.5.1 TEST 446-5

Sequence photographs of Test 446-5 are shown in Figure 8.5.2. This test was proposed to observe the steel slotted fuse plate connection design which was a preliminary design based upon the laboratory tests described in Chapter 4, Part III. The base released at 15 milliseconds after initial contact (b), and the maximum fuse plate slip occurred 19 milliseconds later (c). Note that the fuse plate did not become disengaged (d), however, the support post was stripped from the windbeams (e), with sufficient angular velocity to clear the vehicle. This behavior is considered satisfactory since the vehicle damage was minor, however the fuse plate design did not permit the desired behavior in which the upper part of the post would have remained attached to the windbeams.

The choice of fuse plate thickness and bolt diameter were apparently over-designed from the viewpoint of desirable collision behavior. These sequence photographs illustrate the behavior of an overdesigned fuse plate.

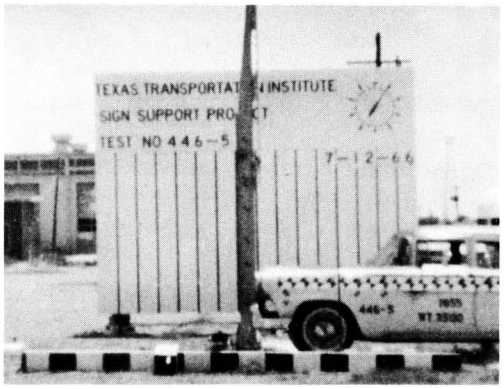

(a) INITIAL CONTACT (t = 0.000 SEC)

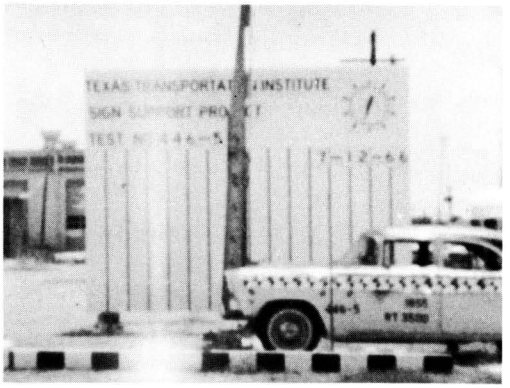

(b) BASE RELEASE (t = 0.015 SEC)

(c) MAX. FUSE PLATE SLIP (t = 0.034 SEC)

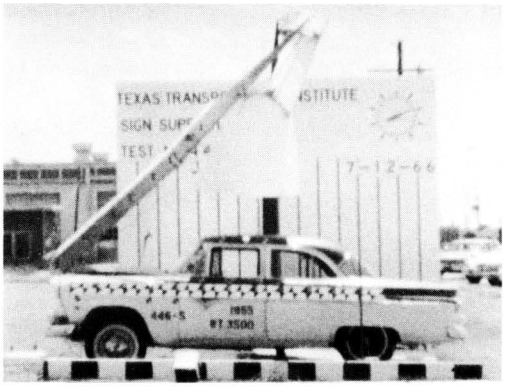

(d) LOSS OF CONTACT (t = 0.136 SEC)

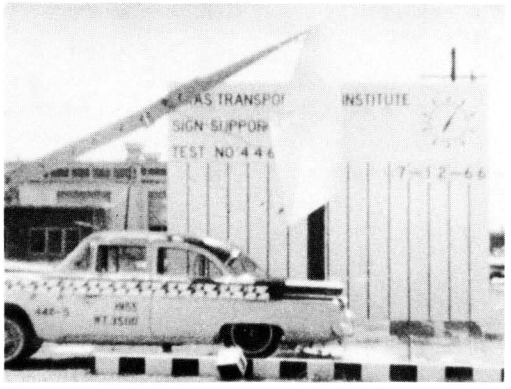

(e) POST CLEARS VEHICLE (t = 0.237 SEC)

FIGURE 8.5.2. SEQUENCE PHOTOGRAPHS OF TEST 446-5

Before and after views of the front of the crash vehicle are presented in Figure 8.5.3; in (a) the guide rail and pulling and release mechanism are shown in the foreground. The deformation of the bumper, grille, and hood are shown in (b). The vehicle damage caused by the 8WF20 steel shape was minor even though the fuse plate did not function in the collision incident. The support post used in this test weighs in excess of 200 pounds.

It should be emphasized that the stripping of the support post from the windbeams provided satisfactory safety behavior in this crash test. This behavior illustrates the added safety feature provided by the windbeam connection in case the fuse connection does not operate properly. It should be noted that in this test the support post was bolted to the aluminum windbeam with steel bolts.

It is estimated that the crash vehicle was traveling 47.3 miles per hour prior to impact (see Table 7.3.1, Part III), and the change in velocity caused by the collision was 3.3 miles per hour. A peak deceleration of 15.7 g's was recorded at 20.7 milliseconds after impact. These values compare favorably with data from previous tests[17] in which the fuse connection did disengage.

(a) BEFORE

(b) AFTER

FIGURE 8.5.3 TEST 446-5, TEST VEHICLE DAMAGE

Support damage in this test is shown in Figure 8.5.4; in (a) the support post and upper windbeam, which was stripped from the sign panel can be seen, in (b) the damage to the plywood sign face is shown, and in (c) the incomplete slippage of the fuse plate is apparent. The fuse plate slipped approximately 3/4 inch, but the combination of the tension in the 7/8 inch diameter bolts and the bending resistance of the 9/16 inch thick fuse plate was too great to permit the fuse to disengage completely.

Discussion. Frame-by-frame analysis of the high-speed films coupled with parameter studies from mathematical simulation led to the recommendations for designing the fuse connection presented in Section 5.1, Part II. It is apparent that the fuse plate thickness must be very nearly equal to the rolled shape flange thickness. In addition, the selection of bolt size must be chosen to provide moment capacity adequate to resist wind load. When these two requirements are satisfied, optimum fuse behavior can be anticipated in a collision incident.

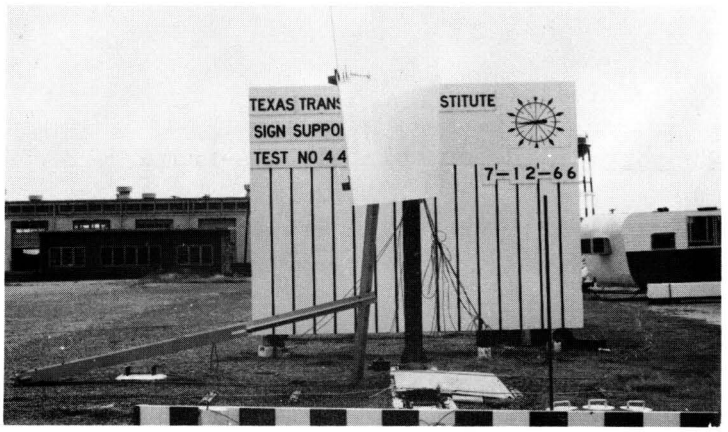

(a)

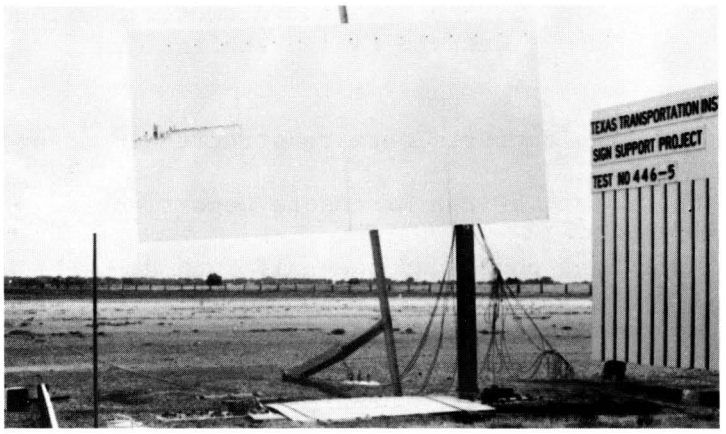

(b)

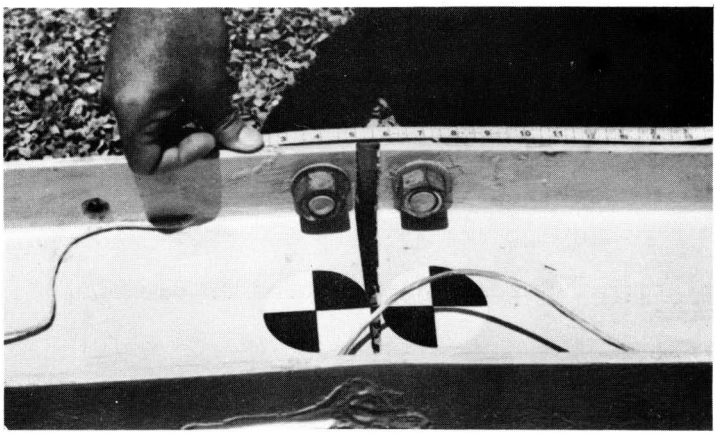

(c)

FIGURE 8.5.4 TEST 446-5, SUPPORT DAMAGE

8.6 Description of Test 446-7

Type of Sign Support: Deformable Steel A-frame

Construction Details: (see Figure 8.6.1)

Sign Face:	8' x 14' x 0.10", Sheet Aluminum
Support Posts:	4 lb./ft. Rail Steel "U" section (perforated)
Windbeams:	4 lb./ft. Rail Steel "U" section (perforated)
Foundation:	Set in one foot diameter non-reinforced concrete filled shafts five feet deep.

The sign and sign supports were constructed in accordance with plans and specifications of the Minnesota Department of Highways. The rail steel "U" sections contained one-half inch diameter holes spaced at six inches on centers. This type of section is widely used in the United States for small sign installations.

Crash Vehicle: A 1955 Ford two door sedan, weighing 3480 pounds, was employed in this test.

Crash Vehicle Instrumentation: The vehicle instrumentation was identical to that described in Test 446-5.

Post Instrumentation: Strain gages mounted on diagonal strut, as described in Table 6.3.1, were installed.

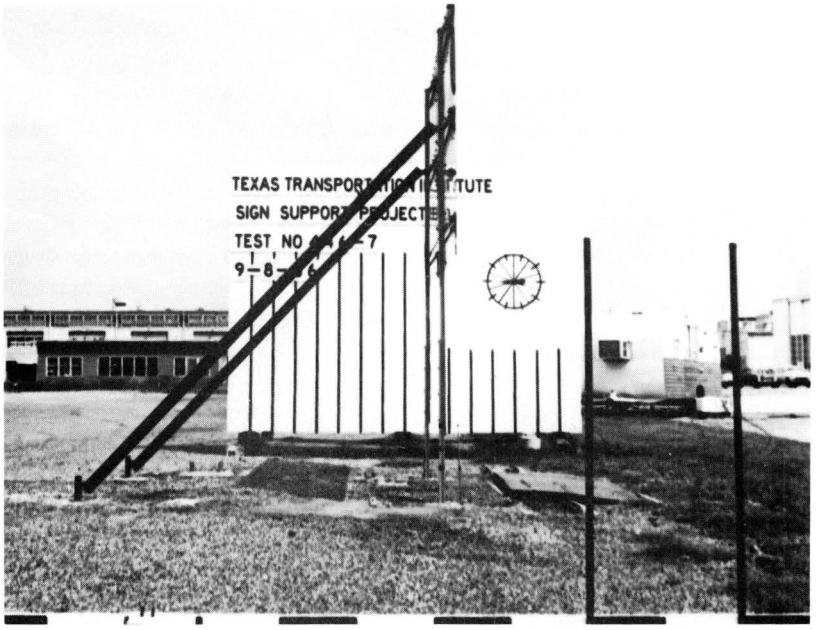

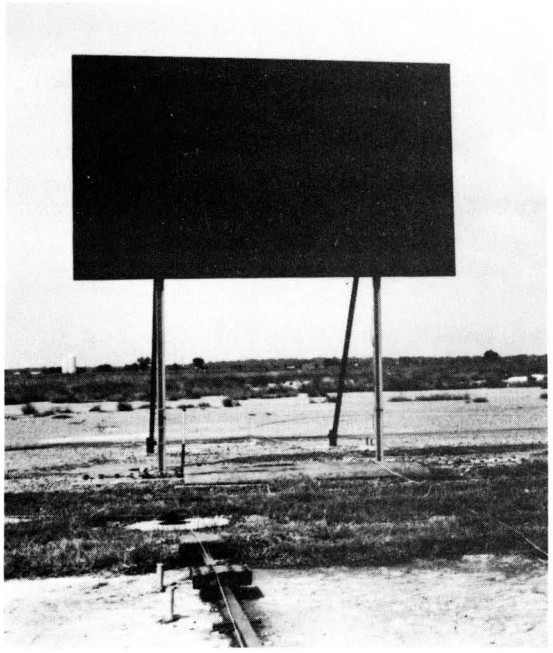

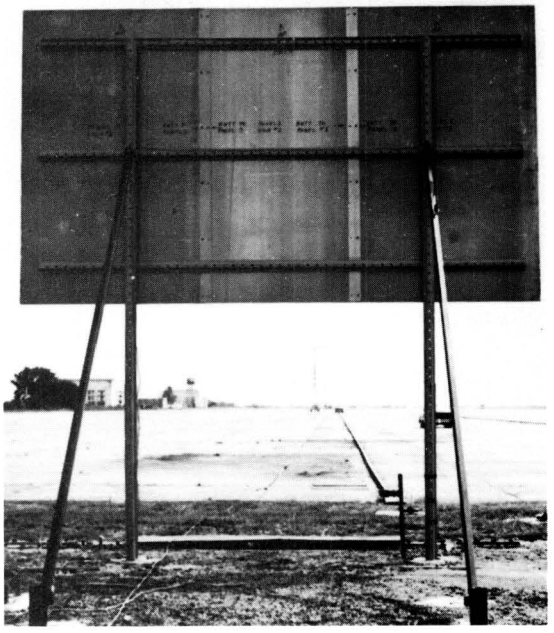

FIGURE 8.6.1 TEST 446-7

The vertical forward support posts and short rear stubs were embedded in one foot diameter, plain concrete shafts, five feet deep. Each diagonal strut was bolted to the forward vertical post approximately ten feet above grade, and to the rear stub approximately six inches above grade. Each rear stub was located approximately ten feet behind the forward vertical post. The bolted connections were made with 3/8 inch stainless steel bolts employing angle sections to permit the connection.

Sequence photographs of the collision incident are displayed in Figure 8.6.2. The first photograph (a) shows the initial vehicle contact with the vertical support post. Frame by frame analysis of the high-speed films indicated that the vertical post sheared at a hole near bumper height approximately 13 milliseconds after contact by the vehicle (b). The diagonal strut connection to the rear stub failed at approximately 179 milliseconds by shearing of the connecting bolts (c), allowing the diagonal strut to pivot about the bolted connection at the upper end of the strut. The portion of the vertical support, extending down from the sign background, struck the top of the crash vehicle at the windshield. The vertical support was deflected to the right of the vehicle path and the diagonal strut was deflected in front of the vehicle at 207 milliseconds (d). A view of the collision incident at 357 milliseconds after contact shows the vertical post at the right of the crash vehicle and the diagonal strut above the vehicle (e). The sign face partially separated at one of the panel joints.

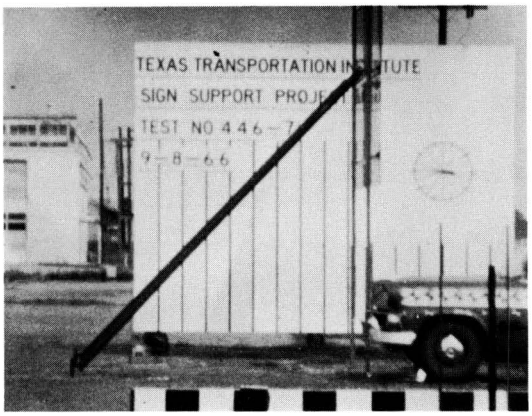

(a) CONTACT (t=0.000 SEC.)

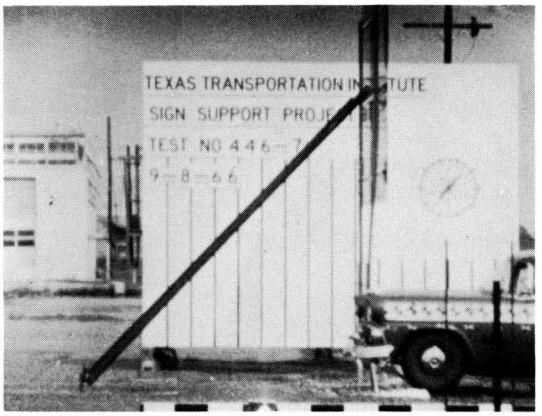

(b) POST SHEARS (t=0.013 SEC.)

(c) REAR STRUT FAILS (t=0.179SEC.)

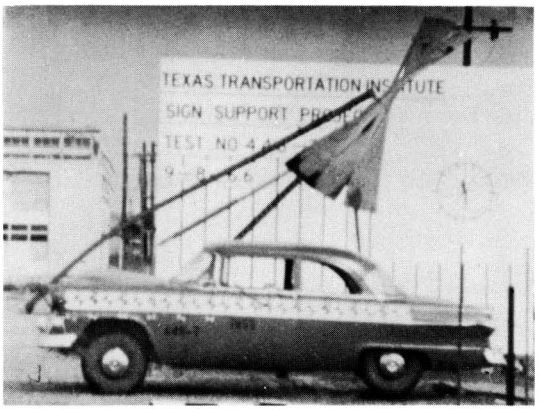

(d) LOSS OF CONTACT (t=0.207 SEC.)

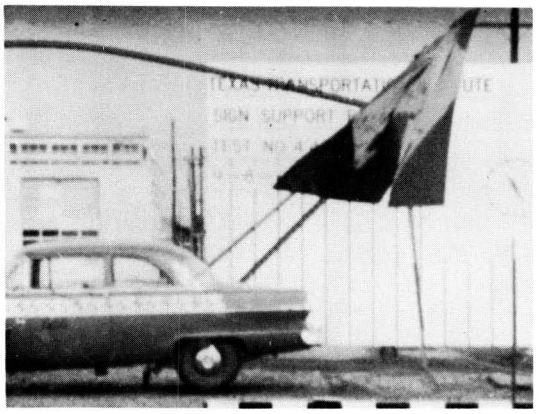

(e) STRUT CLEARS VEHICLE (t=0.357 SEC.)

FIGURE 8.6.2. SEQUENCE PHOTOGRAPHS OF TEST 446-7

A comparison of before and after photographs of the crash vehicle is made in Figure 8.6.3. The crumpled bumper, grille, and hood of the crash vehicle can be seen in Figure 8.6.3 (b). The top of the automobile was dented slightly and the windshield was cracked. The vehicle damage was not severe from the viewpoint of vehicle occupants.

It is estimated from the data obtained in this crash test that the vehicle was slowed 4.3 miles per hour by the collision. The peak deceleration recorded was 19.5 g's at 18.2 milliseconds after impact. This is a tolerable reduction in speed from the 43.7 miles per hour vehicle velocity prior to impact (see Table 7.3.1, Part III). The peak deceleration is comparable to that recorded in previous tests[17] and in Test 446-5 on the break-away post concept.

The change in velocity and peak deceleration values provides a numerical comparison for the several tests, but the relatively light damage to the vehicle is an important indicator of the relative safety aspect of the deformable A-frame concept.

(a) BEFORE

(b) AFTER

FIGURE 8.6.3 TEST 446-7, TEST VEHICLE DAMAGE

Damage to the sign support system is shown in Figure 8.6.4; it should be noted that the sign support system remained standing although the vertical supports were bent. Shearing and bending of the forward vertical post and the cracked foundation are shown in photograph (d), the crash vehicle approached from the right, and the twisted vertical leg which remained erect can be seen in the background.

Discussion. The collision behavior of this concept is considered satisfactory as a safety device except for the roof and windshield damage. However, this damage may not be as significant as it first appears, when one considers that the test was conducted as a "head-on" collision in which the vertical member was pushed into the diagonal member. The films show that the diagonal strut actually stopped the upward swing of the vertical support. Had this test been conducted at an angle, such as might be expected when a vehicle leaves the roadway, the vertical support probably would have missed the diagonal member and rotated clear of the colliding vehicle.

This secondary impact might be eliminated by placing a horizontal strut between the vertical and diagonal members near the bottom of the sign, which might cause the vertical member to bend upward over the vehicle. However, any variations of this concept should be proven by testing before being applied in the field.

It should be emphasized that the design wind load for this structure was approximately 20 psf, and thus the structural members are relatively light in weight. Extrapolation of the results of this test to heavier sections for larger signs or greater wind loads could prove to be an unsafe procedure.

(a)

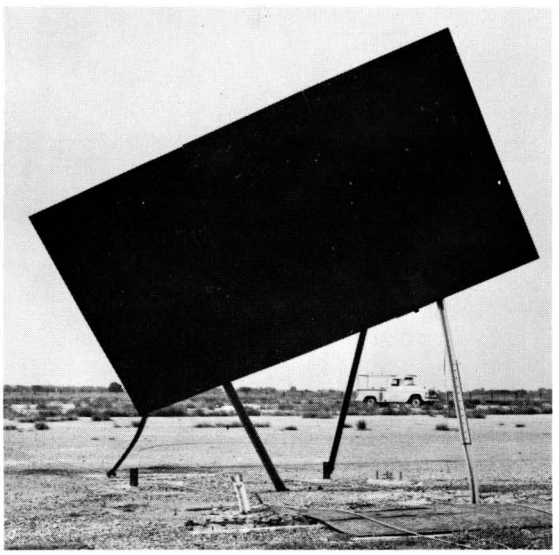

(b)

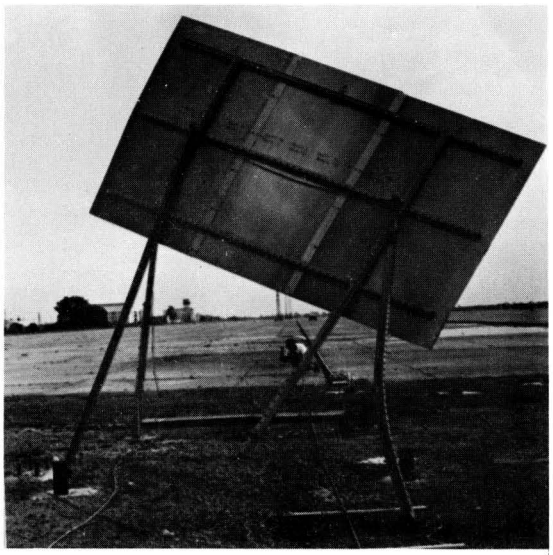

(c)

(d)

FIGURE 8.6.4 TEST 446-7, SUPPORT DAMAGE

8.7 Description of Test 446-8

Type of Sign Support: Deformable Steel A-frame

Construction Details: (see Figure 8.7.1)

Sign Face:	8' x 14' x 0.10", Sheet Aluminum
Support Posts:	4 lb./ft. Rail Steel "U" section (perforated)
Windbeams:	4 lb./ft. Rail Steel "U" section (perforated)
Foundation:	Posts driven four feet into natural ground (stiff clay in this installation).

The sign and sign supports were constructed in accordance with plans and specifications of the Minnesota Department of Highways. The rail steel "U" sections contained one-half inch diameter holes spaced at six inches on centers. This type of section is widely used in the United States for small sign installations.

Crash Vehicle: A 1955 Ford two door sedan, weighing 3460 pounds, was employed in this test.

Crash Vehicle Instrumentation: The vehicle instrumentation was identical to that described in Test 446-5.

Crash Instrumentation: One strain gage mounted on diagonal strut, as described in Table 6.3.1.

FIGURE 8.7.1 TEST 446-8

This test employed a sign support identical to test 446-7 except for the post foundations. In this installation the vertical forward posts were driven to a depth of four feet into the natural ground. The soil at the test site is a stiff clay. Figure 8.7.2 shows the sequence of events in the collision incident. Note that the behavior is essentially the same as in Test 446-7. The vertical post sheared at a hole near bumper height as in the previous test. However, the restraint offered by the soil was less than that provided by the concrete and the shearing of the post (b) occurred approximately 15 milliseconds later than in test 446-7. The time of failure of the diagonal strut connection at the rear stub occurred approximately 13 milliseconds earlier (c) than in the previous test, but this is not considered significant. Once again the forward vertical support post struck the top of the crash vehicle at the windshield. The vertical post was deflected to the right and the diagonal strut was deflected in front of and lost contact with the vehicle at 194 milliseconds (d). The sequence photograph (e) shows the vertical post and the diagonal strut deflected away from the vehicle at 300 milliseconds.

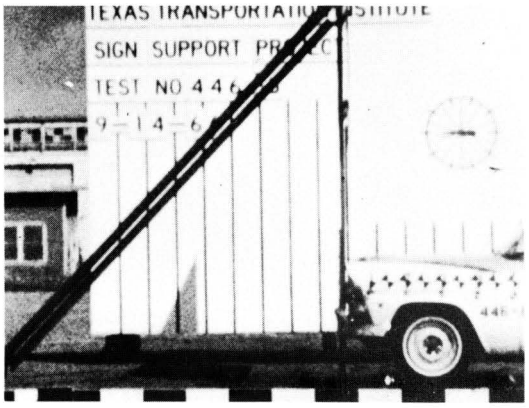

(a) CONTACT (t=0.000 SEC)

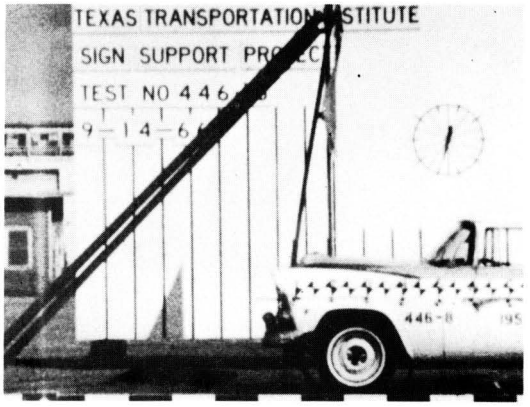

(b) POST SHEARS (t=0.028 SEC.)

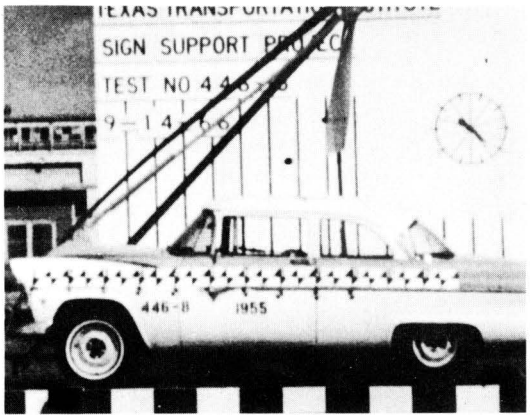

(c) REAR STRUT FAILS (t=0.166 SEC)

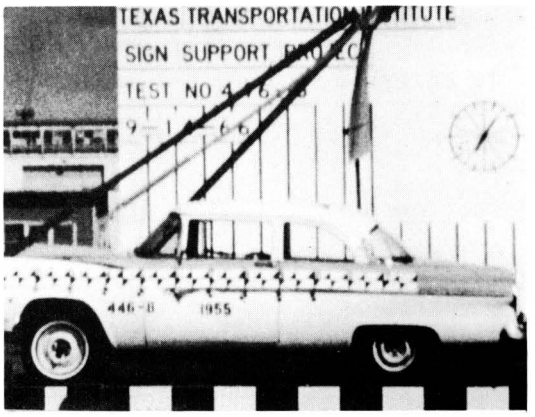

(d) LOSS OF CONTACT (t=0.194 SEC.)

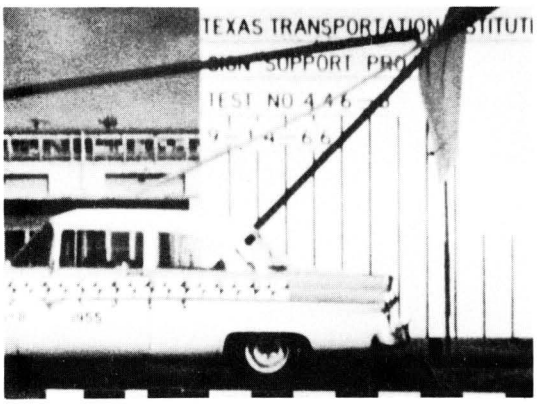

(e) STRUT CLEARS VEHICLE (t=0.300 SEC.)

FIGURE 8.7.2. SEQUENCE PHOTOGRAPHS OF TEST 446-8

The crumpled bumper, grille, and hood of the crash vehicle are shown in Figure 8.7.3. Once again the top of the vehicle was dented slightly and the windshield was cracked by the forward support post. The vehicle damage was not severe from the viewpoint of possible vehicle occupants.

The crash vehicle velocity prior to impact was determined to have been 42.7 miles per hour (see Article 7.3, Part III); and the vehicle was slowed approximately 3.7 miles per hour by the collision. This is a tolerable reduction in speed. The peak deceleration recorded was 22.6 g's at 46.0 milliseconds after impact. The peak deceleration is comparable to that recorded in previous tests[17] and in Test 446-5 on the break-away post concept.

It should be emphasized that the damage to the roof and windshield in each test on the deformable A-frame concept is not desirable. Careful examination of the high-speed films indicate that this results from the vertical forward post striking the diagonal strut and then the vehicle.

(a) BEFORE

(b) AFTER

FIGURE 8.7.3 TEST 446-8, TEST VEHICLE DAMAGE

Damage to the sign support system is shown in Figure 8.7.4; once again the sign support system remained standing following the collision incident. The vertical post and diagonal strut were deformed by the collision, and the sign background was warped. The shearing and bending of the forward vertical post are shown in photograph (d).

Discussion. The damage to the roof and windshield could be a detrimental factor in collisions involving convertibles or sports cars. Except for this, however, the collision behavior of the deformable A-frame is considered satisfactory. The variability in soil could affect the behavior of a post driven into natural ground. It is considered prudent therefore to embed the support posts and rear stubs in concrete. It is recommended that the use of light weight structural members (approximately 4 lb./ft.) be specified. Heavier members in the A-frame concept would probably produce more damage to the vehicle owing to the energy required to cause shearing of the vertical post and bolt at the rear stub.

The deformable A-frame concept, as tested, appears to be a satisfactory alternate to the cantilever break-away support from the viewpoint of safety.

(a)

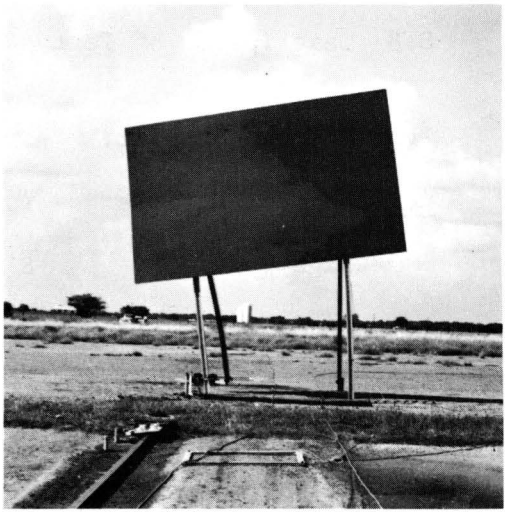

(b)

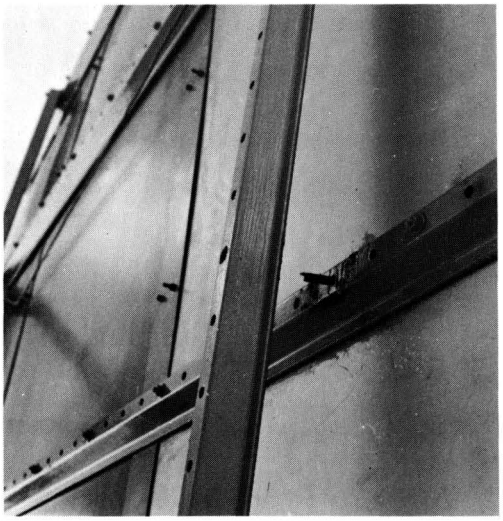

(c)

(d)

FIGURE 8.7.4 TEST 446-8, SUPPORT DAMAGE

8.8 Description of Test 446-9

Type of Sign Support: Fracture Joint A-Frame

Construction Details: (see Figure 8.8.1)

Sign Face:	8' x 16' Alcoa Type A Panel
Support Posts:	3"T2.72 6063-T6 Aluminum (vertical post) 3" O.D. x 1/8" wall 6063-T6 Aluminum (diagonals)
Windbeams:	Integral with panel
Foundation:	Reinforced concete 12" diameter x 4' - 0" deep with 3/8" A325 anchor bolts

Crash Vehicle: A 1955 Ford four door sedan, weighing 3580 pounds, was employed in this test.

Crash Vehicle Instrumentation: The vehicle instrumentation was identical to that described in Test 446-5.

Post Instrumentation: None

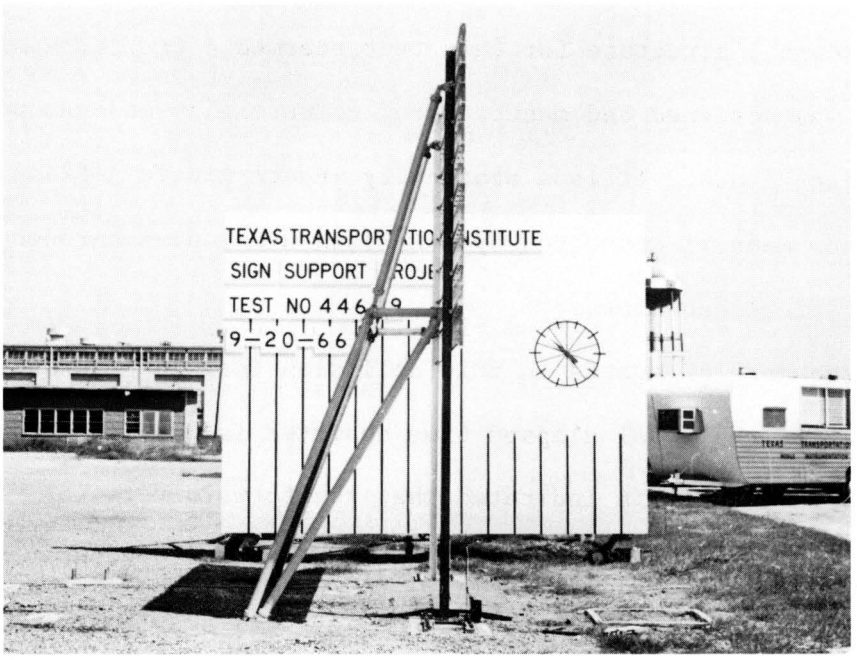

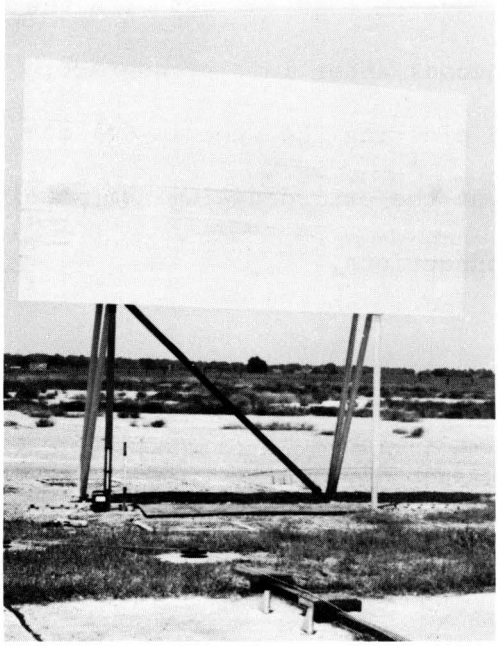

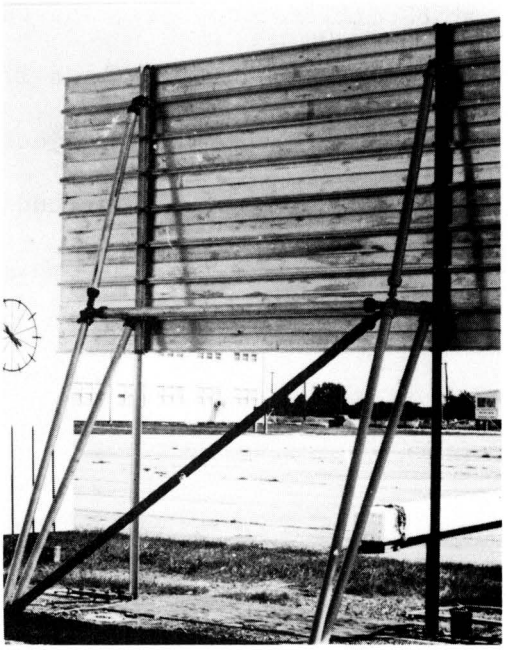

FIGURE 8.8.1 TEST 446-9

The support structure for this test, termed a fracture-joint A-frame, was designed and manufactured commercially and was purchased with project funds. It is a statically indeterminate A-frame made up of aluminum members connected by stainless steel pins through cast aluminum joint connectors.

The sequence of events in this collision incident are shown in Figure 8.8.2, the total elapsed time depicted is 336 milliseconds. Frame by frame analysis indicated that the forward vertical "T-section" support was bent (b) and the base casting fractured 14 milliseconds after initial contact, and the vertical support post remained in contact with the crash vehicle until contact was made with the diagonal strut at the rear. The rear casting at the base fractured at 82 milliseconds (c), and the support system lost contact with the front of the vehicle (d) at 126 milliseconds after initial contact. The support system was projected upward clearing the vehicle (e) at approximately 336 milliseconds, note that the extruded aluminum panel sections separated at several bolted connections.

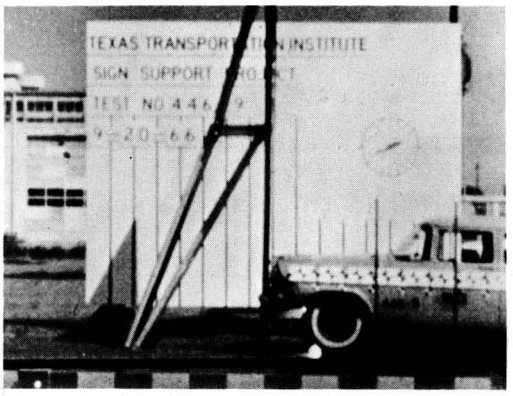

(a) INITIAL CONTACT (t=0.000 SEC.)

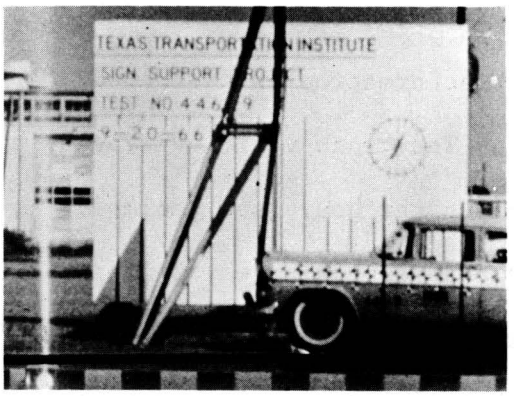

(b) FRONT CASTING FRACTURED (t=0.014 SEC.)

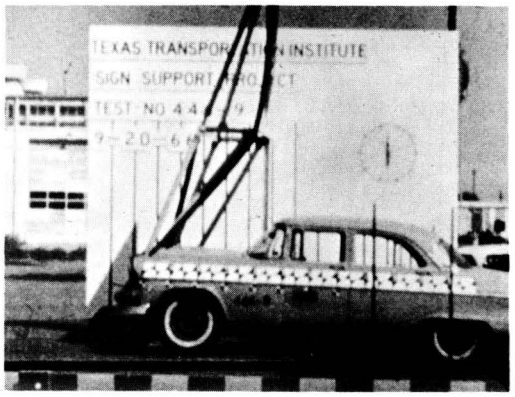

(c) REAR CASTING FRACTURED (t=0.082 SEC.)

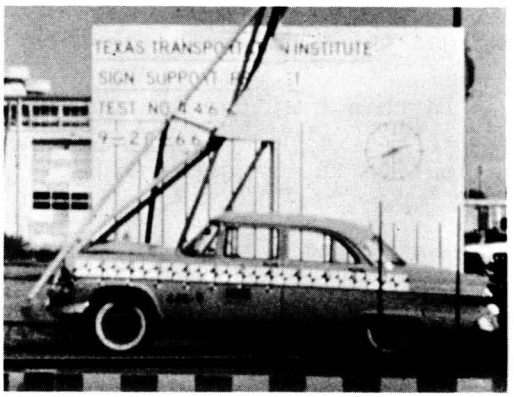

(d) LOSS OF CONTACT (t=0.126 SEC.)

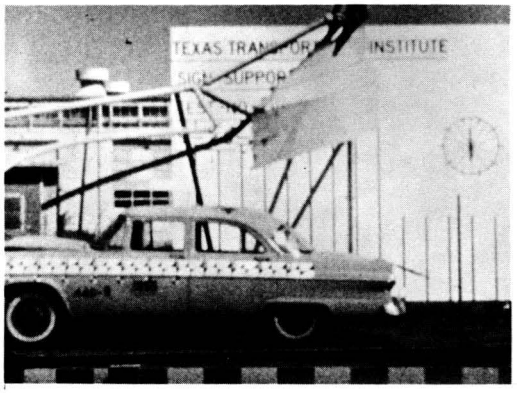

(e) SUPPORT CLEARS VEHICLE (t=0.336 SEC.)

FIGURE 8.8.2. SEQUENCE PHOTOGRAPHS OF TEST 446-9

Damage to the crash vehicle, shown in Figure 8.8.3, was limited to deformation of the bumper, grille and hood.

The crash vehicle velocity prior to impact was approximately 45 miles per hour (see Table 7.3.1, Part III); and the vehicle was slowed approximately 2.1 miles per hour by the collision. The peak recorded deceleration was 13.2 g's at 5.75 milliseconds after impact. This is a tolerable reduction in speed, and the peak deceleration is comparable to that recorded in previous tests,[17] and to that recorded in Test 446-5 on the break-away sign support.

In this test the fracture joints performed satisfactorily with respect to the crash vehicle.

(a) BEFORE

(b) AFTER

FIGURE 8.8.3 TEST 446-9, TEST VEHICLE DAMAGE

The aluminum fracture-joint support system collapsed following the collision incident as seen in Figure 8.8.4 (a); the separation of the extruded background panels noted earlier contributed to this collapse, because the torsional stiffness and structural integrity of the background was reduced. When the vehicle impacted the vertical support post, the base plate casting was fractured as shown in Figure 8.8.4 (c), allowing the post to buckle in the area of high bending moment near the upper connection point. This allowed the support to ride up on top of the hood. As the vehicle contacted the rear legs the base casting was fractured, see Figure 8.8.4 (d), allowing the support to move away from the vehicle. At this point in time, shown in Figure 8.8.2 (d), the aluminum sign background panels began to separate, this caused a loss of torsional stiffness and structural integrity and resulted in further distruction of joints and total collapse of the support. It should be noted that a transverse diagonal strut (see Figure 8.4.13) provides lateral support to the structure. This transverse member contributes to the strength of the structure, but makes collision behavior dependent upon which forward vertical support is struck.

Discussion. The sign support, as tested, functioned satisfactorily from the viewpoint of safety, but was partially demolished. Approximately half of the castings were destroyed. Some of the connecting members appeared to be re-usuable.

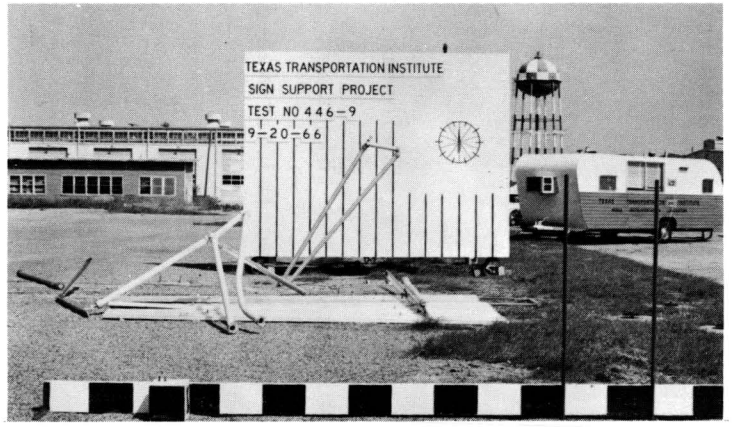

(a)

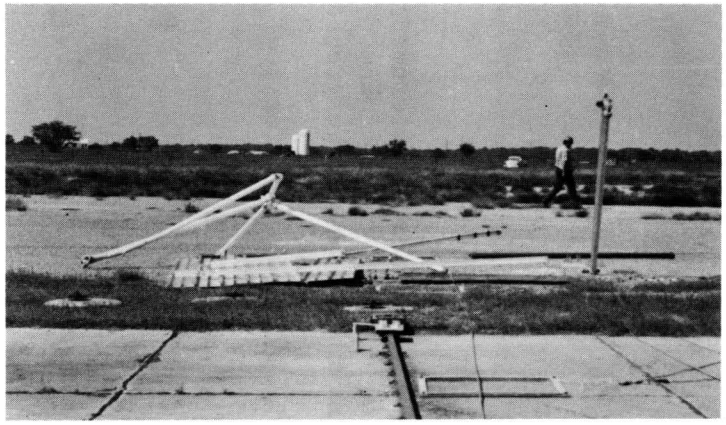

(b)

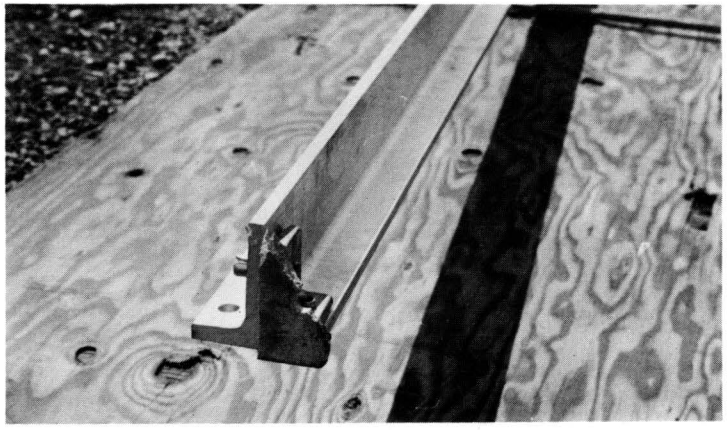

(c)

(d)

FIGURE 8.8.4 TEST 446-9, SUPPORT DAMAGE

8.9 Description of Test 446-10

Type of Sign Support: Modified Deformable Steel A-Frame

Construction Details: (see Figure 8.9.1)

Sign Face:	8' x 14' x 0.10", Sheet Aluminum
Support Posts:	4 lb./ft. Rail Steel "U" section (perforated) with V-shaped notches cut into edge of the vertical supports seven feet above the ground.
Windbeams:	4 lb./ft. Rail Steel "U" secton (perforated)
Foundation:	Posts driven into soil four feet.

With the exception of the modification in the support posts, the sign and supports were constructed in accordance with plans and specifications of the Minnesota Department of Highways. The rail steel "U" sections contained one-half inch diameter holes spaced at six inches on centers. This type of section is widely used in the United States for small sign installations.

Crash Vehicle: A 1955 Ford four door sedan, weighing 3300 pounds, was employed in this test.

Crash Vehicle Instrumentation: One Endevco piezoelectric accelerometer and one Statham oil-damped accelerometer were utilized in this test; the details of installation were the same as those described in Test 446-5.

Post Instrumentation: None

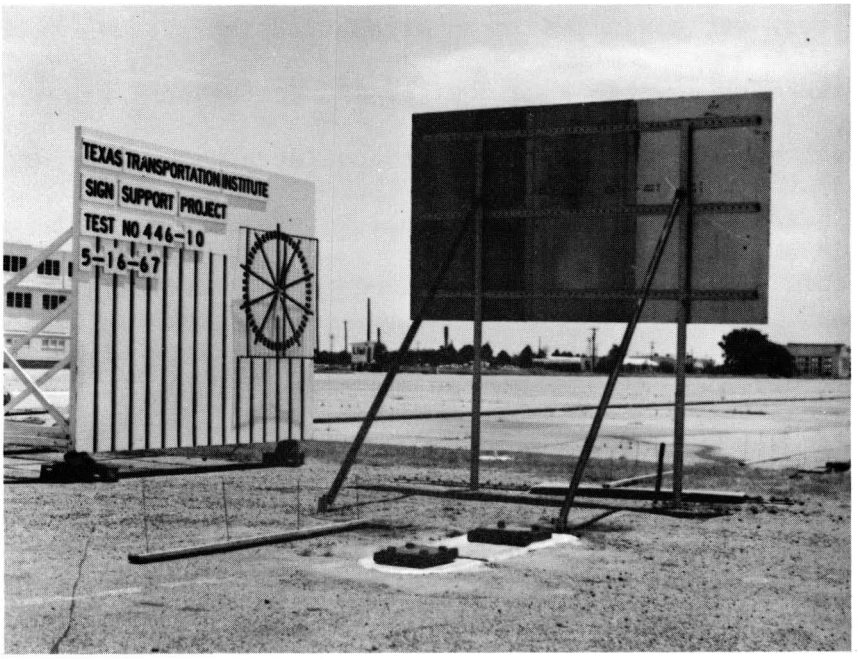

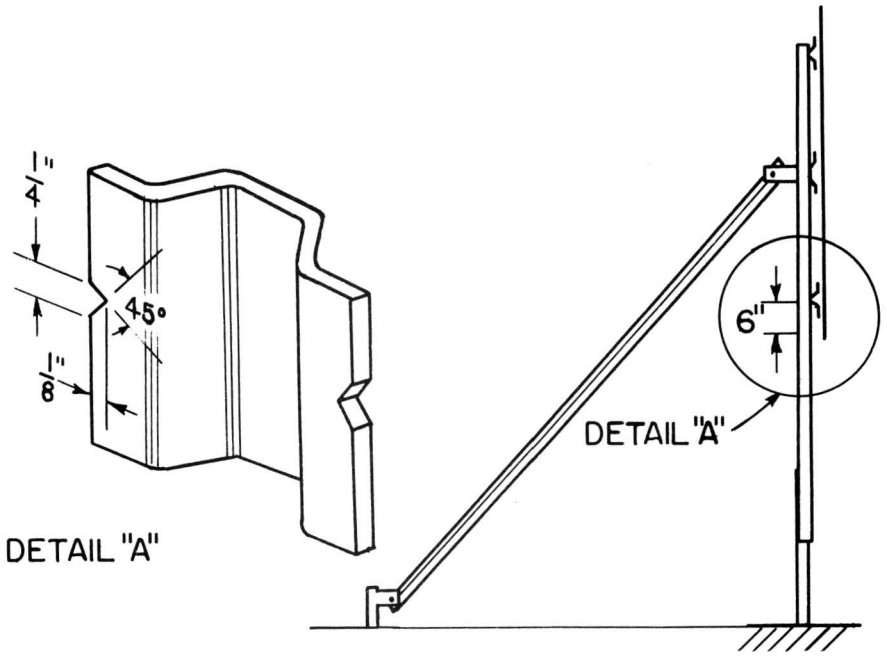

FIGURE 8.9.1 TEST 446-10

This test was conducted in an attempt to improve the behavior of the deforming post A-frame design. In Tests 446-7 and 446-8, it was noted that the severed front support post struck the roof of the vehicle at the windshield area. Modifications were made in an attempt to correct this situation. It was decided to introduce a stress riser in the forward vertical support post near the bottom of the sign background. This was intended to cause a crack to initiate at the stress riser and result in brittle fracture of the vertical support and allowing the support to hinge.

The support structure used in this test was constructed of parts salvaged from Tests 446-7 and 446-8. The front support posts were driven four feet in the soil as in Test 446-8. Figure 8.9.2 illustrates the sequence of events, which shows that the stress-riser did not operate as anticipated. The support sheared, as in the previous tests, but the bolt connecting the vertical target post to the windbeam failed before the bending moment built up sufficiently to cause the stress-riser to function. The support did function safely, however, in spite of the fact that the attempted modification was not satisfactory.

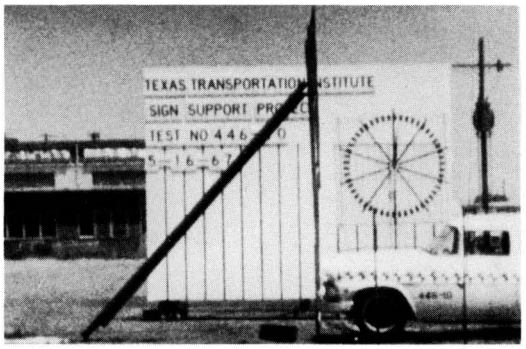

(a) CONTACT (t = 0.000 SEC.)

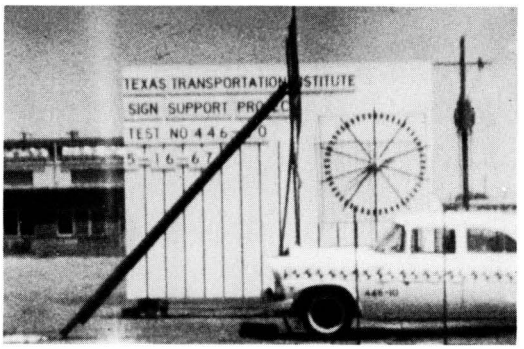

(b) POST SHEARS (t = 0.017 SEC.)

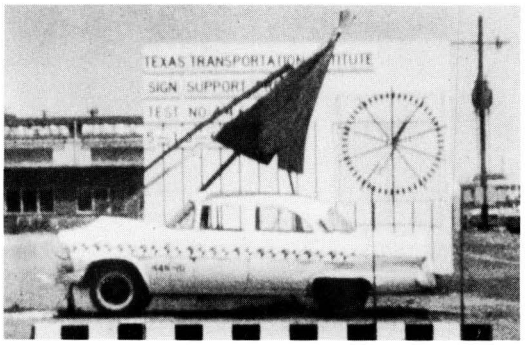

(c) REAR STRUT FAILS (t = 0.186 SEC.)

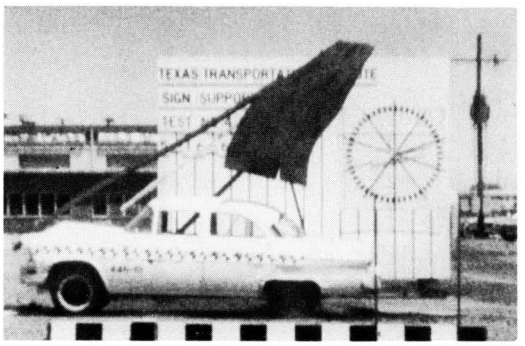

(d) LOSS OF CONTACT (t = 0.228 SEC.)

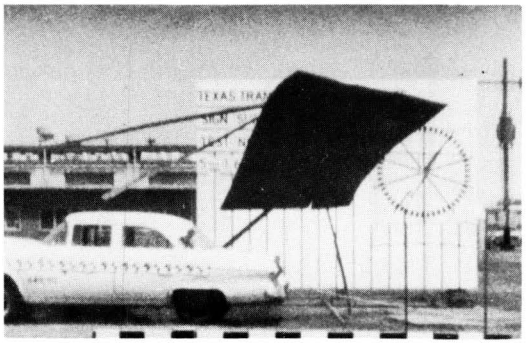

(e) STRUT CLEARS VEHICLE (t = 0.337)

FIGURE 8.9.2. SEQUENCE PHOTOGRAPHS OF TEST 446-10

Damage to the crash vehicle,as seen in Figure 8.9.3, was again limited to deformation of the bumper, grille, and hood. It should be noted that the top of the car and windshield were not struck by the support post as in previous designs. This behavior indicates that the vertical support post cleared the diagonal strut in this test. This behavior is not attributed to the modifications in the vertical support post. The time lapses following initial contact for the several events in the collision incident are comparable to those observed in Tests 446-7 and 446-8.

In this test the vertical post was deflected to the right of the crash vehicle as in the previous tests on this deforming A-frame. This strengthens the recommendation that the rear stub be placed out of line with the forward posts, probably one foot to the left of these posts.

Analysis of the high-speed film of the collision incident indicated that the crash vehicle velocity prior to impact was 43.7 miles per hour, and the collision caused a reduction in speed of 7.2 miles per hour. The reduction in speed was greater than that observed in the previous tests on this type of support; it is approximately three times greater than that computed for the break-away concept in earlier studies,[17] and is more than twice that computed in Test 446-5. The peak deceleration recorded at 125 milliseconds was 13.9 g's. The peak deceleration is close to values obtained in previous tests and in Test 446-5 on the break-away design.

(a) BEFORE

(b) AFTER

FIGURE 8.9.3 TEST 446-10, TEST VEHICLE DAMAGE

The sign support collapsed following the collision incident as seen in Figure 8.9.4; this collapse is partially attributed to the fact that the structural members had been previously crash tested. The rail steel may have been strain hardened in the earlier tests with a reduction in toughness of the material. However, the extreme torsion of the off-hit leg shown in Figure 8.9.4 (a) appears to have been the major contributor to the total collapse of the support system following the collision incident. The other photographs in Figure 8.9.4 illustrate details of the collapsed structure. It is noted in Figure 8.9.4 (d) that the shearing of the vertical support post did not occur at a hole as in the previous tests.

Discussion. The modified deformable A-frame sign support functioned satisfactorily from the viewpoint of safety, but collapsed after the vehicle passed. The behavior is not attributed to the modifications incorporated in the support post system. The V-notches were ineffective and are not recommended.

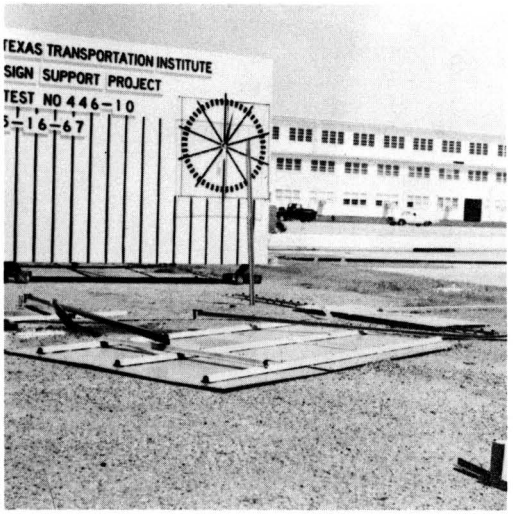

(a)

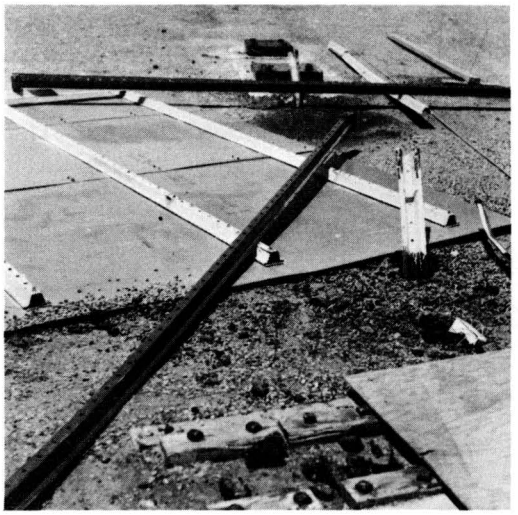

(b)

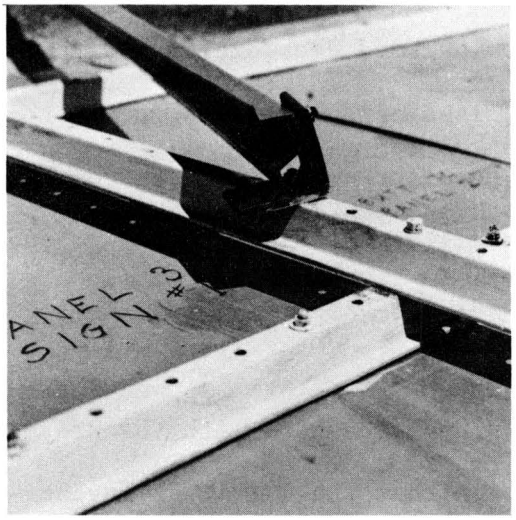

(c)

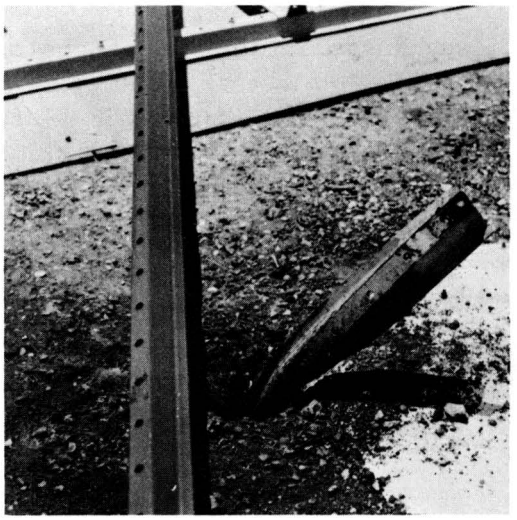

(d)

FIGURE 8.9.4 TEST 446-10, SUPPORT DAMAGE

CHAPTER 9

LOCATION AND INSTALLATIONS OF ROADSIDE SIGNS

9.1 Introduction

When a vehicle is involved in a collision with a break-away or other sign support with safety devices it proceeds with a small decrease in velocity. Vehicles which have collided with break-away support installations have remained under the control of the vehicle operator. Tire tracks at accident scenes indicate no loss of control, and in the majority of the reported collisions, the vehicle did not remain at the scene. In several accidents involving break-away sign supports the colliding vehicle subsequently struck another obstacle located near the break-away installation. Such obstacles have included deep drainage ditches, culvert headwalls, and guard posts. It is apparent, therefore, that the entire roadway environment must be considered in designing for safety. Attention must be given to the rigid obstacles and other potentially hazardous features in the area behind and adjacent to break-away installations.

Discussion of the roadside and its appurtenances with the Project Policy Committee led to the recommendation that the TTI staff investigate a limited number of break-away installations and present the results of the investigation. The purpose of this study was to find examples of sign placement which would illustrate the location of break-away supports in relation to the immediate roadside environment. Consequently, in the summer of 1966 an investigation was conducted of actual installations

of break-away sign support structures. Interstate Highway 10 near Beaumont, Texas, was selected because all supports had been converted to break-away structures. The conversion from conventional fixed base supports to break-away base supports had been accomplished in the field; thus no relocation was involved since the existing foundations and signs were employed. This portion of highway presented some excellent examples of unfavorable placement of break-away structures. Two photographs showing conventional nonbreak-away installations on Interstate Highway 45 are included to illustrate the conditions which exist prior to conversion.

9.2 Case Studies

The following photographs and discussion provide an indication of unfavorable location practices. This discussion does not imply criticism of the engineers who were responsible for the location of the sign installations discussed in this study. It must be recalled that no safety criteria for sign location existed at the time these signs were installed, and these signs and other appurtenances were installed in accordance with policies and acceptable practices.

The case studies shown in Figures 9.2.1 through 9.2.7 are presented with the recommendation that careful attention be given to proper location of break-away sign supports.

(a) View of break-away roadside sign located adjacent to shoulder.

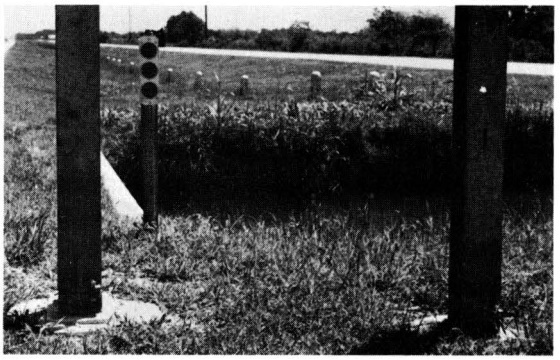

(b) Note proximity of drainage ditch and headwall to supports.

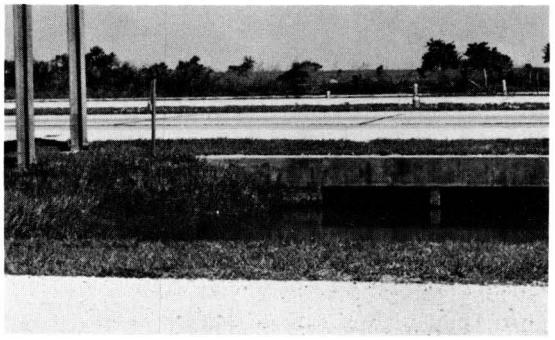

(c) Side view showing location of sign with respect to ditch.

FIGURE 9.2.1 CASE STUDY 1 - SIGN SUPPORT LOCATION ON I. H. 10

(a) Break-away roadside sign located near guardrail and bridge.

(b) Note relation of sign to guardrail, headwalls, and ditch.

FIGURE 9.2.2 CASE STUDY 2 - SIGN SUPPORT LOCATION ON I. H. 10

(a) Typical roadside break-away location.

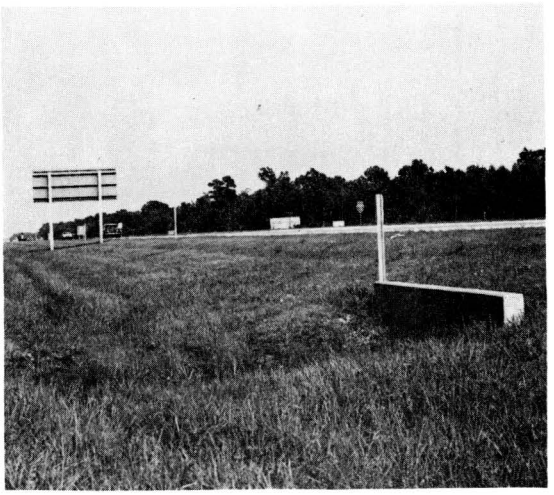

(b) Rear view showing location of sign with respect to culvert headwalls.

FIGURE 9.2.3 CASE STUDY 3 - SIGN SUPPORT LOCATION ON I. H. 10

(a) View of break-away sign located on side slope.

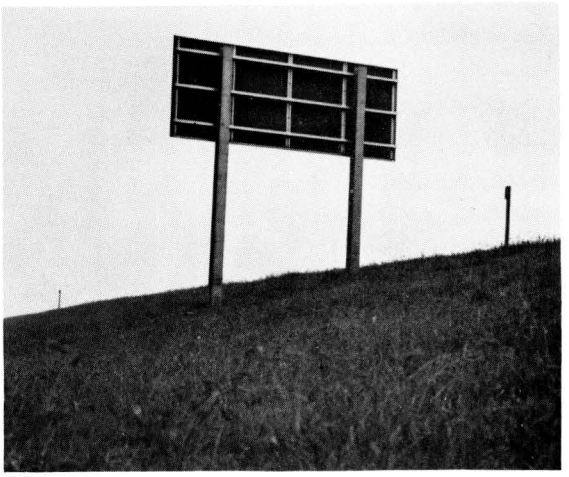

(b) View of sign from access road at bottom of slope.

FIGURE 9.2.4 CASE STUDY 4 - SIGN SUPPORT LOCATION ON I. H. 10

(a) View of break-away exit sign located in the gore.

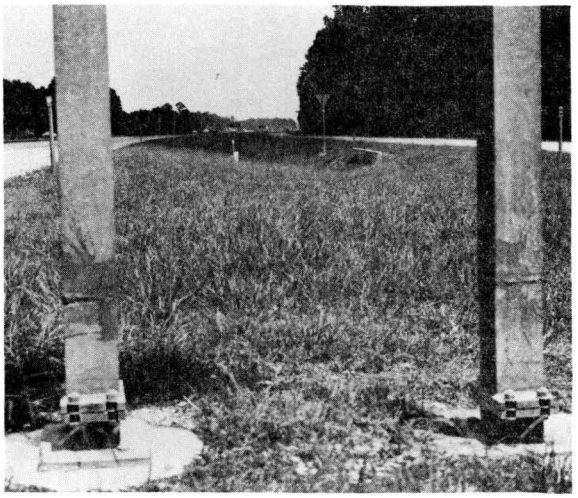

(b) Close up view shows the presence of culvert headwall behind sign. Note the weld above break-away base, base plate, and foundation at ground level in this field modified installation.

FIGURE 9.2.5 CASE STUDY 5 - SIGN SUPPORT LOCATION ON I. H. 10

(a) Typical break-away rest area exit sign located in the gore.

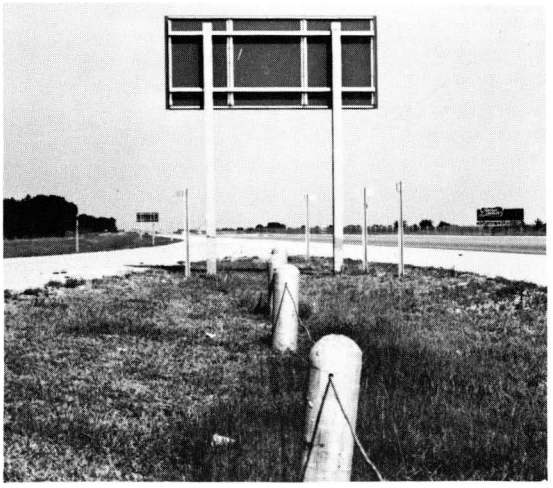

(b) Rear view of sign, showing guard posts and steel cable.

FIGURE 9.2.6 CASE STUDY 6 - SIGN SUPPORT LOCATION ON I. H. 10

(a) Conventional nonbreak-away signs located in gore. Note guard posts placed in front of the signs.

(b) Conventional nonbreak-away signs located in gore. Note the guardrail installation and the concrete foundation protruding above finished grade.

FIGURE 9.2.7 CASE STUDY 7 - SIGN SUPPORT LOCATIONS ON I. H. 45

Discussion. It is recognized that location and installation practice must be responsive to the needs of two highway categories: (1) those highways which are in operation and (2) those highways which are to be built in the future. In the first category, conventional support locations have already been made, and conversion of the in-place supports may be accomplished without considering the immediate environment. It is recommended that such conversion be made only at existing installations where adjacent obstacles will not present as great a hazard as the conventional support. Where existing hazards exist it is recommended that the break-away supports be relocated in order to avoid an aggravated collision incident involving one or more hazards. Such a relocation should be considered when a conventional support is located immediately in front of an overpass structure. The sign might better be installed on the overpass or at a point beyond the overpass.

In planning for signing of highways in the second category, future construction, the designer has more latitude in selecting sign placement. Safety requirements for the roadway environment must include consideration of the three dimensional nature of the roadway. Thus plan, profile, and cross section of the roadway must be given careful attention. The placement of signs must also be made with these three views of the roadway in mind. Flatter side slopes, horizontal alignment at and ahead of decision-making points, vertical alignment to provide adequate sight distance, and the nature of fixed,immovable obstacles such as bridge ends must be considered in

locating future sign installations.

A report[18] of the Special AASHO Traffic Safety Committee published in February 1967 contains a review of signing practices and traffic safety conditions made through on-the-scene observations by the committee. Nineteen conclusions and recommendations were presented concerning Roadside Design and Appurtenances. The following excerpts[19] from this report are recommended as excellent guidelines for improving sign location practices.

1. "In the development of plans for highway improvements, all elements of design should be reviewed to insure that any feature likely to be associated with injury or accident to the highway user is eliminated or minimized in its effect. Special attention must be directed to the safety characteristics of the roadside so that they two are the result of deliberate design and not an unpredictable byproduct of grading, drainage or other construction activity.

2. An intensive crash program to remove roadside hazards on existing streets and highways and to engineer the roadsides of new facilities with safety as a major criterion should have a paramount place in the highway program of each State. Only in this way will the motorist who inadvertently leaves the traveled way have adequate protection against death or injury.

3. Design standards more liberal than the minimums prescribed will often increase safety. Constant field checks of the operating conditions with existing and new designs are recommended for evaluation of their effectiveness and cost efficiency.

4. Embankment and cut slopes 6:1 or flatter can often be negotiated by a vehicle with some chance for recovery and these should therefore be provided where possible.

5. A full shoulder width should be carried across all structures. Shoulders should be flush with the adjoining through lane. Contrast in color or texture or both, and the use of a conspicuous edge-line marking are recommended for the guidance of drivers and to discourage use of shoulders by through traffic.

6. To increase safety when vehicles leave the pavement, a clear recovery area, free of physical obstruction, should be provided along the roadway 30 feet or more from the edge of the traveled way in rural areas. Corrective programs should be undertaken at once to eliminate

from the roadway or to relocate to protected positions such hazardous fixed objects as trees, drainage structures, massive sign supports, utility poles, and other ground-mounted obstructions that are now exposed to traffic. Where this is impracticable, an adequate guardrail or other type of protection should be provided.

7. The gore area at the divergence of two roadways, as at the exit a freeway, must be kept clear of heavy structures, unyielding sign supports and similar installations that would not readily give way if struck by a vehicle out of control. The standard EXIT sign is a permissible installation in the gore but should always be mounted on a breakaway type support.

8. The use of appurtenances along the roadside must be reviewed continually to minimize the number of such objects that can be struck by vehicles. Each jurisdiction should periodically review its signing and retain only the essential signs. The continuing demands for additional nonessential highway signs must be firmly resisted.

9. Many ground-mounted highway signs can be placed farther from the pavement, laterally, and still retain their effectiveness. Under favorable viewing conditions, a minimum distance of 30 feet from the edge of pavement to the edge of sign is recommended. The detailed location of all individual signs and sign supports should be subjected to a field review of existing highway conditions prior to installation whenever possible to assure maximum effectiveness and safety.

10. On multilane facilities with heavy traffic volumes, additional use of overhead sign locations is recommended to provide information equally visible to all traffic and for specific lane assignment.

11. Much greater use of overhead crossing structures for support of overhead signs is recommended.

12. The adoption and use of a suitable breakaway or yielding design for lighting and sign supports by all jurisdictions is recommended. Concrete bases for these supports should be flush with the ground level.

13. A consistent nationwide policy for the application of guardrail should be established at the earliest possible date. Designers must keep in mind that the objective of guardrail installation is to lessen the hazard to highway users, and not to protect any part of the roadway. Guardrail should only be used where the result of striking an object or leaving the roadway would be more severe than striking the rail."

REFERENCES

1. Foisy, J. E., "Analysis of Nut and Bolt Torques," Report No. R64SE45, General Electric Company, Lynn, Massachusetts, 1964, p. 48.

2. Project Number 8-5-63-68, sponsored by the Texas Highway Department in cooperation with the U. S. Department of Transportation, Bureau of Public Roads.

3. Specifications for Joints Using ASTM A325 or A490 Bolts, March, 1964.

4. "A Primer on Brittle Fracture," Steel Design File, Design Data From Bethlehem Steel, AlA, File No. 13-A, p. 7.

5. Barton, F. W. and Hall, W. J., "A Study of Brittle Fracture Initiation in Mild Steel," Technical Report No. SSC-147 to the Ship Structure Committee, through Department of the Navy, July 15, 1963, for sale by U. S. Department of Commerce, Office of Technical Services, Washington, D. C., 20230, p. 28.

6. Timoshenko, S. B. and Goodier, J. N., Theory of Elasticity, McGraw-Hill Book Company, Inc., Second Edition, 1951, p. 302.

7. Ibid, p. 273.

8. Rowan, N. J., Olson, R. M., Edwards, T. C., Gaddis, A. M., Williams, T. G. and Hawkins, D. L., "Impact Behavior of Sign Supports - II, A Staff Progress Report," Research Report No. 68-2, Texas Transportation Institute, Texas A&M University, College Station, Texas, September, 1965, Appendix B, Table IV.

9. Ibid, p. 13.

10. Olson, R. M., "Instrumentation and Photographic Techniques for Determining Displacement, Velocity Change, and Deceleration of Vehicles with Break-Away Sign Structures," Research Report 68-3, Texas Transportation Institute, Texas A&M University, College Station, Texas, September, 1966, p. 34.

11. Ibid, p. 50.

12. Severy, D. M., Mathewson, J. H. and Siegel, A. W., "Barrier Collisions. IV. An Evaluation of Motorist Force and Injury Control Systems," Highway Research Board Proceedings, Vol. 40, 1961, p. 541-556.

13. Severy, D. M. and Mathewson, J. H., "Automobile-Barrier Impacts," Highway Research Board Bulletin 91, 1954, p. 39-54.

14. Stonex, K. A. and Skeels, P. C., "Development of Crash Research Techniques at the General Motors Proving Ground," Highway Research Record No. 4, 1963, p. 32.

15. Beaton, J. L., "Full Scale Tests of Concrete Bridge Rails Subjected to Automobile Impacts," Highway Research Board Proceedings, Vol. 35, 1956, p. 251-267.

16. McAlpin, G. W., Graham, M. D., Burnett, W. C. and McHenry, R. R., "Development of an Analytical Procedure for Prediction of Highway Barrier Performance," Highway Research Record No. 83, 1965, p. 191.

17. Olson, op. cit., p. 49.

18. "Highway Design and Operational Practices Related to Highway Safety," A Report of the Special AASHO Traffic Safety Committee, American Association of State Highway Officials, Washington, D. C., February, 1967, 71 pages.

19. Ibid., p. 1-2.

APPENDIX

Test Visicorder Records

Figures 1 through 6 are reproductions of the Visicorder traces for all tests where data were recorded. In Test 446-1 and Test 446-4, no data were recorded because of equipment malfunctions. On each record the transducer that produced the trace is identified and its calibration is noted. The vertical distance between the horizontal lines represents 1/2 inch on the original trace.

FIGURE 1 VISICORDER RECORD, TESTS 446-2 AND 446-3

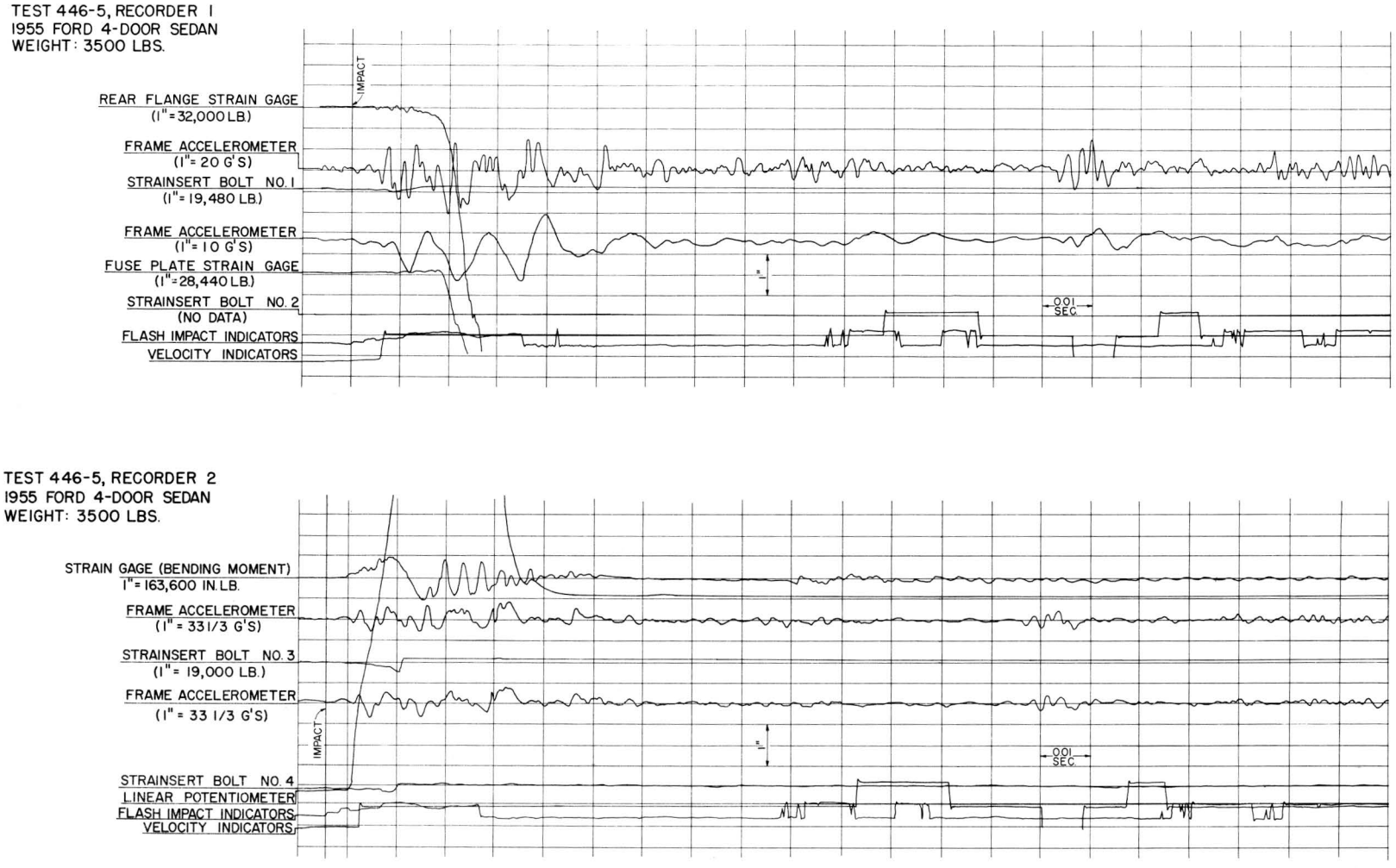

FIGURE 2 VISICORDER RECORD, TEST 446-5

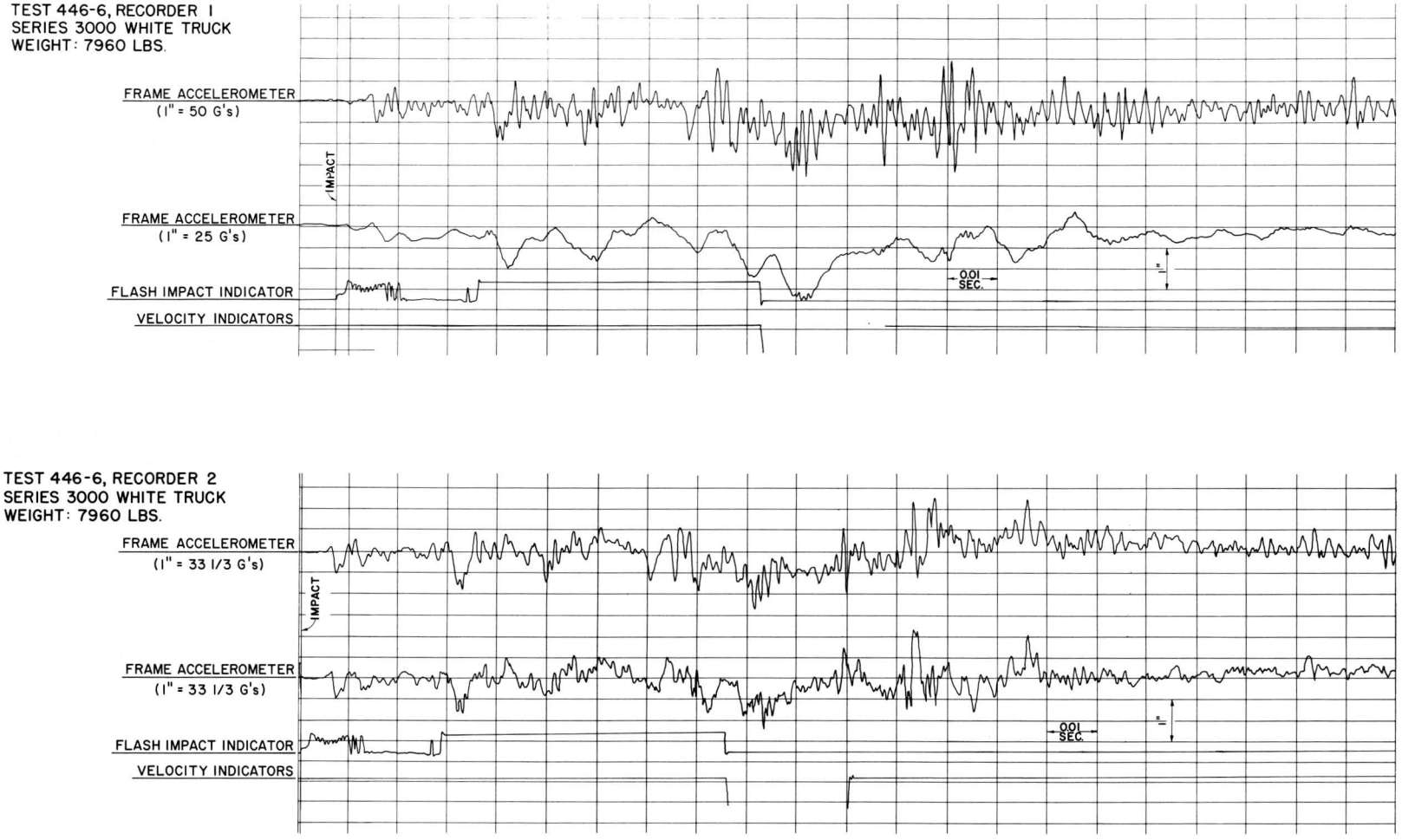

FIGURE 3 VISICORDER RECORD, TEST 446-6

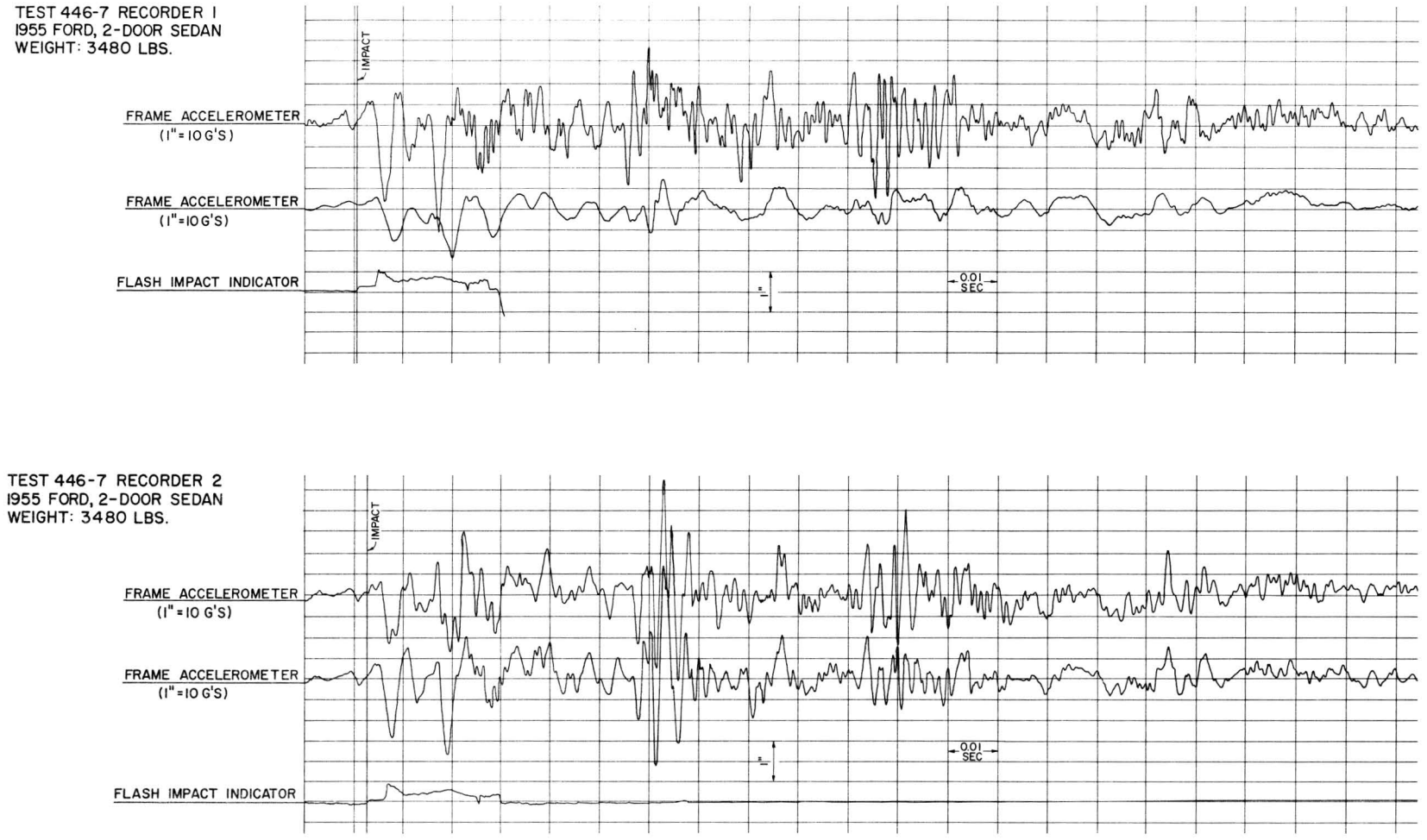

FIGURE 4 VISICORDER RECORD, TEST 446-7

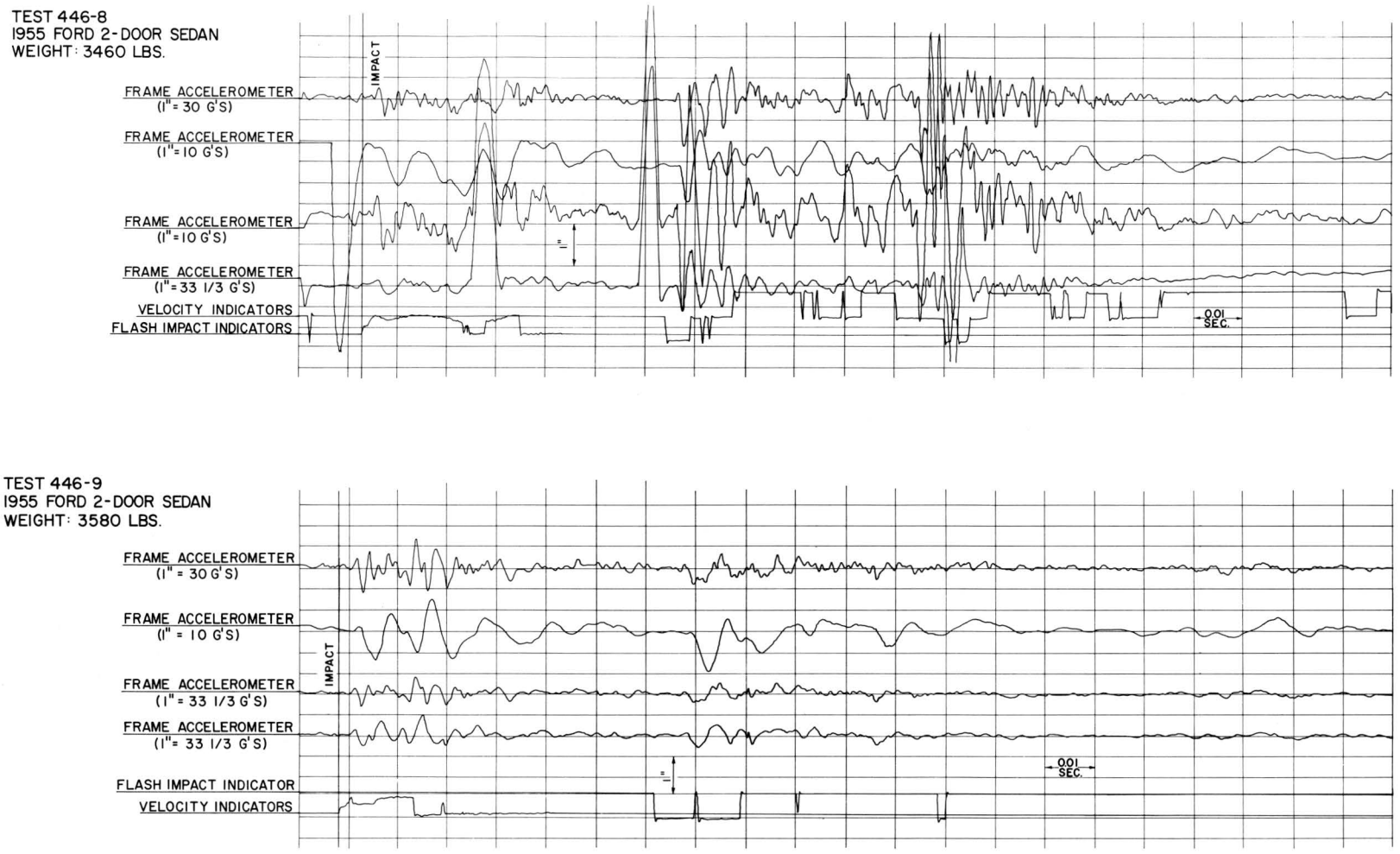

FIGURE 5 VISICORDER RECORD, TEST 446-8 AND 446-9

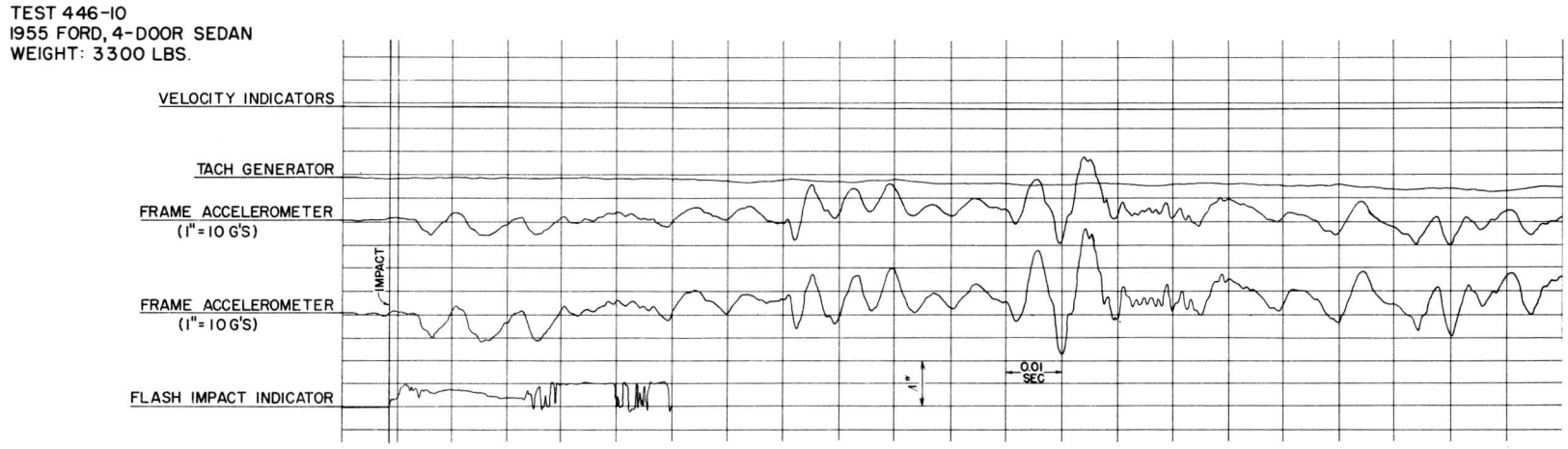

FIGURE 6 VISICORDER RECORD, TEST 446-10